TECHNISCHE UNIVERSITÄT MÜNCHEN
Lehrstuhl für Bauchemie

A Comprehensive Study on Calcium Silicate Hydrate – Polycarboxylate Superplasticizer (C-S-H – PCE) Nanocomposites as Accelerating Admixtures in Cement

Vipasri Kanchanason

Vollständiger Abdruck der von der Fakultät für Chemie der
Technischen Universität München
zur Erlangung des akademischen Grades eines

Doktors der Naturwissenschaften (Dr. rer. nat.)

genehmigten Dissertation.

Vorsitzender:	Univ.-Prof. Dr. Michael Schuster
Prüfer der Dissertation:	1. Univ.-Prof. Dr. Johann P. Plank
	2. apl.Prof. Dr. Anton Lerf

Die Dissertation wurde am 23.01.2018 bei der Technischen Universität München eingereicht und durch die Fakultät für Chemie am 12.03.2018 angenommen.

“The moon and the stars reside up high,

one must climb a long ladder to reach them”

The Royal Guidance of His Majesty the King Bhumipol Adulyadej

Acknowledgements

I would like to express my deepest gratitude to my supervisor, Prof. Dr. Johann Plank, who has provided me the great opportunity to conduct my doctoral study here at the Chair for Construction Chemistry, Technische Universität München, and who has given me the valuable guidance, encouragement, motivation, and immense knowledge throughout my Ph.D work. Without his continuous support and patience it would not be possible to achieve this research. I greatly appreciate the precious opportunities he has offered to improve my soft skills via working as an assistant in lab courses and oral presentations at international conferences.

I would also like to gratefully thank SCG Cement-Building Materials for financial support of my study at TUM.

I would like to acknowledge Prof. Dr. Sevil Weinkauf, Dr. Peter Carsten and Dr. Marianne Hanzlik from the center of Electron Microscopy at TUM's Chemistry department for their technical support with TEM. A special "thank you" is also extended to Florian Weigl and Jasmin Haberl from department of Analytical Chemistry at TUM for conducting the ICP-OES measurements.

Special thanks go to my senior Ph.D. colleagues Salami Taye, Constantin Tiemeyer, Nan Zou, Thomas Pavlitschek, Stefan Baueregger, Ahmad Habbaba, Alex Lange, Julia Pickelmann, Markus Meier, Teresa Pique, Teepakorn Napharatsamee, Huiqun Li, Michael Kaul, Lei Lei, Johanna de Reese, Laura Severin and Thomas Hurnaus for their help and suggestions. Also, I would like to express my gratitude to Dr. Oksana Storcheva for her help

regarding the ^{29}Si NMR and TEM measurements. Thanks to our secretaries Anke Kloiber and Liu Jingnu for all their administrative work.

I owe my deepest gratitude to my other colleagues for their friendly assistance, cheerfulness, and creative suggestions: Somruedee Klaithong, Timon Echt, Maike Müller, Manuel Ilg, Markus Schönlein, Johannes Stecher, Mouala Moumin, Stefanie Gruber, Claudia Chomyn, Marlene Schmid, Alexander Engbert, My Linh Vo, Florian Hartmann, Michael Spörl, Magdalena Strobl, Christopher Schiefer, Johann Mekulanetsch, Haijing Yang, Dr. Theau Conte, Eileen Quek Ee Ling, Nabisha Syed Ali, Wenjun Li and Dagmar Lettrich.

The great appreciation also goes to the Analytical and Testing Lab of Siam Research and Innovation Company (SRI) for providing the XRF measurements and for conducting the concrete tests. I truly thank my colleagues at the Admixture and Advanced Materials Research group of SRI for their technical support and valuable discussions.

I am grateful to TUM English Writing Center for consulting in English writing of my thesis.

And finally I would like to thank my mother Kruewun Kanchanason, my father Somboon Kanchanason, my sister Kanchana Puangjit and her family, my brother Kittipong Rakchuay, and my beloved Thai friends here and in Thailand for their love, support and encouragement over all these years. Without all of you, this work would have not been successful.

List of Publications

This thesis includes the following publications:

Peer reviewed SCI(E) journal:

1) V. Kanchanason, J. Plank

   Role of pH on the structure, composition and morphology of C-S-H – PCE nanocomposites and their effect on early strength development of Portland cement

   Cement and Concrete Research, 102, **2017**, 90-98.

2) V. Kanchanason, J. Plank

   Effectiveness of a calcium silicate hydrate – polycarboxylate ether (C-S-H–PCE) nanocomposite on early strength development of fly ash cement

   Construction and Building Materials, 169, **2018**, 20-27.

Non-review conference papers:

3) V. Kanchanason, J. Plank

   Early nucleation and crystal growth of C-S-H – PCE nanocomposites used as strength enhancers in cement

   The 12th International Conference on Superplasticizers and Other Chemical Admixtures in Concrete, Beijing, China, October 28 - October 31, **2018**, accepted

4) V. Kanchanason, J. Plank

Relationship between the structure and morphology of C-S-H – PCE nanocomposites and their accelerating effect in cement

Tagung Bauchemie, Bauhaus-Universität Weimar, Tagungsband 1, Weimar, Germany, GDCh-Monographie, 52, **2017**, 36-40.

5) V. Kanchanason, J. Plank

Effectiveness of C-S-H – PCE Nanocomposites Possessing Globular and Foil-Like Morphology on Early Strength Development of Portland Cement

2nd ICCCM International Conference on the Chemistry of Construction Materials, Technische Universität München, Munich, Germany, GDCh-Monographie, 50, **2016**, 85-88.

6) V. Kanchanason, J. Plank

C-S-H – PCE nanocomposites for enhancement of early strength of cement

19. ibausil, Bauhaus-Universität Weimar, Tagungsband 1, Weimar, Germany, **2015**, 759-766.

7) V. Kanchanason, J. Plank

C-S-H – PCE Nanocomposites for Enhancement of Early Strength of Portland Cement

Proceedings of the 14th ICCC International Congress on the Chemistry of Cement, Abstract book p. 326, Proceedings CD, Section 4: Admixtures, Beijing, China **2015**.

List of abbreviations

General abbreviations:

APEG	α-allyl-ω-methoxy or ω-hydroxy poly(ethylene glycol)
API	American Petroleum Institute
bwoc	By weight of cement
CEM I	Portland cement with maximum 5 wt. % of minor constituents
CEM II	Portland composite cement
d_{50}	Average particle size (50 % of particles by number are below that value)
DEA	Diethanol amine
DEIPA	Diethanolisopropanol amine
DI water	Deionized water
DIN	The German national standards organization
DLS	Dynamic Light Scattering
EO	Ethylene oxide
eq/g	Equivalent amount per gram of polymer
FT-IR	Fourier-transform infrared
g	gram
GGBFS	Ground granulated blast furnace slag
hr	Hour
HPEG	α-methallyl-ω-methoxy or ω-hydroxy poly(ethylene glycol)
IPEG	Isoprenyl oxy poly(ethylene glycol)
I_p	C-S-H inner product in hardened cement
J	Joule
LOI	Loss on ignition
m	Meter
MA	Methacrylic acid
MAS	Magic angle spinning
MCL	Mean chain length
min	Minute
mL	Milliliter
M_n	Number average molecular weight
MPEG	Methoxy poly(ethylene glycol)
MPEG-MA	ω-methoxy poly(ethylene glycol) methacrylate ester

M_w	Weight average molecular weight
nm	Nanometer
NMR	Nuclear magnetic resonance
O_p	C-S-H outer product in hardened cement
OPC	Ordinary Portland cement
Pa	Pascal
PAAM	Polyamidoamine
PCE	Polycarboxylate (ether)
pH	Pondus hydrogenii
PDI	Polydispersity index
PEG	Polyethylene glycol
PEO	Polyethylene oxide
Poly-DADMAC	Poly diallyl dimethylammonium chloride
PVA	Polyvinylalcohol
rpm	Rotations per minute
SCC	Self-compacting concrete
SCM	Supplementary cementitious material
sec	Second
TEA	Triethanol amine
TEM	Transmission electron microscopy
TIPA	Triisopropanol amine
TOC	Total organic carbon
UHPC	Ultra-high strength concrete
W	Watt
wt. %	Weight percent
w/b ratio	Water-to-binder ratio
w/c ratio	Water-to-cement ratio
VPEG	α-vinyl-ω-hydroxy poly(ethylene glycol)
XRD	X-ray diffraction
XRF	X-ray fluorescence
µ	Micro

Notation in cement chemistry:

Notation	Chemical formula	Mineral name
A	Al_2O_3	Aluminium oxide
C	CaO	Calcium oxide
F	Fe_2O_3	Iron oxide
H	H_2O	Water
S	SiO_2	Silicon dioxide
$	SO_3	Sulfur trioxide
C_3S	$Ca_3(SiO_4)O$	Tricalcium silicate
C_2S	$Ca_2(SiO_4)$	Dicalcium silicate
C_3A	$Ca_9Al_6O_{18}$	Tricalcium aluminate
C_4AF	$Ca_4Al_2Fe_2O_{10}$	Tetracalcium alumino ferrite
CH_2$	$CaSO_4 \cdot 2H_2O$	Gypsum
$C_6A\$_3H_{32}$ ($C_3A \cdot 3C\$ \cdot H_{32}$)	$[Ca_6Al_2(OH)_{12}](SO_4)_3 \cdot 26H_2O$	Ettingite
$C_4A\$H_{12}$ ($C_3A \cdot C\$ \cdot H_{12}$)	$[Ca_4Al_2(OH)_{12}](SO_4) \cdot 6H_2O$	Monosulfoaluminate
C-S-H	$xCaO \cdot ySiO_2 \cdot zH_2O$	Calcium silicate hydrate

Contents

1 Introduction

CO_2 emissions from cement production are generated from the decarbonation of limestone ($CaCO_3$), the calcination, and the milling process. About 900 kg of CO_2 are released for every ton of clinker produced, thus producing approximately 5 - 7 % of global anthropogenic carbon dioxide emissions [1-3]. In order to reduce the environmental impact of CO_2 emissions from cement production, a part of the clinker can be substituted with supplementary cementitious materials (SCMs) such as fly ash, blast furnace slag, limestone, etc. These are known as blended cements (CEM II/III) that are more environmentally more friendly than Portland cement. However, the disadvantage of blended cements is their slow early strength development, owing to a reduced rate of cement hydration and the slow pozzolanic reaction of SCMs.

Generally, calcium based salts such as calcium chloride, nitrate or formate are used as accelerators to increase the rate of hydration and to boost the early strength of Portland cement [4]. In blended cements, many reports showed an increase of early strength through addition of accelerating admixtures, such as calcium chloride, calcium formate, sodium sulfate, sodium thiocyanate, alkanolamines, and glycerol [5-8]. However, those admixtures sometimes lead to a decreased final strength.

Calcium silicate hydrate (C-S-H) is well-known as the main hydration product of ordinary Portland cement. The layered structure of C-S-H consists of linear silicate chains which are aligned in “dreierketten” sequences and share oxygen atoms with calcium ions in plane [9]. Recently, synthetic C-S-H has been introduced as a seeding material for acceleration of cement hydration [10-12]. However, only a minor acceleration can be observed from C-S-H due to rapid agglomeration and/or OSTWALD ripening of the initially formed nanofoils. In order to maximize acceleration, the size of the C-S-H particles has to be controlled to their

original nanoscale by adding polymeric dispersants such as polycarboxylate (PCE) superplasticizers [13-16].

PCE copolymers are known as high-range water-reducing admixtures for concrete. They are structured in a comb-like shape that consists of a backbone grafted with side chains. The backbone contains carboxylate anchor groups that are negatively charged and responsible for the adsorption onto the positively charged surface of e.g. cement particles. The non-ionic side chains made of polyethylene glycol (PEG) promote dispersion via a steric hindrance effect. Based on this specific molecular structure, PCEs can be applied to adsorb on freshly formed C-S-H and to produce C-S-H particles of particularly large surface area which is very beneficial for effective acceleration of cement hydration [17,18].

In this thesis, C-S-H – PCE nanocomposites were synthesized and used as seeding materials for the purpose of early strength enhancement in Portland cement and blended cements. Four main studies were carried out to obtain the superior C-S-H – PCE crystal seeds and to understand their mode of action. First, the influence of different molecular structures of PCEs, such as the side chain lengths and the grafting density, on the size of the C-S-H particles and their ability to accelerate the early strength development of mortar was investigated. Second, the impact of composition, structure and morphology of the synthesized C-S-H – PCE nanocomposites on their strength enhancement in Portland cement was studied mechanistically. Third, the effectiveness of the C-S-H – PCE nanocomposite on the early strength development of mortar and concrete made from fly ash and slag blended cements was determined. Based upon these investigations, a model for the interaction between PCE and C-S-H was proposed and the mechanism of the C-S-H – PCE seeding admixture in cement was revealed. Finally, the nucleation and crystallization of C-S-H in the presence and absence of a PCE superplasticizer were investigated.

2 Aims and scope

This PhD work aims to study and optimize C-S-H – PCE nanocomposites as seed crystals for the hydration of silicate phases in cement; to achieve the strongest seeding effect in cement hydration, as demonstrated by the largest gain in early strength of mortar and concrete; and to measure the key parameters controlling the size and the characteristics of the C-S-H – PCE nanocomposites.

Therefore, the process variables during the synthesis of C-S-H – PCE, such as the molecular structure of PCE, pH value, Ca/Si ratio, temperature and ageing time, were looked at. The characteristics of the synthesized C-S-H – PCE nanocomposites were determined in the context of their ability to accelerate the early strength development of mortar and concrete made from Portland or blended cements. Moreover, the mode of action of the C-S-H – PCE nanocomposite in cement was elucidated. Finally, the study on the nucleation and crystallization of C-S-H in the presence and absence of PCE is of relevance to understand the development of C-S-H in actual cement.

2.1 Influence of different PCE structures on the strength enhancing effect of C-S-H particles

The aim of this part is to use PCE superplasticizers of different molecular structures to stabilize and control the size of the C-S-H particles. This part describes the effect of side chain length and grafting density of MPEG PCEs on the size and characteristics of C-S-H particles. The effectiveness of the synthesized C-S-H – PCE nanocomposites in Portland cement was determined by 16 hour mortar strength tests. The impact of the C-S-H – PCE nanocomposites in cement was investigated based on heat flow calorimetry and ^{29}Si MAS NMR spectroscopy.

2.2 Effect of synthesis conditions on the effectiveness of C-S-H – PCE nanocomposites as accelerators in Portland cement

The impact of several process parameters during the C-S-H synthesis on the characteristics and performance of the C-S-H – PCE nanocomposites was investigated. A design of experiments (DOE) was used to determine the relationship between process parameters (e.g. pH value, Ca/Si ratio and temperature) and early strength of mortar. After that, the dominant parameter impacting the early strength of mortar was identified with regard to the structure, composition and morphology of C-S-H – PCE nanocomposites by using XRD, FT-IR, ^{29}Si MAS NMR, TOC, TEM, etc. measurements. Additionally, a structural model for the C-S-H – PCE nanocomposite was proposed.

2.3 Application of the C-S-H – PCE nanocomposite as an accelerator in blended cements

Blended cements have a relatively slow early strength development. The first objective of this section was to study the effectiveness of the C-S-H – PCE nanocomposite on early strength development of mortar and concrete made from fly ash, slag and calcined clay blended cements. Secondly, the behavior of the C-S-H – PCE seeding admixture in the blended cements was studied via in-situ XRD and calorimetric measurements.

2.4 Nucleation and growth of C-S-H – PCE nanocomposites

The very early nucleation and subsequent crystallization of C-S-H in the presence and absence of an IPEG PCE was monitored via transmission electron microscopy (TEM). Moreover, the effectiveness of C-S-H – PCE nanocomposites prepared at different ageing times on the early strength development of mortar was determined.

3 Theoretical background and state of the art

3.1 Calcium silicate hydrate (C-S-H)

Calcium silicate hydrates (C-S-H) consist of CaO, SiO_2 and H_2O in different stoichiometry. Their structures are variable in the range from crystalline to semicrystalline and nearly amorphous [9,19]. Generally, more than 30 crystalline minerals of C-S-H are known such as tobermorite, jennite, wollastonite, xonolite, etc. The semicrystalline phases have been reported as imperfect forms of 1.4-nm tobermorite; C-S-H (I) and jennite; C-S-H (II). Poorly ordered C-S-H (which mistakenly is also called “C-S-H gel”) is the main hydration product of Portland cement. It forms up to 60 % of hardened cement and presents the binding phase which is responsible for the strength properties and durability in hardened cement.

3.1.1 Formation of calcium silicate hydrate

a) Nucleation theories

Nucleation is the most important stage to create the first tiny solid aggregates. It includes the conglomeration of atoms, ions or molecules to form the first sub-microscopic cluster or nucleus of the solid crystal [20,21].

i. The classical nucleation theory (CNT) distinguishes between two main processes: primary and secondary nucleation. Primary nucleation involves the formation of the first nucleus which occurs in the absence of a solid interface in the solution (homogeneous nucleation) or in the presence of a solid interface of a foreign seed (heterogeneous nucleation). Opposite to this, crystal nuclei produced from a pre-existing crystal is known as secondary nucleation [21].

The classical nucleation theory considers the formation of a molecular or ionic

cluster [22]. The rate of nucleation (*J*) is given by a simple Boltzmann approach (**Equation 1**).

$$J = K \exp\left(\frac{-\Delta G_T}{kT}\right) \qquad \textbf{Equation 1}$$

where *k* is the Boltzmann constant, ΔG_T is the change in Gibbs free energy, and *K* is the kinetic prefactor.

The Gibbs free energy change (barrier height) resulting from cluster formation is expressed in the CNT as the sum of surface and volume energies (**Equation 2**). It is associated with the formation of a spherical cluster of radius "r" that is given by **Equation 3**.

$$\Delta G_T = \Delta G_S + \Delta G_V \qquad \textbf{Equation 2}$$

$$\Delta G_T = 4\pi r^2 \sigma - \frac{4}{3}\frac{\pi r^3}{V_m}\Delta\mu \qquad \textbf{Equation 3}$$

where σ is the interfacial free energy based on a unit surface area between the forming phase and the metastable phase, and $\Delta\mu$ is the difference in the specific free energy between liquid and solid.

The growth of a cluster to achieve a stable nucleus depends on the competition between the surface and volume energies. The surface term, which hinders the formation of a new phase, increases with r^2 whereas the volume energy term which typically drives nucleation decreases with r^3. The net free energy change (ΔG_T) increases with the increase in the cluster size until it reaches a maximum, then the net free energy decreases at further growth (**Figure 1**). The size of the cluster corresponding to the maximum free energy change is known as the critical nucleus

size (r^*) that is the smallest crystalline unit capable of growing further into a larger crystal. From the critical nucleus size the clusters can overcome the nucleation barrier energy, form a stable crystal nucleus and grow further. Therefore, at a high level of supersaturation the rate at which clusters reach the critical nucleus size increases and nucleation occurs more rapidly.

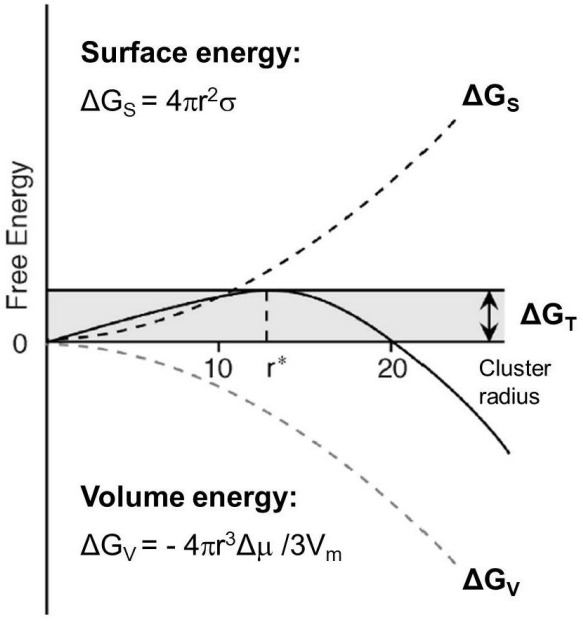

Figure 1: Graphical representation of the free energy change of a cluster as a function of its radius (redrawn after [22])

ii. Non-classical nucleation theory

This concept presents that the morphology of the precritical clusters can differ significantly from that of the final bulk crystal (**Figure 2**) [23-25]. The mechanisms can involve formation of liquid droplets [26,27] or amorphous nanoparticles (possibly formed after aggregation of stable prenucleation clusters) as precursors [28,29]. The nucleated amorphous solid phase subsequently crystallizes to generate the final stable crystal product.

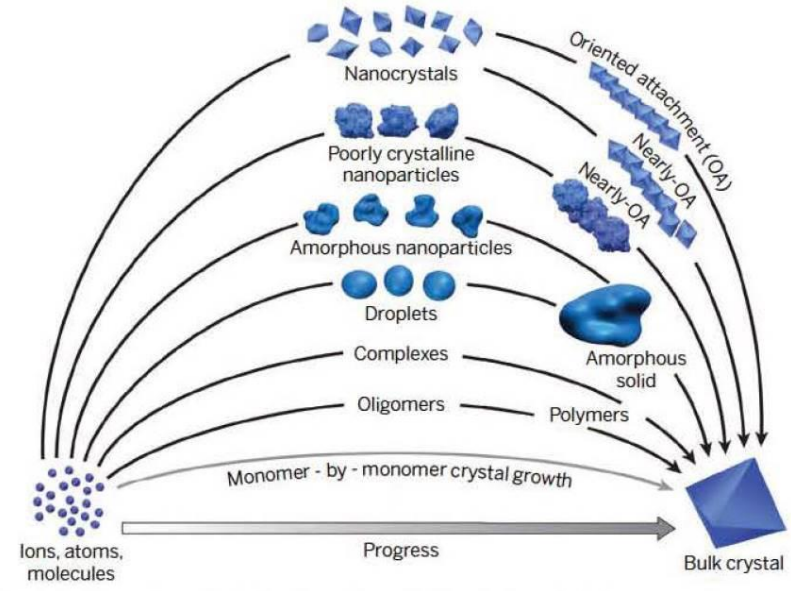

Figure 2: Known pathways to crystallization by particle attachment (from [24])

b) Formation of C-S-H in cement

Ordinary Portland cement (OPC) consists of four main compounds including the two silicate phases; tricalcium silicate (C_3S) and β-dicalcium silicate (C_2S); and two aluminate phases; tricalcium aluminate (C_3A) and tetracalcium aluminoferrite (C_4AF) [9]. Yet, the main component of cement is C_3S representing ~ 50 - 70 %.

When the cement grains make first contact with water, C-S-H is produced together with Portlandite ($Ca(OH)_2$) as a by-product during the hydration of the C_3S and C_2S phases via dissolution-precipitation reaction, as originally proposed by Le Chatelier [30]. This reaction proceeds in several steps (**Equations 4-6** for C_3S hydration), including the dissolution of the silicate phases, the nucleation of metastable and stable forms of C-S-H, and the growth of the stable C-S-H precipitates [31-33]. So far, it was believed that the C-S-H precipitation follows a classical nucleation process [34].

C_3S dissolution

$$Ca_3SiO_5 + 3H_2O \rightarrow 3Ca^{2+} + 4OH^- + H_2SiO_4^{2-}$$ **Equation 4**

C-S-H precipitation

$$1.7Ca^{2+} + 1.4OH^- + H_2SiO_4^{2-} \rightarrow (CaO)_{1.7}–(SiO_2)–(H_2O)_{1.7}$$ **Equation 5**

$Ca(OH)_2$ precipitation

$$1.3Ca^{2+} + 2.6OH^- \rightarrow 1.3Ca(OH)_2$$ **Equation 6**

- ***Dissolution***

The reaction between C_3S and water starts immediately after wetting. At first, Ca^{2+} ions are extracted from the surfaces of C_3S and C_2S while the silicate anions remain in the solid phases, thus signifying a rare incongruent dissolution behavior. After several hours (~ 2 - 3 hrs), the silicate anions start to dissolve as well until the concentrations of calcium and silicate in the pore solution reach an equilibrium (**Equation 4**). The dissolution rates can be monitored by analyzing the evolution of the ionic concentrations in the pore solution over time. The dissolution rate of C_3S at undersaturated condition has been tracked by analyzing the Si concentration in the pore solution [35-38]. Generally, the dissolution rate in undersaturated condition depends on the solubility of the ionic species, specific surface area, structure of the crystalline lattice, temperature, ionic concentration in solution [39], and crystallographic defects [40-42]. Over time, the solution gets more enriched with calcium and silicate ions and then supersaturated with respect to C-S-H which consequently precipitates. However, the formation of a protective layer of hydration products [43,44], or the presence of aluminum [42] on the surface of the C_3S particles limit the dissolution, leading to delayed nucleation and growth of C-S-H.

- ***Nucleation***

Currently it is believed that the precipitation of C-S-H in cement follows a classical nucleation process (heterogeneous nucleation). C-S-H can nucleate and grow on the C_3S grains after the concentrations of calcium and silicate in solution increase until reaching the level of supersaturation. It has been reported that the lime ($Ca(OH)_2$) concentration in solution is the most important parameter to control the heterogeneous nucleation process during the hydration of C_3S and C_2S [34]. The number of C-S-H nuclei formed in the first minutes controls the hydration kinetics of the induction period. It depends on the dissolution rate of C_3S, the volume of the solution (w/c ratio) and the initial concentration of calcium, silicate and hydroxide in the solution. A higher number of precipitated C-S-H nuclei implies a faster hydration [45,46].

- ***Growth of C-S-H***

The growth mode of C-S-H mainly controls the acceleration period of cement hydration. Nuclei of stable C-S-H continue to grow around the alite grains until complete coverage of the surface is reached. The C-S-H growth is anisotropic which occurs at two different rates parallel and perpendicularly to the surface [46]. The rate of growth depends on the number of active growth sites on the cement grains and the lime concentration in solution [47]. The growth mechanism of C-S-H has been described via two structural developments such as the defective sheets of silicate and aggregation of nanoparticles. In the first scenario, Gartner et al. [48,49] proposed a mechanism whereby C-S-H grows as branching sheets from localized nanocrystalline regions of existing C-S-H (**Figure 3**). These sheets grow in two dimensions and can build a defect into the layer. This leads to a distorting of the sheets and a disordering of the crystalline structure. According to the second model, the initial C-S-H nanoparticles aggregate. As such, the growth of C-S-H is limited until their size reaches a few nanometers.

These C-S-H nanoparticles can provide new sites for further heterogeneous nucleation or the agglomeration with previously precipitated C-S-H nanoparticles [50-54].

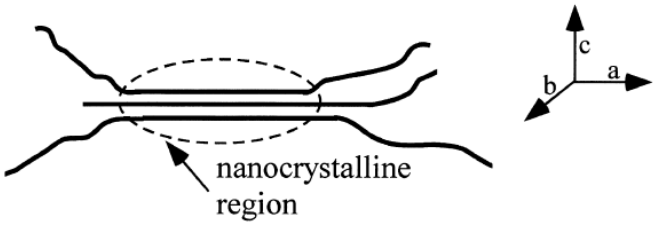

Figure 3: Schematic representation of the nanocrystalline region in C-S-H (from [49])

c) Synthetic C-S-H

C-S-H can be synthesized via a silica-lime reaction, co-precipitation and other processes. The precipitation of C-S-H from aqueous supersaturated solution is described as a sequence of nucleation and growth processes. First, the nucleation of C-S-H in aqueous solution (**Equation 7)** occurs at conditions in which the degree of supersaturation exceeds a critical value. Once the C-S-H nucleus has reached the supercritical size, it can grow.

$$Ca^{2+}_{(aq)} + H_2SiO_4^{2-}{}_{(aq)} \rightarrow CaH_2SiO_{4(s)} \qquad \textbf{Equation 7}$$

The homogeneous nucleation of C-S-H has been studied from different supersaturated solutions by mixing solutions of lime and silica, or – more preferably – calcium salts (e.g. $Ca(NO_3)_2$) with a soluble silicate (e.g. $Na_2SiO_3 \cdot 5H_2O$). The degree of supersaturation is the main parameter to control the homogeneous nucleation rate. High levels of supersaturation lead to a reduction in the time required to induce C-S-H nucleation (induction time); however, nucleation at very low supersaturation becomes heterogeneous [34]. Moreover, it

has been reported that the pH value plays an important role in the kinetics relative to the formation of C-S-H precipitates. An increase in pH value (e.g. from 10 to 12) at constant supersaturation can slow down the rate of precipitation and produces C-S-H crystallites of larger size [55].

3.1.2 Types of calcium silicate hydrate

a) Crystalline C-S-H

Among the various crystalline calcium silicate hydrates, the structures of 1.4-nm tobermorite and jennite are best characterized.

The crystal structure of 1.4-nm tobermorite, $Ca_5Si_6O_{16}(OH)_2 \cdot 8H_2O$, consists of a central Ca–O layer with attached linear silicate chains on both sides. These silicate chains are aligned in sequences of "dreierketten" which present a repeating unit of three silica tetrahedra. Two of the silica tetrahedra (pairing tetrahedra) are linked to the calcium oxide layer, while the third silica tetrahedron is bridged two pairing tetrahedra (**Figure 4**). 1.4-nm tobermorite exhibits a layered structure which has a layer thickness of 1.4 nm, as determined by XRD. The interlayer spaces of tobermorite contain water molecules and additional calcium cations [9,19,56,57].

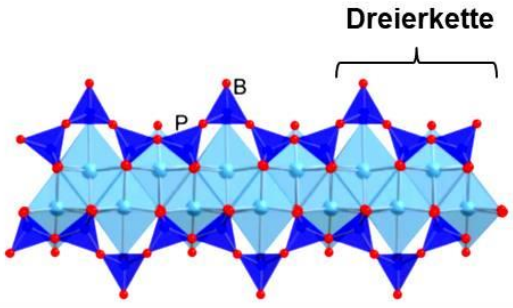

Figure 4: Schematic diagram of dreierketten chains present in 1.4-nm tobermorite (redrawn after [19])

The layered structure of jennite, $Ca_9(Si_6O_{18})(OH)_6 \cdot 8H_2O$, contains ribbons of edge-sharing calcium octahedra flanked on both sides by silicate tetrahedra (**Figure 5**). These main layers are linked by additional calcium octahedra on inversion centers. The hydroxyl groups are bonded to three calcium cations while no SiOH groups are observed [58]. Thus, jennite has a much higher Ca/Si ratio of ~ 1.5 vs. 0.83 in tobermorite and its layer thickness is 1.05 nm.

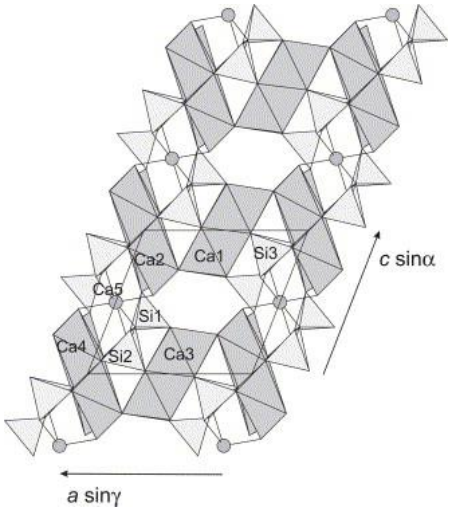

Figure 5: Schematic diagram of the silicate chains present in jennite (from [58])

b) Less crystalline C-S-H

- ***"C-S-H gel"***

The C-S-H present in hardened Portland cement is poorly crystalline. Many reports have described the structure of C-S-H in hardened cement using a defect tobermorite structure [9,19,59] where some of the silicate tetrahedra are missing.

Generally, C-S-H is composed of silicate tetrahedra which are aligned in a dreierketten structure [60-63]. These silicate tetrahedra share oxygen atoms with calcium in plane and are stacked in a layer structure (**Figure 6**). The mean silicate chain length of C-S-H obtained during the hydration of Portland cement is in the range of 5-8 tetrahedra only [61,64]. The

interlayer of C-S-H is also occupied by water, calcium ions and other ions which influence the distance of the interlayer space.

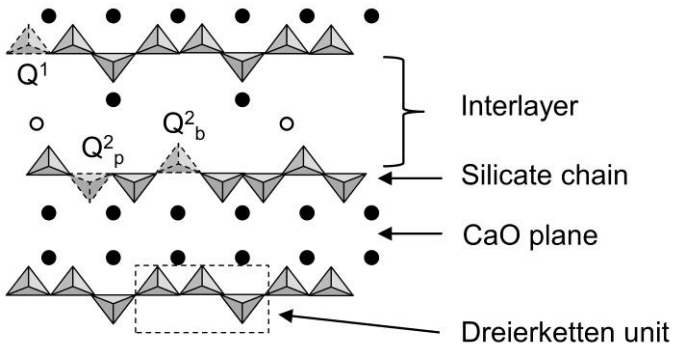

Figure 6: Schematic structure of C-S-H (from [9]). Triangles: silica tetrahedra; black circles: calcium atoms/ions in CaO planes and calcium ions; empty circles: species in the interlayer (water). Q_n: n represents the number of SiO_4 units attached to an individual silicate tetrahedron, p: pairing units, b: bridging sites

The composition of C-S-H in hardened cement is variable and depends on the water-to-cement (w/c) ratio, ageing time, concentration of calcium and silicate in solution, etc. Moreover, Ca^{2+} is the main parameter controlling the hydration kinetics, stoichiometry and structure of C-S-H. Generally, the Ca/Si molar ratio of C-S-H formed in cement hydration is greater than 1.5, with a mean of ~ 1.7 [62,63,65-69]. In hardened cement, C-S-H occurs in various morphologies, namely as small globular particles with diameters of ~ 6 - 8 nm in the inner product (Ip), and with fibrillar morphology in the outer product (Op) (**Figure 7**) [19,65,70,71].

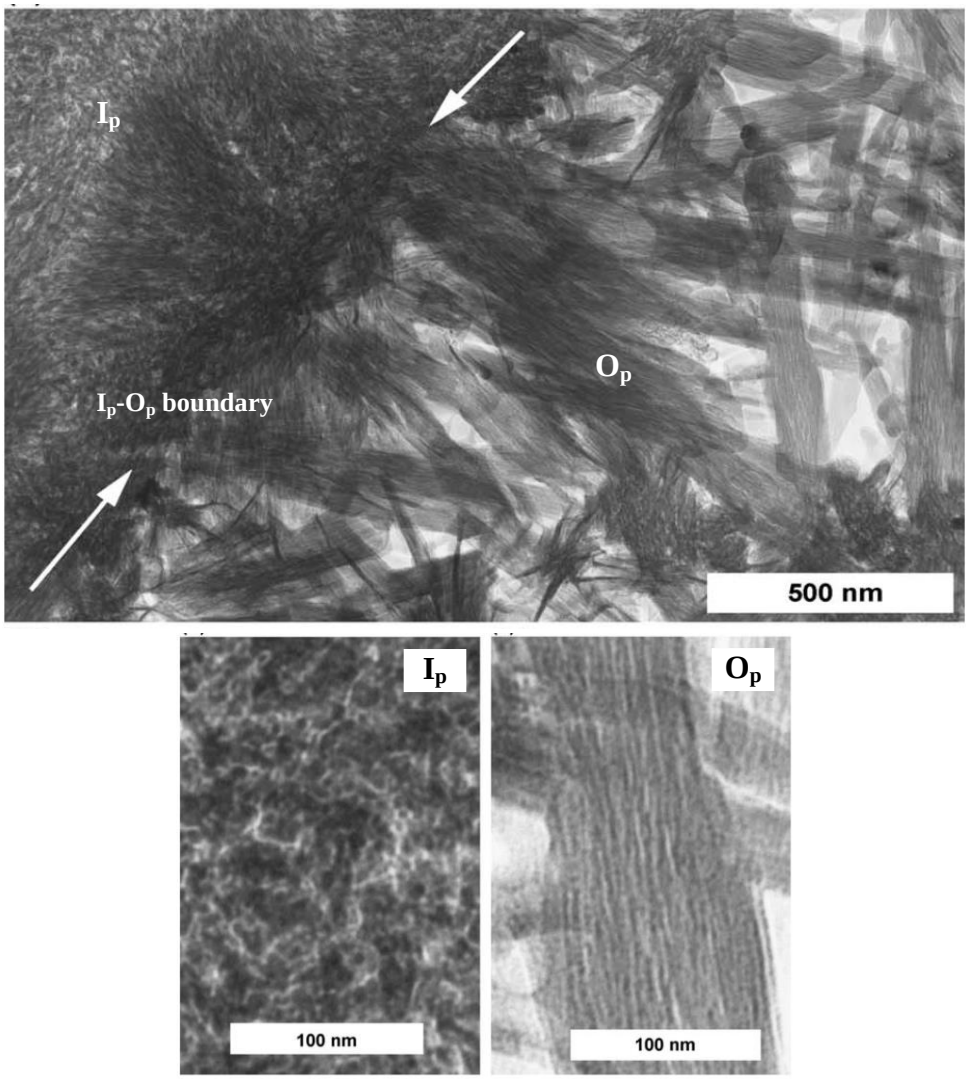

Figure 7: TEM micrograph showing the inner product (Ip) and the outer product (Op) of C-S-H present in a hardened C_3S paste (from [71])

- ***Synthetic C-S-H***

Most studies focus on the variations of composition, structure and morphology of synthetic C-S-H produced by controlled C_3S hydration, silica-lime reaction, co-precipitation, etc.

Synthetic C-S-H has been categorized in several systems including semicrystalline C-S-H which exhibits an intermediate structure between 1.4-nm tobermorite, jennite and C-S-H gel. The semicrystalline C-S-H formed at room temperature has been classified as C-S-H (I) and

C-S-H (II) [9,72,73]. They are known as an imperfect version of 1.4-nm tobermorite and jennite, respectively. Additionally, Nonat et al. have proposed three types of C-S-H including C-S-H (α), C-S-H (β) and C-S-H (γ) [74,75].

Composition

The composition of C-S-H is typically characterized by the molar ratio of calcium to silicon in its structure (Ca/Si ratio). The Ca/Si ratio can vary from 0.7 to 2.0 [70]. Generally, specific compositions of C-S-H can be found in crystalline phases such as 1.4-nm tobermorite ($Ca_5Si_6O_{16}(OH)_2 \cdot 8H_2O$; Ca/Si = 0.83) and jennite ($Ca_9(Si_6O_{18})(OH)_6 \cdot 8H_2O$; Ca/Si = 1.5) [9]. For semicrystalline C-S-H, the Ca/Si ratios of the C-S-H (I) vary in the range from 0.67 to 1.5 while the Ca/Si ratios of C-S-H (II) are nearly 2.0 [9,72,73]. Furthermore, for C-S-H (α) a Ca/Si ratio of 0.7 - 1.0, for C-S-H (β) a Ca/Si of 1.0 - 1.5 and for C-S-H (γ) a Ca/Si > 1.5 have been reported [74,75].

The Ca/Si ratios depend on several factors such as the initial mixture of raw materials, the activity of the ions in the equilibrium solution, pH value, temperature, synthesis approach, etc. Also, the correlation between the concentrations of calcium and silicate ions in the solutions and the Ca/Si ratio has been highlighted [76]. There, a decreased silicate concentration and rise in the calcium concentration in solution led to an increased Ca/Si ratio of the C-S-H products. The lowest and highest Ca/Si ratios found in C-S-H were at ~ 0.7 and ~ 1.45, respectively. Amorphous silica and calcium hydroxide were also detected in C-S-H with Ca/Si ratios lower than 0.7 and greater than 1.45, respectively. Recently, a uniform C-S-H (without contamination by calcium hydroxide phase) possessing controlled Ca/Si ratios up to 2.0 was produced using a micro mixer system [77]. Moreover, strongly alkaline solutions led to an increase in the Ca/Si ratios in the C-S-H [78-81].

Composition of the silicate chain

^{29}Si MAS NMR presents a very useful technique for the characterization of silicate chains present in C-S-H precipitated during cement hydration or in synthetic C-S-H. Evidence from ^{29}Si NMR spectroscopy suggests linear silicate chains for the synthetic C-S-H arranged in dreierketten. The silicate chains generally contain terminal silicate groups (Q^1, δ = -79 ppm) and chain members linked to two neighboring silicate units (Q^2), as shown in **Figure 8**. The Q^2 silica tetrahedra positioned in the middle of the chains can arrange in a "dreierketten" structure whereby a dimer of silicate tetrahedra (paring tetrahedra; Q^2_p, δ = -85 ppm) connects to the bridging tetrahedron (Q^2_b, δ = -83 ppm) [82-87]. It has been shown that the number of bridging tetrahedra decreases when the Ca/Si ratio increases [80,88,89].

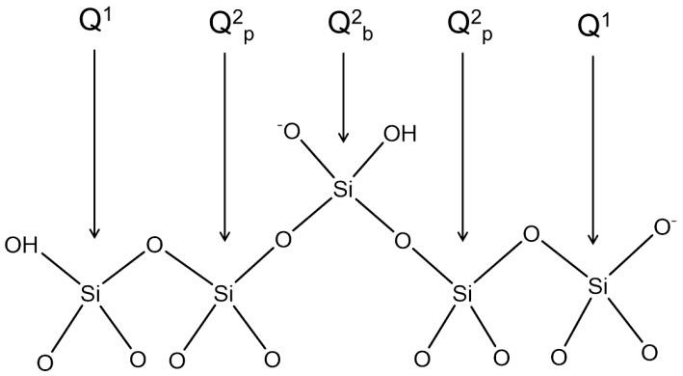

Figure 8: Schematic representation of a pentameric silicate chain of the type present in the dreierketten-based model for the structure of C-S-H

Deconvolution of the spectrum in terms of three resonances allows an estimation of the mean chain length (MCL) that can be calculated by following **Equation 8** [89]. It has been observed experimentally that the silicate chain in C-S-H contains 3*n*-1 tetrahedra, where *n* is an integer [19]. When all bridging tetrahedra are missing in the silicate chain, then the chain represents a series of dimeric anions thus giving the shortest MCL.

$$MCL = \frac{2\,(Q^1+Q^2_b+Q^2_p+Q^3)}{Q^1}$$ **Equation 8**

The MCL of silicate chains in C-S-H depends on the degree of polymerization (Q^2/Q^1). An increase in the mean chain length reflects a higher degree of polymerization. Moreover, the mean chain length increases with decreasing Ca/Si ratio, particularly Ca/Si ratios of ~ 1.1 - 1.3 [80,84,88-94]. High pH conditions lead to an increase in Q^1 units and a decrease in the MCL of the silicate chains [80,81,86,95,96]. Furthermore, several reports have revealed that the substitution of Si by aluminium Al(IV) in the bridging positions of the silica dreierketten structure [97-103] increases the mean chain length of the silicate chain [95].

Surface charge of C-S-H

Generally, the external surfaces of C-S-H contain silanol groups attached to the bridging tetrahedra (Q^2_b) and the end-chain tetrahedra (Q^1) (**Figure 8**). These silanol groups are ionized in highly alkaline condition and result in a negatively charged surface (**Equation 9**). However, most often this charge is changed via complexation by dissolved calcium ions (**Equation 10**). Consequently, in cement the surfaces of C-S-H exhibit a slightly positive charge as determined by zeta potential measurement [104-106]. Several factors affect the surface charge of C-S-H such as Ca/Si, pH value, calcium concentration, type of alkaline cations, etc. A negative zeta potential of C-S-H is measured at very low calcium concentrations and low Ca/Si ratios. While at higher calcium concentrations and high Ca/Si ratios, sorbed calcium overcompensates the negatively charged surface, resulting in an apparent charge reversal [105,107,108]. Moreover, a reduction in the zeta potential of C-S-H in the presence of various alkaline cations such as Na^+, K^+, Cs^+, etc. has been reported. This indicates that these monovalent ions partially replace the calcium ions in the interlayer and on the surfaces of C-S-H (**Equation 11**) [95,105,109,110].

$$SiOH \rightarrow SiO^- + H^+ \quad \textbf{Equation 9}$$

$$\equiv Si{-}O^- + Ca^{2+} \rightarrow \equiv Si{-}O\,Ca^+ + H^+ \quad \textbf{Equation 10}$$

$$\equiv Si{-}O^- + M^+ \rightarrow \equiv Si{-}OM + H^+ \quad \textbf{Equation 11}$$

(where M is a monovalent ion)

Morphology

The morphology of C-S-H has been studied via transmission electron microscopy (TEM). Various morphologies have been reported for synthetic C-S-H (**Figure 9**) which depend on the Ca/Si ratio, pH value, synthesis method, and temperature.

The morphology of C-S-H changes from foils at low Ca/Si ratio to fibres at high Ca/Si [89,111]. At high Ca/Si ratios, a mixture of C-S-H and a fibrous lime-rich phase is observed [112]. At low Ca/Si ratio of 1.0, a globular-like morphology of C-S-H is found at low pH values < 10.9 while a foil-like morphology of C-S-H is always observed at pH values ≥ 11.7 [81].

The synthetic C-S-H fabricated via silica-lime reaction attains a foil-like morphology at Ca/Si ratios of ~ 0.7 - 1.5, whereas a fibrillar morphology is observed at higher lime concentrations of CaO > 22 mmol/L and Ca/Si ratios > 1.58 in the controlled C_3S hydration method [89]. Additionally, the C-S-H samples prepared by mechano-chemical reaction show a coarser foil-like morphology when compared to the C-S-H obtained from the silica-lime reaction. Under hydrothermal conditions of the silica-lime reaction, the morphologies of C-S-H can vary from sheet to long reticular fibers as the Ca/Si ratios increase from 1.0 to 1.7 [114,115].

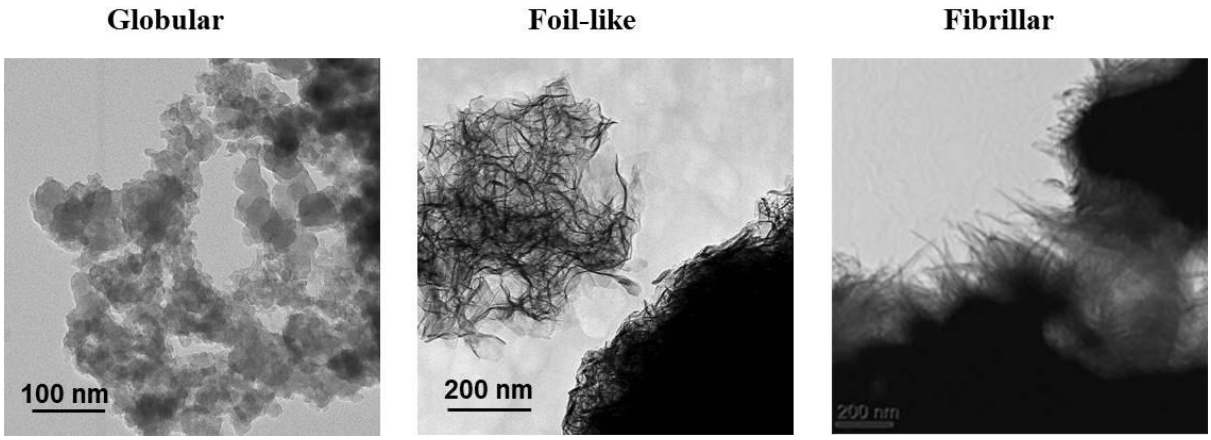

Figure 9: TEM images of various morphologies of synthetic C-S-H observed at ambient temperature (from [81,89])

3.1.3 Structure of C-S-H

a) Structural models for C-S-H

Several papers have presented models for the mesostructure of C-S-H. These concepts rely on two different theories, namely the colloidal model and the layer model.

The first model was developed by Power and Brownyard which is known as the P-B model [116]. They assumed that the C-S-H gel is as a colloidal structure made of small bricks with interstitial gel pores.

On the other side, Feldman and Sereda (F-S) presented a model of the C-S-H network as formed by irregular C-S-H layers with adsorbed and interlayered water molecules (**Figure 10**). They suggested that the interlayered water can be reversibly removed upon drying, thus instead of using water as a medium in the sorption isotherms, they studied the diffusion of helium into the C-S-H structure to provide evidence for the layered structure of the C-S-H gel [117].

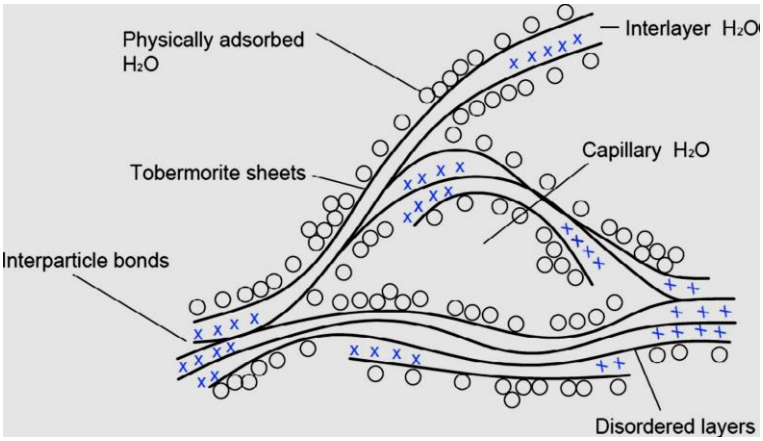

Figure 10: Schematic representation of the Feldman and Sereda model (from [118])

Afterward, the colloidal model I (CM-I) which combined the F-S and P-B concepts was developed by Jennings. This model defines the size, density, and packing efficiency of C-S-H basic building blocks. Moreover, the structure of calcium silicate hydrate between 1 and 100 nm was described through a series of SANS and SAXS analyses. The basic units of C-S-H are small spheres with a diameter of ~ 2.2 nm that flocculate to form larger globules (= basic building block) of ~ 5.6 nm diameter. The globules pack together to form low density (LD) and high density (HD) C-S-H depending on the packing densities [119]. The combination of these units leads to a formation of the microstructure of C-S-H.

According to Jennings' colloidal model-II (CM-II) [120], the nanostructure of C-S-H can be described based on the analysis of water sorption isotherms. The C-S-H gel is assumed as a fractal structure consisting of an assembly of C-S-H flocs formed as globules (not identical with the globules shown later in this work here) with a cross section of ~ 5 nm. These "globules" are multilamellar objects and contain interlayer spaces and intraglobular spaces (IGP) in which water can be located. The stacking of the "globules" can create two types of pores: the small gel pores (SGP) of 1 - 3 nm and the large gel pores (LGP) of 3 - 12 nm.

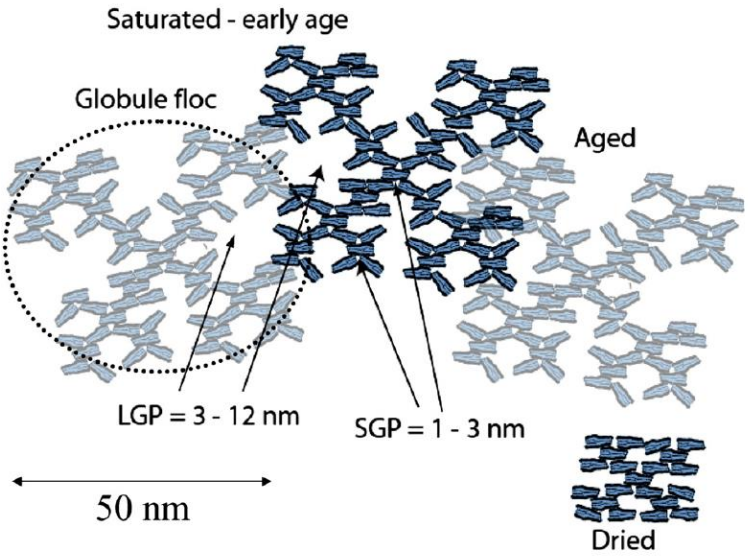

Figure 11: Schematic presentation of the nanoscale structure of C-S-H according to the CM-II model (from [120])

b) Molecular models for C-S-H

Most models proposed for the nanostructure of C-S-H are based on linear silicate chains, similar to those which are present in 1.4-nm tobermorite, the known dreierkette-based models.

The first dreierkette-based model for C-S-H was proposed by Bernal et al. [121]. The crystallographic tests were performed on two synthetic C-S-H products; C-S-H (I) and C-S-H (II) produced by hydration of C_3S. It was found that C-S-H (I) had a layer structure, similar to the natural mineral 1.1-nm tobermorite (Ca/Si = 0.83) that contains infinite linear silicate chains of dreierketten (bridging tetrahedron which link to paired tetrahedra) in which the paring silicate tetrahedra share O–O edges with the CaO plane.

The structure of poorly crystalline and amorphous C-S-H phases is described as a layered structure built up from CaO_x polyhedra sandwiched between two dimeric or polymeric

silicate chains [122]. The layers of C-S-H are separated by an interlayer which contains H_2O, Ca^{2+}, OH^-, and other ions.

Taylor's model [61] revealed that the structures of C-S-H containing Ca/Si ratios above 0.83 are characterized by the removal of some bridging tetrahedra which are substituted by calcium ions. The Ca/Si ratios of the C-S-H gels were in the range of 0.83 - 2.25 as present in 1.4-nm tobermorite and jennite at low and high Ca/Si ratios, respectively. The silicate chains in their structures are aligned in dreierketten with the length of 3*n*-1 tetrahedra (where n = 1, 2, 3, ...). The dimeric structural units representing the shortest silicate chains are obtained from omission of all bridging tetrahedra from the tobermorite and jennite structures.

Richardson and Groves proposed models for C-S-H which were classified into two different combinations of structures such as the T/J (tobermorite/jennite) and T/CH (tobermorite/calcium hydroxide) structure [123]. These models have been applied to describe the nanostructure of C-S-H in real cement pastes. There, the Ca/Si ratios of C-S-H were extended to the range of 0.67 - 2.5. The tobermorite-like core is the part of the braces which consists of a highly disordered layer structure containing finite silicate chains at a length of 3*n* - 1. The Ca^{2+} ions are in the main layer and the interlayer which is required for charge-balance. The position of Ca^{2+} ions in the T/J and T/CH structures is different: in the T/J structure, the Ca^{2+} ions form part of the main jennite-based layers, as Si–O–Ca–OH, while on the T/CH structure the Ca^{2+} ions are present in layers of CH which occupy the space between the silicate layers of the tobermorite-like structure. Moreover, the model was also applied to the C-S-H structure present in blended cements [124] where bridging Si^{4+} was substituted by Al^{3+} in the silicate chains, resulting in C-A-S-H.

3.2 Polycarboxylate based superplasticizers

Polycarboxylate (PCE) superplasticizers are known as high-range water-reducing admixtures in concrete [125], such as ready-mix concrete, self-compacting concrete (SCC), ultra-high strength concrete (UHPC) [126-128], etc. PCEs improve the rheology of concrete through the dispersion of particles [129,130]. Consequently, the water consumption in the mix proportion of concrete is reduced, leading to an improvement of compressive strength and durability of hardened concrete [131,132].

3.2.1 Molecular structure of PCEs

The structure of comb-like PCE copolymers generally consists of a main chain (backbone) to which side chains are attached. The backbone carries carboxylate anchor groups (COO^-) that have a negative charge and are responsible for adsorption of the polymer onto the positively charged surface sites of cement particles and hydration products like ettringite [133-136]. The non-ionic side chains grafted to the backbone of PCEs are normally made from polyethylene glycol (PEG) which is accountable for the dispersing ability via a steric hindrance effect [130,137,138].

Currently, several types of PCE superplasticizers are used in the concrete industry, including MPEG-type PCEs, APEG-type PCEs, VPEG-type PCEs, HPEG-type PCEs, IPEG-type PCEs, and PAAM-type PCEs [139] (**Figure 12**).

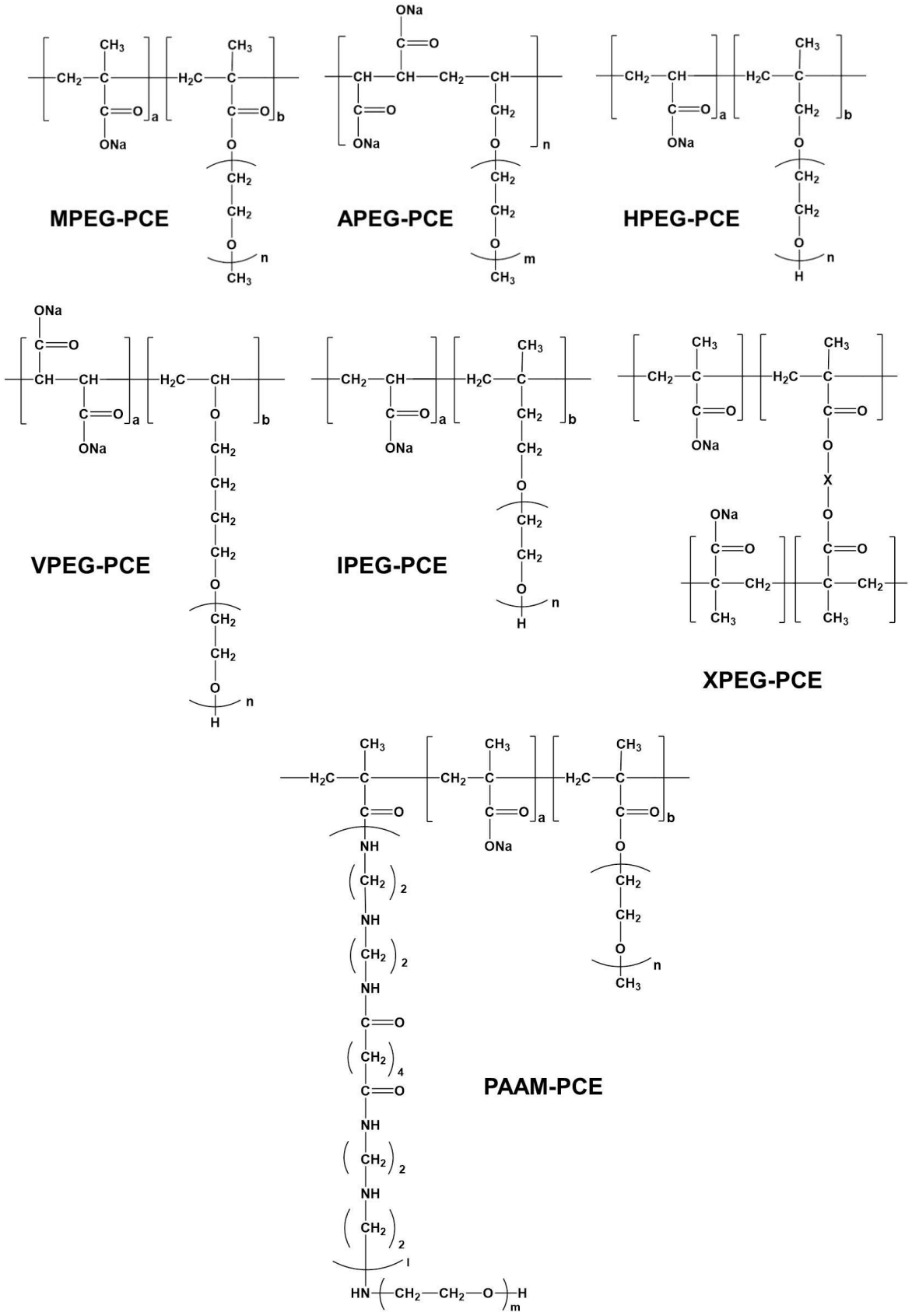

Figure 12: Chemical structures of various PCE superplasticizers

3.2.2 Preparation of PCEs

There are two main synthetic routes used for producing PCEs (**Figure 13**) [139,140]:

(a) Esterification of carboxylic groups in polyanionic trunk chains with poly(ethylene glycol) can be used to synthesize MPEG-based PCEs. This procedure produces a highly uniform PCE with statistical distribution of the side chains along the backbone. However, this method is less popular in the industry because of high cost, long reaction time, and low conversion rate.

(b) Free radical copolymerization of a monomer carrying carboxylic groups and a monomer bearing the side chain (macromonomer) is normally used in the industry due to its simpler procedure and higher cost-effectiveness. This process produces a gradient polymer with non-homogeneous distribution of the side chains along the main chain. Recently, reversible addition-fragmentation chain-transfer or RAFT polymerization technique has been used for the production of specific gradient polymers such as MPEG PCEs with a well-controlled structure [141], and MPEG PCEs with large anionic blocks that can adsorb more strongly on cement [142]. Several kinds of PCE can be synthesized via free radical copolymerization such as:

- MPEG-type PCEs are prepared from ω-methoxy poly(ethylene glycol) methacrylate ester macromonomer with methacrylic acid [143].
- APEG-type PCEs are made from α-allyl-ω-methoxy or ω-hydroxy poly(ethylene glycol) ether and maleic anhydride or acrylic acid [144].
- VPEG-type PCEs are synthesized by aqueous free radical copolymerization of 4-hydroxy butyl-poly(ethylene glycol) vinyl ether and maleic anhydride or acrylic acid [145].
- HPEG-type PCEs are made from the macromonomer α-methallyl-ω-methoxy or ω-hydroxy poly(ethylene glycol) with e.g. acrylic acid [146].

- IPEG-type PCEs (also called TPEG-PCE) are prepared from isoprenyl oxy poly(ethylene glycol) ether as macromonomer by copolymerization with e.g. acrylic acid [147].

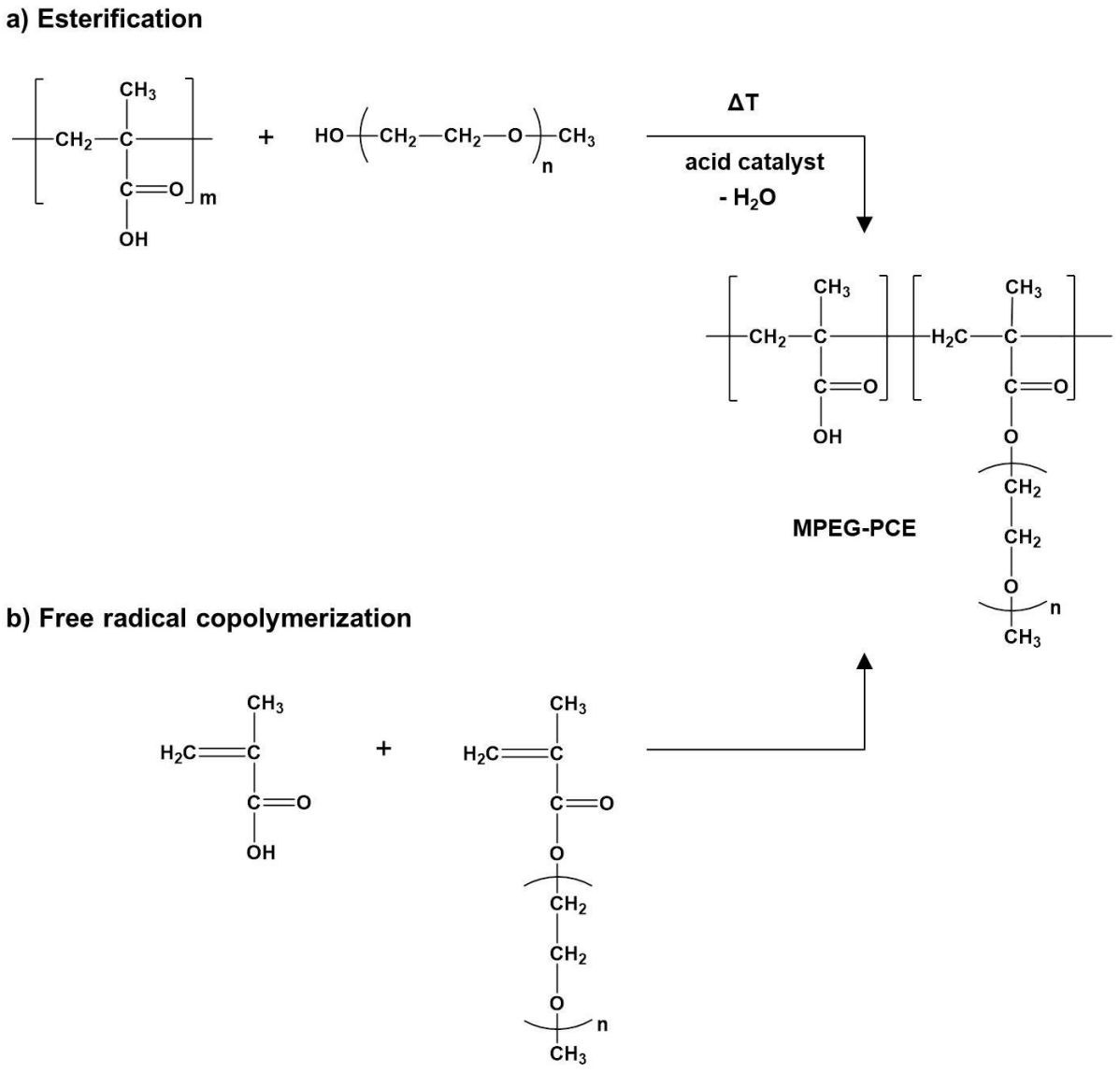

Figure 13: Two synthetic methods for producing MPEG-type PCEs

3.2.3 Impact of PCE structure on adsorption and dispersion

The adsorption of PCE copolymers on the surfaces of cement particles is one of the most important parameters influencing the rheological properties such as fluidity and slump loss of concrete. The charged surfaces of the particles, as measured by zeta potential, are a key factor for PCE adsorption via electrostatic interaction. A highly positive zeta potential leads to a high PCE adsorption [135,136,148].

The various architectural structures in PCE superplasticizers control their adsorption and dispersing effect [139,149-155] which include:

- length of the backbone
- chemical composition of the backbone (acrylic, methacrylic, maleic etc.)
- length of side chains
- grafting density of side chains (polyether/ester to carboxylate ratio)
- distribution of the side chains along the backbone (random, gradient)

The density of ionic groups in the polymer backbone relates to the anionic charge density of a PCE which can be determined experimentally by titration with a cationic polyelectrolyte such as polydadmac, etc. The anionic charge density of the PCE plays a vital role for its adsorption behavior and, consequently, its dispersing power. Generally, PCE adsorption increases with an increase in the density of ionic groups on the backbone [149,154]. However, a decreased PCE adsorption can be observed for PCE copolymers possessing a long side chain at the same grafting density [149,152]. Moreover, the pH value of the aqueous solution and calcium ions present in the cement pore solution affect the anionic charge of the PCE [156]. The anionic charge of PCEs increases with increasing pH values due to a deprotonation of the carboxylate ($–COO^-$) groups in the polymer backbone. However, a reduction in anionic charge results from the presence of calcium ions that can coordinate with the carboxylate groups, both through complexation and counter-ion

condensation. Generally, the $–COO^-$ groups can coordinate Ca^{2+} as a monodentate or bidentate ligand (**Figure 14**) which depends on the architecture of the PCE. In PCEs possessing a high side chain density, the $–COO^-$ group is shielded by the side chains and preferably coordinates with Ca^{2+} as bidentate ligand, producing a neutral Ca^{2+}–PC complex. Consequently, this type of PCE shows almost no anionic charge in cement pore solution. PCEs exhibiting a high density of $–COO^-$ possess anionic character in pore solution due to monodentate complexation of Ca^{2+}.

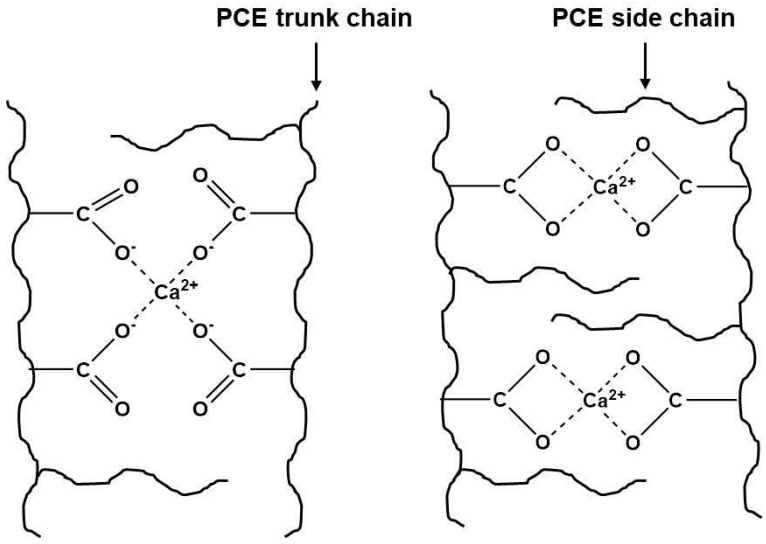

Figure 14: Schematic illustration of monodentate (left) and bidentate (right) complexation of Ca^{2+} by PCEs possessing different molecular structures (redrawn after [156])

The different side chain lengths (n_{EO}) of PCE copolymers lead to different molecular conformations in solution such as flexible backbone worm (FBW), stretched backbone worm (SBW), stretched backbone star (SBS), etc. which are derived from the model of Gay and Raphäel [157] (**Figure 15**).

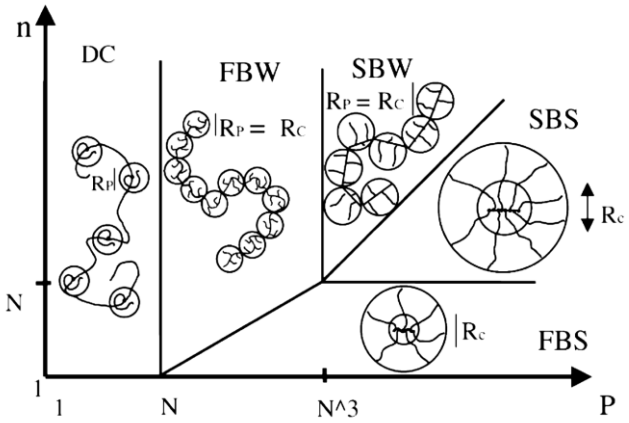

Figure 15: Behavior of a non-ionic comb-like polymer in a good solvent (from [157])

The molecular conformations of PCEs affect the adsorbed amount of PCE on cement particles [152,153]. There, the worm-like copolymers with $n_{EO} \leq 7$ adsorb flat ("train type") and form a densely packed layer leading to higher adsorbed amounts of the copolymer. Whereas star copolymers possessing long side chains ($n_{EO} \geq 34$) prefer perpendicular adsorption on the cement surfaces ("tail" type) resulting in the higher surface occupancy via their extended graft chains (**Figure 16**). Consequently, a lower amount of PCE adsorbed can be observed.

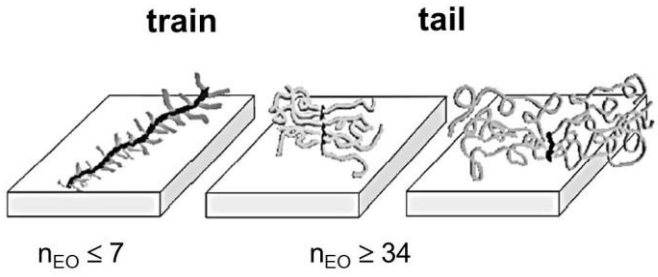

Figure 16: Adsorbed conformations of PCEs on a cement grain (redrawn after [152])

The different distribution of the negatively charged groups and side chains along the PCE backbone like in gradient or random copolymers influences the dispersing behavior of these comb copolymers. A gradient polymer can adsorb on cement surfaces stronger than the random polymer, leading to a higher dispersing effect [142].

The PEG side chain is the most important part to disperse cement particles via a steric hindrance effect (**Figure 17**). It has been reported that the steric repulsion originating from the graft chains correlates to the adsorbed layer thickness (ALT) of the adsorbed polymer. Generally, the steric repulsion originating from PCEs increases with increased adsorbed layer thickness of the PCE [137,158,159]. Moreover, assuming full coverage of the cement surface by PCEs, the dispersive power of PCEs possessing long side chains is higher than that from PCEs having short side chains [160].

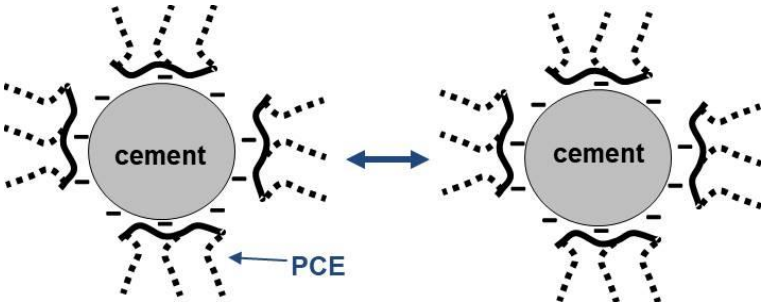

Figure 17: Illustration of the dispersion mechanism via steric hindrance effect of PCEs

Several authors have also studied PCE adsorption on supplementary cementitious materials and inert materials such as calcite, fly ash, silica fume, clays, slag, etc. [148,161-167]. Moreover, PCEs are applied in other significant applications such as iconic concrete structures, shotcrete for high speed railway tracks, gypsum wallboard, cement grinding agent, etc. [139]. Recently, another attractive application of PCEs includes their use for the preparation of C-S-H – PCE nanocomposites as seeding materials to enhance the early

strength development of concrete [13,17,18,168]. To better understand the role and the relevance of PCE adsorption on C-S-H to achieve a superior seeding material, the effect of PCE superplasticizer structure on properties of the C-S-H – PCE nanocomposites was investigated. This topic will be discussed in the next section.

3.3 C-S-H-based nanocomposites

The improvement of properties (e.g. modulus of elasticity and compressive strength) and durability of concrete have been studied for a long time via the modification of C-S-H by using organic compounds such as anionic, cationic, non-ionic polymers etc. Moreover, PCE superplasticizers present essential components and are widely used to improve the fluidity of concrete. So far, only few reports have described the interaction between PCE copolymers and C-S-H. Importantly, the mode of interaction between C-S-H and the organic component depends on the characteristics of C-S-H and type of the organic compound.

3.3.1 Mode of interaction between C-S-H and organic compounds

a) Surface adsorption via calcium complexation

As presented before, C-S-H formed at Ca/Si ratios above 1.0 attains a positively charged surface due to an overcompensation of the deprotonated silanol groups by adsorbed calcium ions (**Equation 9**) [110,111,169]. This way, anionic organic compounds such as PCEs, amino acids, PAAm-co-PAA; poly(acrylamide-co-acrylic acid) are able to adsorb on these surfaces via the complexation of calcium ions [13,81,170-174].

In such a PCE copolymer, the carboxylate groups present on the backbone of the polymer can coordinate via monodentate complexation of calcium species in solution (**Figure 18**) [81,172,173]. The various architectural structures of PCEs [13-16,175,176] control their adsorption on the C-S-H surfaces. The PCEs possessing low grafting density show an increased anionic charge density leading to a higher amount of adsorbed PCE on C-S-H particles. However, a lower adsorbed amount of PCE on C-S-H can be observed at low pH values such at pH = 10.4 as a result of a lower specific anionic charge density of PCE and a less positively charged surface of C-S-H [81]. The molecular structure of PCEs also affects the conformation and the layer thickness of adsorbed PCEs on C-S-H [159]. It was observed

that the conformation of PCEs with very long side chains corresponds to a flexible backbone star (FBS). Furthermore, the layer thickness of PCEs adsorbed onto C-S-H surfaces increases with increased side chain length and the grafting ratio (C/E; carboxylate to ester groups) of the PCE copolymer.

The surface chemistry of C-S-H also depends on the Ca/Si ratio and the pH value. It has been reported that at low Ca/Si ratio of 0.66 and pH = 10.3, the zeta potential value of C-S-H is negative because the silanol groups on the C-S-H surfaces are partially deprotonated and poorly compensated by calcium ions. Thus, electrostatic interactions between the deprotonated silanol groups and positively charged organic compounds are favored [171].

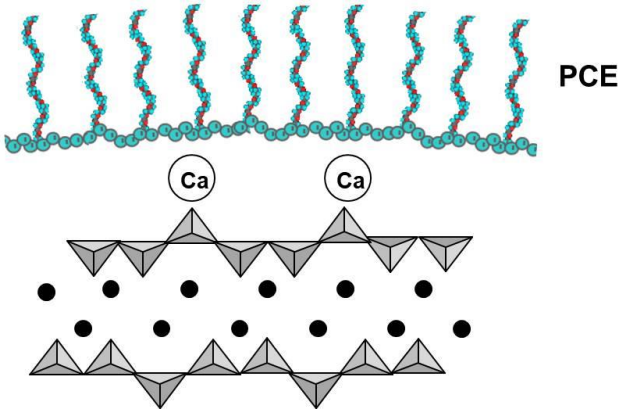

Figure 18: Model illustrating the electrochemical double layer formed on the surface of C-S-H at high pH value resulting from interaction between PCE, Ca^{2+} and the chains of C-S-H

b) Grafting at the defect sites on the silicate chains

The number of missing bridging silica tetrahedra on the silicate chains of C-S-H generally increases with an increase in Ca/Si ratio (Ca/Si > 1.0). These defect sites can provide the possibility of adsorption of organic compounds such as poly(ethylene glycol), poly(acrylic acid), methylene blue, hexadecyltrimethylammonium, etc. [177-180] via H-bonds or Van der

Waals interactions (**Figure 19**). These evidences have been investigated via ^{29}Si MAS NMR spectroscopy which indicated a rise in the number of Q^2 sites leading to an increase in the Q^2/Q^1 ratio and the mean chain length of the silicate chains in the structure of C-S-H modified with organic/polymer molecules.

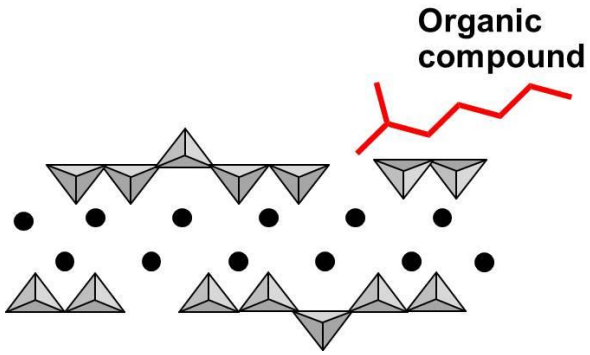

Figure 19: Schematic representation of an organic compound adsorbed at a defect site of the C-S-H surface

c) Intercalation into the interlayer galleries of the C-S-H

Generally, the interlayer spaces of C-S-H contain water molecules and additional calcium ions which balance the negatively charged sites of the C-S-H. The distance between the interlayers of C-S-H can be retrieved from the basal spacing (d002) as evidenced in the XRD pattern [9].

Charged linear polymers can intercalate into the interlayer spaces of C-S-H (**Figure 20**) leading to an increase in the interlayer spacing. The degree of expansion depends on several factors such as chemical composition and structure of C-S-H, type of polymer, concentration of used polymer, etc. [181-185].

It has been reported that the Ca/Si ratio of C-S-H limits the extent of intercalation of polymer. Anionic polymers such as poly(methacrylic acid), poly(acrylic acid) and nonionic

polymers like poly(vinyl alcohol) preferably intercalate into C-S-H structures containing Ca/Si ratios ≥ 0.7 [181,183-185], whereas the intercalation of cationic polymers into the galleries of C-S-H such as poly(diallyl dimethylammonium chloride), poly(4-vinylbenzyl trimethylammonium chloride), etc. were favored at Ca/Si ratios ≤ 1.0 [182,183]. Moreover, a shift of the d002 basal spacing to smaller angles (larger d-spacing) was found in the C-S-H synthesized at high concentrations of polymers.

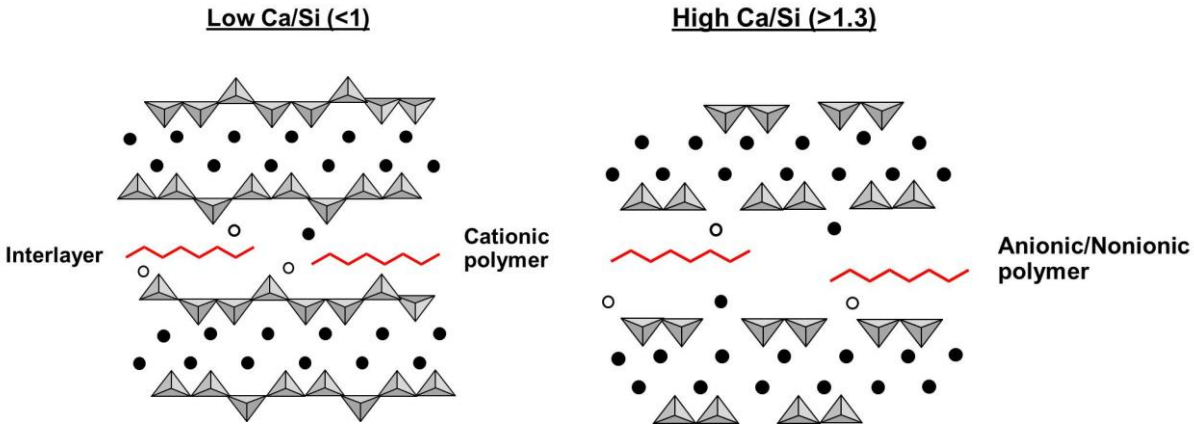

Figure 20: Schematic representation of the intercalation of cationic, anionic or nonionic polymers into the C-S-H nanostructure

d) Covalent bonding of organic compounds with C-S-H

Novel hybrid organic-inorganic calcium silicate hydrate materials were synthesized via a sol-gel process from a mixture of organo trialkoxy silane and tetraethoxy silane with calcium salt in alkaline media. The organic compounds covalently bonded at the end and in the middle of the C-S-H chains (**Figure 21**) as evidenced by NMR measurements. Moreover, the organic compounds can incorporate into the interlayer space of C-S-H depending on the length of the alkyl chains. In the case of highly hydrophobic organic groups, a phase separation was observed [186,187].

Additionally, some reports have described the interaction via covalent bonds between PCEs containing silyl functionalities (PCE-Sil) and the surfaces of C-S-H. This covalent bond occurs through siloxane bridges between silanol groups of silylated PCE and the silanol groups in dimers of C-S-H [173,188].

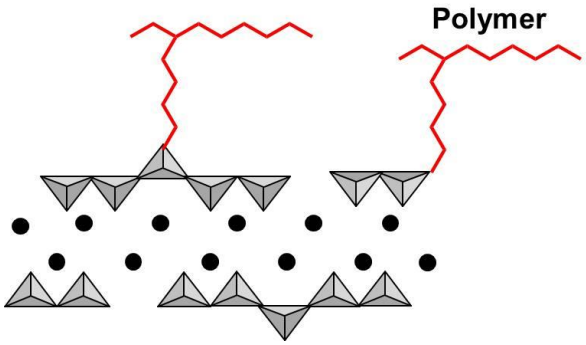

Figure 21: Schematic representation of polymers bonded to silicate tetrahedra in C-S-H

3.4 Hydration kinetics of Portland cement

Ordinary Portland cement contains four major components including C_3S, C_2S, C_3A, and C_4AF. The chemical reactions between anhydrous cement, or one of its constituent phases, and water begin immediately after wetting, which is known as hydration. The rate of hydration of Portland cement can be tracked by using isothermal heat flow calorimetry. The overall progress of hydration at ambient temperature is divided into five stages (**Figure 22**), which include pre-induction, induction, acceleration, deceleration, and final hydration period [31,32,189-192].

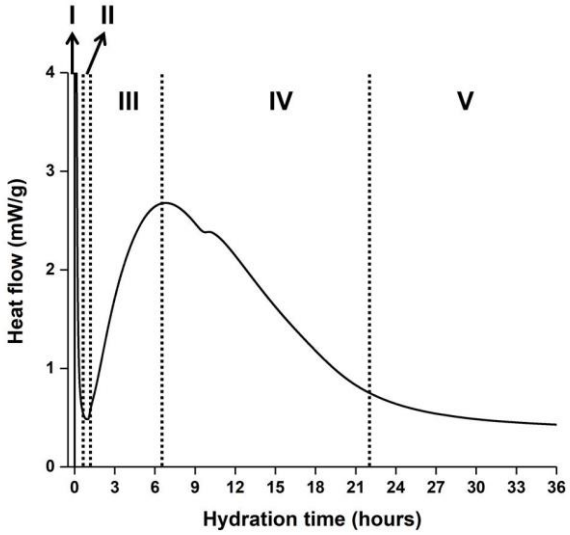

Figure 22: Rate of cement hydration as a function of time as evidenced by isothermal calorimetry measurement

I. Pre-induction period (Initial dissolution and nucleation)

The first, highly exothermic signal in isothermal calorimetry signifies the rapid dissolution of the anhydrous phases in clinker such as C_3A and C_3S, and the precipitation of hydration products such as ettringite and metastable C-S-H. This period lasts only slowly (a few minutes) and is then followed by induction period.

C_3A is the most reactive phase in cement leading to flash set. For this reason, calcium sulfate like gypsum is always added to Portland cement clinker during the grinding process. The high heat release from the hydration of C_3A in the presence of calcium sulfate indicates the dissolution of C_3A and the rapid precipitation of ettringite ($C_6A\$_3H_{32}$) on the anhydrous grains (**Equation 12**). It has been reported that the rate of C_3A dissolution can be slowed down by adsorption of sulfate ions on reactive sites [192].

$$C_3A + 3C\$H_2 \rightarrow 26H + C_6A\$_3H_{32} \qquad \textbf{Equation 12}$$

The rapid dissolution of C_3S contributes an increase of the Ca^{2+}, $H_2SiO_4^{2-}$, and OH^- concentrations in the liquid phase and a thin, metastable layer of C-S-H precipitates on the cement grains. After that, the dissolution rate of C_3S decelerates. The mechanism of this early deceleration of C_3S hydration has been discussed. For its explanation, two hypotheses including the metastable barrier hypothesis and the slow dissolution step hypothesis have been proposed [31,32].

II. Induction period

In this stage, the hydration of all clinker phases is very slow. For the hydration of C_3S, the metastable C-S-H phases still form during the induction period. The termination of this

period can be detected once the C-S-H nuclei reach a certain critical size and start to grow [193].

III. Acceleration period

The main peak of heat release stems from a heterogeneous nucleation and growth of the C-S-H, and the precipitation of Portlandite. Moreover, the calcium sulfate completely dissolves and the concentration of sulfate decreases due to the formation of AF_t and possibly the adsorption of sulfate on the C-S-H surfaces. Accelerating admixtures or mineral admixtures such as limestone powder, clay minerals etc. [194-196] can affect the hydration kinetics of cement; for example, by shifting the onset of the acceleration period to earlier times, and increasing the total heat released during the accelerating period.

IV. Deceleration period

Here, the hydration rate slows down and is controlled by a diffusion process. The C-S-H phase continuously precipitates at the interface between non-hydrated cement grains and originally formed C-S-H. Moreover, a second peak representing the sulfate depletion point occurs during this deceleration. This peak corresponds to a higher dissolution of C_3A and a faster precipitation of AF_t.

V. Final hydration period

The last stage of heat release shows a low activity due to the slow diffusion of species in the hardened cement. Furthermore, a third peak corresponding to the precipitation of monosulfoaluminate (AF_m; $C_4A\$H_{12}$) from the reaction between ettringite and C_3A is observed (**Equation 13**).

$$2C_3A + C_6A\$_3H_{32} \rightarrow 4H + 3C_4A\$H_{12} \qquad \textbf{Equation 13}$$

3.5 Hardening accelerators

An accelerating admixture is a material that is normally used in concrete for improving the development of early strength and increasing the rate of cement hydration at early ages [4,194]. Various admixtures are used in various applications such as in blended cements, urgent repair works, concrete works performed in cold climates, or speeding up the production in precast concrete plants etc.

3.5.1 Accelerating chemicals

The American Concrete Institute (ACI) *Manual of Concrete Practice* (Committee 212.3R-10) [197] has divided accelerators into four groups as follow:

i. Soluble inorganic salts such as chlorides, bromides, fluorides, carbonates, thiocyanates, nitrites, nitrates, thiosulfates, silicates, aluminates, and alkaline hydroxides can accelerate the setting of Portland cement.
ii. Soluble organic compounds consisting of triethanol amine (TEA), calcium formate, calcium acetate, calcium propionate, and calcium butyrate.
iii. Quick setting admixtures are used in shotcrete applications which promote setting in a few minutes. These admixtures contain sodium silicate, sodium aluminate, aluminum chloride, sodium fluoride, and calcium chloride.
iv. Miscellaneous solid admixtures include calcium aluminate, silicate minerals, finely ground magnesium carbonate and calcium carbonate.

Among those admixtures, calcium chloride ($CaCl_2$) is most widely used in concrete because of its ready availability, low cost, and high performance. However, it is not recommended for use in reinforced or prestressed concrete because of its tendency to promote the corrosion of steel. According to the mechanism of acceleration with calcium chloride [198], it acts as catalyst and mainly affects the hydration of C_3S phase leading to an

increase in the rate of C-S-H formation, thus increasing the early strength. While a minor accelerating effect on early hydration is obtained from the reaction between C_3A and calcium chloride is observed. In the presence of gypsum, calcium chloride has an accelerating effect on the reaction between C_3A and gypsum resulting in a series of hydration products. The sequence of reactions possible in the system $C_3A/CaCl_2/CaSO_4/H_2O$ is shown in **Equations 14-16**.

$$C_3A + 3CaSO_4 + 32H_2O \rightarrow C_3A \cdot 3CaSO_4 \cdot 32H_2O \quad \textbf{Equation 14}$$

$$CaCl_2 + C_3A + 10H_2O \rightarrow C_3A \cdot CaCl_2 \cdot 10H_2O \quad \textbf{Equation 15}$$

$$C_3A \cdot 3CaSO_4 \cdot 32H_2O + 2C_3A \cdot Ca(OH)_2 \cdot 12H_2O \rightarrow 3C_3A \cdot CaSO_4 \cdot 12H_2O + 20H_2O + 2Ca(OH)_2 \quad \textbf{Equation 16}$$

Non-chloride accelerating admixtures have been commercially used such as calcium formate, calcium nitrate, sodium aluminate, triethanol amine, etc. Calcium formate ($Ca(HCOO)_2$) acts as an accelerator [199] in the same manner as calcium chloride, but higher dosages (~ 3 - 5 times) are required and its solubility is limited. Calcium nitrate ($Ca(NO_3)_2$) can also be used for shortening the time of setting and hardening for concrete, and it is also a very effective corrosion inhibitor for metal imbedded in concrete [200]. Furthermore, there have been many studies on alkanolamine-based additives such as triethanol amine (TEA), triisopropanol amine (TIPA), etc. TEA is well-known as an effective grinding aid, and also used as an accelerator in cement [201,202]. It accelerates the hydration of C_3A and the formation of ettringite during the induction period. However, higher dosages of TEA (> 0.5 % by weight of cement) lead to retardation of the C_3S phase. Recently, binary and ternary hardening accelerating admixtures have been studied in Portland cement and blended

cements; for example, calcium nitrate and TEA, $CaCl_2$ and diethanol-isopropanol amine (DEIPA), sodium thiocyanate (NaSCN), diethanol amine (DEA) and glycerol, etc. [203-205]. However, the gain in early strength by using those admixtures is limited and sometimes leads to a decreased final strength.

3.5.2 C-S-H as an accelerator

Several authors have reported that synthetic C-S-H particles can be used as an accelerator in cement [10-12,206]. C-S-H can serve as a seeding material to reduce the activation energy barrier which needs to be overcome to initiate the nucleation of C-S-H gel in hydrated cement (**Figure 23**).

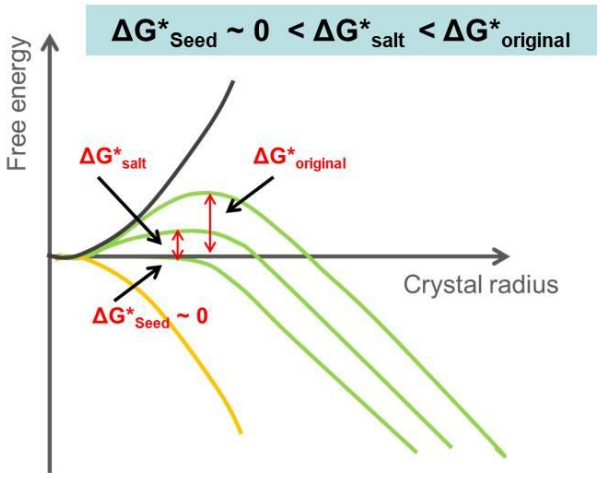

Figure 23: Schematic illustration of the reduction of the energy barrier height ($\Delta G^*_{original}$) after adding conventional accelerators (ΔG^*_{salt}) and seed crystals (ΔG^*_{seed})

C-S-H seeds can provide new nucleation sites in the capillary pores of the cement paste for generating the C-S-H gel (**Figure 24**) [10]. This way, hydration of the silicate phases C_3S and

C_2S is initiated much earlier and leads to an increase in the degree of hydration, as detected via isothermal heat flow calorimetry and ^{29}Si NMR spectroscopy [10,11]. The influence of addition of the synthetic C-S-H particles on the acceleration effect on cement depends on the particle size, surface area, composition and the dosage of C-S-H, the characteristics of cement, etc. Importantly, a high surface area of the C-S-H seeds is necessary to provide a massive number of seeds for the formation of C-S-H. This promotes the nucleation of C-S-H and accelerates the rate of hydration in cement. However, the C-S-H seeds produced according to [206] produce only a minor accelerating effect, owed to their relatively large size, possibly due to agglomeration and/or OSTWALD ripening. To avoid these effects, the size of the C-S-H seeds must be stabilized to their original nanosize by addition of polymeric dispersants such as polycarboxylate (PCE) based superplasticizers [13-16,207].

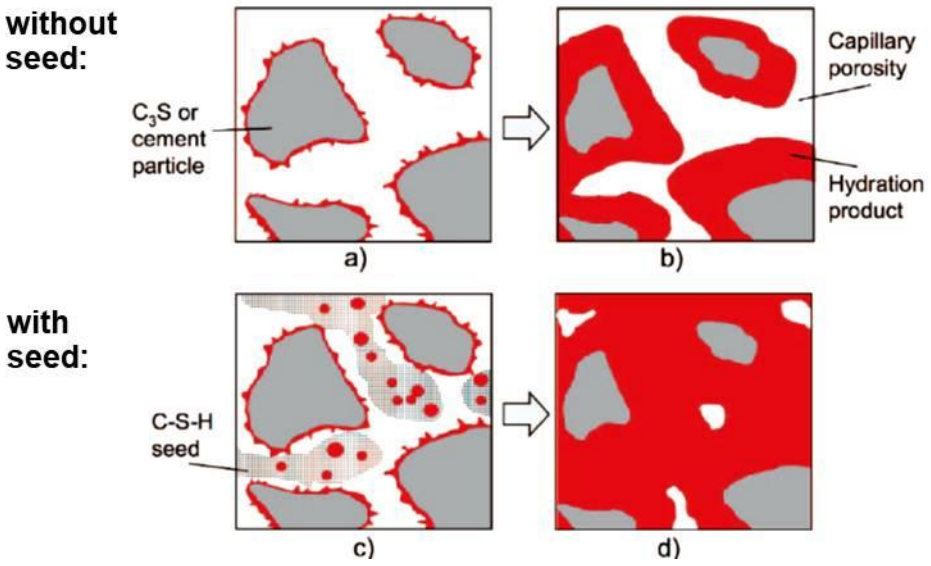

Figure 24: Schematic illustration of the hydration of C_3S or cement particles with and without C-S-H seeds (from [10])

In 2011, BASF invented finely dispersed C-S-H particles that have been commercialized under the trade name of X-SEED® [168,208-211]. In this product, the C-S-H particles are

stabilized by the addition of PCE comb copolymers. These C-S-H particles exhibit a high surface area and low aggregation and turned out to be a highly effective cement hardening accelerator [17,18,212-214]. However, intensive scientific studies are still required to improve the effectiveness of this admixture, and to further understand how the accelerating mechanism relates to the material characteristics. These are resolved by this thesis.

4 Materials and methods

This chapter provides an overview of all materials and essential techniques used in this thesis. The preparation steps to obtain C-S-H – PCE nanocomposites and the principals of the techniques used in this work are also described.

4.1 Materials

4.1.1 Chemicals for the synthesis of C-S-H

The starting materials used in the synthesis of C-S-H were $Ca(NO_3)_2 \cdot 4H_2O$ (PanReac AppliChem, Germany) and $Na_2SiO_3 \cdot 5H_2O$ (VWR Prolabo BDH Chemicals, Germany). Moreover, HNO_3 65 wt. % (VWR Prolabo BDH Chemicals, Germany) and NaOH (Merck KGaA, Germany) were used to adjust the pH value during the synthesis.

4.1.2 Polycarboxylate superplasticizers (PCEs)

MPEG PCEs

A series of methacrylate based polycarboxylate superplasticizers with varying side chain lengths and molar ratio of methacrylic acid (MAA) to ω-methoxy polyethylene glycol methacrylate ester (MPEG-MA) were used for the synthesis of the C-S-H – PCE nanocomposites (**Section 5.1**). Their general chemical structure is shown in **Figure 25**.

Five methacrylic acid–co–ω–methoxy poly(ethylene glycol) (MPEG) methacrylate ester polymers possessing different side chain lengths were synthesized by aqueous free radical copolymerization [133]. The samples were denoted as xPC6, whereby 6 refers to the molar ratio between methacrylic acid and ω–methoxy poly(ethylene glycol) methacrylate ester,

while x corresponds to the side chain length which varied from 8, 17, 25, 45 to 114 ethylene oxide (EO) units.

Furthermore, another three MPEG PCEs were synthesized with side chains made of 45 ethylene oxide (EO) units and molar ratios of methacrylic acid (MAA) to ω-methoxy polyethylene glycol methacrylate ester (MPEG-MAA) between 2:1, 6:1 and 8:1. The properties of all synthesized MPEG PCE samples are listed in **Table 1**.

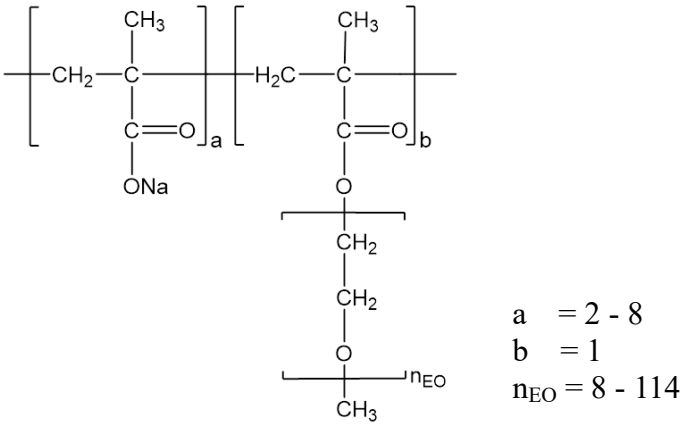

Figure 25: Chemical structure of the methacrylic acid–co–ω–methoxy poly(ethylene glycol) (MPEG) methacrylate ester based PCE superplasticizers used in the study

IPEG PCE

A commercial isoprenyl oxy poly(ethylene glycol) based superplasticizer (IPEG PCE) was employed in the synthesis (**Section 5.2** and **5.3**). The solid content of this PCE solution was 40 % by weight and the chemical structure of this PCE polymer is presented in **Figure 26**. Its molecular properties and anionic charge amount measured at different pH values are summarized in **Table 2**.

Table 1

Molecular properties and specific anionic charge density of the MPEG PCE samples

PCE polymer sample	Property						
	MAA : MPEG-MA (a : b)	Ethylene oxide (EO) units (n_{EO})	Molar mass, M_w (g/mol)	Molar mass, M_n (g/mol)	Polydispersity index *(PDI)*	Specific anionic charge density in NaOH (µeq/g)	Solid content (%)
8PC6	6:1	8	14,250	6,425	2.2	9,014	31.7
17PC6	6:1	17	15,290	7,601	2.0	5,119	35.3
25PC6	6:1	25	16,820	8,750	1.9	4,036	37.5
45PC6	6:1	45	26,060	14,900	1.7	3,641	18.4
114PC6	6:1	114	65,730	35,390	1.9	1,734	36.0
45PC2	2:1	45	43,410	23,020	1.9	1,320	36.4
45PC6	6:1	45	26,060	14,900	1.7	3,641	18.4
45PC8	8:1	45	28,860	15,130	1.9	4,098	20.2

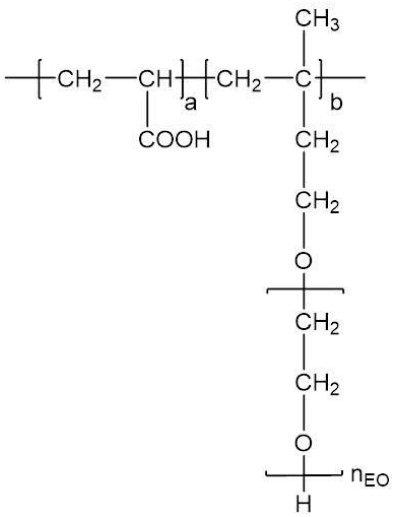

Figure 26: Chemical structure of the isoprenyl oxy poly(ethyleneglycol) (IPEG) based PCE superplasticizer used in the study

Table 2

Molecular properties and pH-dependent specific anionic charge density of the IPEG PCE sample used in the study

Molar masses (g/mol)		Polydispersity index	Specific anionic charge density in NaOH (µeq/g) at pH value				Solid content (%)
M_w	M_n	(*PDI*)	10.4	11.7	12.4	13.8	
35,100	15,700	2.2	1,800	2,750	2,140	-*	40.0

*****No stable value obtained

4.1.3 Cement

Ordinary Portland cement

An ordinary Portland Cement (OPC) sample (Type CEM I 42.5R) obtained from Schwenk Cement Company (Allmendingen, Germany) was used in this study. Its phase composition was determined by quantitative XRD including *Rietveld* refinement and thermogravimetric analysis of the calcium sulfate hydrates. The results are listed in **Table 3**. Its specific surface area (*Blaine*) and mean particle size (d_{50} value) were found at 2,990 cm^2/g and 17 µm, respectively.

A slowly hydrating Ordinary Portland Cement (OPC) sample (API Class G oil well cement, corresponding to a CEM I 32.5N) obtained from Dyckerhoff GmbH (Germany) was used for testing the early strength development of mortars. This cement was selected for its particularly slow development in early strength. Its phase composition was determined by quantitative XRD including *Rietveld* refinement and thermogravimetric analysis of the calcium sulfate hydrates. The results are listed in **Table 3**. Its specific surface area (*Blaine*) and mean particle size (d_{50} value) were found at 3,000 cm^2/g and 17 µm, respectively.

Table 3

Phase composition of the OPC samples as determined by quantitative XRD using *Rietveld* refinement and thermogravimetry

Phase	CEM I 42.5 R cement (wt.%)	API Class G cement (wt.%)
C_3S	54.7	59.3
C_2S	16.2	19.5
C_3A	6.7	1.7
C_4AF	11.3	14.1
free CaO	0.8	< 0.3
$CaSO_4 \cdot 1/2H_2O$ *	0.1	0.2
$CaSO_4 \cdot 2H_2O$ *	4.7	4.6
Anhydrite	1.4	< 0.1
Arcanite	< 0.1	< 0.1
Calcite	1.7	-
Dolomite	1.3	-
Quartz	0.4	-
Total	99.3	99.7

* Determined by thermogravimetry

Blended cement

A fly ash-blended cement (Type IP according to ASTM C595, corresponding to a CEM II/B-V) containing 35 wt. % of fly ash Class F was used in the tests. Oxide composition (determined by XRF), density and specific surface area (*Blaine*) of this cement are listed in **Table 4**.

The slag-blended cement was prepared from 35 wt. % of ground granulated blast-furnace slag (GGBFS) that was obtained from Schwenk Cement Company, Karlstadt, Germany. Mineralogical composition of the slag sample was investigated by XRD measurement and the XRD spectrum is exhibited in **Figure 27**.

The calcined clay-blended cement was prepared from 35 wt. % of a calcined clay that was obtained from Bavaria/Germany. The oxide composition (determined by XRF), specific surface area (*Blaine*), mean particle size (d_{50} value) and density of the slag and calcined clay samples are listed in **Table 4**.

Table 4

Chemical composition and physical properties of fly ash-blended cement, GGBFS and calcined clay samples

Composition (%)	Fly ash-blended cement	GGBFS	Calcined clay
SiO_2	24.9	35.9	52.6
CaO	50.8	42.8	5.7
Al_2O_3	9.9	11.4	22.2
MgO	1.7	6.4	2.2
TiO_2	0.3	0.8	1.0
K_2O	0.9	0.3	2.8
Na_2O	1.1	0.3	0.3
Fe_2O_3	7.1	0.5	8.4
Mn_3O_4	-	0.3	-
SO_3	2.4	2.4	1.4
SrO	-	0.1	-
ZrO_2	-	< 0.1	-
BaO	-	0.1	-
LOI*	0.9	-	2.9
Blaine value (cm^2/g)	4,100	4,000	-
d_{50} value (μm)	12.0	13.2	14.2
Density (g/cm^3)	3.0	2.9	2.6

*Loss on ignition

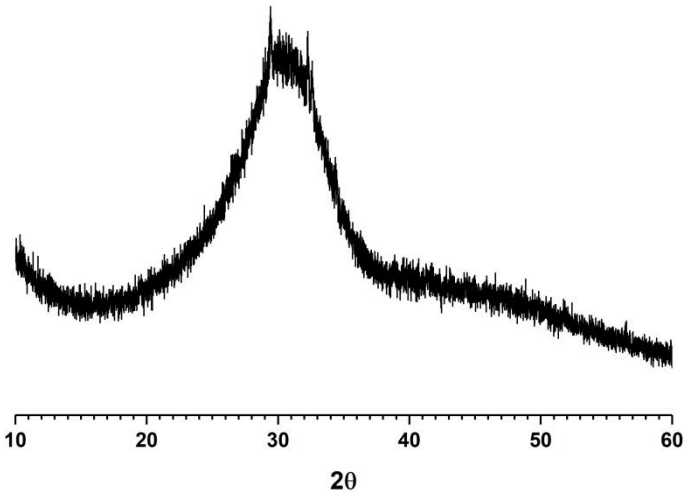

Figure 27: XRD spectrum of the GGBFS used in the slag-blended cement

4.2 Methods

This section, the preparation of the C-S-H – PCE nanocomposites, their characterization, performance testing, and investigations relating to their mode of action in cement are described.

4.2.1 Preparation and characterization of C-S-H – PCE nanocomposites

An overview of the preparation and characterization of the C-S-H – PCE nanocomposites is presented in **Figure 28**.

The C-S-H – PCE nanocomposites were prepared by the co-precipitation method. The general setup of this synthesis is shown in **Figure 29**. First, aqueous $Ca(NO_3)_2$ and Na_2SiO_3 solutions were prepared in a water bath at 75 ° C to achieve fast and complete dissolution and were then cooled to ambient. After that, both solutions were continuously added at a constant dosing rate to the PCE solution while stirring at 20 ° C under N_2 atmosphere. Moreover, the pH of the reaction solution was continuously monitored using a pH electrode submerged in

the solution and was adjusted to 10.4 or 11.7 by the addition of 1M HNO_3, or to 12.4 and 13.8 by adding 30 wt. % NaOH as needed. When the addition of $Ca(NO_3)_2$ and Na_2SiO_3 was finished, the white suspensions were stirred for another 24 hours at room temperature. Detailed process parameters used in the synthesis of the C-S-H – PCE nanocomposites are listed in **Table 5**.

The C-S-H – PCE nanocomposites were then characterized by several techniques including XRD, FT-IR, ^{29}Si MAS NMR spectroscopy, TEM, particle size analysis, TOC measurement, etc. Moreover, their effectiveness in cement was tested in mortar and concrete. The working mechanism of these nanocomposites in cement was investigated via isothermal heat flow calorimetry, in-situ XRD and ^{29}Si MAS NMR spectroscopy.

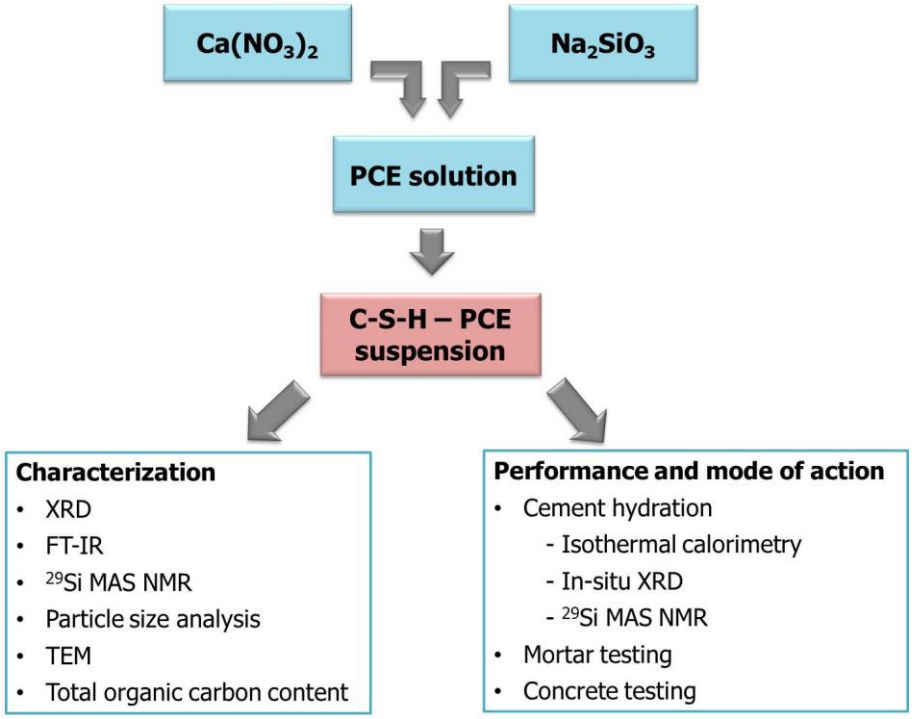

Figure 28: Sequence of steps performed in the preparation and characterization of the C-S-H – PCE nanocomposites

Figure 29: Experimental setup for the synthesis of the C-S-H – PCE nanocomposites

Table 5

Process parameters used in the synthesis of the C-S-H – PCE nanocomposites

Parameters	Experiment *				
	A1	A2	A3	A4 **	A5
Mode of addition	Drop wise	Drop wise	Drop wise	Drop wise	Drop wise
Ca/Si ratio	1.5	1.5	1.0	1.0	1.0
Type of PCE	MPEG - 8PC6 - 17PC6 - 25PC6 - 45PC6 - 114PC6	MPEG - 45PC2 - 45PC6 - 45PC8	IPEG	IPEG	IPEG
Concentration (wt. %)					
- $Ca(NO_3)_2$	42.4	42.4	42.6	42.6	42.6
- Na_2SiO_3	15.1	15.1	20.0	20.0	20.0
- PCE	3.85 mM	9.1 %	6.7 %	6.7 %	6.7 %
Dosing rate (mL/min)					
- $Ca(NO_3)_2$	0.52	0.52	0.61	6.8	0.61
- Na_2SiO_3	1.16	1.16	1.16	13.0	1.16
- HNO_3	-	-	0.51	6.3	0.51
pH	11.3	11.3	10.4 - 13.8	11.7	11.7
Temperature (°C)	20	20	20	20	20
Mixing speed (rpm)	300	300	300	300	300
Atmosphere	N_2	N_2	N_2	N_2	N_2
Reaction time					
- Addition time (min)	8	8	8	18	8
- Ageing time (hrs)	24	24	24	24	0 - 24

* Experiment: A1 in paper #1, A2 in paper #2, A3 in paper #3 - #5, A4 in paper #6 and A5 in paper #7

** This was a 1 L batch; all other batches 20 mL only.

4.2.2 Principal techniques

Specific charge amount

The anionic charge amount of the PCE polymers was measured by polyelectrolyte titration using a particle charge detector PCD 03 pH (BTG Mütek GmbH, Herrsching, Germany).

The principle of this method is based on the measurement of a streaming current generated by charged polymer molecules which adsorb via van der Waals forces on a moving surface. Charge neutralization is achieved by addition of an oppositely charged polyelectrolyte which can form a polyelectrolyte complex and leads to a zero streaming current (isoelectric point).

First, the aqueous anionic polymer is filled into the plastic measuring cell with a fitted piston. Dissolved polymer molecules adsorb on the surface of the piston and on the wall of the cell. The piston is vertically oscillated in the cell by a motor leading to separation of the free counter-ions from the adsorbed polymer. At the Platinum electrodes, the counter-ions induce a current which is amplified and finally shown on the display. During the polyelectrolyte titration, a standard solution of 0.001 N cationic poly-DADMAC (polydiallyl dimethyl ammonium chloride) was dropped continuously to the PCE solution until the isoelectric point was reached [156]. The titration of each sample was done three times and the average of the specific charge amount was calculated as follows **Equation 17**.

$$q = \frac{V*c}{m} \qquad \textbf{Equation 17}$$

where V: consumption of poly-DADMAC (L)

c: concentration of poly-DADMAC (eq/L)

m: mass of PCE in the aqueous solution (g)

q: specific anionic charge density (eq/g)

Particle size analysis

The particle size of the C-S-H or C-S-H – PCE nanocomposites was determined via dynamic light scattering (DLS) which is a technique for measuring the random changes in the intensity of light scattered from a suspension or colloidal solution. Generally, particles suspended in solution undergo a random motion known as Brownian motion. A monochromatic light source, typically a laser, is shot into a sample and then the molecules scatter the light in all directions. The Brownian motion of particles or molecules in suspension leads to different intensities of the scattered light. Analysis of these intensity fluctuations is detected at a known scattering angle θ by a fast photon detector and from this the particle size is calculated by using the Stokes-Einstein equation (**Equation 18**).

$$D_h = \frac{k_B T}{3\pi\eta D_t} \qquad \textbf{Equation 18}$$

where D_h is the hydrodynamic diameter

D_t is the translational diffusion coefficient

k_B is Boltzmann's constant

T is thermodynamic temperature

η is dynamic viscosity

X-ray diffraction

X-ray diffraction (XRD) is a powerful technique for characterizing crystalline materials. It provides information on the crystal structure, crystal orientation and other structural parameters such as grain size, crystallinity, strain and crystal defects.

X-ray diffraction peaks are produced by constructive interference of a monochromatic beam of X-rays diffracted at specific angles from each set of lattice planes in a sample which is described by Bragg's law (**Equation 19**). The peak intensities are determined by the distribution of atoms within the lattice. Consequently, the X-ray diffraction pattern is the fingerprint of the periodic atomic arrangements in a given material. Comparison with spectra from the ICDD (International Centre for Diffraction Data) database of X-ray diffraction patterns enables the phase identification of a large variety of crystalline samples. The XRD patterns of C-S-H and C-S-H – PCE nanocomposites obtained from a BRUKER AXS D8 diffractometer are shown in **chapter 5**.

$$n\lambda = 2d \sin\theta \qquad \textbf{Equation 19}$$

where *d* refers to the spacing between the atomic planes in the crystalline phase and λ is the X-ray wavelength**.**

Fourier-transform infrared spectroscopy

Fourier-transform infrared (FT-IR) spectroscopy is an analytical technique used to identify organic, polymeric, and in some cases inorganic materials (e.g. silica polymorphs). Moreover, IR is most useful in providing information about the presence or absence of specific functional groups. This technique measures the infrared radiation absorbed by a material at resonant frequencies which is a characteristic of its molecular component and structure.

Generally, a beam of the middle infrared light (400 - 4,000 cm^{-1}) is generated by an IR source and passed through the sample. The IR radiation induces stronger molecular vibrations in covalent bond of the material including stretching, bending, scissoring, rocking and twisting. The absorption occurs when the frequency of the IR is the same as the vibrational

frequency of a bond or collection of bonds in a molecule. The signal of the transmitted light obtained from the detector is an interferogram which can be Fourier transformed to get the actual spectrum. The FT-IR spectrum is basically presented as a plot of intensity of the transmission versus transmitted frequency or wavenumber.

Nuclear magnetic resonance spectroscopy

Nuclear magnetic resonance (NMR) is a physical phenomenon in which nuclei in a magnetic field (B_0) absorb and re-emit electromagnetic radiation. This energy is at a specific resonance frequency which depends on the strength of the magnetic field and the magnetic properties of the isotope of the atoms.

Solid-state ^{29}Si NMR spectroscopy is a nondestructive technique and powerful tool for investigating the structure and dynamics of crystalline and amorphous silicate materials. In silicates, the ^{29}Si chemical shifts reflect the degree of polymerization of the SiO_4 tetrahedra. In cement-based systems, this technique has played an important role in the characterization of the silicate chain structure in calcium silicate hydrate (C-S-H) which is the main hydration product of Portland cement.

The binding motif of silicate present in the synthesized C-S-H and C-S-H – PCE nanocomposites was identified by ^{29}Si MAS NMR spectroscopy using a Bruker Avance 300 MHz instrument operating at a resonance frequency of 59.595 MHz. The powder samples were sifted into a 7 mm zirconia rotor and spun at 5 kHz. All spectra were recorded with a relaxation delay of 45 seconds, and tetrakis(trimethylsilyl)silane was used as external standard. The ^{29}Si NMR spectra were analysed by deconvolution of the different signals for the Q^n species using Origin93 software. The linewidth and lineshape of the spectra were fit according to the *Voigt* model.

Total organic carbon content

The total organic carbon (TOC) content of the C-S-H – PCE nanocomposites was determined using a High TOC II instrument (Elementar, Hanau, Germany). First, the total organic carbon present in the PCE polymer and the non-adsorbed part of PCE remaining in the aqueous phase after 24 hours of stirring were measured. From this, the amount of PCE adsorbed on C-S-H surfaces was calculated from the difference between the amount of PCE added and the amount remaining in the filtrate (depletion method).

In the High TOC II apparatus, the sample containing organic carbon is oxidized in a combustion tube packed with a platinum catalyst at 900 °C in synthetic air. The concentration of the carbon dioxide generated from the oxidation process is measured via a non-dispersive infrared (NDIR) detector. The amount of organic carbon present in the sample is calculated based on the values obtained for mono potassium phthalate which is used as calibration standard.

Transmission electron microscopy

Transmission electron microscopy (TEM) is a microscopic technique used to observe features such as structure, crystallization, morphology and stress of very small specimens. This technique uses an accelerated beam of electrons which is transmitted through an ultra-thin specimen (less than 100 nm thick) or a suspension on a grid to form an image. The lighter areas of the image represent the places where a greater number of electrons are able to pass through the sample and the darker areas reflect the denser areas of the object.

A transmission electron microscope is composed of several components such as an electron gun, electromagnetic lenses, vacuum chamber, condensers, specimen stage and phosphorescent screen. An electron gun creates electrons which are accelerated to extremely high speeds using electromagnetic coils. The electrons are focused into a small beam by a

condenser lens and passes through the specimen. Then, the objective lens focuses the portion of the beam that is emitted from the sample into an image. The image produced by TEM is called a micrograph which is observed onto a phosphorescent screen.

In this thesis, morphology of the C-S-H – PCE samples was captured by TEM performed on a JEOL JEM 2011 instrument (JEOL, Japan) equipped with a LaB_6 cathode. The C-S-H – PCE suspensions were diluted with water or isopropanol and dispersed in an ultrasonic bath for 5 minutes. After plasma surface treatment, the dispersed samples were dropped on a 300 Cu mesh with carbon support films (Quantifoil Micro Tools GmbH, Germany).

Isothermal heat flow calorimetry

Isothermal heat flow calorimetry is a powerful technique used for measurement of heat production during the hydration of cement which is exothermic and for monitoring the hydration kinetics of cement at a constant temperature. The heat production in a sample is detected by a heat flow sensor as heat is conducted to a heat sink (surrounding) that is in contact with the air thermostat. For each sample, it is necessary to have a reference sample that is on a parallel heat flow sensor. This arrangement reduces the noise in the measurements from temperature fluctuations entering the instrument. The output from the calorimeter is the difference between the sample signal and the reference signal which is recorded continuously and in real time.

The determination of heat flow relies on the so-called Seebeck effect which is the direct conversion of temperature differences to electric voltage. Then, the thermal power is calculated by the following **Equation 20**.

$$P = \varepsilon(U - U_0) \qquad \textbf{Equation 20}$$

where P is the thermal power (in watts), ε is the calibration coefficient (in watts/volt), U is the voltage (in volts) and U_0 is the baseline voltage (in volts).

Hydration kinetics of cement paste in this study was tracked by isothermal heat flow calorimeter (TAM AIR, Thermometric, Järfälla, Sweden) at 20 ° C. A cement paste was prepared from 4 g of (blended) cement and 1.8 g of DI water (w/c = 0.45), mixed in a glass ampule for 2 minutes and placed into the calorimeter. Dosages of the C-S-H and C-S-H–PCE nanocomposites were 0.35 - 2.0 % (as solid) by weight of cement (bwoc).

Mortar testing

The method for determination of the compressive and flexural strengths of mortar was according to DIN EN 196-1.

The mortar consisted of 450 g of cement, 1,350 g of standard CEN sand and 225 g of water (w/c = 0.5 for CEM I 42.5R) or 198 g of water (w/c = 0.44 for API Class G cement). Moreover, the C-S-H – PCE suspensions were used in a standard mortar at the dosage of 0.35 – 2.0 % (as solid) by weight of cement (bwoc). The mixing operation was carried out automatically as follows:

Amounts of DI water and cement were placed into the mixing bowl and then the mixer was immediately started at low speed. After 30 sec of mixing, the sand was added and steadily stirred for 30 sec. Then, the mixer was switched to high speed and mixing continued for additional 30 sec. After that, the mixer was stopped for 90 sec and a plastic scraper was used to homogenize the mortar adhering to the wall and bottom part of the bowl. Then mixing was continued again at high speed for 60 sec.

The spread flow of fresh mortar was measured via flow table test. After that, the mortar was cast into 40 x 40 x 160 mm prism steel molds and compacted on a vibrating table for 2

minutes. The specimens were then covered with a plate of glass and cured for 6, 8, 12, 16 and 24 hours in a climate chamber at a temperature of 20 ± 1 ° C and 90 % relative humidity. To obtain the strength values after 28 days, the specimens were demolded after 1 day and then cured in water at 20 ± 1 ° C. After curing, the compressive and flexural strengths were measured using an instrument from Toni Technik, Berlin, Germany (**Figure 30**). The compressive and flexural strengths were calculated by following **Equations 21** and **22**, respectively.

$$R_c = \frac{F_c}{1600} \qquad \textbf{Equation 21}$$

where R_c is the compressive strength (MPa), F_c is the maximum load at fracture (N), and 1600 is the area of the auxiliary plates; 40 mm x 40 mm (mm^2).

$$R_f = \frac{1.5 * F_f * l}{b^3} \qquad \textbf{Equation 22}$$

where R_f is the flexural strength (MPa), b is the side of the square section of the prism (mm), F_f is the load applied to the middle of the prism at fracture (N), and l is the distance between the supports (mm^2).

Figure 30: Test apparatus used to determine the compressive and flexural strengths of mortar

Concrete testing

Concrete was prepared in a 30 L pan-type mixer according to ASTM C192 at 23 ± 2 ° C. The mix proportion of concrete is listed in the paper in **section 5.3**. The fly ash blended cement was used at 400 kg/m^3, the ratio of aggregates-to-cement was 4.5 and the w/c ratio was fixed at 0.41. IPEG-PCE superplasticizer was used to adjust the workability of the fresh concrete to a slump value of 16 ± 0.5 cm. The dosages of the C-S-H – PCE composite tested were 0.8 % and 2.0 % bwoc. Additionally, a defoamer (DOWFAX DF141 from Dow Chemical, USA) was used to achieve a constant fresh concrete density of 2,420 ± 10 kg/m^3.

First, dried aggregates including gravel and sand were put to the pan-type mixer and soaked with half the amount of water for 5 min. After that, cement was added to the mixer and the rest of water and other admixtures were continuously added into the concrete mixture during the mixing process. The total mixing time was 5 min. From the fresh concrete, the temperature was measured and tested for slump, density and air content. Moreover, concrete samples were cast into 100 x 100 x 100 mm molds and cured for 6, 8, 10, 12, 16 and 24 hours in a climate room at 23 ± 2 ° C and a relative humidity > 95 %. To obtain the 7 and 28 day values, the specimens were removed from the molds after 1 day and then cured in a saturated lime solution. The compressive strength data were collected from an UH-2000kNI instrument from Shimadzu Corporation, Kyoto, Japan (**Figure 31**).

Figure 31: Compressive strength test apparatus for concrete

5 Results and discussion

This chapter presents the main results which are presented in the publications organized in four main topics:

5.1 Influence of different PCE structures on the properties of C-S-H particles and their effectiveness as strength accelerators in ordinary Portland cement

5.2 Effect of synthesis parameters on the accelerating effectiveness of C-S-H – PCE nanocomposites in Portland cement

5.3 Application of the C-S-H – PCE nanocomposite as an accelerator in blended cements

5.4 Mechanism of the nucleation and growth of C-S-H – PCE nanocomposites

5.1 Influence of different PCE structures on the strength enhancing effect of C-S-H particles

This section describes the role of the molecular architecture of PCE superplasticizers on the size of the C-S-H particles and their strength enhancing effect. Moreover, the structures of the C-S-H – PCE nanocomposites were studied. A special focus was placed on MPEG PCE superplasticizers possessing different side chain lengths and grafting density (molar ratio of methacrylic acid to methoxy polyethylene glycol methacrylate ester).

5.1.1 Effect of the side chain length of PCE

C-S-H – PCE nanocomposites were synthesized by the co-precipitation method from Na_2SiO_3 and $Ca(NO_3)_2$ in the presence of the MPEG PCE copolymers. The molar ratio of CaO/SiO_2 present in the starting materials was 1.5. Here, five MPEG PCEs possessing the same grafting density (MAA : MPEG-MA molar ratios of 6:1), but different side chain lengths (8, 17, 25, 45 and 114 ethylene oxide (EO) units) were employed in the precipitation.

For the structure of the synthesized products, a semi-crystalline composition like in C-S-H (I) was determined via XRD. Moreover, evidence from FT-IR and TOC measurements suggested that the PCE polymers were adsorbed onto the surface of the C-S-H particles. More bulky PCEs such as those exhibiting long side chains occupied the surfaces of the initial C-S-H foils more densely which better prevented the further growth of C-S-H. This led to smaller sizes of the C-S-H particles as detected by dynamic light scattering (DLS). The PCE polymer with the longest pendant groups (114 EO units) produced the smallest particle sizes of the C-S-H – PCE composite and exhibited the strongest seeding effect for the hydration of the silicate phases in cement, as was observed via isothermal heat flow calorimetry. Accordingly, this nanocomposite achieved the largest gain in early compressive

and flexural strengths of mortar, with an ~ 80 % increase over that of the neat OPC sample (**Figure 32**).

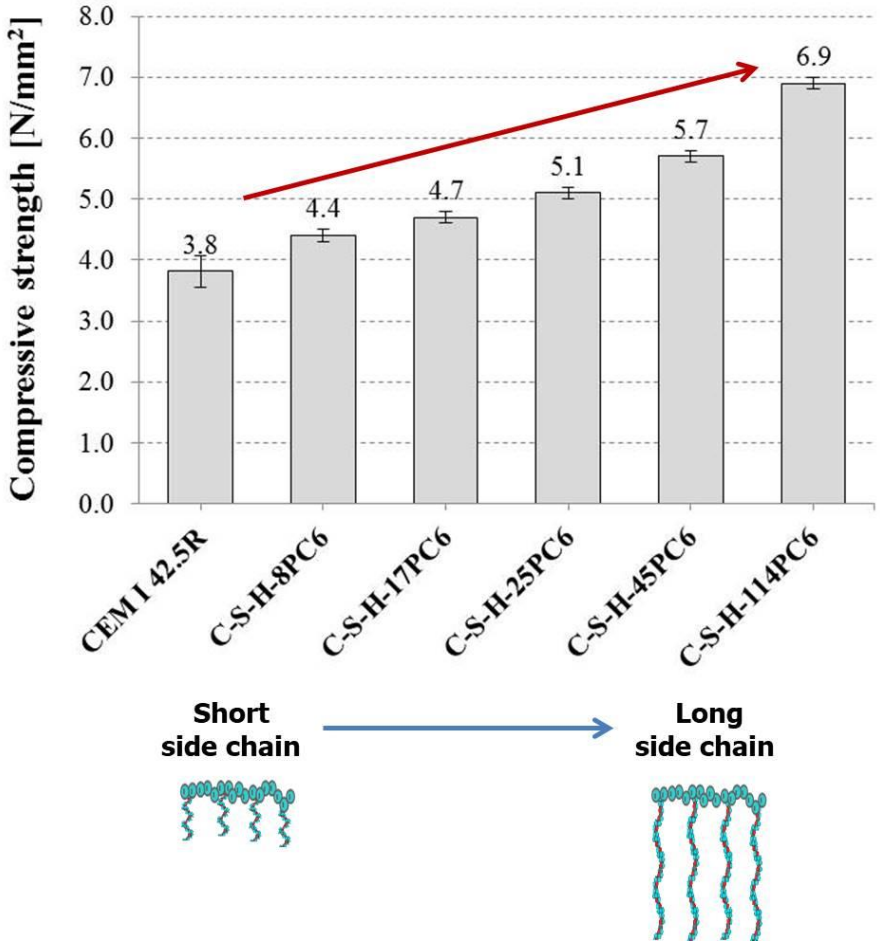

Figure 32: Compressive strength of mortars cured for 16 hours and admixed with 0.35 % wt. of the C-S-H – PCE nanocomposites synthesized by using different PCE polymers

Paper #1

C-S-H - PCE nanocomposites for enhancement of early strength of Portland cement

(Effect of the side chain length of PCE)

V. Kanchanason, J. Plank

Proceedings of the 14th ICCC International Congress on the Chemistry of Cement,

Abstract book p. 326, Proceedings CD, Section 4: Admixtures, Beijing, China 2015.

C-S-H - PCE Nanocomposites for Enhancement of Early Strength of Portland Cement

Kanchanason, V. [a, b] and Plank, J. [a]*

[a] *Technische Universität München, Chair of Construction Chemistry, 85747 Garching, Germany*

[b] *Siam Cement Group, 1 Siam Cement Road, Bangsue, Bangkok, 10800, Thailand*

Abstract

Common cement hydration accelerators such as e.g. calcium or aluminium salts achieve higher early strength at the sacrifice of final strength which is undesirable. In this study, the effectiveness of C-S-H – polycarboxylate (PCE) nanocomposites as strength enhancing admixtures was studied. Different MPEG-PCE copolymers exhibiting side chain lengths from 8, 17, 25, 45 to 114 ethylene oxide (EO) units were used to prepare the nanocomposites by precipitating C-S-H from Na_2SiO_3 and $Ca(NO_3)_2$ in the PCE solution. It was found that the longer the side chain of the PCE, the smaller is the particle size of the precipitated C-S-H, and the higher is the strength enhancing effect. Thus, the MPEG PCE sample possessing a side chain made of 114 EO units produces C-S-H particles of ~ 30 nm, as was measured via dynamic light scattering, and increases early strength (16 hrs) up to 80 %. Opposite to this, the C-S-H particle size obtained from a PCE possessing only 8 EO units in the side chain was ~ 600 nm, and it showed only minimal effect on early strength.

Structural investigation of the C-S-H – PCE nanocomposites via X-ray diffraction revealed a semi-crystalline composition like in C-S-H (I). Moreover, from FT-IR spectroscopy and total organic carbon (TOC) measurements, a structural model was developed which suggests that in the nanocomposite the PCE polymers are adhered the surface of C-S-H particles. Furthermore, TEM imaging revealed a layered structure of individual C-S-H nanofoils with an approximate length of 100 nm and a basal spacing of 2.1 nm, thus signifying a relatively narrow interlayer distance. Apparently, the PCE polymer is entrapped between individual C-S-H nanofoils and perhaps also became incorporated into its lamellar structure.

Finally, the mode of action of the C-S-H – PCE nanocomposite was assessed. When dispersed in highly alkaline cement pore solution, the aggregated C-S-H particles disintegrate into individual nanofoils which then effectively initiate the nucleation of C-S-H from the pore solution. Accordingly, the effect of the C-S-H – PCE nanocomposite relies on eliminating the activation energy barrier for the C-S-H crystallization which in normal cement has to be overcome to initiate C-S-H crystallization from the dissolved clinker phases C_3S and C_2S, respectively.

Originality

C-S-H – PCE nanocomposites were synthesized which can greatly enhance the early strength (from 6 to ~ 24 hrs) of Portland cement without sacrifice on the final strength. Dependence of their effectiveness on PCE molecular structure (particularly the length of the side chain), as well as a model for the C-S-H – PCE nanocomposites is presented. Furthermore, the mechanism for the nucleation enhancing effect of the C-S-H – PCE composites is elucidated.

Keywords: *C-S-H; polycarboxylate; early strength; nanocomposite; nucleation*

*** Corresponding author: Email sekretariat@bauchemie.ch.tum.de; Tel +49 89 289 13151, Fax +49 89 289 13152**

1. Introduction

CO_2 emission from cement production is generated from the calcination and milling processes (WBCSD and IEA., 2009). Clinker substitution with supplementary cementitious materials (SCMs) like in blended cements (CEM II/III) is highly advantageous from an environmental point of view because in their production, less CO_2 is released compared to Portland cement. However, their drawback is a reduced rate of hydration leading to slow development of early strength. As a potential cure, accelerators based on calcium salts (e.g. Ca nitrate or formate) have been applied to enhance early strength, but at the same time they also significantly reduce the final strength which is undesirable.

Calcium silicate hydrate ($xCaO{\cdot}ySiO_2{\cdot}zH_2O$, C-S-H) is well known as the main hydration product of Portland cement. Various types of crystalline calcium silicate hydrates (1.4 nm tobermorite, jennite, etc.) and less crystalline hydrates (C-S-H (I), C-S-H (II) and C-S-H gel) can form under hydrothermal conditions and near room temperature. Both tobermorite and jennite exhibit layered structures whereby the tetrahedrons of silicate present in the "dreierketten" share oxygen atoms with calcium in plane (H.F.W. Taylor., 1997). For the size of synthetic, disk-like C-S-H which was synthesized from C_3S at different concentrations in water, diameters between 13 nm and 19 nm and thicknesses from 4 to 12 nm signifying stacks of 4 - 11 layers were found by small-angle neutron scattering (SANS) technique (Chiang W-S. *et al*., 2012). Such nano-scale discs are thought to present subunits which make up the larger C-S-H foils.

In the past, numerous attempts have been made to promote cement hydration via addition of synthetic crystalline C-S-H particles. It was thought that the addition of well-dispersed C-S-H as seeding material can increase the early hydration rate and generally accelerate the hydration of cement (Thomas J.J. *et al*., 2009). However, it was found that the accelerating effect of C-S-H at early age either was only minor or did not show at all, possibly due to agglomeration and OSTWALD ripening which leads to C-S-H particles which are too large to enact sufficient nucleation seeding. To avoid these effects, the C-S-H particles have to be stabilized in their original nanosize by addition of polymeric dispersants. The external surface of C-S-H contains silanol groups ionized in high alkaline solution which chelate calcium ions from the pore solution (Viallis-Terrisse H. *et al.,* 2001 and Nonat A., 2004). Consequently, C-S-H exhibits a slightly positive surface charge, thus allowing stabilization with anionic polymers such as superplasticizers.

Polycarboxylate (PCE) superplasticizers are also known as high range water reducers. They improve the flow property of concrete via an electrosteric effect (Uchikawa H. *et al*., 1997). C-S-H stabilized by the addition of such comb copolymers demonstrated low aggregation and turned out to be a highly effective cement hardening accelerator (Nicoleau L. *et al*., 2011 and 2013).

In this study, the impact of different PCE structures (here: the side chain lengths) on the size of the C-S-H particles and their strength enhancing effect was investigated. Moreover, a model for the interaction between PCE and C-S-H is proposed and the strength enhancing effect is explained mechanistically.

2. Experimental

2.1. Raw Materials

The compounds used for C-S-H preparation were $Ca(NO_3)_2 \cdot 4H_2O$ (PanReac AppliChem) and $Na_2SiO_3 \cdot 5H_2O$ (Prolabo Chemicals).

As PCE superplasticizers, five methacrylic acid–co–ω–methoxy poly(ethylene glycol) (MPEG) methacrylate ester polymers possessing different side chain lengths were synthesized by aqueous free radical copolymerization (Plank J. *et al.,* 2008). Their general chemical structure is shown in **Figure 1**. The samples were denoted as xPC6, whereby 6 refers to the molar ratio between methacrylic acid and ω–methoxy poly(ethylene glycol) methacrylate ester, while x corresponds to the side chain length which varied from 8, 17, 25, 45 to 114 ethylene oxide (EO) units. The properties of the synthesized MPEG PCE samples are listed in **Table 1**.

Moreover, Ordinary Portland Cement (OPC) type CEM I 42.5 R obtained from Schwenk Zement KG (Germany) was used for testing the early strength. Its phase composition (determined by XRD

with RIETVELD refinement, acid titration according to FRANKE for free lime and DSC/TG for the calcium sulfate hydrates) is presented in **Table 2**. Deionized water obtained from a Millipore Synergy apparatus was used for all tests.

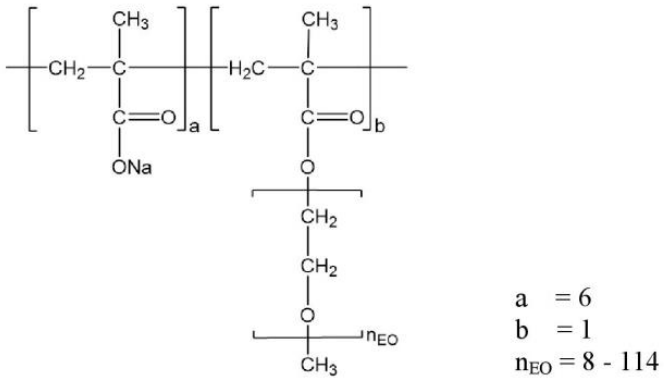

Figure 1: Chemical structure of the methacrylic acid–co–ω–methoxy poly(ethylene glycol) (MPEG) methacrylate ester based superplasticizers used in the study

Table 1 Molecular properties and specific anionic charge density of the MPEG PCE samples used in the study

PCE polymer sample	Property				
	Molar mass, M_w (g/mol)	Molar mass, M_n (g/mol)	Polydispersity index (PDI)	Ethylene oxide (EO) units	Specific anionic charge density (μeq/g)
8PC6	14,250	6,425	2.2	8	9,014
17PC6	15,290	7,601	2.0	17	5,119
25PC6	16,820	8,750	1.9	25	4,036
45PC6	26,060	14,900	1.7	45	3,641
114PC6	65,730	35,390	1.9	114	1,734

2.2. Experimental Procedures

Synthesis of C-S-H – PCE nanocomposites

The C-S-H – PCE particles were synthesized by the co-precipitation method (Matsuyama H. *et al.*, 2000). The molar ratio of CaO/SiO_2 present in the starting materials was 1.5. First, 0.0285 mmol of individual PCE were dissolved at room temperature in 7.4 mL of water (3.85 mM) and the pH of the solution was adjusted to 7 ± 0.5 by using aqueous 30 wt % NaOH. Next, solutions of 1.7 g of sodium silicate in 4.8 mL of water (0.008 mol) and 2.8 g of calcium nitrate in 1.8 mL of water (0.012 mol) were prepared and then pumped to the PCE solution at a speed of 1.16 mL/min and 0.52 mL/min, respectively while stirring under N_2 atmosphere. The pH of the suspension was kept at 11.3 (Matsuyama H. *et al.*, 2000 and Garcia-Lodeiro I. *et al.*, 2008). After 24 hours of stirring, the resulting suspensions were either used as is, or transformed into powder by centrifugation until a clear solution was obtained, followed by washing with CO_2-free de-ionized water and freeze drying. The powders were utilized for XRD and FT-IR analysis. In all other experiments, the liquid suspensions from above were used without any further treatment.

Table 2 Phase composition of the CEM I 42.5 R sample, as determined via Q-XRD including Rietveld refinement

Content (wt.-%)												
C_3S, m	C_2S, m	C_3A, c	C_3A, o	C_4AF	Lime	Periclase	Arcanite	Gypsum	Anhydrite	Calcite	Quartz	Total
55.1	15.9	4.5	2.0	10.2	0.1	0.4	1.4	3.5	2.3	4.0	0.5	100

Characterization techniques

Particle sizes of the C-S-H – PCE nanocomposites were determined by dynamic light scattering (DLS) using a Zetasizer Nano ZS apparatus (Malvern Instruments, Workestershire, UK). Nanocomposite concentration was 0.1 g/L. Powder x-ray diffraction (XRD) patterns were acquired from a BRUKER AXS D8 diffractometer (Karlsruhe, Germany) operating at 30 kV and 30 mA with Cu Kα radiation. The patterns were obtained in the range of 2θ angles between 0.6° and 60°. Furthermore, the C-S-H – PCE composites were characterized by Fourier Transform Infrared Spectroscopy (FTIR) using the BRUKER Vertex 70 spectrometer (Bruker, Ettlingen, Germany) with ATR cell in the range of 400 - 4000 cm^{-1}. The amount of PCE adsorbed on C-S-H was determined via total organic carbon (TOC) content on a High TOC II instrument (Elementar, Hanau, Germany). Here, at first the organic carbon present in the PCE used in the reaction and the non-adsorbed PCE remaining in the filtrate after the reaction were measured. After that, the adsorbed amount of PCE was calculated from the difference between the organic carbon resulting from the PCE present in the filtrate. Morphology of the C-S-H – PCE nanocomposites was observed by transmission electron microscopy (TEM) performed on a JEOL JEM 2011 instrument (JEOL, Japan) equipped with a LaB_6 cathode.

Mortar test

The C-S-H – PCE precipitates were tested for their effectiveness as strength enhancing admixture in a standard mortar prepared according to DIN EN 196-1. The dosage of the C-S-H – PCE suspension was 0.35 % (as solid) by weight of cement (bwoc). The water to cement (w/c) ratio of the mortar was 0.5. The mortar was cast into 40 x 40 x 160 mm prism steel molds and cured at 20 ± 1 ° C and 90 % relative humidity for 6, 8 and 16 hours. After curing, the compressive and flexural strengths were measured on a test apparatus provided by Toni Technik (Berlin, Germany).

Calorimetry

Hydration kinetics was tracked by isothermal heat flow calorimetry. A cement paste was prepared from 4 g of cement and 2 g of DI water (w/c = 0.5), mixed in a glass ampule and placed into the calorimeter (TAM AIR, Thermometric, Järfälla, Sweden) at 20°C. Dosages of the C-S-H – PCE suspensions were the same as in the mortar tests.

3. Results and discussion

3.1. Characterization of C-S-H – PCE nanocomposites

Fig. 2 shows the X-ray diffraction patterns of the synthesized products obtained in the co-precipitation process. Pure C-S-H and the C-S-H – PCE nanocomposites exhibit the diffraction pattern of semi-crystalline C-S-H (I) which represents an imperfect version of 1.4 nm tobermorite. For pure C-S-H, the main hk0 reflections (100, 110, 200, 020) appear at 16.7, 29.0, 31.9 and 49.7 ° 2θ, respectively. The 002 reflection observed at 7.0 ° 2θ signifies a basal spacing between the silicate layers of 1.2 nm. In contrast, for the C-S-H – PCE nanocomposites no such reflections indicating the basal spacing were detected in the range of 5 - 10 ° 2θ. Thus, it is possible that the interlayers of the C-S-H – PCE crystallites are disturbed by the incorporation of PCE. Furthermore, considering the bulky nature of the PCE molecules, the interlayer distances might be such wide that the corresponding reflection appears at very low 2θ angles which are not detectable by our instrument. Several authors have reported about the expansion of the interlayer spacing of C-S-H resulting from the intercalation of anionic polymers (Matsuyama H. *et al.,* 1999a and Matsuyama H. *et al.,* 1999b).

Next, the FT-IR spectra of pure C-S-H, of PCE polymer 114PC6 and of all synthesized C-S-H – PCE nanocomposites were recorded (**Fig. 3**). In pure C-S-H and the C-S-H nanocomposites, a broad peak of valence vibration from the crystal water can be observed between 3700 and 3200 cm^{-1}. It can be related to the stretching modes of hydroxyl groups present in the interlayer region of C-S-H as physically bound water. The absorbances of the alkyl C–H stretches of PCE are found at 2875 cm^{-1}. Furthermore, the characteristic bands at ~ 1560 and ~ 1465 cm^{-1} correspond to the asymmetric and symmetric vibrations of the COO^- group present in the main chain of PCE. The peaks of the C–O valence vibration of the ether bond present in the side chain of PCE are detected at 1100 cm^{-1}. For the

C-S-H – PCE composites, the stretching and vibrational bands of the silicate sheets appear at 960 cm^{-1} (ν Si–O) and at 665 cm^{-1} (δ Si–O–Si), respectively. Thus, appearance of the bands characteristic for PCE provides assertive evidence for the presence of PCE in the synthesized precipitates. However, the spectra do not provide information about whether the PCE polymers are only surface-adsorbed or perhaps even chemically incorporated into the C-S-H structure.

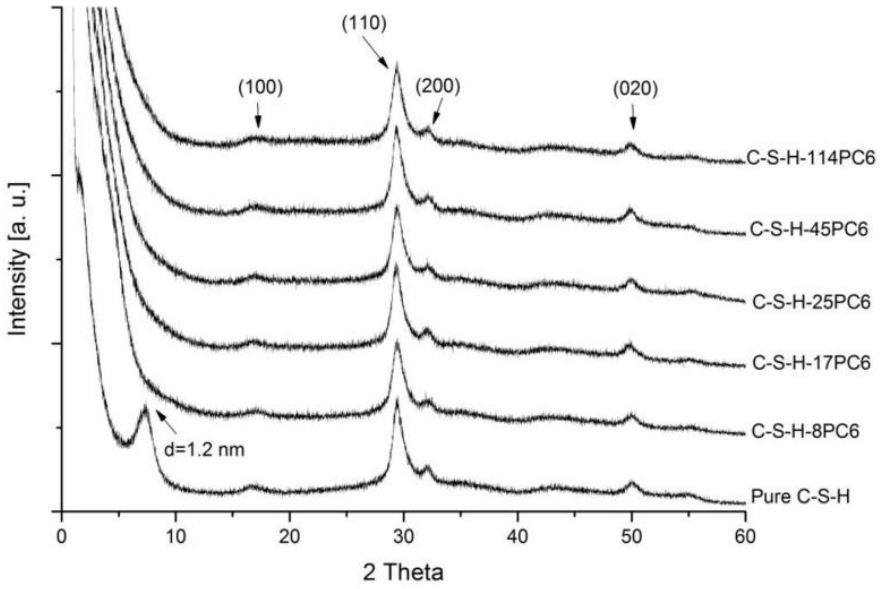

Figure 2: XRD patterns of synthesized pure C-S-H and of the C-S-H – PCE nanocomposites obtained from different PCE superplasticizers

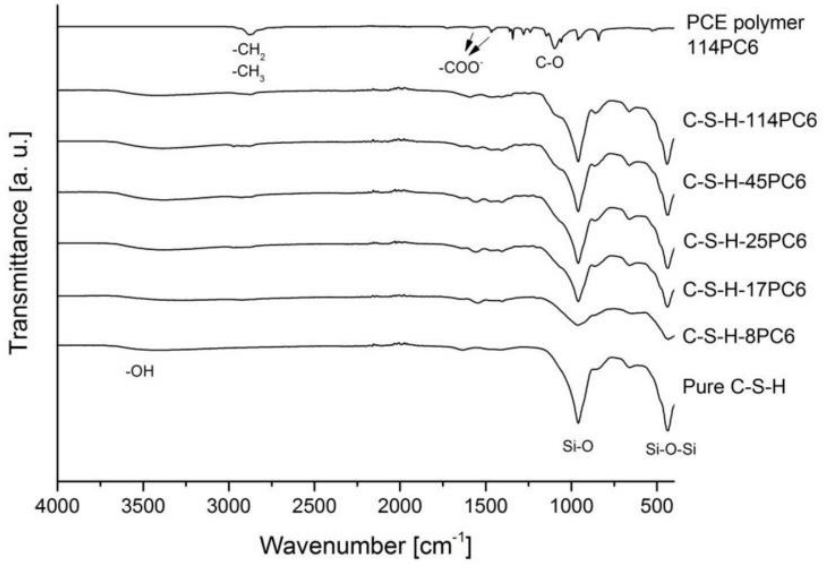

Figure 3: FT-IR spectra of pure C-S-H, of PCE polymer 114PC6 and of the synthesized C-S-H – PCE nanocomposites

3.2. Effect of side chain length on particle size of C-S-H

The particle size distributions of the C-S-H – PCE composites as measured by dynamic light scattering (DLS) in term of number and intensity are presented in **Fig. 4**. In term of intensity, bimodal particle size distributions were found for all C-S-H – PCE composites. This implies that the C-S-H – PCE composites contain a mixture of small and large particles. However, when presented by intensity,

the larger particles appear grossly overrepresented, because they scatter light much stronger than smaller particles. When looking at the particle size in terms of number it becomes clear that only the nanocomposites prepared from PCE polymers possessing side chain lengths of 8 and 17 EO units exhibit bimodal particle size distributions. Whereas all other composites show monomodal distributions. Generally, the C-S-H particle size (in term of number) decreases with increased side chain length of the PCE polymer. The MPEG PCEs possessing a side chain made of 8 or 17 EO units produce C-S-H particles with a bimodal particle size distribution, with an average particle size for the fraction of small size at ~ 100 and ~ 90 nm, and for the large size fraction at ~ 600 and ~ 500 nm, respectively. The latter is nearly the same as the particle size of pure C-S-H shown at ~ 530 nm. In case of 25 EO units in the pendant groups, the mean particle size is smaller than in C-S-H – 17PC6 and displays at ~ 80 nm. In comparison, the average C-S-H particle sizes obtained from the PCEs possessing 45 and 114 EO units in their side chains are ~ 60 and ~ 30 nm, respectively. This signifies that PCEs can effectively modulate the particle size of C-S-H, and that PCEs possessing longer side chains (45-114 EO units) produce particularly small C-S-H particles, as is desirable for a strong seeding effect.

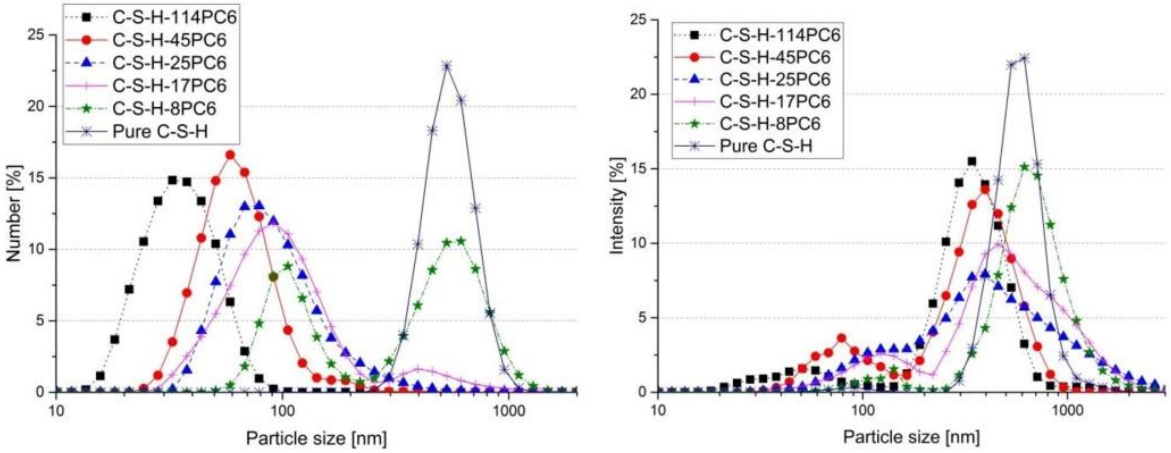

Figure 4: Particle size distributions (left : number-based ; right : intensity-based) of pure C-S-H and of the synthesized C-S-H – PCE nanocomposites

3.3. PCE sorption on C-S-H

The amount of PCE sorbed on C-S-H was quantified (**Fig. 5**). After 24 hours of reaction, the molar amounts of PCEs sorbed on C-S-H increase slightly with increased side chain length of the PCE. However, when the mass sorbed on C-S-H is looked at, then the differences between the PCE polymers become even were pronounced, i.e. from PCE polymer 114PC6, ~ 550 mg sorb per g of C-S-H while from the short-chain polymer 8PC6, only ~ 110 mg/g C-S-H are consumed. This observation explains why the more bulky PCE 114PC6 leads to smaller C-S-H composites. It occupies the surfaces of the initial C-S-H foils more densely, and this prevents their further growth.

3.4. Effect on early strength

Mortars admixed with 0.35 wt % of the C-S-H – PCE nanocomposites were tested after 16 hours of curing, and the compressive and flexural strengths were determined. The results are displayed in **Fig. 6**. It was found that the enhancement in early strength clearly depends on the C-S-H particle size which is controlled by side chain length (EO units) of the PCE polymers. Consequently, the compressive strength of the mortar prepared from the nanocomposite with the smallest particle size (C-S-H – 114PC6) reaches ~ 7.0 N/mm^2 which presents an 80 % increase over the neat OPC sample. Whereas the C-S-H – 45PC6 nanocomposite exhibits a compressive strength of 5.7 N/mm^2 or a 50 % increases, only over the neat CEM I 42.5 R. Furthermore, the C-S-H composites exhibiting larger particle sizes (> 60 nm) including C-S-H – 25PC6, C-S-H – 17PC6 and C-S-H – 8PC6 are even less

effective and increase compressive strengths only between 35 and 15 %. For the flexural strengths of the mortars, a similar trend was found. For example, the C-S-H – 114PC6 nanocomposite produces the highest flexural strength of 2.1 N/mm^2 whereas the others show values between 1.3 and 1.6 N/mm^2. Furthermore, the compressive strengths after 12 hours of curing were investigated (individual data not shown here). Again, a much superior strength development was found for the C-S-H – 114PC6 nanocomposite.

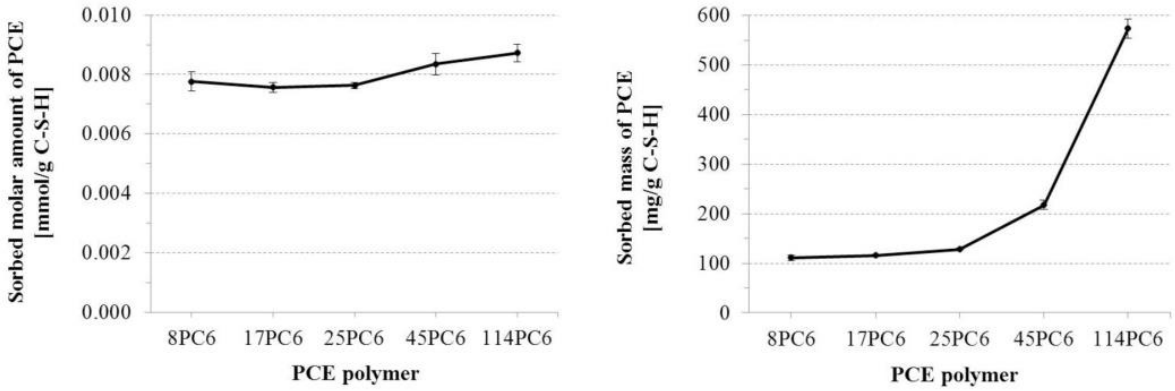

Figure 5: Molar (left) and mass amounts (right) of PCE polymers sorbed by the C-S-H nanocomposites

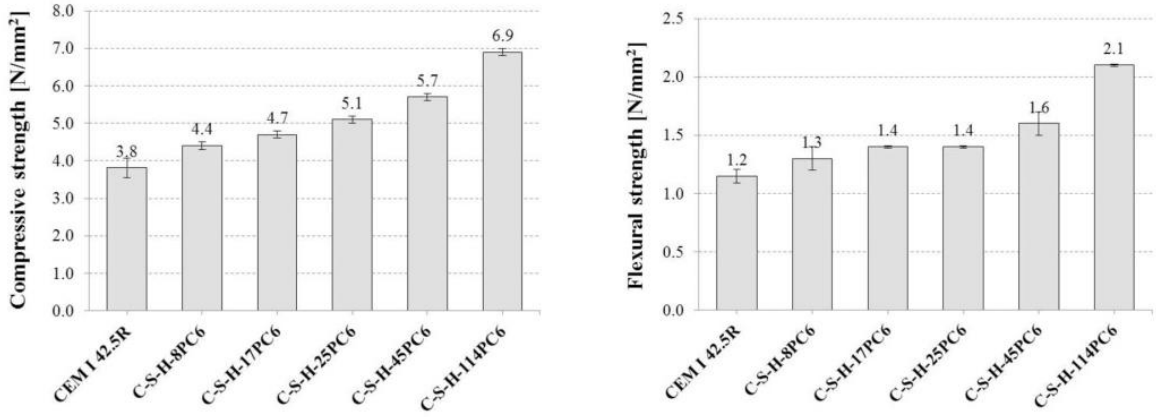

Figure 6: Compressive and flexural strengths of mortars cured for 16 hrs and admixed with 0.35 % bwoc of the synthesized C-S-H – PCE nanocomposites

3.5. Calorimetric investigation

The impact of the C-S-H – PCE nanocomposites on cement hydration was studied via isothermal heat flow calorimetry. As examples, the curves obtained for the two extremes in PCE composition, 8PC6 and 114PC6, are displayed in **Fig. 7**. Generally, addition of the C-S-H – PCE nanocomposites increases the peak assigned to the silicate reaction, indicating enhanced hydration of the clinker phases C_3S and C_2S. Even for the C-S-H – 8PC6 nanocomposite which consists of large particles, a noticeable increase in hydration is observed. The most effective composite, C-S-H – 114PC6 modified the shape of the silicate hydration curve whereby the peak commonly assigned to the conversion of AF_t to AF_m has disappeared. Instead, a very pronounced peak is observed which possibly subsumes both the late silicate reaction and the $AF_t \rightarrow AF_m$ conversion.

3.6. Structural model of C-S-H – PCE

TEM imaging clearly revealed a foil-like morphology for the C-S-H – PCE nanocomposites. The sizes of individual foils vary between 100 and 300 nm. As an example, the images from C-S-H –

114PC6 are shown in **Fig. 8**. Furthermore, a lamellar structure was observed for this composite whereby a d spacing of approximately 2.1 nm was found which is higher than that for pure C-S-H which was at 1.2 nm as determined by XRD (**Fig. 2**). This suggests that the polymer not only is adsorbed onto the surfaces of individual C-S-H foils, but also became chemically incorporated into the interlayer region of C-S-H, hence resulting in a C-S-H – PCE composite on the nano scale.

Based on the integrated XRD, FT-IR, sorption and TEM results first a model for the formation of the C-S-H – PCE nanocomposites as shown in **Fig. 9** can be presented. During the precipitation of C-S-H, the anionic comb polymers occupy the surfaces of individual C-S-H foils. PCE polymers possessing long pendant groups such as in 114PC6 prevent the further growth of the early C-S-H foils and thus keep their size small. Whereas short-chain PCEs are less effective and produce significantly larger C-S-H particles. TEM imaging provided a clear evidence that in the nanocomposites the PCE polymer is not only surface adsorbed, but becomes even chemically incorporated into the C-S-H layered structure. This finding is highly important and requires further study, e.g. using SAXS analysis.

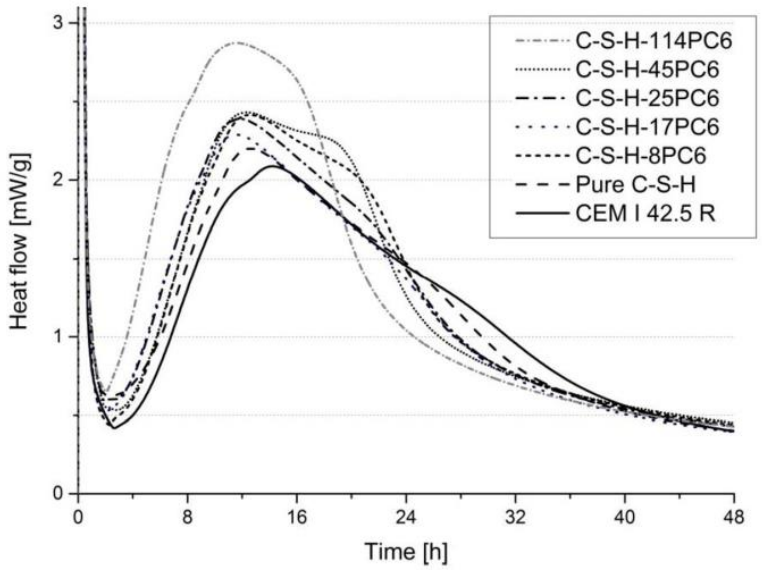

Figure 7: Heat evolution during hydration of pure CEM I 42.5 R (w/c = 0.5) and admixed with 0.35 % bwoc of the C-S-H – PCE nanocomposites, determined via isothermal calorimetry

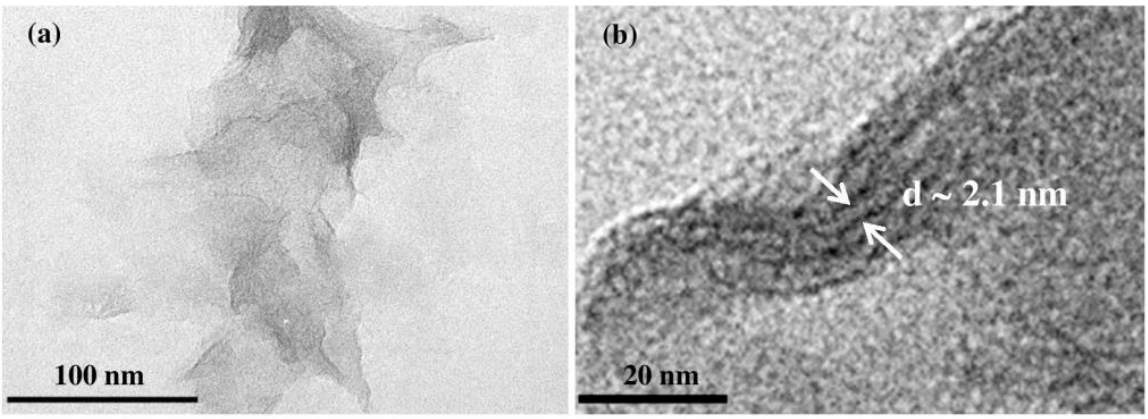

Figure 8: TEM micrographs of the C-S-H – 114PC6 nanocomposite : (a) overview displaying the particle morphology and (b) image revealing the lamellar nano structure of the foils

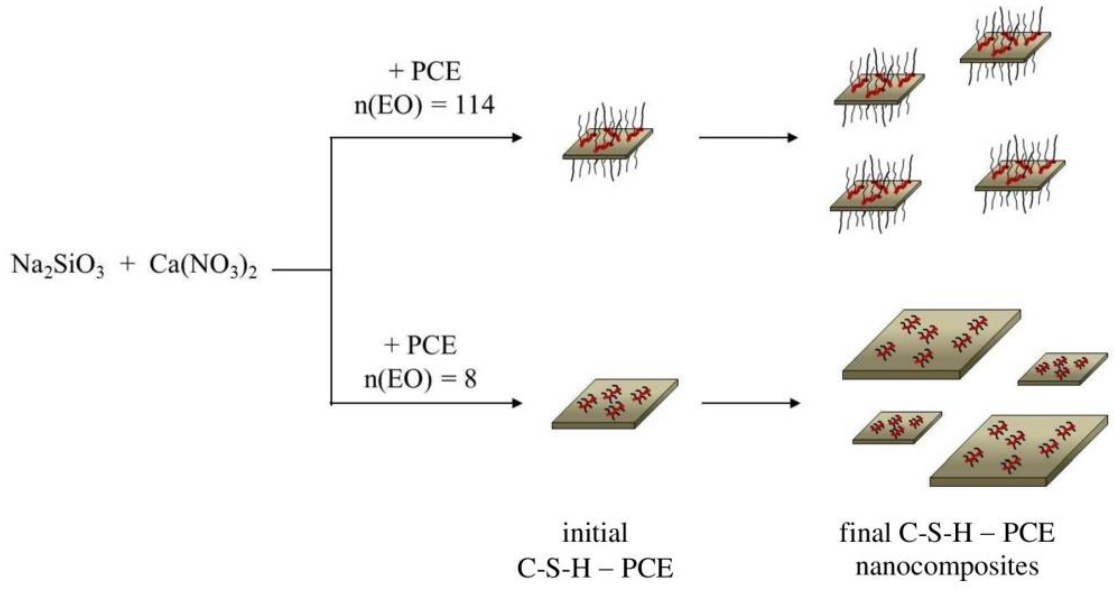

Figure 9: Illustration of the effect of different PCE molecules in modulating the size of the C-S-H – PCE nanocomposites

4. Conclusion

C-S-H – PCE nanocomposites were successfully synthesized by co-precipitation of Na_2SiO_3 and $Ca(NO_3)_2$ in the presence of anionic MPEG PCE copolymers. Using different PCE molecules with varied side chain lengths, it is possible to control the average size of the C-S-H – PCE composites. A PCE polymer with very long pendant groups was found to produce the smallest particle sizes for the C-S-H – PCE composite and exhibited the strongest seeding effect for the hydration of the silicate phases C_3S and C_2S. Accordingly, this nanocomposite achieved the largest gain in early compressive and flexural strengths of mortar.

Future studies should focus on the impact of chemically different PCE copolymers (e.g. MPEG- versus IPEG-type PCEs) and on the nano structure of the C-S-H – PCE composites. Furthermore, interaction of nano C-S-H with polymers other than PCEs (e.g. polyethylene imines, phosphated polymers, etc.) should be looked at.

Acknowledgements

This work was performed at the "TUM Center For Advanced PCE Studies". The authors would like to thank Dr. Marianne Hanzlik (TUM, Division of Electron Microscopy) for taking the TEM images. We also thank Schwenk Zement KG for the supply of CEM I 42.5 R and the Siam Cement Group (SCG) for financial support.

References

- Chiang W-S., Fratini E., Baglioni P., Liu D., Chen S-H., **2012**. Microstructure determination of Calcium-Silicate-Hydrate globules by Small-Angle Neutron Scattering. *The Journal of Physical Chemistry C*, 116, 5055 - 5061.
- Garcia-Lodeiro I., Fernández-Jiménez A., Blanco-Varela M. T., Palomo A., **2008**. FTIR study of the sol–gel synthesis of cementitious gels: C–S–H and N–A–S–H. *Journal of Sol-Gel Science and Technology*, 45, 1 63 - 72.
- DIN Deutsches Institut für Normung e.V., **2005**. DIN EN 196-1: Methods of testing cement - Part 1: Determination of strength.
- H.F.W. Taylor, Cement Chemistry, 2nd ed., Section: Hydration of the calcium silicate phases, Academic Press, London, U.K., **1997**, pp. 123 - 166.

- Matsuyama H., Young J. F., **1999a**. Synthesis of calcium silicate hydrate/polymer complexes: Part I. Anionic and nonionic polymers. *Journal of Materials Research,* 14, 8 3379 - 3387.
- Matsuyama H., Young J. F., **1999b**. Intercalation of polymers in calcium silicate hydrate: Anew synthetic approach to biocomposites?. *Chemistry of Materials,* 11, 16 - 19.
- Matsuyama H., Young J. F., **2000**. Effects of pH on precipitation of quasi-crystalline calcium silicate hydrate in aqueous solution. *Advances in Cement Research,* 12, 1 29 - 33.
- Nicoleau L., Albrecht G., Lorenz K., Jetzlsperger E., Fridrich D., Wohlhaupter Thomas., Dorfner R., Leitner H., Vierle M., Schmitt D., Braeu M., Hesse C., Pancera S.M., Zuern S., Kutschera M., **2011**. Plasticizer-Containing Hardening Accelerator Composition. *Patent US 20110269875 A1*.
- Nicoleau L., Gädt T., Chitu L., Maier G., Paris O., **2013**. Oriented aggregation of calcium silicate hydrate platelets by the use of comb-like copolymer. *Soft Matter*, 9, 4864 - 4874.
- Nonat A., **2004**. The structure and stoichiometry of C-S-H. *Cement and Concrete Research*, 34, 1521 - 1528.
- Plank, J., Pöllmann, K., Zouaoui N., Andres, P. R., Schaefer, C., **2008**. Synthesis and performance of methacrylic ester based polycarboxylate superplasticizers possessing hydroxy terminated poly(ethylene glycol) side chains. *Cement and Concrete Research*, 38, 1210 - 1216.
- World Business Council for Sustainable Development (WBCSD) and International Energy Agency (IEA), **2009**. Cement Technology Roadmap 2009: Carbon emissions reductions up to 2050, 1 - 36.
- Thomas J.J., Jennings H. M., Chen J.J., **2009**. Influence of nucleation seeding on the hydration mechanisms of tricalcium silicate and cement. *The Journal of Physical Chemistry C,* 113, 4327 - 4334.
- Uchikawa H., Hanehara S., Sawaki D., **1997**. The role of steric repulsive force in the dispersion of cement particles in fresh paste prepared with organic admixture. *Cement and Concrete Research,* 27, 1 37 - 50.
- Viallis-Terrisse H., Nonat A., Petit J-C., **2001**. Zeta-potential study of calcium silicate hydrates interacting with alkaline cations. *Journal of Colloid and Interface Science,* 244, 58 - 65.

5.1.2 Effect of the grafting density of PCE

As mentioned before, anionic PCE copolymers can adsorb on the C-S-H surfaces and the length of side chains of the PCE polymers presents the key to restrict the C-S-H particles to their original nanosize, as is desirable for a strong seeding effect in cement.

In this part, three PCE superplasticizers possessing different grafting densities (the molar ratio of methacrylic acid (MAA) to methoxy polyethylene glycol (MPEG) methacrylate ester was varied between 2:1, 6:1 and 8:1), yet exhibiting the same side chain lengths of 45 EO units were employed in the precipitation of C-S-H. The C-S-H – PCE nanocomposites were successfully synthesized as confirmed by XRD and FT-IR measurements.

It was found that, the amount of the PCEs adsorbed on C-S-H increased with increasing anionic character of the PCE resulting from a higher MAA content in the PCE. Here, higher molar ratios of MAA : MPEG-MA (> 6:1) led to a higher adsorbed amount of PCE on C-S-H and produced a larger portion of small size C-S-H particles (d_{50} ~ 100 nm).

These particularly small C-S-H – PCE nanocomposites are most advantageous to boost the early compressive strength of mortar after 12 and 16 hours which increased about 60 % over the neat cement (**Figure 33**).

The mechanism behind is that the C-S-H – PCE nanocomposites accelerate the polymerization of the mono silicates to polysilicates in cement, as was found by ^{29}Si MAS NMR spectroscopy.

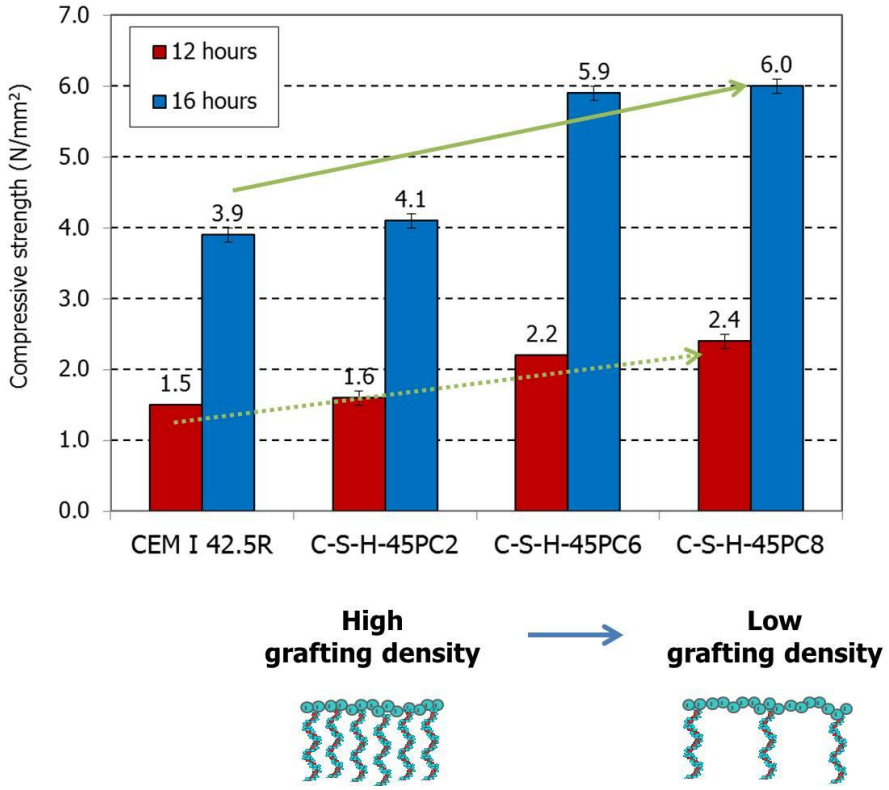

Figure 33: Compressive strength development of mortars cured for 16 hours and admixed with 0.35 % wt. of the C-S-H – PCE nanocomposites synthesized from PCEs exhibiting different grafting density (anionicity)

Paper #2

C-S-H – PCE nanocomposites for enhancement of early strength of cement

(Effect of the grafting density of PCE)

V. Kanchanason, J. Plank

19. ibausil, Bauhaus-Universität Weimar, Tagungsband 1, Weimar, Germany (2015) 759 – 766.

V. Kanchanason and J. Plank

C-S-H – PCE Nanocomposites for Enhancement of Early Strength of Cement

1. Introduction

Carbon dioxide which is responsible for the greenhouse effect is emitted from the calcination and grinding processes in cement manufacture. A potential way to reduce the environmental impact from cement is the replacement of clinker by using Supplementary Cementitious Materials (SCMs) such as fly ash, blast furnace slag, limestone etc. in blended cements (CEM II/III). However, a more widespread use of blended cements is limited especially by their low early strength.

Generally, cement hydration can be accelerated by using synthetic calcium silicate hydrate (C-S-H) crystals as seeding material. The accelerating effect is influenced by the size of the C-S-H particles and is lost when particle agglomeration occurs. To prevent this deleterious effect, the size of the C-S-H particles has to be controlled and stabilized by addition of polymeric dispersants such as anionic polycarboxylate (PCE) superplasticizers.

In this study, the influence of PCE superplasticizers possessing different grafting density (molar ratio of methacrylic acid (MAA) to methoxy polyethylene glycol (MPEG) methacrylate ester) and anionic character on the particle size of C-S-H – PCE nanocomposites and their strength enhancing effect was investigated. Apparently, the C-S-H – PCE nanocomposites reduce the activation energy (ΔG) necessary to initiate C-S-H nucleation to zero and thus allow much faster hydration of the silicate phases C_3S and C_2S, as was evidenced by isothermal heat flow calorimetry and ^{29}Si MAS NMR spectroscopy.

2. Experimental program

2.1. Raw Materials

The chemicals used for C-S-H synthesis were $Ca(NO_3)_2 \cdot 4H_2O$ (PanReac AppliChem, Darmstadt, Germany) and $Na_2SiO_3 \cdot 5H_2O$ (VWR Prolabo Chemicals, Leuven, Belgium). The PCE superplasticizers were synthesized in our laboratories and contained side chains made of 45 ethylene oxide (EO) units and the molar ratio of methacrylic acid (MAA) to ω-methoxy polyethylene glycol methacrylate ester (MPEG-MAA) were varied between 2:1, 6:1 and 8:1. The properties of the MPEG PCE samples are shown in **Table 1**. Furthermore, Ordinary Portland Cement (OPC) type CEM I 42.5 R obtained from Schwenk Zement KG (Germany) was used for testing the strength development. The main phase composition (wt. %) of the OPC consisted of 55.1 % C_3S, 15.9 % C_2S, 6.5 % C_3A and 10.2 % C_4AF.

Table 1:
Molecular properties and specific anionic charge density of the MPEG PCE samples

PCE polymer sample	Molar mass, M_w (g/mol)	Molar mass, M_n (g/mol)	Polydispersity index (PDI)	Specific anionic charge density (µeq/g)
45PC2	43,410	23,020	1.9	1,320
45PC6	26,060	14,900	1.7	3,641
45PC8	28,860	15,130	1.9	4,098

2.2. Experimental Procedures

Synthesis of C-S-H – PCE nanocomposites

The C-S-H – PCE nanocomposites were prepared by precipitating C-S-H from Na_2SiO_3 and $Ca(NO_3)_2$ in the presence of PCE. Firstly, 0.7 g of PCE powder were dissolved in 7.4 mL of water and the pH of the solution was controlled at 7 ± 0.5 by using 30 wt. % NaOH. After that, solutions of 1.7 g of $Na_2SiO_3 \cdot 5H_2O$ (0.008 mol) in 4.8 mL of water and 2.8 g of $Ca(NO_3)_2 \cdot 4H_2O$ (0.012 mol) in 1.8 mL of water were prepared and then added simultaneously to the PCE solution while stirring under N_2 atmosphere to prevent carbonation of the $Ca(OH)_2$. After 24 hours of stirring, the pH of the suspension had dropped from ~ 11.6 to 11.3 and the resulting precipitates were centrifuged, washed with deionized (DI) water, transformed into a powder by freeze drying and then characterized by XRD and FT-IR analysis. Furthermore, the liquid suspensions of the nanocomposites as obtained in the synthesis were directly used in other measurements such as particle size analysis, heat flow calorimetry and mortar tests.

Characterization techniques

Particle size of the C-S-H – PCE nanocomposites (c = 0.1 g/L) were determined by dynamic light scattering (DLS) using a Zetasizer Nano ZS apparatus (Malvern Instruments, Workestershire, UK). Powder x-ray diffraction (XRD) patterns (2θ = 0.6 ° - 60 °) were obtained from a BRUKER AXS D8 diffractometer (Karlsruhe, Germany) operating at 30 kV and 30 mA with Cu Kα radiation. Furthermore, the C-S-H – PCE composites were characterized by Fourier Transform Infrared Spectroscopy (FTIR) using the BRUKER Vertex 70 spectrometer (Bruker, Ettlingen, Germany) with ATR cell in the range of 400 - 4000 cm^{-1}. The amount of PCE adsorbed on C-S-H was investigated by total organic carbon (TOC) content on a High TOC II instrument (Elementar, Hanau, Germany).

Mortar test

The C-S-H – PCE precipitates were measured for their efficiency as strength enhancer in a standard mortar prepared from CEM I 42.5 R (w/c = 0.5) at a cement-to-sand ratio of 1 : 3 according to DIN EN 196-1. The dosage of the C-S-H – PCE suspension was 0.35 % (as solid) by weight of cement (bwoc). The compressive and flexural strengths were measured after curing for 12 and 16 hours (Toni Technik, Berlin, Germany).

Cement hydration

Hydration kinetics was investigated by isothermal heat flow calorimeter (TAM AIR, Thermometric, Järfälla, Sweden) at 20°C. A cement paste was prepared from 4 g of cement and 2 g of DI water (w/c = 0.5). Dosage of the C-S-H – PCE suspensions was

0.35 % (as solid) bwoc. To study the structure of the hydration products, hydration of the cement paste was stopped after 16 hours by addition of acetone, the residue was dried overnight in an oven at 50 ° C and ^{29}Si MAS NMR spectra were recorded on a Bruker Avance 300 instrument. There, powder samples of the composite were filled into a 7 mm Zirconia rotor and spun at 5 KHz. Tetrakis(trimetylsilyl)silane was used as external standard.

3. Results and Discussion

3.1 Characterization of the C-S-H – PCE nanocomposites

The XRD patterns of the synthesized products are exhibited in **Fig. 1**. Pure C-S-H and the C-S-H – PCE nanocomposites show the diffraction pattern of semi-crystalline C-S-H (I) which constitutes an imperfect version of 1.4 nm tobermorite. The main hk0 reflections (100, 110, 200, 020) appear at 16.7, 29.0, 31.9 and 49.7 ° 2θ, respectively. Only in pure C-S-H, the 002 reflection can be observed at 7.0 ° 2θ which signifies a d spacing between the silicate layers of 1.2 nm.

Fig. 2 shows the FT-IR spectra of pure C-S-H, of PCE polymer 45PC6 and of the C-S-H – PCE nanocomposites obtained in the co-precipitation process when PCE samples 45PC2, 45PC6 and 45PC8 were present. In pure C-S-H, a broad, weak band of the stretching modes of hydroxyl groups from the crystal water can be observed between 3700 and 3200 cm^{-1}. In pure PCE polymer 45PC6, the absorbances of the alkyl C–H stretches of PCE polymer are found at 2875 cm^{-1}. Moreover, the peaks of the asymmetric and symmetric vibrations of the COO^- group present in the main chain of PCE are detected at ~ 1565 and ~ 1460 cm^{-1}, respectively. The characteristic bands at ~ 1100 cm^{-1} correspond to the C–O valence vibration of the ether bond present in the side chain of PCE. For the C-S-H – PCE composites, the stretching and vibrational bands of the silicate chains appear at 963 cm^{-1} (ν Si–O), 664 cm^{-1} (δ Si–O–Si) and 448 cm^{-1} (δ Si–O), respectively. Furthermore, display of the characteristic bands of the PCE copolymers in the spectra of the C-S-H – PCE nanocomposites confirms the presence of PCE in the synthesized C-S-H precipitates.

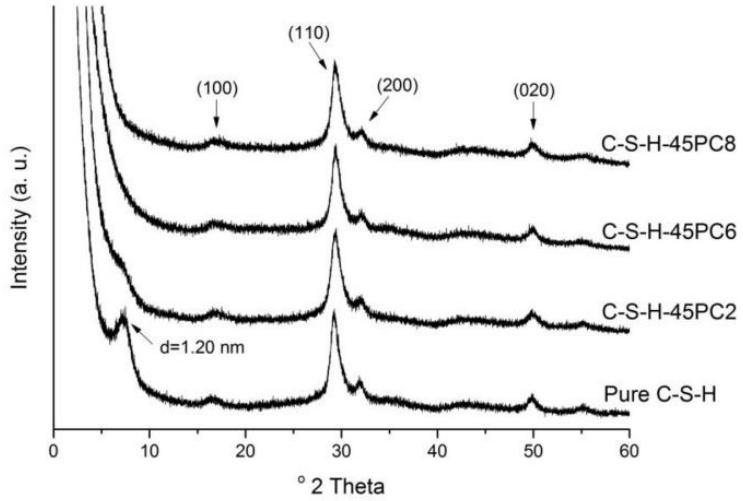

Figure 1: XRD patterns of synthesized pure C-S-H and of the C-S-H – PCE nanocomposites precipitated in the presence of PCE polymers 45PC2, 45PC6 and 45PC8

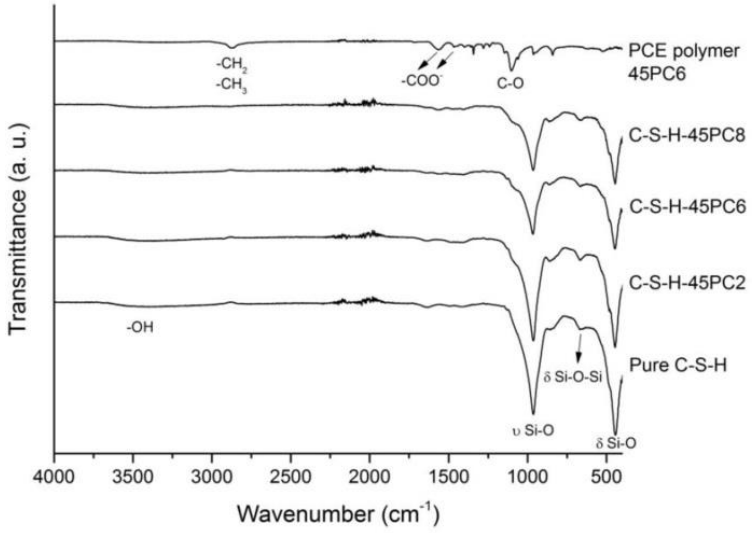

Figure 2: FT-IR spectra of synthesized pure C-S-H, of pure PCE copolymer 45PC6 and of the synthesized C-S-H – PCE nanocomposites

3.2 Effect of molar ratio in PCE on particle size of C-S-H – PCE

The particle size distribution in pure C-S-H and in the synthesized C-S-H composites is presented in **Fig. 3**. The particle size of C-S-H decreases with increased ratio of MAA to MPEG-MAA of the PCE polymer. The MPEG PCE possessing a low ratio of MAA to MPEG-MAA of 2 : 1 produces C-S-H particles with a monomodal particle size distribution and an average particle size at ~ 400 nm which is nearly the same as the particle size of pure C-S-H (~ 530 nm). In contrast, the other composites show bimodal particle size distributions. For the PCEs made of MAA : MPEG-MAA at molar ratios of 6 : 1 and 8 : 1, a small particle fraction shows at ~ 100 nm, while the large size fraction is observed at ~ 400 nm. The latter is similar to the size of the C-S-H composites obtained in the presence of 45PC2. This indicates that from PCEs possessing the optimum molar ratio of MAA : MPEG-MAA of > 6 : 1, a larger portion of small size C-S-H particles is obtained which is advantageous for the seeding effect in cement.

3.3 Sorption of PCE on C-S-H

Normally, in the highly alkaline pore solution loaded with calcium ions, the external surface of C-S-H particles exhibits a positive surface charge, thus allowing adsorption and stabilization by highly anionic PCE molecules. The amount of PCE sorbed on C-S-H was investigated by TOC (**Fig. 4**). The mass amount of the PCEs sorbed on C-S-H increases with increased anionic character of the PCE resulting from an increase of the MAA content in the PCE. For PCE polymer 45PC2 exhibiting the lowest anionic charge, ~ 180 mg sorb per g of C-S-H while from the PCEs of higher anionic charge density, ~ 200 mg/g C-S-H are consumed. However, when the molar amount of sorbed PCEs on C-S-H is considered, then a district difference in PCE sorption between low and high anionic charge densities of PCE is observed. This result suggests that PCEs of higher anionic charge density sorb in slightly higher amount on C-S-H and presumably lead to a smaller size of the C-S-H composites.

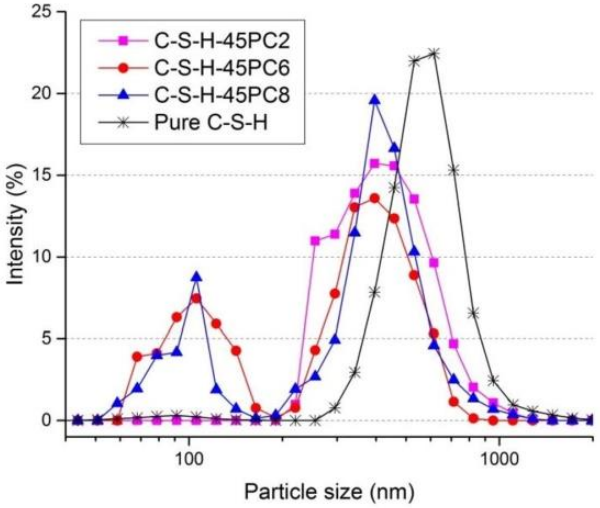

Figure 3: Particle size distribution of pure C-S-H and of the C-S-H – PCE nanocomposites obtained in the synthesis

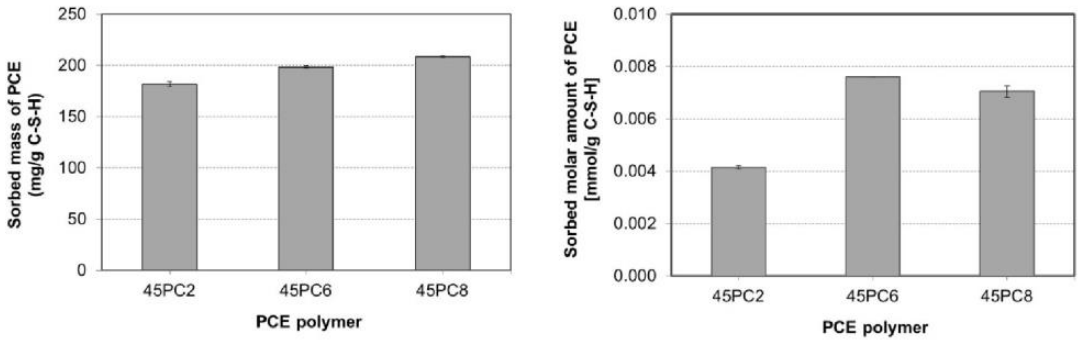

Figure 4: Mass amounts (left) and molar amount (right) of the PCE polymers sorbed by C-S-H

3.4 Effect on early strength of mortar

Mortars admixed with 0.35 wt % of the C-S-H – PCE nanocomposites were prepared and their compressive and flexural strengths were measured after 12 and 16 hours of curing. The results (**Fig. 5**) indicate that the improvement in early strength clearly depends on the particle size of the C-S-H – PCE nanocomposites which again is controlled by the amount of PCE sorbed on C-S-H. As a result, the compressive strengths of the mortar admixed with nanocomposite C-S-H – 45PC8 containing the smallest particle size (~ 100 nm) reach 2.4 and 6.0 N/mm^2 after 12 and 16 hours, respectively. These values signify an enhancement of ~ 60 % over the neat CEM I 42.5 R. Similar values were found for the C-S-H – 45PC8 nanocomposite (2.2 and 5.9 N/mm^2 for 12 and 16 hours, respectively). However, the compressive strengths of the mortars prepared from nanocomposite C-S-H – 45PC2 holding only a large size fraction (~ 400 nm) is comparable with that of the neat Portland cement. A similar trend was found for the flexural strengths of the mortars after 16 hours of curing. In case of the nanocomposites C-S-H – 45PC6 and C-S-H – 45PC8, the flexural strengths show at 1.6 and 1.7 N/mm^2, respectively whereas that of C-S-H – 45PC2 exhibited a value of

1.2 N/mm^2 only. The final strengths of the mortars (28 days) admixed with C-S-H – 45PC6 and C-S-H – 45PC8 were still the same as for the neat OPC sample (~ 58 and ~ 8 N/mm^2 for compressive and flexural strengths, respectively).

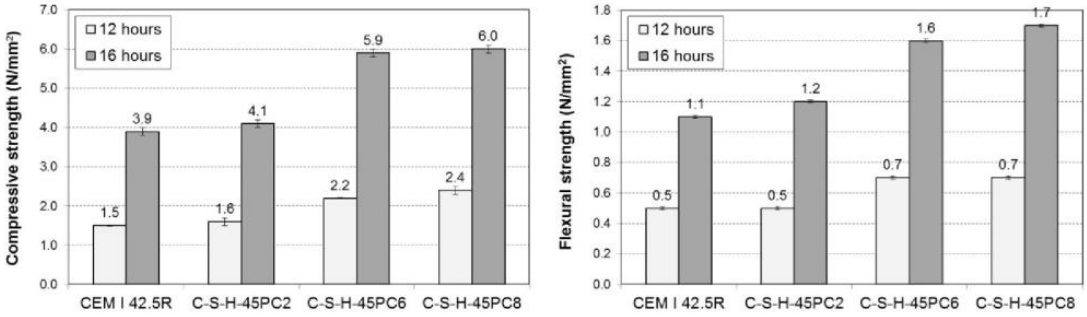

Figure 5: Compressive and flexural strengths of mortars cured for 12 and 16 hrs and admixed with 0.35 % bwoc of the synthesized C-S-H – PCE nanocomposites

3.5 Effect on cement hydration

The effect of the synthesized C-S-H – PCE nanocomposites on cement hydration was studied via isothermal heat flow calorimetry (**Fig. 6**). Addition of the C-S-H – PCE nanocomposites increases the heat flow during the acceleration period which is dominated by the nucleation and growth of the C-S-H phases, indicating enhanced hydration of the clinker phases C_3S and C_2S. Furthermore, the peak generally assigned to the conversion of AF_t to AF_m occurs at earlier hydration times. These effects are most pronounced for those composites (C-S-H – 45PC6 and C-S-H – 45PC8) which contain small particle size fractions and enhance mortar strength considerably.

The degree of condensation of C-S-H formed in cement after 16 hours of hydration was studied via ^{29}Si MAS NMR spectroscopy. As examples, the ^{29}Si MAS NMR spectra from the pure cement paste and from OPC admixed with C-S-H – 45PC6 nanocomposite are shown in **Fig. 7**. In the pure paste of CEM I 42.5 R, the signal at - 71 ppm corresponds to Q^0 of non-hydrated C_3S and C_2S while at - 79 ppm a Q^1 signal signifying an end chain silicate appears. In principle, these two signals are also observed in the OPC hydrated with nanocomposite C-S-H – 45PC6. However, there the Q^1 signal is stronger than in the neat OPC; and two small signals located at about - 82 and - 84 ppm corresponding to Q^2 groups (bridging silicate unit) are detectable now. They signify that when the nanocomposite C-S-H – 45PC6 containing the small size particle fraction is admixed, then the polymerization of the mono silicates to polysilicates present in C-S-H is greatly accelerated which leads to a significantly higher early strength of the mortar.

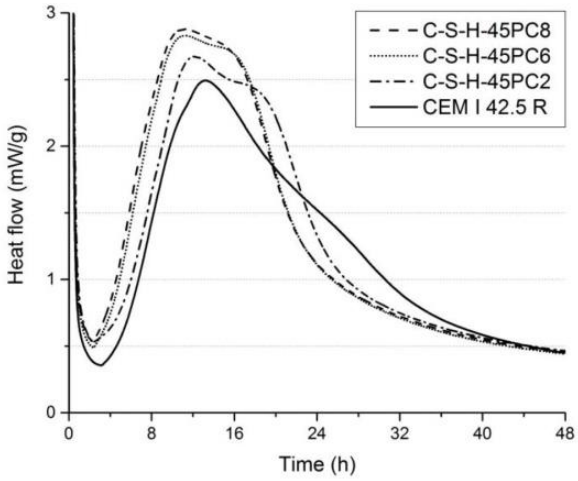

Figure 6: Heat evolution during hydration of neat CEM I 42.5 R (w/c = 0.5) and the pure cement admixed with 0.35% bwoc of C-S-H – PCE nanocomposites

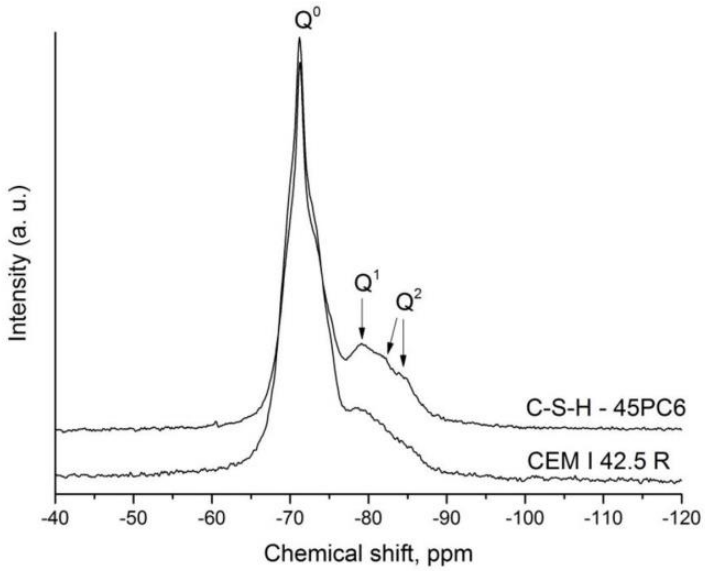

Figure 7: ^{29}Si MAS NMR spectra of neat CEM I 42.5 R (w/c = 0.5) and of the pure cement admixed with 0.35% bwoc of nanocomposite C-S-H – 45PC6

4. Conclusions

C-S-H – PCE nanocomposites were prepared by co-precipitation from Na_2SiO_3 and $Ca(NO_3)_2$ in the presence of anionic MPEG PCE copolymers. Using different PCE molecules with varied grafting density (molar ratio of MAA to MPEG-MAA), it is possible to control the average particle size of the C-S-H – PCE composites. Therefore, a PCE polymer with high molar ratio of MAA : MPEG-MAA (> 6 : 1) produces particularly small particle sizes of C-S-H – PCE nanocomposites and shows the strongest seeding effect on the hydration of C_3S and C_2S. Accordingly, this nanocomposite achieves a higher degree of polymerization of the mono silicates to C-S-H and achieves the largest gain in early strengths of the mortar.

References

[1] Cong X., Kirkpatrick R. *^{29}Si MAS NMR study of the structure of calcium silicate hydrate,* Advanced Cement Based Materials, (1996)3, 114 – 156.

[2] H.F.W. Taylor, Cement Chemistry, 2nd ed., Section: *Hydration of the calcium silicate phases*, Academic Press, London, U.K., (1997), pp. 123 - 166.

[3] Matsuyama H., Young J. F. *Synthesis of calcium silicate hydrate/polymer complexes: Part I. Anionic and nonionic polymers*. Journal of Materials Research, (1999a) 14, 8 3379 - 3387.

[4] DIN Deutsches Institut für Normung e.V. DIN EN 196-1: *Methods of testing cement - Part 1: Determination of strength*, 2005.

[5] Garcia-Lodeiro I., Fernández-Jiménez A., Blanco-Varela M. T., Palomo A. *FTIR study of the sol–gel synthesis of cementitious gels: C–S–H and N–A–S–H*. Journal of Sol-Gel Science and Technology, (2008) 45, 1 63 - 72.

[6] Thomas J.J., Jennings H. M., Chen J. J. *Influence of nucleation seeding on the hydration mechanisms of tricalcium silicate and cement*. The Journal of Physical Chemistry C, (2009) 113, 4327 - 4334.

[7] Alizadeh R., Raki L., Makar J. M., Beaudoin J. J., Moudrakovski I. *Hydration of tricalcium silicate in the presence of synthetic calcium-silicate-hydrate*. Journal of Materials Chemistry, (2009) 19, 7937 – 7946.

[8] Nicoleau L., Albrecht G., Lorenz K., Jetzlsperger E., Friedrich D., Wohlhaupter T., Dorfner R., Leitner H., Vierle M., Schmitt D., Braeu M., Hesse C., Pancera S.M., Zuern S., Kutschera M. *Plasticizer-Containing Hardening Accelerator Composition*. Patent US 20110269875 A1, 2011.

Authors:

M. Sc. Vipasri Kanchanason
Prof. Dr. Johann Plank

Technische Universität München
Lehrstuhl für Bauchemie
Lichtenbergstraße 4 85747 Garching

Corresponding author: Email sekretariat@bauchemie.ch.tum.de;
Tel +49 89 289 13151, Fax +49 89 289 13152

5.2 Effect of synthesis conditions on the effectiveness of C-S-H – PCE nanocomposites as accelerators in Portland cement

This section describes the influence of process parameters during the synthesis of the C-S-H – PCE nanocomposites on their characteristics and performance. A commercial isoprenyl oxy poly(ethylene glycol) based superplasticizer (IPEG PCE) possessing very long side chain lengths (93 EO units) was employed in the synthesis of C-S-H. Moreover, various factors such as pH value, Ca/Si ratio and temperature were adjusted during the preparation of the C-S-H – PCE nanocomposites to achieve a 100 % increase over the neat OPC sample for the 16 hour compressive strength of mortar.

5.2.1 Effectiveness of C-S-H – PCE nanocomposites in Portland cement

First, the experiments were designed via a tool called Box-Behnken Design (BBD) by using the MINITAB software. C-S-H – PCE nanocomposites synthesized under 16 different conditions were admixed at 0.35 wt. % to mortar which was then tested for compressive strength after 16 hours of curing. Thereafter, the relation between the synthetic variables and the resultant mortar strengths was analyzed via the regression equation.

The strength results are presented in **Figure 34**. It was found that addition of the C-S-H – PCE compounds synthesized under different conditions clearly promoted the early strength development of mortars. The highest compressive strength value was obtained from a C-S-H – PCE nanocomposite synthesized at a Ca/Si ratio of 1.0, at pH = 11.7 and a temperature of 50 ° C. The increase was ~ 10 N/mm^2 which represents a 100 % increase over that of the control sample. In comparison, the C-S-H – PCE compound prepared at the low pH value of 10.9 and high temperature (75 ° C) did not show an accelerating effect in cement. It produced a compressive strength value which was comparable to that of the neat cement.

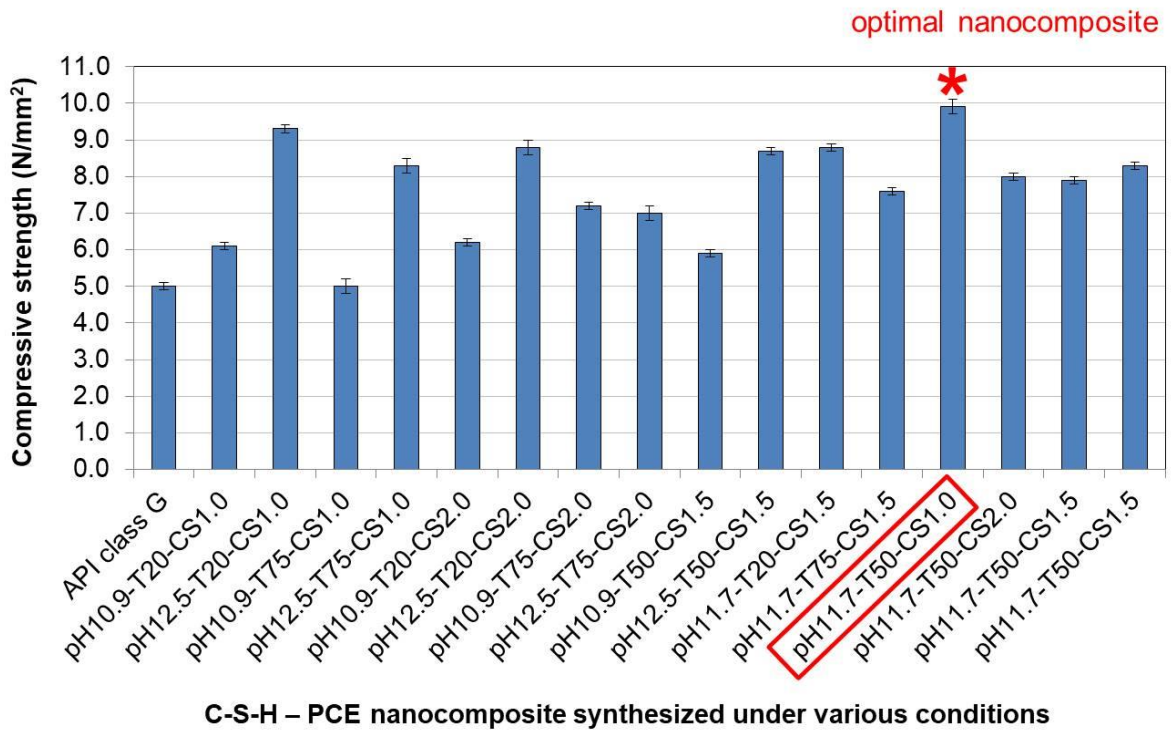

Figure 34: Compressive strengths of mortars cured for 16 hours and admixed with 0.35 % bwoc of C-S-H – PCE nanocomposites synthesized under various conditions

To quantify the dominant control factor, the response surface regression was analyzed and the results are shown in **Table 6**. According to the theory, the p-values of factors less than 0.05 are most effective and should be considered. It was observed that only the pH value played a dominant role during the synthesis of the nanacomposite and significantly impacted the early strength of mortar, while the Ca/Si ratio and temperature were less important factors. According to this, the optimum condition to achieve the largest gain in compressive strength as obtained from the regression equation (**Equation 23**) was: pH = 12.3, Ca/Si = 1.0 and 20 ° C, as is shown in **Figure 35**.

To verify this result, the effect of pH values (pH = 10.4 - 13.8) during the synthesis on structure, composition and morphology of C-S-H – PCE compounds and their effectiveness

on early strength of mortar was studied in another series of experiments. This is presented in the following **section 5.2.2**.

Strength = -283.244 + 46.6676a - 0.0146972b + 14.7106c - 1.84971(a*a) - 1.28125(a*c)

Equation 23

Table 6

Variance analysis according to the BBD model relating to the compressive strengths of mortars admixed with differently synthesized C-S-H – PCE nanocomposites

Parameter	**Compressive strengths of mortar samples**		
	P	**T**	**Coefficient**
Constant	0.000	29.123	8.4412
pH (a)	0.000	5.217	1.1700
Temp (b)	0.101	-1.804	-0.4042
Ca/Si (c)	0.546	-0.624	-0.1400
pH*pH (a*a)	0.009	-3.231	-1.1838
pH*Ca/Si (a*c)	0.068	-2.044	-0.5125

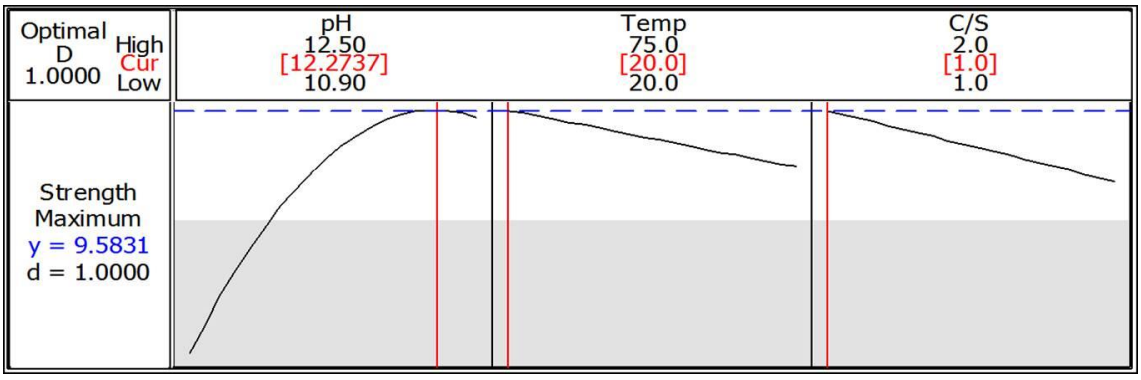

Figure 35: Finding the optimal condition for the synthesis of the C-S-H – PCE nanocomposite

5.2.2 Effect of pH on the composition, structure and morphology of C-S-H – PCE nanocomposites

As was shown in **section 5.2.1**, the pH value during the synthesis had the strongest effect on the performance of the synthesized C-S-H – PCE nanocomposite used as a strength enhancer in cement. For this reason, studies on the influence of the pH conditions on the characteristic properties of the C-S-H – PCE nanocomposite were performed. The results are presented in three papers that follow this section.

First of all, C-S-H – PCE was precipitated from Na_2SiO_3 and $Ca(NO_3)_2$ solutions in an isoprenolether (IPEG) - based PCE solution at pH values of 10.4, 11.7, 12.4 and 13.8. It was confirmed that the pH value plays a critical role for the nanostructure, composition (Ca/Si ratio) and morphology of the C-S-H – PCE products obtained. Furthermore, it influences the PCE adsorption on C-S-H.

An increase of pH value from 10.4 to ≥ 11.7 changed the C-S-H structure from amorphous to semi-crystalline, as was evidenced by XRD measurement. A decrease in the basal spacing in the semi-crystalline structure was also found when the pH increased. However, no evidence from XRD supported the intercalation of the IPEG-PCE into the C-S-H lamellar structure.

Furthermore, the silicate chains present in the C-S-H – PCE nanocomposites were investigated via ^{29}Si MAS NMR spectroscopy. According to this, branched silicate chains in C-S-H – PCE developed only at the low pH of 10.4. At higher pH values, no more bridging sites occurred and the degree of polymerization of the silicate chains decreased, leading to shorter chain lengths in C-S-H.

The composition of C-S-H is typically described by the Ca/Si ratio. The Ca/Si ratio of the nanocomposites increased with a rise in pH and reached a value close to the initial ratio of 1.0.

The morphology of the C-S-H – PCE nanocomposites was also affected by the pH. It was found that at pH = 10.4, globular, agglomerated C-S-H particles were precipitated which at pH ≥ 11.7 transformed to a foil-like morphology.

Additionally, the pH value influenced PCE adsorption on C-S-H which controls the particle size of the product. The results revealed a reduction in the amount of PCE adsorbed on the C-S-H foils at pH above 11.7, resulting from the decreased anionic charge of PCE owed to counter-ion condensation. The highest PCE adsorption was observed at pH = 11.7, leading to the highest amount of ultra-small nanofoils.

In summary, it became apparent that the pH value during the synthesis of C-S-H – PCE nanocomposites besides the PCE composition presents the most important factor to control the nanostructure, morphology and particle size of the nanocomposites. The C-S-H – PCE nanocomposite obtained at pH = 11.7 consisted of the smallest foil-like particles, performed the strongest seeding effect on cement hydration, and produced the largest gain in the early strength of mortar. In comparison, globular C-S-H – PCE particles prepared at pH = 10.4 exhibited only a minor accelerating effect on cement hydration.

Paper #3

Role of pH on the structure, composition and morphology of C-S-H – PCE nanocomposites and their effect on early strength development of Portland cement

V. Kanchanason, J. Plank

Cement and Concrete Research, 102 (2017) 90 – 98.

Cement and Concrete Research 102 (2017) 90–98

Contents lists available at ScienceDirect

Cement and Concrete Research

journal homepage: www.elsevier.com/locate/cemconres

Role of pH on the structure, composition and morphology of C-S-H–PCE nanocomposites and their effect on early strength development of Portland cement

V. Kanchanason[a,b], J. Plank[a,*]

[a] Technische Universität München, Chair of Construction Chemistry, Lichtenbergstraße 4, 85747 Garching, Germany
[b] Siam Research and Innovation Company, 51 Moo 8, Tub Kwang, Kaeng Khoi, Saraburi 18260, Thailand

ARTICLE INFO

Keywords:
C-S-H (B)
Polycarboxylate (D)
Nanocomposite
pH (A)
Early strength (C)

ABSTRACT

Synthetic C-S-H–PCE nanocomposites are known to act as seeding material in Portland cement. Here, C-S-H–PCE was precipitated from Na_2SiO_3 and $Ca(NO_3)_2$ solutions in an isoprenolether (IPEG)-based PCE solution at pH values of 10.4, 11.7, 12.4 and 13.8. It was found that at pH = 10.4 the C-S-H–PCE precipitate is amorphous, possesses a disordered structure, consists of partially branched silicate chains and exhibits a globular morphology. At pH = 11.7, the precipitate is semi-crystalline and consists of shorter, non-branched silicate chains. Moreover, it contains the highest amount of ultra-small nanofoils (< 50 nm) and can sorb the largest amount of PCE (~250 mg/g C-S-H). It shows optimal seeding effect in cement when compared with globular or foils of C-S-H–PCE exhibiting larger size (> 200 nm) obtained at pH = 12.4 and 13.8, respectively.

1. Introduction

Clinker substitution with supplementary cementitious materials (SCMs), like in blended cements (CEM II/III), presents an attractive way to reduce the environmental impact of CO_2 emission from cement production. However, the disadvantage of blended cements is a slow development of early strength. Additionally, when concrete is used in cold climates, such condition delays its hydration leading to a decrease in early strength. In recent years, synthetic calcium silicate hydrate (C-S-H) has been introduced as a potential accelerator to speed up cement hydration [1–7].

Calcium silicate hydrate ($xCaO{\cdot}ySiO_2{\cdot}zH_2O$, C-S-H) is well known as the main hydration product of Portland cement. It presents the binding phase and is responsible for the strength properties of hardened cement. The C-S-H generated in hydrated Portland cement is of low crystallinity, has a Ca/Si molar ratio of ~1.6–1.9 which depends on the water-to-cement (w/c) ratio and other parameters [8–11]. It also occurs in various morphologies such as small globules in the inner product (I_p) and fibrous particles in the outer product (O_p) C-S-H [12–14].

Generally, C-S-H is composed of silicate tetrahedra which are aligned in a dreierketten structure. They share oxygen atoms with calcium in plane and are stacked in a layer structure [15] (Fig. 1). However, for synthetic C-S-H, a huge number of variations in composition, structure and morphology are possible. They depend on many factors such as the initial Ca/Si ratio, pH value, the preparation method etc. For example, the C-S-H synthesized via silica-lime reaction using the controlled C_3S hydration method [16] attained a foil like morphology at Ca/Si molar ratios of ~0.7–1.5 whereas a fibrillar morphology was observed at higher lime concentrations (Ca/Si > 1.58). In another experiment, nanofoils of C-S-H were detected upon dropwise addition of calcium nitrate into a sodium silicate solution at a high Ca/Si ratio of 2.0 and pH = 13.3 [17,18]. Many reports based on evidence from ^{29}Si NMR spectroscopy describe linear silicate chains for synthetic C-S-H which contains terminal silicate groups (Q^1) and chain members linked to two neighboring silicate units (Q^2). The Q^2 silica tetrahedra positioned in the middle of the chains can arrange in a dreierketten structure whereby a dimer of silica tetrahedra (paring tetrahedra) connects to the bridging tetrahedron.

The chain length of C-S-H depends on its composition relative to the Ca/Si ratio. At Ca/Si ratios > 1.0, short silicate chains and no more bridging tetrahedra were found [19,20]. Moreover, strongly alkaline conditions and high pH values caused an increase in Q^1 units and a reduction in the mean chain length of the silicate chains [20–23]. Furthermore, for this C-S-H, a decreased interlayer space and Ca/Si ratio were observed [24].

Synthetic C-S-H can serve as a seeding material in cement. The influence of the size of the C-S-H particles on their seeding efficiency has been considered and can be controlled by the addition of polymeric

* Corresponding author.
E-mail address: sekretariat@bauchemie.ch.tum.de (J. Plank).

http://dx.doi.org/10.1016/j.cemconres.2017.09.002
Received 24 February 2017; Received in revised form 9 August 2017; Accepted 8 September 2017
Available online 20 September 2017

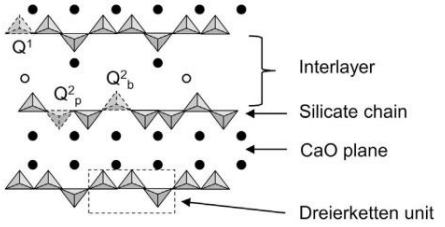

Fig. 1. Schematic structure of C-S-H. Triangles: silica tetrahedra; black circles: calcium atoms/ions in CaO planes and calcium ions; empty circles: species in the interlayer (water). Q^n: n represents the number of SiO_4 units attached to an individual silicate tetrahedron, p: pairing units, b: bridging sites.
(Adapted from [15])

dispersants such as polycarboxylates (PCEs). Generally, the external surfaces of C-S-H contain silanol groups which are ionized in high alkaline condition and are able to complex with dissolved calcium ions [25–27]. Consequently, the surfaces of C-S-H exhibit a positive charge which can facilitate the adsorption of anionic comb-like copolymers such as PCE superplasticizers [28,29]. Based on this mechanism, *meso* crystals composed of C-S-H nanofoils occupied with adsorbed PCE polymers are formed which represent a nanocomposite [30]. The various architectural structures possible in PCEs [31] control their adsorption on the C-S-H surfaces which in turn affects the size of the C-S-H particles. As such, specific PCE molecules result in C-S-H particles exhibiting a huge surface area which is highly beneficial for effective cement acceleration [4,30,32,33]. Moreover, the impact of anionicity and type of PCE on the composition and the length of the silicate chains in C-S-H have been reported [28,29,34,35]. However, so far the correlation between the composition, structure, morphology and particle size of individual C-S-H–PCE nanocomposites and their seeding efficiency in cement has not yet been disclosed.

In this paper, the effect of pH varied between 10.4 and 13.8 during the co-precipitation of calcium nitrate and sodium silicate (molar ratio Ca/Si = 1.0) on the composition, structure and morphology of pure C-S-H and C-S-H–PCE nanocomposites was investigated using XRD, FT-IR, ^{29}Si MAS NMR spectroscopy, XRF and TEM measurements. Additionally, the amount of PCE adsorbed on C-S-H obtained at different pH values which strongly affects the size of the C-S-H particles was measured via total organic carbon (TOC) method. Based upon these findings, a mechanism of interaction between PCE and C-S-H is proposed for the different pH conditions. Finally, those results are linked with the effectiveness of the synthesized C-S-H–PCE nanocomposites relative to their ability to accelerate the early strength development of mortar. The correlation between structure, morphology and particle size of the C-S-H–PCE nanocomposites and their strength enhancing effect is revealed.

2. Materials and methods

2.1. Raw materials

The starting materials used in the synthesis of C-S-H were $Ca(NO_3)_2{\cdot}4H_2O$ (PanReac AppliChem, Germany) and $Na_2SiO_3{\cdot}5H_2O$ (VWR Prolabo BDH Chemicals, Germany). Moreover, HNO_3 65 wt% (VWR Prolabo BDH Chemicals, Germany) and NaOH (Merck KGaA, Germany) were used to adjust the pH values during the synthesis.

A commercial isoprenyl oxy poly(ethylene glycol) based superplasticizer (IPEG PCE) was employed in the synthesis. The solid content of this PCE solution was 40% by weight and the chemical structure of this PCE polymer is presented in Fig. 2. Its molecular properties and anionic charge amount at different pH values are summarized in Table 1.

Furthermore, a slowly hydrating Ordinary Portland Cement (OPC) sample (API Class G oil well cement, corresponding to a CEM I 32.5 N) obtained from Dyckerhoff GmbH (Germany) was used for testing the early strength development of mortars. This cement was selected for its particularly slow development in early strength. Its phase composition was determined by XRD including *Rietveld* refinement and thermogravimetric analysis of the calcium sulfate hydrates. The results are listed in Table 2. Its specific surface area (*Blaine*) and mean particle size (d_{50} value) were found at 3000 cm^2/g and 11 μm, respectively.

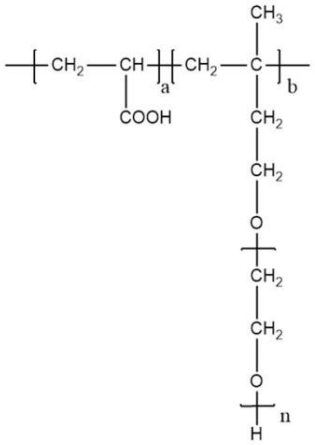

Fig. 2. Chemical structure of the isoprenyl oxy poly(ethylene glycol) (IPEG) based PCE superplasticizer used in the study.

Table 1
Molecular properties and pH-dependent specific anionic charge densities of the IPEG PCE sample.

Molar masses (g/mol)		Polydispersity index	Specific anionic charge density in NaOH (μeq/g)			
M_w	M_n	(*PDI*)	At pH value			
			10.4	11.7	12.4	13.8
35,100	15,700	2.2	1800	2750	2140	–[a]

[a] No stable value obtained.

2.2. Preparation of C-S-H and C-S-H–PCE nanocomposites

The C-S-H and C-S-H–PCE nanocomposites were prepared by the co-precipitation method. Aqueous $Ca(NO_3)_2$ and Na_2SiO_3 solutions were fed into water or the IPEG-PCE solution to obtain pure C-S-H or C-S-

Table 2
Phase composition of the OPC sample as determined by XRD using *Rietveld* refinement and thermogravimetry.

Phase	[wt%]
C3S	59.3
C2S	19.5
C3A, cubic	1.7
C4AF	14.1
free CaO	< 0.3
$CaSO_4{\cdot}1/2H_2O$[a]	0.2
$CaSO_4{\cdot}2H_2O$[a]	4.6
Anhydrite	< 0.1
Arcanite	< 0.1
Total	99.7

[a] Determined by thermogravimetry.

H–PCE nanocomposites. The initial molar ratio of CaO/SiO_2 based on the starting materials was 1.0. In preparation of the C-S-H–PCE nanocomposite, 4.2 g of the IPEG-PCE solution were diluted with 20.8 mL of water (resulting in a 6.7 wt% PCE solution) and the pH of this PCE solution was adjusted to 8.5 ± 0.1 by using aqueous 30 wt% NaOH. Next, solutions of 4.2 g (18 mmol) of $Ca(NO_3)_2{\cdot}4H_2O$ in 2.7 mL of water ($Ca(NO_3)_2$ concentration 42.6 wt%) and 3.8 g (18 mmol) of $Na_2SiO_3{\cdot}5H_2O$ in 7.2 mL of water (sodium silicate concentration 20 wt %) were prepared in a water bath at 75 °C to achieve fast and complete dissolution and were then cooled to ambient. After that, both solutions were continuously added at 0.61 mL/min and 1.16 mL/min, respectively, to 23.3 mL of DI water or 24.3 mL of PCE solution while stirring at 20 °C under N_2 atmosphere. Total addition time was 8 min. Moreover, the pH of the reaction solution was continuously monitored using a pH electrode submerged in the solution and was adjusted to 10.4 or 11.7 by the addition of 1 M HNO_3, or to 12.4 and 13.8 by adding 30 wt% NaOH as needed. When the addition of $Ca(NO_3)_2$ and Na_2SiO_3 was finished, the white suspensions were stirred for another 24 h at room temperature and then used as is in TEM measurement, particle size analysis and mortar testing. Additionally, part of the samples were transformed into a powder by centrifugation, washing with CO_2-free de-ionized water and freeze drying for 24 h. The powders were characterized by XRD, FT-IR and ^{29}Si MAS NMR spectroscopy and XRF. Furthermore, the white suspensions were centrifuged by using a filter tube with an inset membrane with a nominal molecular weight limit of 100 kDa (Merck Millipore, Cork, Ireland). From the clear filtrate, the PCE and Ca^{2+} contents were determined by TOC and ICP-OES measurements, respectively.

2.3. Characterization techniques

The anionic charge amount of the PCE was measured by polyelectrolyte titration using a particle charge detector PCD 03 pH (BTG Mütek GmbH, Herrsching, Germany). First, the anionic PCE was dissolved in NaOH solution at different pH values of 10.4, 11.7, 12.4 and 13.8 (PCE concentration 0.2 mg/mL). Then, the PCE solution was titrated with a standard solution of 0.001 N cationic poly-DADMAC (polydiallyl dimethyl ammonium chloride) until charge neutralization was obtained [36].

Powder X-ray diffraction (XRD) patterns were obtained from a BRUKER AXS D8 diffractometer (Karlsruhe, Germany) with *Bragg - Brentano* geometry working at 30 kV and 35 mA with Cu Kα radiation between 3.0° and 60° 2θ.

FT-IR spectra of the C-S-H–PCE nanocomposites were recorded on a BRUKER Vertex 70 spectrometer (Bruker, Ettlingen, Germany) equipped with ATR cell in the range of 400–4000 cm^{-1}.

The binding motif of silicate present in the synthesized C-S-H and C-S-H–PCE nanocomposites was identified by ^{29}Si MAS NMR spectroscopy using a Bruker Avance 300 MHz instrument operating at a resonance frequency of 59.595 MHz. The powder samples were sifted into a 7 mm zirconia rotor and spun at 5 kHz. All spectra were recorded with a relaxation delay of 45 s, and tetrakis(trimethylsilyl)silane was used as external standard. The ^{29}Si NMR spectra were analysed by deconvolution of the different signals for the Q^n species using Origin93 software. The linewidth and lineshape of the spectra were fit according to the *Voigt* model.

The molar ratios of CaO/SiO_2 and Na_2O/SiO_2 present in the C-S-H and C-S-H–PCE samples were assessed by X-ray fluorescence (XRF) using a BRUKER S8 TIGER (Karlsruhe, Germany) instrument with rhodium X-ray tube. The C-S-H powders were molten in a mixture of lithium tetraborate and lithium metaborate as a fluxing agent and pressed into a tablet before measurement.

Morphology of the C-S-H and C-S-H–PCE samples was captured by transmission electron microscopy (TEM) performed on a JEOL JEM 2011 instrument (JEOL, Japan) equipped with a LaB_6 cathode. The C-S-H or C-S-H–PCE suspensions were diluted with water and dispersed in an ultrasonic bath for 5 min. After plasma surface treatment, the dispersed samples were dropped on a 300 Cu mesh with carbon support films (Quantifoil Micro Tools GmbH, Germany). The size of the C-S-H and C-S-H–PCE nanoparticles were measured by using ImageJ software.

The total organic carbon (TOC) content of the C-S-H–PCE nanocomposites was determined using a High TOC II instrument (Elementar, Hanau, Germany). First, the total organic carbon present in the PCE polymer and the non-adsorbed part of PCE remaining in the aqueous phase after 24 h of stirring were measured. From this, the amount of PCE sorbed on C-S-H was calculated from the difference between the amount of PCE added and the amount remaining in the filtrate (depletion method). Furthermore, the concentration of free, non-reacted Ca^{2+} ions present in the filtrate was measured using an inductively coupled plasma optical emission spectrometer (ICP-OES; iCAP 7000 Series, Thermo Scientific, Waltham, USA).

Particle size of C-S-H or C-S-H–PCE nanocomposites was measured via dynamic light scattering (DLS) using a Zetasizer Nano ZS apparatus (Malvern Instruments, Worcestershire, UK). The samples were suspended in water at a concentration of 0.1 g/L. An ultrasonic bath was used to disperse the particles for 15 min prior to measurement.

Zeta potential of the C-S-H suspensions was captured on an electrophoretic instrument (Zetasizer Nano ZS apparatus from Malvern Instruments, Worcestershire, UK). The samples were diluted to a liquid/solid ratio (wt/wt) of 500 using filtrate obtained via centrifugation of the suspension produced in the synthesis. Prior to measurement, the diluted suspensions were sonicated in an ultrasonic bath for 15 min.

2.4. Mortar tests

The C-S-H–PCE suspensions precipitated at different pH values were tested for their effectiveness as strength enhancers in a standard mortar prepared according to DIN EN 196-1. The dosage of the C-S-H–PCE nanocomposite was 0.35% (as solid) by weight of cement (bwoc). The water to cement (w/c) ratio of the mortar was set at 0.44. The mortar was cast into 40 × 40 × 160 mm prism steel molds and cured at 20 ± 1 °C and 90% relative humidity for 16 h. After curing, the compressive and flexural strengths were measured using an instrument from Toni Technik, Berlin, Germany. To ensure comparable results, all mortar specimens were adjusted to the same fresh mortar density of 2310 kg/m^3 by applying a defoamer, and the density was checked for each sample to be within ± 10 kg/m^3 deviation.

3. Results and discussion

3.1. Nanostructure and composition of C-S-H and C-S-H–PCE nanocomposites

3.1.1. XRD analysis

The XRD patterns of the synthesized products obtained at different pH values are shown in Fig. 3.

At pH = 10.4, a broad peak indicating a highly disordered structure was detected for both C-S-H and C-S-H–PCE, suggesting amorphous character. While at pH values above 10.4, for both species semi-crystalline C-S-H was observed, with the main hk0 reflections (100, 110, 200 and 020) at 16.7, 29.0, 31.9 and 49.7° 2θ, respectively [15,24,37].

The (002) reflection of the C-S-H occurring between 7.0 and 9.0° 2θ allows to determine the basal spacing between silicate layers in the C-S-H structure. According to this analysis, the d spacing of pure C-S-H decreased from 1.28 to 1.05 nm when the pH value was increased to 13.8. This reduction can be explained by the absence of bridging silica units in the dreierketten structure [24] or the substitution of charge balancing calcium ions by sodium ions from the NaOH solution [38]. To compare, in the C-S-H–PCE nanocomposites the (002) reflections signifying the basal spacing were also observed at pH = 11.7, 12.4 and 13.8, and the same d spacing as in pure C-S-H was found.

This result implies that at all pH values studied and using our

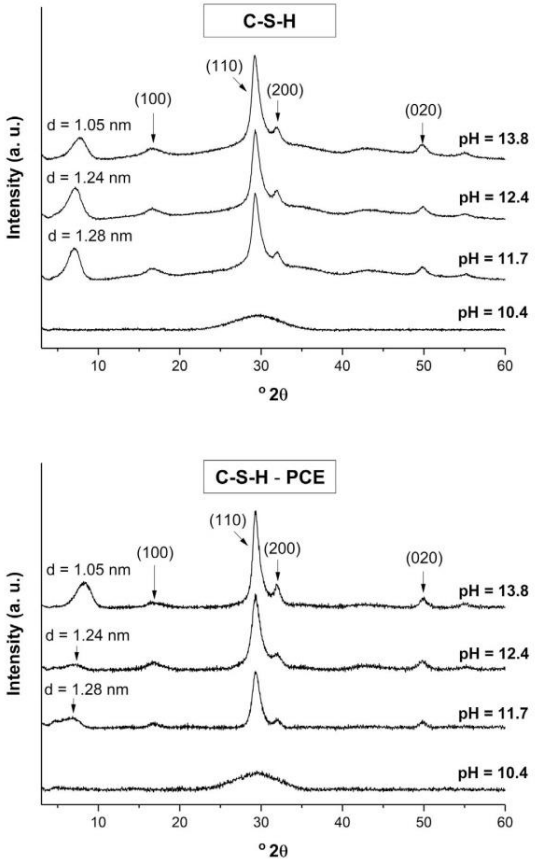

Fig. 3. XRD patterns of C-S-H and C-S-H–PCE nanocomposites synthesized at different pH values.

synthesis method always structurally similar C-S-H products are formed, independent of whether the PCE is present or not, and that the comb-shaped PCE copolymer does not intercalate into the C-S-H structure, as was recently reported for silylated PCEs [39]. This distinguishes our method from other works which reported an expansion of the interlayer spacing of C-S-H resulting from the intercalation of linear anionic polymers such as poly(methacrylic acid), poly(acrylic acid) etc. However, these experiments were performed at an initial Ca/Si ratio of 1.3 and at pH ~ 13 [37,40].

3.1.2. FT-IR analysis

The FT-IR spectra of the pristine IPEG PCE polymer and the C-S-H–PCE composites obtained at different pH values are shown in Fig. 4. The broad peaks characteristic for hydroxyl groups present as crystal water in C-S-H which occur between 3700 and 3200 cm^{-1} and at ~1640 cm^{-1} were found for all C-S-H–PCE samples. The absorbance band signifying the alkyl (C—H) stretches in PCE was observed at ~2875 cm^{-1}. Additionally, the bands at ~1560 and ~1460 cm^{-1} correspond to the asymmetric and symmetric vibrations of the COO^- groups present in the main chain of PCE while the peak assigned to the ether bonds (C—O) in the PCE side chain was detected at ~1100 cm^{-1}. As expected, in the C-S-H–PCE composites, the absorbances for the carboxylate (COO^-) and the ether (C—O) groups (the latter visible as a shoulder only) appear much weaker than in the pristine PCE polymer,

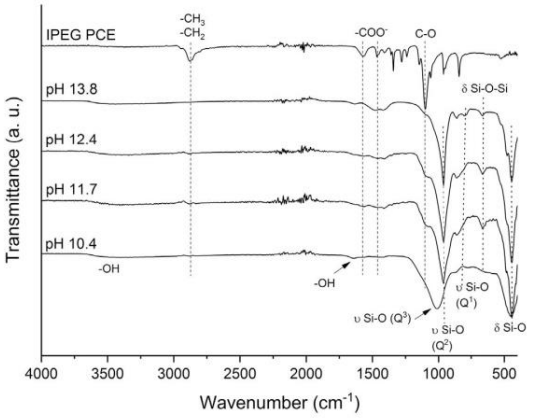

Fig. 4. FT-IR spectra of the pristine IPEG PCE polymer and of the C-S-H–PCE nanocomposites synthesized at various pH values.

especially in the composites obtained at pH = 10.4 and 13.8, respectively, thus signifying lower polymer contents in these two composites. This finding was confirmed later by adsorption measurements presented in Section 3.4. To conclude, the presence of PCE superplasticizer in the synthesized C-S-H precipitates is confirmed by the display of the characteristic bands of PCE in the spectra of the C-S-H–PCE nanocomposites.

Relative to the C-S-H skeleton, the stretching and vibrational bands of the silicate units appeared at ~1010 cm^{-1} (ν Si—O of Q^3 sites, only observed in the sample obtained at pH = 10.4, reflecting a higher degree of silicate polymerization due to the presence of Q^3 sites in the silica-rich C-S-H gel [41]), ~960 cm^{-1} (ν Si—O of Q^2 sites), ~815 cm^{-1} (ν Si—O of Q^1 sites), ~663 cm^{-1} (δ Si—O—Si) and ~445 cm^{-1} (δ Si—O of SiO_4), respectively. As alkalinity increased, the band of the Si—O asymmetric stretching vibrations of Q^2 tetrahedra shifted to lower frequencies, indicating a lower degree of polymerization of the silicate chains [42]. Moreover, the band of Si—O stretching of Q^1 tetrahedra increased in intensity with increasing pH values. These trends were confirmed later using ^{29}Si MAS NMR spectroscopy (see Fig. 5).

3.1.3. Analysis of the silicate chain

From ^{29}Si MAS NMR measurements, the different coordination species of the silicon atoms occurring in the chains of C-S-H can be identified and assigned as terminal chain unit (Q^1, $\delta \sim -79.5$ ppm), bridging unit (Q^2_b at $\delta \sim -83.5$ ppm) or a unit connected to two pairing sites (Q^2_p at $\delta \sim -85.3$ ppm) [21,24,43,44] (Fig. 1).

The ^{29}Si MAS NMR spectra of pure C-S-H and the C-S-H–PCE nanocomposites synthesized at various pH values are presented in Fig. 5. At pH = 10.4, the spectra for both C-S-H and C-S-H–PCE showed a broad peak covering the entire range for Q^1, Q^2 and Q^3 species, thus suggesting coexistence of silica units positioned as terminal, chain member and branching site [24,43].

However, at higher pH values (> 10.4), the spectra of both C-S-H and C-S-H–PCE clearly suggest that with increasing pH value, the branching units disappear and the average chain length is reduced, as is evidenced by the rise of the Q^1 signal as pH increases. Furthermore, a slight shift of the Q^1 and Q^2 signals for the C-S-H synthesized at the highly alkaline pH value of 13.8 to a less negative value was found. A similar downfield shift for the silica sites has been reported for C-S-H in alkali hydroxide solution. It resulted from differences in the shielding of the silicate units [21,22,45]. Generally, a lower shielding effect for the silica tetrahedra by alkalis leads to a downfield chemical shift when compared to calcium [19,46]. This suggests that sodium ions which are

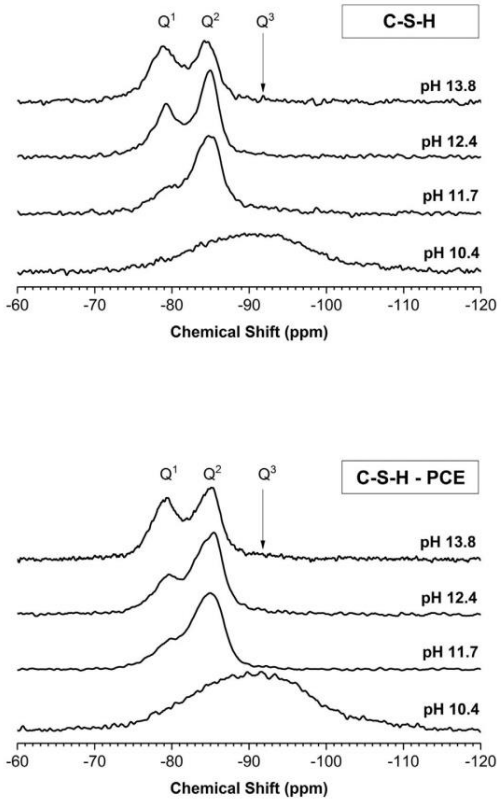

Fig. 5. ^{29}Si MAS NMR spectra of C-S-H and C-S-H–PCE obtained at various pH values.

Table 3
Oxide compositions of C-S-H and C-S-H–PCE nanocomposites precipitated at different pH values.

pH	CaO/SiO_2		Na_2O/SiO_2	
	C-S-H	C-S-H–PCE	C-S-H	C-S-H–PCE
10.4	0.48	0.45	0.01	0.01
11.7	0.83	0.89	0.03	0.03
12.4	0.91	0.94	0.03	0.05
13.8	0.91	0.95	0.05	0.09

increasingly present in our synthesis at pH ≥ 12.4 (at such conditions the Ca^{2+} concentration decreases) are able to compete with and substitute calcium ions bound to deprotonated silanol groups present along the C-S-H chain. This concept is supported by the increasing Na_2O/SiO_2 ratios displayed in Table 3.

According to spectra deconvolution (one example exhibited in Fig. 6), Q^2_b signals at δ ~ − 83 ppm were observed in both C-S-H and C-S-H–PCE nanocomposites at pH > 10.4. The relative population of the silicate species (Q^2/Q^1) and the mean chain length (MCL, calculated according to Eq. (1) [16]) are tabulated in Table 4.

$$MCL = \frac{2\,(Q^1 + Q^2{}_b + Q^2{}_p + Q^3)}{Q^1} \quad (1)$$

There, the percentage of Q^1 units increased significantly at higher pH values (> 10.4) while the total amount of Q^2 units decreased accordingly. This reduction in the fraction of Q^2 resulted from both

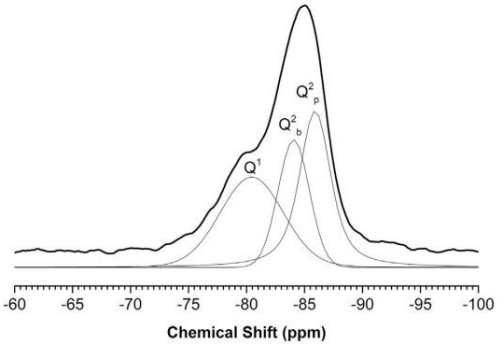

Fig. 6. Example of a deconvoluted ^{29}Si MAS NMR spectrum presented for the C-S-H–PCE nanocomposite synthesized at pH = 11.7.

Table 4
Chemical shift, percentages of the silicate species and mean silicate chain length (MCL) of the C-S-H and C-S-H–PCE samples, respectively.

pH values	Q^1		Q^2_b		Q^2_p		Q^2/Q^1	MCL (silica units)
	(ppm)	(%)	(ppm)	(%)	(ppm)	(%)		
C-S-H								
10.4	–	–	–	–	–	–	–	–
11.7	−79.2	28.2	−83.4	14.4	−85.5	54.7	2.5	7.1
12.4	−79.2	45.1	−83.1	12.0	−85.0	42.9	1.2	4.4
13.8	−78.8	59.5	–	–	−84.5	40.5	0.7	3.4
C-S-H–PCE								
10.4	–	–	–	–	–	–	–	–
11.7	−79.6	27.0	−83.5	17.1	−85.3	55.9	2.7	7.4
12.4	−79.7	33.8	−83.7	18.1	−85.7	48.1	2.0	5.9
13.8	−79.1	45.3	−83.4	12.2	−85.4	42.5	1.2	4.4

absence of bridging sites (Q^2_b) and fewer pairing units (Q^2_p). Consequently, the degree of polymerization (Q^2/Q^1) and the MCL of the silicate chains decreased which reflects a lower degree of polymerization. Furthermore, the reduced amount of Q^2_b sites led to a decrease in the basal spacing between the silicate layers which is in agreement with the XRD results as mentioned before (see Fig. 3).

The highest degree of polymerization and mean chain length were found in the C-S-H sample synthesized at pH = 11.7. Its MCL was ~7 which signifies that the average silicate chain consists of five Q^2 and two Q^1 units. Shorter silicate chains (3–4 units) were found at pH values above 11.7.

In the presence of the IPEG PCE, the mean chain length of C-S-H increased as is evidenced by a lower proportional amount of Q^1 and a higher occurrence of Q^2 units, (Table 4). This increment in the MCL of C-S-H–PCE nanocomposites is probably owed to the polymer being attached to the C-S-H at sites where the bridging silica tetrahedra are missing [34]. Within the series of C-S-H–PCE nanocomposites, a higher pH value led to a decreased amount of Q^2 sites, Q^2/Q^1 ratios and MCL of the silicate chains, thus showing the same trend as in pure C-S-H. As such, the highest degree of polymerization for the C-S-H–PCE nanocomposites again was observed at pH = 11.7 representing a chain of ~7 silica units while the shortest chain was found at pH = 13.8.

This implies that the chain length of both the C-S-H and C-S-H–PCE nanocomposite depend on the pH value present during the synthesis whereby higher pH values lead to shorter silicate chains (Fig. 7). In addition, the presence of the PCE polymer favors the polymerization of the mono silicate, thus leading to longer C-S-H chains which has been observed before in other studies [35,39].

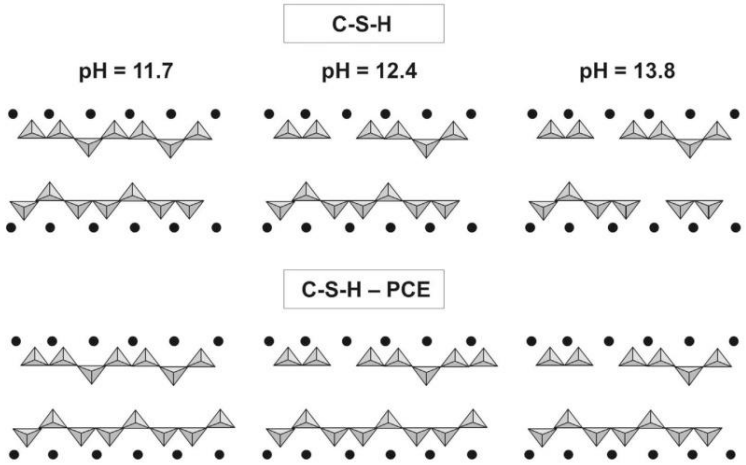

Fig. 7. Schematic representation of the silicate chains present in C-S-H and C-S-H–PCE nanocomposites synthesized at different pH values (triangles: silica tetrahedron; black circles: calcium atoms in CaO planes).

3.1.4. C-S-H composition

The CaO/SiO_2 and Na_2O/SiO_2 ratios of the synthesized C-S-H and C-S-H–PCE nanocomposites are displayed in Table 3.

The results signify that the Ca/Si ratios of the C-S-H and C-S-H–PCE samples rise with increased pH values. The Ca/Si ratios were generally lower than the molar ratio of 1.0 present in the feeding components $Ca(NO_3)_2/Na_2SiO_3$. The lowest value for the CaO/SiO_2 ratio was recorded for both systems at pH = 10.4. This reflects the dominant amount of silicate species present in these C-S-H structures. The difference in the Ca/Si ratios between C-S-H and C-S-H–PCE was only minor. The highest Ca/Si ratios were found at pH = 12.4 and 13.8, respectively. This suggests that high alkaline condition leads to more CaO planes in the C-S-H structure. Additionally, at pH = 13.8 more sodium ions occupy the coordination sites of CaO in C-S-H and C-S-H–PCE as has been presented before (Table 3).

Quantification of the residual calcium ions present in the aqueous phase of the C-S-H and C-S-H–PCE suspensions as measured by ICP (Fig. 8) clearly revealed a significant reduction in free calcium at pH values between 10.4 and 12.4. This implies that calcium ions might be consumed for the formation of CaO planes in C-S-H and for the complexation of silanol groups present in C-S-H surfaces (see Section 3.4).

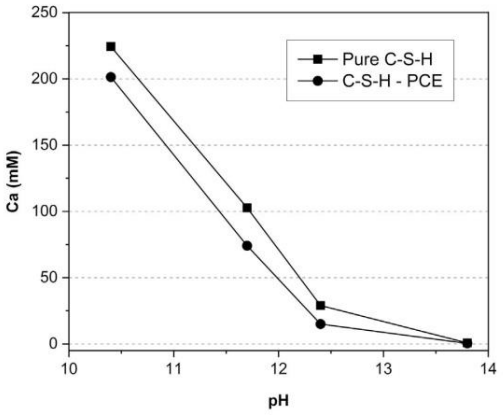

Fig. 8. Concentration of free calcium ions present in the aqueous phase of the C-S-H and C-S-H–PCE nanocomposites synthesized at various pH values.

3.2. Morphology of C-S-H and C-S-H–PCE nanocomposites

TEM images of the synthesized C-S-H and C-S-H–PCE nanocomposites obtained at pH = 10.4, 11.7, 12.4 and 13.8 respectively are presented in Fig. 9. The results clearly reveal differences in the morphology of the samples in dependence of the pH value.

Remarkably, at pH = 10.4 numerous globular and agglomerated particles were observed in both the C-S-H and C-S-H–PCE suspensions, suggesting a non-classical nucleation mechanisms via droplet formation [47,48]. The globules showed a diameter of ~50 nm for individual particles and of 200–800 nm for the agglomerates.

However, a foil-like morphology was always observed when C-S-H and C-S-H–PCE were synthesized at pH values of ≥ 11.7. Generally, for C-S-H–PCE smaller and thinner foils were recorded than for pristine C-S-H. According to the TEM images, the shortest C-S-H–PCE nanofoils resulted at pH = 11.7 (foil length ~ 50 nm). At higher pH values, their size increased and became > 100 nm at pH = 13.8.

3.3. Effect of PCE on particle size of C-S-H–PCE

The size distribution of the synthesized C-S-H–PCE particles is illustrated in Fig. 10. It is evidenced that the pH value adjusted during the preparation significantly affects the particle size of the nanocomposites. Generally, bimodal particle size distributions were observed for all C-S-H–PCE compounds, independent of pH value. This implies that the C-S-H–PCE composites contain a mixture of small and large particles which exhibit an average size of ~50 to ~200 nm, respectively. At pH = 13.8, even a trimodal size distribution comprising particles of ~50 nm, ~300 nm and ~1 μm was captured. Most important, the small size fraction (< 100 nm) of the C-S-H–PCE composites was highest at pH = 11.7 while the large particle fraction (> 100 nm) was highest at pH = 10.4. This suggests that using the proper pH condition during the synthesis such as pH = 11.7, a high amount of particularly small C-S-H particles providing C-S-H of particularly large surface area can be obtained. Exactly this kind of particle size is assumed to work best as seeding material in cement.

Apparently, the C-S-H particles are stabilized best by PCE when a particularly high amount of these superplasticizers are adsorbed. Thus, to achieve a high amount of sorbed PCE on the C-S-H particles which is controlled by the overall architecture and microstructure of the PCE molecule (side chain length, side chain density, repartition of side chains etc.) [49], presents a key parameter to produce particularly small C-S-H precipitates [32,33]. Accordingly, when only a low amount

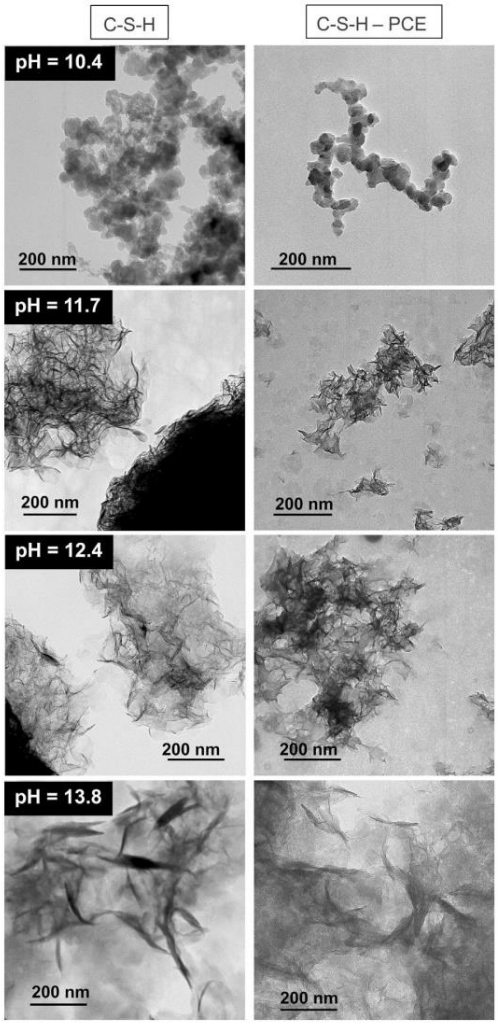

Fig. 9. TEM images of C-S-H and C-S-H–PCE precipitated at different pH values.

of PCE is sorbed on C-S-H such as at pH = 13.8 (see Section 3.4), then predominantly larger size fractions occur. This result corroborates that higher amounts of PCE sorbed on C-S-H surfaces generate and maintain smaller C-S-H particles.

3.4. Adsorption of PCE on C-S-H

When present in a highly alkaline solution containing Ca^{2+} ions, C-S-H attains a positively charged surface (Eq. (2)) [25–27]. This way, anionic organic compounds such as PCEs or amino acids are able to adsorb on these surfaces via the complexation of calcium ions [50,51].

$$\equiv Si-O^- + Ca^{2+} \rightarrow \equiv Si-O\,Ca^+ \quad (2)$$

To account for this interaction, the amount of PCE sorbed on C-S-H was quantified using TOC measurements (Fig. 11). It was found that the adsorbed amount of PCE increased from pH = 10.4 to 11.7. However, when the pH value rose further, PCE sorption declined. At pH = 10.4 the sorbed amount of PCE was ~170 mg/g whereas at pH = 11.7,

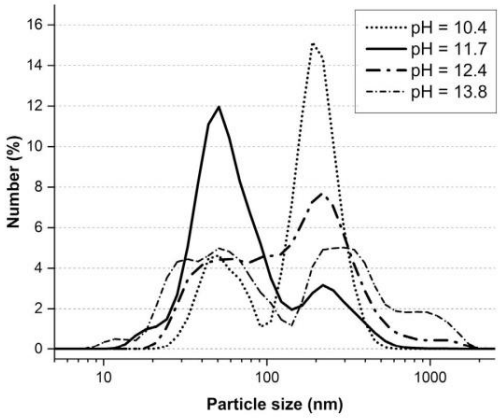

Fig. 10. Particle size distribution by number of C-S-H–PCE synthesized at pH values from 10.4 to 13.8.

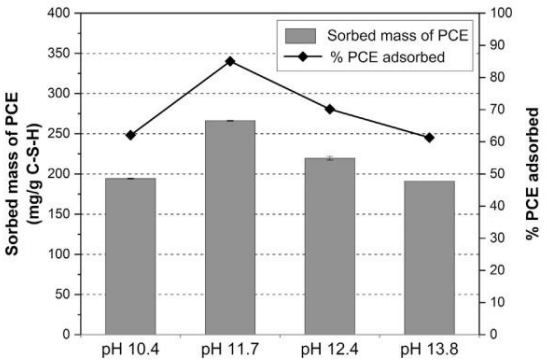

Fig. 11. Amount of PCE polymer contained in the C-S-H–PCE composites at various pH values.

~250 mg/g of PCE were consumed which represents the highest value. At pH = 12.4 and 13.8, the sorbed amounts decreased to ~220 and ~140 mg/g, respectively.

The low sorbed amount of PCE at pH = 10.4 might be owed to the lower specific anionic charge density of the PCE measured at this pH value (~1800 μeq/g versus 2750 μeq/g recorded at pH = 11.7, see Table 1). Additionally, a less positively charged surface was detected for C-S-H at pH = 10.4 (Fig. 12), presumably from fewer deprotonated silanol groups present on the C-S-H surfaces. As a consequence, fewer Ca^{2+} ions can bind to this surface which reduces the number of positively charged sites on C-S-H which facilitate PCE adsorption.

At pH = 12.4, a slight decline in the sorbed amount of PCE was observed (~220 mg/g C-S-H) which continued at the higher pH value of 13.8 (~140 mg/g C-S-H). Presumably, this effect is owed to the decreased concentration of free dissolved Ca^{2+} at such high pH values which reduces the surface charge of C-S-H to less positive until it even turns negative (see zeta potential curve of C-S-H suspension displayed in Fig. 12).

A conceptual sketch of the electrochemical double layer formed as a result of PCE adsorption on the surface of C-S-H is presented in Fig. 13. The model illustrates how the carboxylate groups present on the backbone of the PCE polymer coordinate via monodentate complexation of Ca^{2+} with the silanolate groups at bridging sites of the silicate chain.

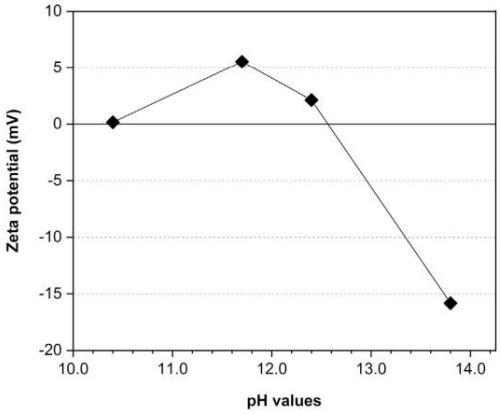

Fig. 12. Zeta potential of the synthesized C-S-H particles at pH = 10.4–13.8.

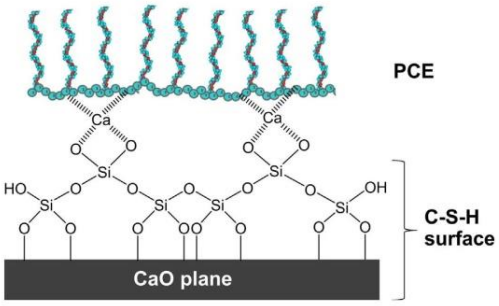

Fig. 13. Model illustrating the electrochemical double layer formed on the surface of C-S-H resulting from interaction between PCE, Ca^{2+} and the chains of C-S-H; note that the PCE molecule shown is not to scale.

3.5. Effectiveness of C-S-H–PCE as hydration accelerator

The 16 hour compressive and flexural strengths of mortars admixed with 0.35 wt% of the C-S-H–PCE particles prepared at pH = 10.4–13.8 are shown in Fig. 14. It was found that the C-S-H–PCE nanocomposites can significantly increase the early strength of mortar. Generally, the compressive strength values were higher for mortars seeded with foil-like C-S-H–PCE (pH = 11.7–13.8) than with globular C-S-H–PCE (pH = 10.4). The C-S-H–PCE compounds precipitated at pH = 11.7 which contained the highest fraction of small nanofoils (~50 nm) showed superior strength development (R_c = 11.7 N/mm^2). When the pH value was increased further, the compressive strengths of the mortars decreased and attained values of 10.5 and 8.8 N/mm^2 representing pH conditions of 12.4 and 13.8, respectively. Apparently, the higher number of large particles (> 100 nm) produces an adverse effect. Least effective were the globular C-S-H–PCE particles obtained at pH = 10.4 (R_c = 7.6 N/mm^2). The same trend was obtained for the flexural strengths (R_f = 1.9, 2.8, 2.6 and 2.2 N/mm^2 at pH = 10.4, 11.7, 12.4 and 13.8, respectively).

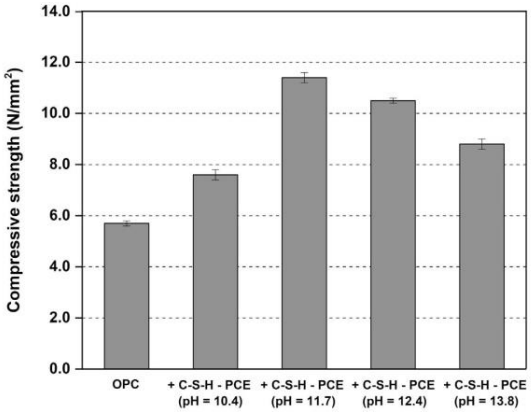

Fig. 14. Compressive strengths of mortars cured for 16 h and admixed with 0.35% bwoc of the C-S-H–PCE composites synthesized at different pH values.

To conclude, the effectiveness of C-S-H–PCE nanocomposites for early strength enhancement of mortar depends on both morphology and particle size, and these parameters are influenced by the pH value adjusted during the synthesis. The seeding effect of C-S-H–PCE appears to rely on nanofoils which act as a template for the growth of fibrillar C-S-H from cement. Apparently, this seeding effect increases with the number (and thus smaller size) of the C-S-H–PCE nanofoils generated in the synthesis.

4. Conclusions

C-S-H–PCE nanocomposites were successfully prepared by co-precipitation from Na_2SiO_3 and $Ca(NO_3)_2$ in the presence of an IPEG PCE copolymer. It was found that the pH conditions existing during the synthesis strongly affect the nanostructure, composition (Ca/Si ratio) and morphology of the C-S-H–PCE products.

An increase of pH value from 10.4 to 11.7 and higher changes the C-S-H structure from amorphous to semi-crystalline. There, the PCE polymer is entrapped between individual C-S-H foils via interaction with calcium ions coordinating to silanolate groups present at the bridging or terminal silica units.

^{29}Si MAS NMR spectroscopy indicates the presence of branched silicate chains in C-S-H–PCE to occur only at the low pH value of 10.4. At higher pH values, no more bridging sites are present and a decline in the number of pairing silica tetrahedra leads to a reduction in the degree of polymerization and shorter chain lengths in C-S-H. The Ca/Si ratio of the C-S-H–PCE composites also increases with a rise in pH and attains a value close to the initial ratio of 1.0 present in the starting components.

The morphology of the C-S-H–PCE nanocomposites is also affected by the pH value. It was found that at pH = 10.4, globular, agglomerated C-S-H particles are precipitated which at pH ≥ 11.7 transform to a foil-like morphology.

Additionally, the pH value plays an important role for PCE sorption on C-S-H which generally controls the particle size of the C-S-H–PCE product. The amount of PCE sorbed on the C-S-H foils decreases from pH > 11.7. The highest amount of PCE sorbed on C-S-H was found at pH = 11.7, resulting from the anionic charge amount of PCE being highest at this pH value and the large number of bridging sites (Q_b^2) of silicate units present in C-S-H. As a result, the C-S-H–PCE nanocomposite synthesized at pH = 11.7 consists of the smallest foil-like particles and exercises the strongest seeding effect in cement hydration, as documented by the largest gain in early (16 h) strength of mortar. In comparison, globular C-S-H–PCE products show only a minor accelerating effect in cement hydration.

Acknowledgements

The authors would like to thank Prof. S. Weinkauf and her team from the center of Electron Microscopy at TUM's Chemistry department for capturing the TEM images, and the department of Analytical Chemistry at TUM for conducting the ICP-OES measurements. We are also grateful to the Central Laboratory of Siam Research and Innovation

Company (SRI) for providing the XRF measurements. V.K. is most indebted to the SCG Cement-Building Materials for financial support of her study.

References

[1] J.J. Thomas, H.M. Jennings, J.J. Chen, Influence of nucleation seeding on the hydration mechanisms of tricalcium silicate and cement, J. Phys. Chem. C 113 (2009) 4327–4334.

[2] R. Alizadeh, L. Raki, J.M. Makar, J.J. Beaudoin, I. Moudrakovski, Hydration of tricalcium silicate in the presence of synthetic calcium-silicate-hydrate, J. Mater. Chem. 19 (2009) 7937–7946.

[3] M.H. Hubler, J.J. Thomas, H.M. Jennings, Influence of nucleation seeding on the hydration kinetics and compressive strength of alkali activated slag paste, Cem. Concr. Res. 41 (2011) 842–846.

[4] L. Nicoleau, Accelerated growth of calcium silicate hydrates: experiments and simulations, Cem. Concr. Res. 41 (2011) 1339–1348.

[5] L. Nicoleau, The acceleration of cement hydration by seeding: influence of the cement mineralogy, ZKG Int. 1 (2013) 40–49.

[6] K. Owens, M.I. Russell, G. Donnelly, A. Kirk, P.A.M. Basheer, Use of nanocrystal seeding chemical admixture in improving Portland cement strength development: application for precast concrete industry, Adv. Appl. Ceram. 113 (8) (2014) 478–484.

[7] G. Land, D. Stephan, Preparation and application of nanoscaled C-S-H as an accelerator for cement hydration, in: K. Sobolev, S.P. Shah (Eds.), Nanotechnology in Construction: Proceedings of NICOM5, Springer International Publishing, Cham, 2015, pp. 117–121.

[8] I.G. Richardson, G.W. Groves, Models for the composition and structure of calcium silicate hydrate (C-S-H) gel in hardened tricalcium silicate pastes, Cem. Concr. Res. 22 (1992) 1001–1010.

[9] I.G. Richardson, G.W. Groves, The incorporation of minor and trace elements into calcium silicate hydrate (C-S-H) gel in hardened cement pastes, Cem. Concr. Res. 23 (1993) 131–138.

[10] I.G. Richardson, The nature of hydration products in hardened cement pastes, Cem. Concr. Compos. 22 (2000) 97–113.

[11] R. Taylor, I.G. Richardson, R.M.D. Brydson, Nature of C-S-H in 20 year old neat ordinary Portland cement and 10% Portland cement – 90% ground granulated blast furnace slag pastes, Adv. Appl. Ceram. 106 (2007) 294–301.

[12] I.G. Richardson, The nature of C-S-H in hardened cements, Cem. Concr. Res. 29 (1999) 1131–1147.

[13] I.G. Richardson, Tobermorite/jennite- and tobermorite/calcium hydroxide-based models for the structure of C-S-H: applicability to hardened pastes of tricalcium silicate, β-dicalcium silicate, Portland cement, and blends of Portland cement with blast-furnace slag, metakaolin, or silica fume, Cem. Concr. Res. 34 (2004) 1733–1777.

[14] I.G. Richardson, The calcium silicate hydrates, Cem. Concr. Res. 38 (2008) 137–158.

[15] H.F.W. Taylor, Cement Chemistry, second ed, Thomas Telford Publishing, London, 1997.

[16] E.T. Rodriguez, I.G. Richardson, L. Black, E. Boehm-Courjault, A. Nonat, J. Skibsted, Composition, silicate anion structure and morphology of calcium silicate hydrates (C-S-H) synthesized by silica-lime reaction and by controlled hydration of tricalcium silicate, Adv. Appl. Ceram. 114 (2015) 362–371.

[17] A. Kumar, P. Bowen, K. Scrivener, Synthetic calcium silicate hydrate with high calcium to silicon ratio, in: C. Shi, Y. Yao (Eds.), 14th ICCC, Beijing, China, 2015, Proceedings CD, Section 2: Hydration of Portland Cement, 2015.

[18] A. Kumar, B.J. Walder, A.K. Mohamed, A. Hofstetter, B. Srinivasan, A.J. Rossini, K. Scrivener, L. Emsley, P. Bowen, The atomic-level structure of cementitious calcium silicate hydrate, J. Phys. Chem. C (2017), http://dx.doi.org/10.1021/acs.jpcc.7b02439.

[19] H. Viallis, P. Faucon, J.-C. Petit, A. Nonat, Interaction between salts (NaCl, CsCl) and calcium silicate hydrates (C-S-H), J. Phys. Chem. B 103 (1999) 5212–5219.

[20] J.J. Chen, J.J. Thomas, H.F.W. Taylor, H.M. Jennings, Solubility and structure of calcium silicate hydrate, Cem. Concr. Res. 34 (2004) 1499–1519.

[21] I. García-Lodeiro, A. Fernández-Jiménez, I. Sobrados, J. Sanz, A. Palomo, C-S-H gels: interpretation of ^{29}Si MAS-NMR spectra, J. Am. Ceram. Soc. 95 (4) (2012) 1440–1446.

[22] E. L'Hôpital, B. Lothenbach, G. Le Saout, D. Kulik, K. Scrivener, Incorporation of aluminium in calcium-silicate-hydrates, Cem. Concr. Res. 75 (2015) 91–103.

[23] G. Zhu, H. Li, X. Wang, S. Li, X. Hou, W. Wu, Q. Tang, Synthesis of calcium silicate hydrate in highly alkaline system, J. Am. Ceram. Soc. 99 (8) (2016) 2778–2785.

[24] H. Matsuyama, J.F. Young, Effects of pH on precipitation of quasi-crystalline calcium silicate hydrate in aqueous solution, Adv. Cem. Res. 12 (1) (2000) 29–33.

[25] L. Nachbaur, P.C. Nkinamubanzi, A. Nonat, J.C. Mutin, Electrokinetic properties which control the coagulation of silicate cement suspensions during early age hydration, J. Colloid Interface Sci. 202 (1998) 261–268.

[26] H. Viallis-Terrisse, A. Nonat, J.C. Petit, Zeta-potential study of calcium silicate hydrates interacting with alkaline cations, J. Colloid Interface Sci. 253 (2001) 140–149.

[27] A. Nonat, The structure and stoichiometry of C-S-H, Cem. Concr. Res. 34 (2004) 1521–1528.

[28] A. Popova, G. Geoffroy, M.F. Renou-Gonnord, P. Faucon, E. Gartner, Interactions between polymeric dispersants and calcium silicate hydrates, J. Am. Ceram. Soc. 83 (10) (2000) 2556–2560.

[29] J. Plank, C. Hirsch, Impact of zeta potential of early cement hydration phases on superplasticizer adsorption, Cem. Concr. Res. 37 (2007) 537–542.

[30] L. Nicoleau, T. Gädt, L. Chitu, G. Maier, O. Paris, Oriented aggregation of calcium silicate hydrate platelets by the use of comb-like copolymer, Soft Matter 9 (2013) 4864–4874.

[31] J. Plank, E. Sakai, C.W. Miao, C. Yu, J.X. Hong, Chemical admixtures – chemistry, applications and their impact on concrete microstructure and durability, Cem. Concr. Res. 78 (2015) 81–99.

[32] V. Kanchanason, J. Plank, C-S-H–PCE nanocomposites for enhancement of early strength of cement, 19th Ibausil, Bauhaus-Universität Weimar, Tagungsband 1, Weimar, Germany, 2015, pp. 759–766.

[33] V. Kanchanason, J. Plank, C-S-H–PCE nanocomposites for enhancement of early strength of Portland cement, in: C. Shi, Y. Yao (Eds.), 14th ICCC, Beijing, China, 2015, Proceedings CD, Section 4: Admixtures, 2015.

[34] J.J. Beaudoin, L. Raki, R. Alizadeh, A ^{29}Si MAS NMR study of modified C-S-H nanostructures, Cem. Concr. Compos. 31 (2009) 585–590.

[35] E. Cappelletto, S. Borsacchi, M. Geppi, F. Ridi, E. Fratini, P. Baglioni, Comb-shaped polymers as nanostructure modifiers of calcium silicate hydrate: a ^{29}Si solid-state NMR investigation, J. Phys. Chem. C 117 (2013) 22947–22953.

[36] J. Plank, B. Sachsenhauser, Experimental determination of the effective anionic charge density of polycarboxylate superplasticizers in cement pore solution, Cem. Concr. Res. 39 (2009) 1–5.

[37] H. Matsuyama, J.F. Young, Synthesis of calcium silicate hydrate/polymer complexes: part I. anionic and nonionic polymers, J. Mater. Res. 14 (8) (1999) 3379–3387.

[38] T.T.H. Bach, E. Chabas, I. Pochard, C. Cau Dit Coumes, J. Haas, F. Frizon, A. Nonat, Retention of alkali ions by hydrated low-pH cements: mechanism and Na^+/K^+ selectivity, Cem. Concr. Res. 51 (2013) 14–21.

[39] C.A. Orozco, B.W. Chun, G. Geng, A.H. Emwas, P.J.M. Monteiro, Characterization of the bonds developed between calcium silicate hydrate and polycarboxylate-based superplasticizers with silyl functionalities, Langmuir 33 (2017) 3404–3412.

[40] H. Matsuyama, J.F. Young, Intercalation of polymers in calcium silicate hydrate: a new synthetic approach to biocomposites? Chem. Mater. 11 (1999) 16–19.

[41] P. Yu, R.J. Kirkpatrick, B. Poe, P.F. McMillan, X. Cong, Structure of calcium silicate hydrate (C-S-H): near-, mid-, and far-infrared spectroscopy, J. Am. Ceram. Soc. 82 (3) (1999) 742–748.

[42] I. García-Lodeiro, D.E. Macphee, A. Palomo, A. Fernández-Jiménez, Effect of alkalis on fresh C–S–H gels. FTIR analysis, Cem. Concr. Res. 39 (2009) 147–153.

[43] X. Cong, R.J. Kirkpatrick, ^{29}Si MAS NMR study of the structure of calcium silicate hydrate, Adv. Cem. Based Mater. 3 (1996) 144–156.

[44] E. Pustovgar, R.P. Sangodkar, A.S. Andreev, M. Palacios, B.F. Chmelka, R.J. Flatt, J.B. d'Espinose de Lacaillerie, Understanding silicate hydration from quantitative analyses of hydrating tricalcium silicates, Nat. Commun. (2016) 1–9.

[45] I. Lognot, I. Klur, A. Nonat, NMR and infrared spectroscopies of C-S-H and Al-substituted C-S-H synthesised in alkaline solutions, in: P. Colombet, et al. (Ed.), Nuclear Magnetic Resonance Spectroscopy of Cement-based Materials, Springer-Verlag, Berlin Heidelberg, 1998, pp. 189–196.

[46] I. Klur, B. Pollet, J. Virlet, A. Nonat, C-S-H structure evolution with calcium content by multinuclear NMR, in: P. Colombet, et al. (Ed.), Nuclear Magnetic Resonance Spectroscopy of Cement-based Materials, Springer-Verlag, Berlin Heidelberg, 1998, pp. 119–141.

[47] H. Cölfen, M. Antonietti, Mesocrystals and Nonclassical Crystallization, John Wiley & Sons Ltd, Chichester, 2008.

[48] J.J. De Yoreo, P.U.P.A. Gilbert, N.A.J.M. Sommerdijk, R.L. Penn, S. Whitelam, D. Joester, H. Zhang, J.D. Rimer, A. Navrotsky, J.F. Banfield, A.F. Wallace, F.M. Michel, F.C. Meldrum, H. Cölfen, P.M. Dove, Crystallization by particle attachment in synthetic, biogenic, and geologic environments, Science 349 (6247) (2015) 1–9.

[49] J. Plank, B. Sachsenhauser, J. de Reese, Experimental determination of the thermodynamic parameters affecting the adsorption behaviour and dispersion effectiveness of PCE superplasticizers, Cem. Concr. Res. 40 (2010) 699–709.

[50] A. Picker, L. Nicoleau, A. Nonat, C. Labbez, H. Cölfen, Identification of binding peptides on calcium silicate hydrate: a novel view on cement additives, Adv. Mater. 26 (2014) 1135–1140.

[51] T. Sowoidnich, T. Rachowski, C. Rößler, A. Völkel, H.M. Ludwig, Calcium complexation and cluster formation as principal modes of action of polymers used as superplasticizer in cement systems, Cem. Concr. Res. 73 (2015) 42–50.

Paper #4

Relationship between the structure and morphology of C-S-H – PCE nanocomposites and their accelerating effect in cement

V. Kanchanason, J. Plank

Tagung Bauchemie, Bauhaus-Universität Weimar, Tagungsband 1, Weimar, Germany,

GDCh-Monograph, 52 (2017) 36 – 40.

Relationship between the structure and morphology of C-S-H – PCE nanocomposites and their accelerating effect in cement

V. Kanchanason and J. Plank
Technische Universität München, Garching, Germany

Abstract

C-S-H – PCE nanocomposites are known to accelerate the hydration of Portland cement. It was found that the pH conditions during the synthesis strongly affect the structure, morphology and particle size of the C-S-H – PCE composites which impact the early strength of cement. The results show that at pH = 11.7 the C-S-H – PCE precipitate is semi-crystalline and contains non-branched silicate chains with the mean chain length of ~ 7. Moreover, it consists of the smallest foil-like particles (< 50 nm) and provides the strongest seeding effect in cement. In comparison, the C-S-H globules obtained at pH = 10.4 show only a minor accelerating effect in cement hydration.

Introduction

Clinker substitution with SCMs, like in blended cements (CEM II/III), allows the reduction of CO_2 emission. However, the drawback of these cements is too slow development of early strength. It has been reported before that synthetic nanoscale C-S-H can accelerate cement hydration /1/. However, the accelerating effect is dependent on the size of the C-S-H particles controlled by the addition of polycarboxylates (PCEs) /2-3/. Furthermore, the structure and morphology of C-S-H depend on many factors such as Ca/Si ratio, temperature, etc. /4/. Until now, the correlation between the structure and morphology of C-S-H – PCE nanocomposites and their seeding performance in cement has not yet been revealed. This study investigates the effect of pH values present during the precipitation of C-S-H on the structure, morphology and particle size of C-S-H – PCE nanocomposites and their influence on early strength enhancement of cement.

Experimental

The C-S-H – PCE nanocomposites were synthesized by co-precipitation method from aqueous 61.3 wt. % $Ca(NO_3)_2 . 4H_2O$ and 34.8 wt. % of $Na_2SiO_3 . 5H_2O$ solutions in the presence of 6.7 wt. % of a commercial IPEG-PCE solution. The pH value of the C-S-H suspensions was controlled at 10.4 and 11.7 by addition of 1 M HNO_3 and at 12.4 and 13.8 by adding 30 wt. % NaOH. After stirring for 24 hours, the suspensions were directly used in the particle size analysis, TEM, and mortar testing. Moreover, the C-S-H – PCE samples were centrifuged, washed with DI water and freeze dried, and then the C-S-H powder was investigated by XRD and ^{29}Si MAS NMR measurements. The amount of PCE adsorbed on C-S-H particles was examined via TOC analysis.

Results and Discussion

The XRD patterns of the C-S-H – PCE nanocomposites are illustrated in **Fig. 1**. The result shows a broad peak at pH = 10.4 signifying an amorphous phase. While at pH values ≥ 11.7, semi-crystalline C-S-H was observed with the main hk0 reflections of 100, 110, 200 and 020 at 16.7, 29.0, 31.9 and 49.7 ° 2θ, respectively. Moreover, the (002) reflection signifying the basal spacing between silicate layers in the C-S-H structure was found only in the C-S-H – PCE synthesized at pH = 13.8 where the same d spacing as in pure C-S-H (d = 1.05 nm) was observed. This probably reveals no incorporation of PCE into the interlayers of the C-S-H at pH = 13.8.

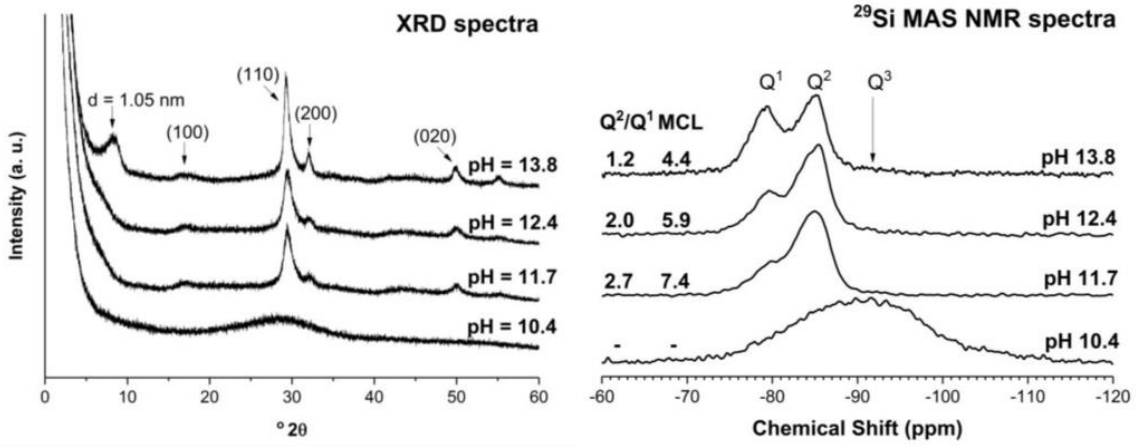

Figure 1: XRD patterns and ^{29}Si MAS NMR spectra of the C-S-H – PCE nanocomposites synthesized at different pH values

In ^{29}Si MAS NMR spectroscopy (**Fig. 1**), the spectrum of C-S-H – PCE nanocomposite synthesized at pH = 10.4 shows a broad peak covering the range for Q^1, Q^2 and Q^3 sites, signifying terminal, middle and branching silicate, respectively. However, at higher pH values

(> 10.4), the spectra illustrate only the Q^1 and Q^2 signals and a reduction in the fraction of Q^2 was detected. This led to a decrease in the degree of polymerization (Q^2/Q^1) and the mean chain length (MCL) of the silicates which reflect a lower degree of polymerization. The highest MCL of ~ 7 was found in the C-S-H sample synthesized at pH = 11.7.

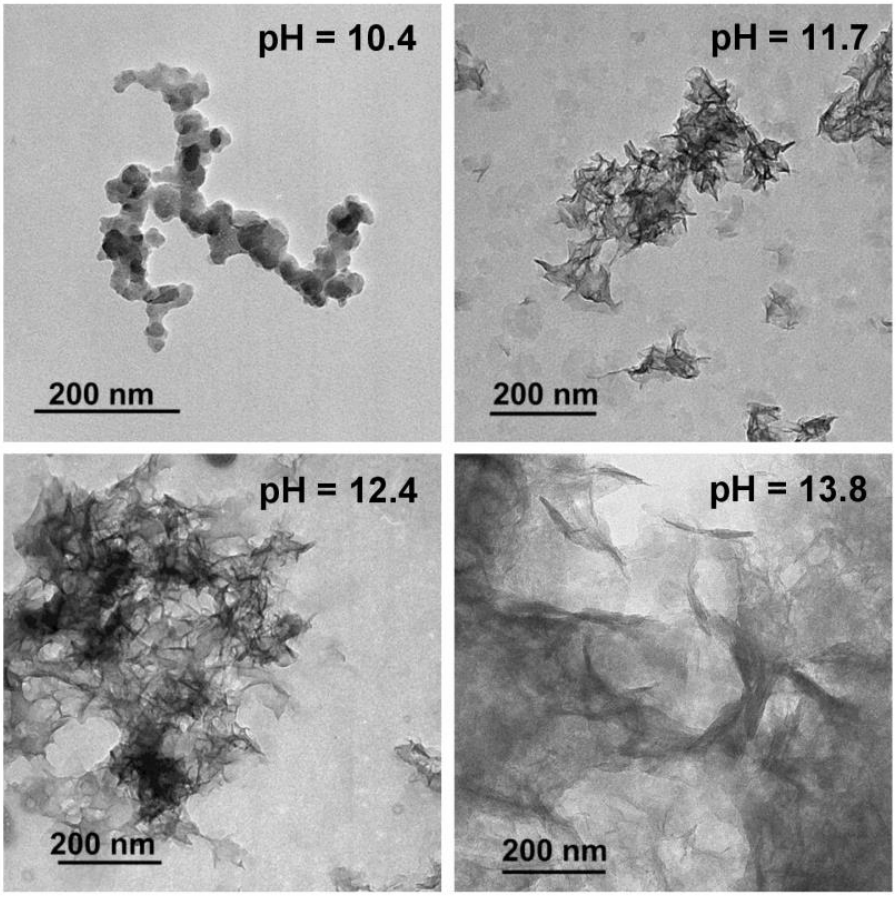

Figure 2: TEM images of C-S-H – PCE particles obtained at pH values from 10.4 to 13.8

TEM images of the synthesized C-S-H – PCE nanocomposites obtained at different pH values are presented in **Fig. 2**. Globular and agglomerated C-S-H particles were clearly found at pH = 10.4. Diameters of globules were ~ 50 nm for single particles and ~ 500 nm for the agglomerates. Foil-like morphology was observed at pH values of ≥ 11.7. The smallest C-S-H – PCE nanofoils with lengths of ~ 50 nm resulted at pH = 11.7. At pH = 13.8, the size of C-S-H foils raised to > 100 nm. Furthermore, DLS analysis (**Fig. 3a**) of the C-S-H – PCE particles prepared at pH 10.4, 11.7 and 12.4 revealed bimodal particle size distributions which contain an average size of ~ 50 to ~ 200 nm. However, at pH = 13.8, a trimodal size distribution consisting of

particles ~ 50 nm, ~ 300 nm and ~ 1 μm was detected. The small size fraction (< 100 nm) of the C-S-H – PCE composites was highest at pH = 11.7, while the larger particle fraction (> 100 nm) was highest at pH = 10.4. The smaller size of C-S-H particles is required for a seeding effect in cement.

Generally, C-S-H attains a positively charged surface when it is applied in a highly alkaline solution containing calcium ions. This allows PCEs to adsorb on their surfaces via calcium complexation. Thus, the main function of PCEs is to stabilize the C-S-H particles into a particular small size. Even, the pH values during the synthesis affected the amount of sorbed PCE on C-S-H (**Fig. 3b**). At pH = 10.4, the sorbed amount of PCE was ~ 170 mg/g, whereas at pH = 11.7, ~ 250 mg/g C-S-H were consumed. Then at pH =12.4 and 13.8, the sorbed amounts decreased to ~ 220 and ~ 140 mg/g, respectively. This result suggests that a higher amount of PCE adsorbed on C-S-H led to a smaller size of the C-S-H composites.

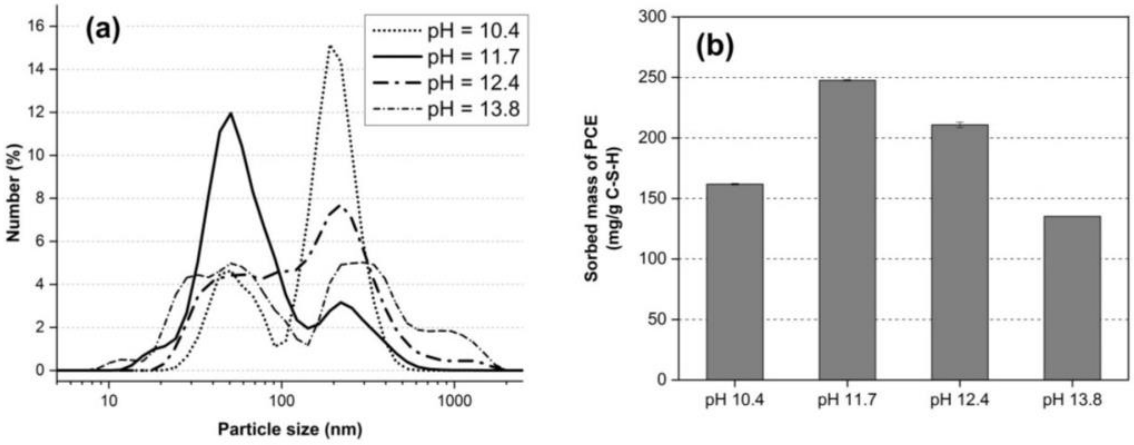

Figure 3: Particle size distribution of the C-S-H – PCE nanocomposites (a) and the amount of PCE sorbed on C-S-H (b) prepared at various pH values

The 16 hours compressive strength of mortar admixed with 0.35 % bwoc (as solid) of C-S-H suspension (pH = 11.7) containing the highest fraction of small nanofolis (~ 50 nm) was found at 11.4 N/mm^2, representing a 100 % increase over the neat cement (**Fig. 4**). However, a higher amount of the large size fraction of C-S-H – PCE nanofoils obtained at pH = 12.4 and 13.8 affected the seeding efficiency in cement, leading to an increase in the compressive strengths of 10.5 and 8.8 N/mm^2, respectively. While, the globule-like C-S-H – PCE nanocomposite (pH = 10.4) consisting of abundant agglomerated particles was less effective as a seeding material, leading to the lowest compressive strength of 7.6 N/mm^2. Thus, the

effectiveness of C-S-H – PCE nanocomposites for early strength enhancement of mortar depends on both morphology and particle size which are influenced by the pH value during the synthesis.

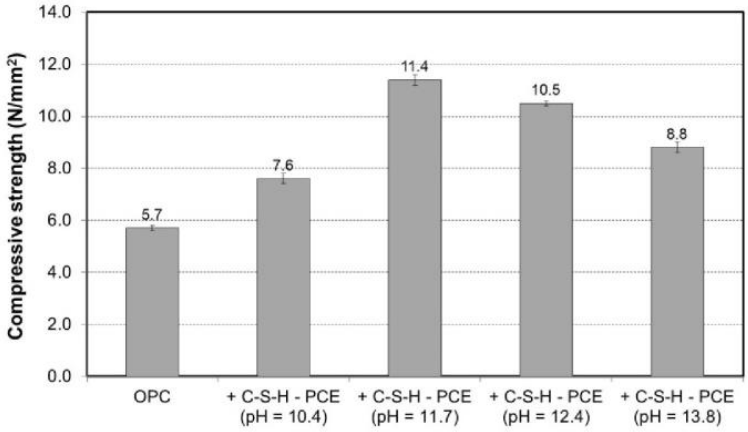

Figure 4: Compressive strength of mortars cured for 16 hrs at 20 ° C, > 95 % RH and admixed with 0.35 % bwoc of the C-S-H – PCE nanocomposites synthesized at different pH values; cement: oil well cement API Class G (Dyckerhoff)

Conclusions

C-S-H – PCE nanocomposites were prepared by co-precipitation from Na_2SiO_3 and $Ca(NO_3)_2$ solutions in the presence of an IPEG PCE copolymer. Different pH conditions existing during the synthesis affect the nanostructure, morphology and the average particle size of the C-S-H – PCE composites. It was found that the C-S-H – PCE nanocomposite synthesized at pH = 11.7 is the semi-crystalline structure and it contains the smallest foil-like particles. As a result, it shows an extreme accelerating effect in cement hydration and achieves the largest gain in early strength of mortar.

References

/1/ J.J. Thomas, H.M. Jennings, J.J. Chen: "Influence of nucleation seeding on the hydration mechanisms of tricalcium silicate and cement"; J. Phys. Chem. C. (2009) 113, 4327-4334

/2/ L. Nicoleau: "Accelerated growth of calcium silicate hydrates: experiments and simulations"; Cem. Concr. Res. (2011) 41, 1339-1348

/3/ V. Kanchanason, J. Plank: "C-S-H – PCE nanocomposites for enhancement of early strength of Portland cement"; in: C. Shi, Y. Yao (Eds.) 14th ICCC, Beijing, China (2015) Proceedings CD, Section 4: Admixtures

/4/ A. Kumar, P. Bowen, K. Scrivener: "Synthetic calcium silicate hydrate with high calcium to silicon ratio"; in: C. Shi, Y. Yao (Eds.) 14th ICCC, Beijing, China (2015) Proceedings CD, Section 2: Hydration of Portland cement

Paper #5

Effectiveness of C-S-H – PCE nanocomposites possessing globular and foil-like morphology on early strength development of Portland cement

V. Kanchanason, J. Plank

2nd ICCCM International Conference on the Chemistry of Construction Materials, Technische Universität München, Munich, Germany, GDCh-Monograph, 50 (2016) 85 – 88.

Effectiveness of C-S-H – PCE Nanocomposites Possessing Globular and Foil-Like Morphology on Early Strength Development of Portland Cement

V. Kanchanason and J. Plank
Technische Universität München, Garching, Germany

Abstract

Nanosized C-S-H – PCE nanocomposites can act as seeding material for Portland cement. It was found that the pH value during the synthesis strongly affects particle size and morphology of the C-S-H – PCE composites. Furthermore, the influence of different particle size and morphology of C-S-H on the early strength of cement was investigated. The results reveal that the nanofoil morphology of C-S-H obtained at pH values > 11.6 consistently provide a superior seeding effect in cement when compared with C-S-H globules obtained at pH = 10.4.

Introduction

Blended cements (CEM II/III) or concrete works performed in cold climates face the problem of too slow development of early strength. It has been established before that synthetic nanoscale C-S-H can accelerate cement hydration /1/. However, the accelerating effect greatly depends on the size of the C-S-H particles and the prevention of C-S-H particle agglomeration controlled by the addition of polycarboxylates (PCEs) /2/. Furthermore, the structure and morphology of C-S-H depends on the process parameters during the synthesis such as pH, molar ratio CaO/SiO_2, temperature, etc. /3-4/.

In this study, the effect of pH present during the precipitation of C-S-H on the particle size and morphology of C-S-H – PCE nanocomposites and their effect on early strength of cement was investigated. Moreover, a mechanism explaining their seeding efficiency in cement based on heat flow calorimetry and ^{29}Si MAS NMR spectroscopy is presented.

Experimental

The C-S-H – PCE nanocomposites were precipitated from aqueous 61.3 wt. % $Ca(NO_3)_2 \cdot 4H_2O$ and 34.8 wt. % of $Na_2SiO_3 \cdot 5H_2O$

solutions in the presence of 6.7 wt. % of an IPEG-PCE (VIVID® 710, Shanghai Sunrise Polymer Material Co., Ltd.). The pH value of the C-S-H suspensions was controlled at 10.4 and 11.6 by addition of 1 M HNO_3 and at 12.4 by adding 30 wt. % NaOH. After stirring for 24 hours, the suspensions were directly used in the measurements such as particle size analysis, TEM, heat flow calorimetry, ^{29}Si MAS NMR spectroscopy and mortar testing.

Results and Discussion

DLS analysis (**Fig. 1**) of the C-S-H – PCE particles revealed a bimodal particle size distribution. The larger size fraction (> 100 nm) of the C-S-H composites was lowest at pH = 11.6 and highest at pH = 10.4. Furthermore, a TEM image **(Fig. 2**) of the C-S-H – PCE nanocomposite prepared at pH = 10.4 shows globular morphology with a diameter of ~ 50 nm for individual particles and ~ 200 nm for agglomerates. Whereas at pH = 11.6 and 12.4, a foil-like morphology of the particles with lengths of ~ 50 nm and 5 nm thickness is observed.

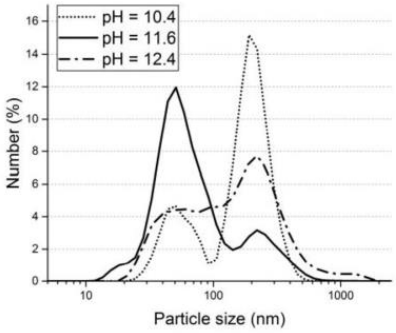

Figure 1: Particle size distribution of the C-S-H – PCE nanocomposites synthesized at different pH values

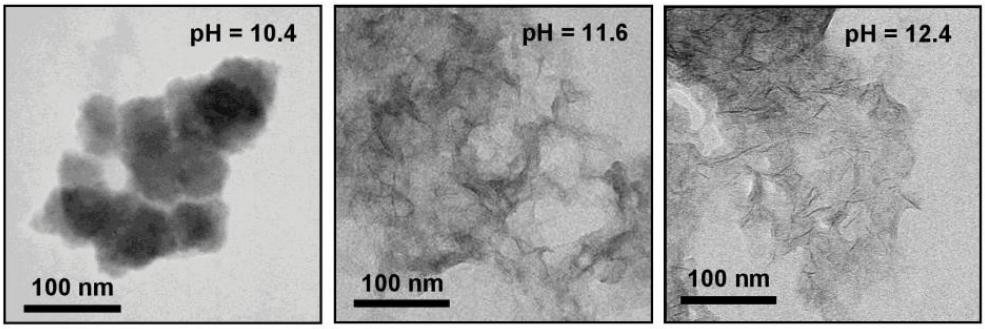

Figure 2: TEM images of C-S-H – PCE particles prepared at different pH values

The 16 hours compressive strengths of mortars admixed with foil-like C-S-H particles (pH = 11.6) which contain the largest amount of the small size fraction (~ 50 nm) were found at 10 N/mm^2, representing a 100 % increase over the neat cement (**Fig. 3**). Furthermore, the C-S-H – PCE nanocomposite synthesized at pH = 12.4 shows a compressive strength of 9 N/mm^2. Whereas, the globule-like C-S-H – PCE nanocomposites (pH = 10.4) containing numerous agglomerated particles are less effective as seeding material and increase the compressive strength only by ~ 30 %. For the flexural strengths of the mortars, the same trend as for the compressive strengths was found. Thus, the enhancement in early strength depends on both morphology and particle size of the C-S-H – PCE nanocomposites which are controlled by the pH during the synthesis.

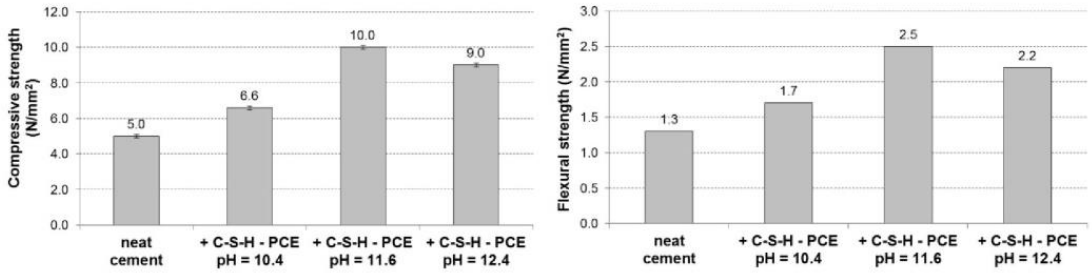

Figure 3: Compressive and flexural strengths of mortars cured for 16 hrs and admixed with 0.35 % bwoc of the C-S-H – PCE nanocomposites synthesized at different pH values; cement : Oil well cement API Class G (Dyckerhoff)

The addition of C-S-H – PCE nanofoils (pH = 11.6 and 12.4) to cement can accelerate and enhance C_3S and C_2S hydration which was also observed via isothermal heat flow calorimetry (**Fig. 4a**). Even for the nanocomposite synthesized at pH = 10.4 which consists of large globules, a slight increase in heat flow during the acceleration period was noticed.

In ^{29}Si MAS NMR spectroscopy, the silicate present in C-S-H produced from cement hydration (**Fig. 4b**) shows signals at - 71 ppm (Q^0 of non-hydrated C_3S and C_2S), at - 79 ppm (Q^1 of terminal silicate) and at - 82 and - 84 ppm (Q^2, Si in the middle of silicate chain). The Q^2/Q^1 ratios of the cement paste admixed with C-S-H – PCE nanofoils (pH = 11.6 and 12.4) are higher than those for globular C-S-H (pH = 10.4) and the pure cement paste. The higher Q^2/Q^1 ratio indicates a higher condensation of mono silicates to polysilicates in C-S-H and explains the higher early strengths of the mortars. The mechanism behind is that nanofoils present a much more adopted template for the

growth of fibrillar C-S-H in cement which requires a linear arrangement of ions. Furthermore, the foils possess a much higher surface area than the globules and therefore are more effective as seeding material.

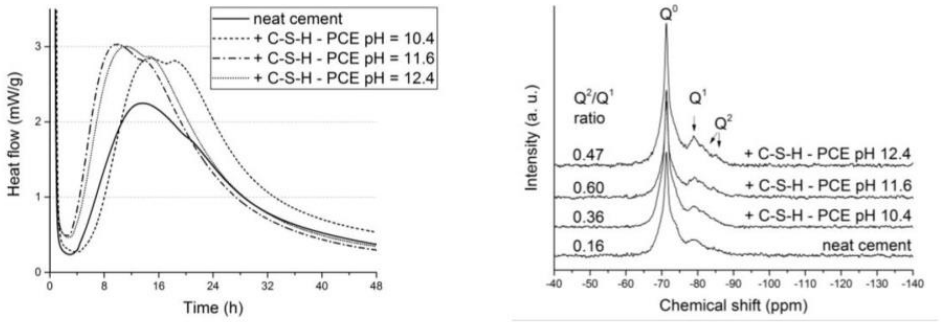

Figure 4: Heat evolution during cement hydration (left), ^{29}Si MAS NMR spectra (right) of pure API class G cement (w/c = 0.44) and admixed with 0.35 % bwoc of the C-S-H – PCE nanocomposites obtained at different pH values

Conclusions

C-S-H – PCE nanocomposites were synthesized by co-precipitation from Na_2SiO_3 and $Ca(NO_3)_2$ solutions in the presence of an IPEG PCE copolymer. Different pH values during the synthesis affect the morphology and the average particle size of the C-S-H – PCE composites. As a result, the C-S-H – PCE nanocomposite prepared at pH = 11.6 consists of the smallest foil-like particles and exhibits the strongest seeding effect for the hydration of cement. Accordingly, such nanofoils achieve the largest gain in early strength of mortar.

References

/1/ R. Alizadeh, L. Raki, J. M. Makar, J. J. Beaudoin, I. Moudrakovski: “Hydration of tricalcium silicate in the presence of synthetic calcium-silicate-hydrate”; J. Mater.Chem. (2009) 19, 7937-7946

/2/ L. Nicoleau, T. Gädt, L. Chitu, G. Maier, O. Paris: “Oriented aggregation of calcium silicate hydrate platelets by the use of comb-like copolymer”; Soft Matter (2013) 9, 4864-4874

/3/ I. G. Richardson: “Tobermorite/jennite- and tobermorite/calcium hydroxide-based models for the structure of C-S-H: applicability to hardened pastes of tricalcium silicate, β-dicalcium silicate, Portland cement, and blends of Portland cement with blast-furnace slag, metakaolin, or silica fume”; Cem. Concr. Res. (2004) 34, 1733-1377

/4/ E. T. Rodriguez, I. G. Richardson, L. Black, E. Boehm-Courjault, A. Nonat, J. Skibsted: “Composition, silicate anion structure and morphology of calcium silicate hydrates (C-S-H) synthesized by silica-lime reaction and by controlled hydration of tricalcium silicate”; Adv. Appl. Ceram. (2015) 114, 362-371

5.3 Application of the C-S-H – PCE nanocomposite as an accelerator in blended cements

The previous studies have demonstrated that the C-S-H – PCE nanocomposite can act as an excellent seeding material for Portland cement and enhances the early strength of e.g. mortar. Here, the effectiveness of a C-S-H – PCE nanocomposite on the early strength development of blended cements made from fly ash, slag and calcined clay was investigated.

5.3.1 Fly ash blended cement

In this publication, the effectiveness of a C-S-H – PCE nanocomposite on the early strength development of mortar and concrete produced from a fly ash blended cement was addressed. Additionally, the mechanism of using the C-S-H – PCE seeding admixture in the blended cement was studied via in-situ XRD and calorimetric measurements.

It was found that the C-S-H – PCE nanocomposite drastically enhanced the early strength of mortar and concrete, particularly at 6 - 24 hours of hydration, without any adverse effect on final strength at 28 days. Furthermore, this admixture improved the workability of fresh mortar and concrete, leading to a significant reduction in the dosage of superplasticizer in the mix design.

The hydration of the silicate phases (C_3S/C_2S) present in the clinker was extremely accelerated by the C-S-H – PCE nanocomposite, as monitored by isothermal heat flow calorimetry. Moreover, a continuous consumption of Portlandite starting at ~ 9 hours of curing was observed via in-situ XRD measurement. This indicated that the C-S-H – PCE nanocomposite can even stimulate the pozzolanic reaction of the fly ash in the blended cement, an extremely important result, as it makes the use of such low CO_2 cements more practical.

Based on these results it can be concluded that the C-S-H – PCE nanocomposite can accelerate both the hydration of cement and the pozzolanic reaction of the fly ash, leading to exceptionally high early strength values.

Paper #6

Effectiveness of a calcium silicate hydrate – polycarboxylate ether (C-S-H–PCE) nanocomposite on early strength development of fly ash cement

V. Kanchanason, J. Plank

Construction and Building Materials, 169 (2018) 20 – 27.

Construction and Building Materials 169 (2018) 20–27

Contents lists available at ScienceDirect

Construction and Building Materials

journal homepage: www.elsevier.com/locate/conbuildmat

Effectiveness of a calcium silicate hydrate – Polycarboxylate ether (C-S-H–PCE) nanocomposite on early strength development of fly ash cement

V. Kanchanason [a,b], J. Plank [a,*]

[a] Technische Universität München, Chair of Construction Chemistry, 85747 Garching, Lichtenbergstraße 4, Germany
[b] Siam Research and Innovation Company, 51 Moo 8, Tub Kwang, Kaeng Khoi, Saraburi 18260, Thailand

HIGHLIGHTS

- Synthetic C-S-H–PCE nanocomposite prepared by co-precipitation from Na_2SiO_3/$Ca(NO_3)_2$.
- C-S-H–PCE enhances early strength (6–24 h) of mortar and concrete of fly ash cement.
- No any adverse effect on final strength.
- C-S-H–PCE accelerates silicate hydration
- C-S-H–PCE also stimulates the pozzolanic reaction of fly ash.

GRAPHICAL ABSTRACT

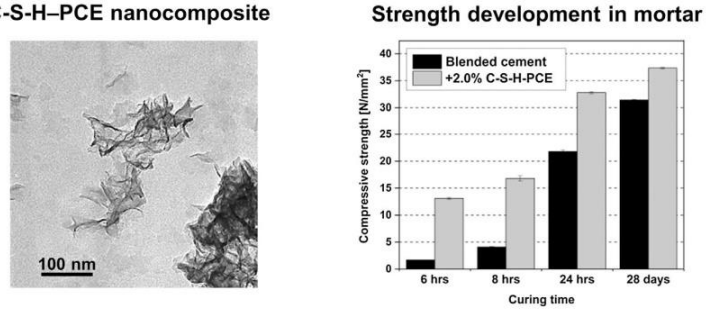

ARTICLE INFO

Article history:
Received 14 July 2017
Received in revised form 5 December 2017
Accepted 7 January 2018

Keywords:
C-S-H
Polycarboxylate
Nucleation
Early strength
Fly ash blended cement

ABSTRACT

C-S-H–PCE nanocomposites are known seeding materials for Portland cement. Here, the effectiveness of a C-S-H–PCE admixture on early strength development of a fly ash blended cement (35 wt% fly ash) was investigated. It was found that addition of C-S-H–PCE drastically increases the compressive strength of mortar and concrete, particularly at 6–24 h of hydration. XRD and calorimetric measurements confirm that the hydration of C_3S/C_2S in cement is greatly accelerated. Most interestingly, however, the C-S-H–PCE nanocomposite also stimulates the pozzolanic reaction of fly ash, thus explaining the exceptionally high early strength values. Accordingly, C-S-H–PCE might also be useful in other CEM II cements holding pozzolanic materials.

1. Introduction

CO_2 emissions resulting from cement production are owed to the decarbonation of $CaCO_3$, the calcination and the milling process. About 900 kg of CO_2 are released for every ton of clinker produced, thus producing approximately 5% of global anthropogenic carbon dioxide emissions [1,2]. Clinker substitution with supplementary cementitious materials (SCMs) such as fly ash, blast furnace slag, limestone etc. such as in blended cements (CEM II/III) allows to reduce CO_2 emission from cement production, making these cements more environmentally friendly. However, the drawback of blended cements is their slow development of early strength owed to the slow pozzolanic reaction of SCMs.

* Corresponding author.
E-mail address: sekretariat@bauchemie.ch.tum.de (J. Plank).

https://doi.org/10.1016/j.conbuildmat.2018.01.053
0950-0618/

Generally, calcium based salts such as calcium chloride, nitrate or formate are used as accelerators to increase the rate of hydration and to boost the early strength of Portland cement [3]. In fly ash blended cements, several studies reported an increase of early strength through addition of accelerating admixtures such as sodium sulfate (Na_2SO_4) [4,5] or alkanolamines (e.g. triethanolamine, TEA; diethanolamine, DEA; tri-isopropanolamine, TIPA etc.) [6,7]. However, those admixtures sometimes led to a decreased final strength.

Recently, several organic-inorganic or pure inorganic nanocomposites have been introduced for the purpose of improving the properties of concrete. Typical examples include polycarboxylate/-graphene oxide nanocomposites [8], polycarboxylate/SiO_2 core shell particles [9], TiO_2-coated nano-SiO_2 [10] and SiO_2/TiO_2 nanocomposites [11]. The main effects sought from them were higher compressive and/or tensile strength and anti-bacterial action.

Calcium silicate hydrate ($xCaO \cdot ySiO_2 \cdot zH_2O$, C-S-H) is well known as the primary hydration product of Portland cement. It acts as the binding phase and is accountable for the strength development and durability of hardened cement. Recently, synthetic C-S-H particles have been used as an accelerator to enhance early cement hydration [12–16]. However, they produce only a minor accelerating effect owed to their relatively large size, possibly due to agglomeration and/or OSTWALD ripening. To avoid these effects, the size of the C-S-H particles can be controlled to nanoscale by the addition of polymeric dispersants such as polycarboxylates (PCEs) [17–19]. Such particularly small C-S-H particles achieved by specific PCE molecules exhibit a huge surface area which produces an extremely strong seeding effect for the hydration of C_3S/C_2S [20,21], leading to significantly higher early strength of Portland cement [22–25]. Consequently, such admixtures based on C-S-H–PCE nanocomposites allow increased production rates e.g. in the manufacturing of precast or prestressed concrete. The improvement of early strength is even more desirable for concrete products made from blended cements. However, so far no report on the effectiveness of C-S-H–PCE nanocomposites on the strength development of a fly ash blended cement has been presented.

In this paper, the effectiveness of a C-S-H–PCE nanocomposite on the development of early strength (6–24 h) of mortar and concrete produced from a fly ash blended cement is investigated. Additionally, the impact of the C-S-H–PCE admixture on the workability of mortar and concrete in terms of superplasticizer consumption to achieve a specific fluidity was addressed. Finally, the working mechanism of the C-S-H–PCE seeding admixture in the blended cement was studied via in-situ X-ray diffraction (XRD) measurements and isothermal heat flow calorimetry.

2. Materials and methods

2.1. Materials

The chemicals used for the preparation of the C-S-H–PCE seeding admixture were $Ca(NO_3)_2 \cdot 4H_2O$ (PanReac AppliChem, Germany) and $Na_2SiO_3 \cdot 5H_2O$ (VWR Prolabo BDH Chemicals, Germany). Moreover, NaOH (Merck KGaA, Germany) and HNO_3 (65 wt%; VWR Prolabo BDH Chemicals, Germany) were used to adjust the pH values of the PCE solution and during the synthesis, respectively. As PCE superplasticizer, a commercial IPEG-PCE ("VIVID" from Sunrise Co., Ltd., Shanghai/China) was used. Its chemical structure is presented in Fig. 1 and the properties of the IPEG-PCE polymer sample are listed in Table 1.

A fly ash-blended cement (Type IP according to ASTM C595, corresponding to a CEM II/B-V) [26] containing 35 wt% of fly ash Class F was used in the tests. Oxide composition (determined by XRF), density and specific surface area (*Blaine*) of this cement are listed in Table 2.

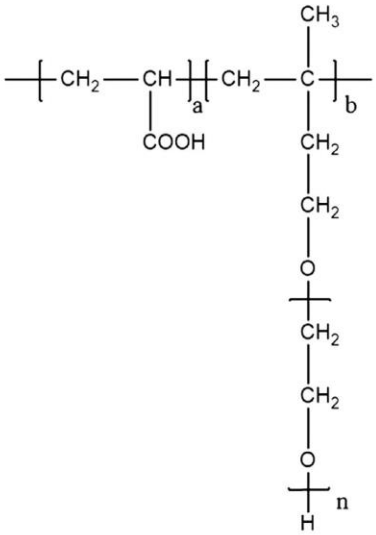

Fig. 1. Chemical structure of the isoprenyl oxy poly(ethyleneglycol) (IPEG) based PCE superplasticizer used in the study.

Table 1
Molecular properties and specific anionic charge density of the IPEG-PCE sample.

Molar masses (g/mol)		Polydispersity index	Specific anionic charge density in NaOH at pH = 11.7
M_w	M_n	(*PDI*)	(μeq/g)
35,100	15,700	2.2	2,750

For mortar preparation, a standard graded sand according to ASTM C778 (particle size of 150–600 μm) was employed. As to concrete, the gradation of the aggregates was based on ASTM C33 [27] and is listed in Table 3.

2.2. Synthesis of C-S-H–PCE nanocomposite

The C-S-H–PCE nanocomposite was prepared by the co-precipitation method whereby aqueous $Ca(NO_3)_2$ and Na_2SiO_3 solutions were fed into a solution of the IPEG-PCE. First, 625.8 g of the IPEG-PCE solution (solids content 6.7 wt%) were placed in a 2 L flask and the pH of this PCE solution was adjusted to 8.0 ± 0.1 by using aqueous 30 wt% NaOH. Next, solutions of 105.0 g (0.45 mol) of $Ca(NO_3)_2 \cdot 4H_2O$ in 66.4 mL of water ($Ca(NO_3)_2$ concentration 42.6 wt%) and 95.9 g (0.45 mol) of $Na_2SiO_3 \cdot 5H_2O$ in 179.8 mL of water (Na_2SiO_3 concentration 20 wt%) were prepared in a water bath at 75 °C and then cooled to ambient. After that, both solutions were constantly fed at 6.8 mL/min (Ca-nitrate) and 13.0 mL/min (Na-silicate) to the PCE solution while stirring at 300 rpm under N_2 atmosphere and at 20 °C. Total addition time was 18 min. Moreover, the pH of the suspension was controlled at 11.7 ± 0.1 by the addition of 1 M HNO_3 as needed. Once the addition of $Ca(NO_3)_2$ and Na_2SiO_3 was finished, the white suspension was stirred for another 24 h at room temperature and then used as is in the tests.

Table 2
Chemical composition and physical properties of the fly ash blended cement.

Composition (%)										Density (g/cm^3)	*Blaine* value (m^2/kg)
CaO	SiO_2	Al_2O_3	SO_3	Fe_2O_3	MgO	K_2O	Na_2O	TiO_2	LOI*		
50.8	24.9	9.9	2.4	7.1	1.7	0.9	1.1	0.3	0.9	3.0	410

* Loss on ignition.

Table 3
Gradation of the aggregates used in the concrete mix.

Sand		Gravel	
Size (mm)	wt%	Size (mm)	wt%
4.75	2	25.00	–
2.36	7	19.00	8
1.18	16	12.50	45
0.60	28	9.50	22
0.30	27	4.75	20
0.15	20	2.36	5

2.3. Test methods

2.3.1. Characterization techniques for C-S-H–PCE nanocomposite

Powder X-ray diffraction (XRD) patterns were obtained from a BRUKER AXS D8 diffractometer (Karlsruhe, Germany) with *Bragg – Brentano* geometry working at 30 kV and 35 mA with Cu Kα radiation between 3.0° and 60° 2θ.

FT-IR spectra of C-S-H, PCE and the C-S-H–PCE nanocomposite were recorded in the range of 400–4000 cm^{-1} on a BRUKER Vertex 70 spectrometer (Bruker, Ettlingen, Germany) equipped with an ATR cell.

Particle size of C-S-H–PCE nanocomposite was measured via dynamic light scattering (DLS) using a Zetasizer Nano ZS apparatus (Malvern Instruments, Workestershire, UK). The sample was suspended in water at a concentration of 0.1 g/L.

Morphology of the C-S-H–PCE nanocomposite was captured on a transmission electron microscopy (TEM) performed on a JEOL JEM 2011 instrument (JEOL, Japan) equipped with a LaB_6 cathode.

2.3.2. Mortar testing

The C-S-H–PCE seeding admixture was tested for its effectiveness as a strength enhancer in a standard mortar prepared from the fly ash blended cement according to ASTM C109 at a water-to-cement (w/c) ratio of 0.41 [28]. Dosages of 0.8%, 1.4% and 2.0% (as solid by weight of cement; bwoc) of the C-S-H–PCE nanocomposite were applied. Moreover, the workability of the mortar was controlled at 20.0 ± 1.0 cm by using the IPEG-PCE superplasticizer. A defoamer (DOWFAX DF141, Dow Chemical, USA) was applied to keep the fresh mortar density at 2300 ± 10 kg/m^3. The freshly prepared mortar was cast into 50 × 50 × 50 mm molds and cured for 6, 8, 12, 16 and 24 h in a climate chamber at a temperature of 23 ± 2 °C and a relative humidity >95%. For each formulation, three cubes were prepared and the values shown later for their compressive strength present the average for the three specimens. The mortar cubes were demolded after 1 day and then cured in saturated lime solution until 28 days. The compressive strength data were collected from an UH-2000kNI instrument from Shimadzu Corporation, Kyoto, Japan (Fig. 2).

2.3.3. Concrete testing

Concrete was prepared in a 30 L pan-type mixer according to ASTM C192 [29] and its mix proportion is listed in Table 4. The fly ash blended cement was used at 400 kg/m^3, the ratio of aggregates-to-cement was 4.5 and the w/c ratio was fixed at 0.41. IPEG-PCE superplasticizer was used to adjust the workability of the fresh concrete to a slump value of 16 ± 0.5 cm. The dosages of the C-S-H–PCE nanocomposite tested were 0.8% and 2.0% bwoc. Additionally, a defoamer (DOWFAX DF141) was used to achieve a constant fresh concrete density of 2420 ± 10 kg/m^3. Concrete samples were cast into 100 × 100 × 100 mm molds and cured for 6, 8, 10, 12, 16 and 24 h in a climate room at 23 ± 2 °C and a relative humidity >95%. Again, three cubes were prepared for each formulation, and the averages were reported later as compressive strengths. To obtain the 7 and 28 day values, the specimens were removed from the molds after 1 day and then cured in saturated lime solution.

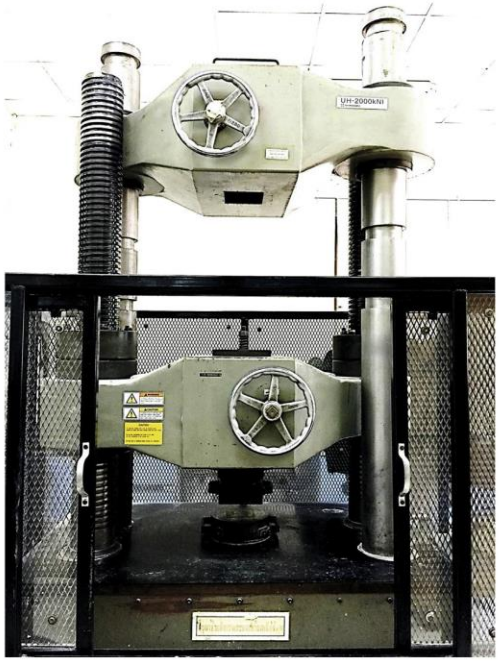

Fig. 2. Compressive strength test apparatus used in the experiments.

2.3.4. Isothermal heat flow calorimetry

Hydration kinetics was tracked by isothermal heat flow calorimetry. A cement paste was prepared from 40 g of cement and 16.4 g of water (w/c = 0.41). Both components were mixed in a plastic container under stirring with a mechanical stirrer (IKA-Werke GmbH & Co. KG, Germany) at 300 rpm for 1 min which was then increased to 600 rpm for another 1 min. From this paste, 3g were transferred to a glass ampule and placed in a calorimeter (TAM AIR, Thermometric, Järfälla, Sweden) equilibrated to 20 °C. Dosages of the C-S-H–PCE nanocomposite were 0.8%, 1.4% and 2.0% (as solid) bwoc.

Table 4
Mix proportions of the concrete samples.

Mixes	Proportion (kg/m^3)				PCE (wt%)	C-S-H–PCE (wt%)	w/c	Slump (cm)
	Cement	Gravel	Sand	Water				
Blended cement	400	1100	710	164	0.21	–	0.41	15.5
+0.8% C-S-H–PCE	400	1100	710	164	0.16	0.8	0.41	16.0
+2.0% C-S-H–PCE	400	1100	710	164	0.08	2.0	0.41	16.5

2.3.5. In situ XRD

The development of phases during the hydration of cement was investigated by in-situ XRD using a BRUKER AXS D8 diffractometer (Karlsruhe, Germany) with *Bragg – Brentano* geometry working at 40 kV and 30 mA with Cu Kα radiation (reflexes between 8° and 44° 2θ evaluated). Total measuring time was 48 h. A cement paste was prepared from 8 g of the blended cement, 3.28 g of water (w/c = 0.41) and optionally 0.79 g (equivalent to 2.0% bwoc) of the C-S-H–PCE nanocomposite, and mixed for 2 min. After that, 4.3 g of this paste were placed on the metal holder and covered with a Kapton foil (7.6 μm thick polyimide) supplied by VHG Labs (Manchester, USA) to minimize carbonation and dehydration during measurement.

3. Results and discussion

3.1. Properties of the C-S-H–PCE nanocomposite

In the following, the composition and some physical properties of the synthesized nanocomposite will be discussed.

The XRD pattern of the C-S-H–PCE nanocomposite (see Fig. 3a) reveals a semi-crystalline material with the main hk0 reflections of 100, 110, 200 and 020 at 16.7, 29.0, 31.9 and 49.7° 2θ, respectively. Moreover, the (002) reflection signifying the basal spacing between individual silicate layers in the C-S-H structure was found to be the same as in pure C-S-H (d = 1.28 nm), thus indicating that the PCE polymer has not been incorporated into the C-S-H structure [25].

Fig. 3b composes the FT-IR spectra of the C-S-H, the pristine PCE polymer and the C-S-H–PCE nanocomposite obtained in the co-precipitation process. The occurrence of absorptions in the nanocomposite which are characteristic for the PCE polymer (e.g. the asymmetric and symmetric vibrations of the COO^- group present in the main chain of PCE at 1565 and 460 cm^{-1}, respectively, or the C-O valence vibration of the ether bond present in the side chain of PCE at 1100 cm^{-1}) confirm the formation of a nanocomposite whereby the PCE polymer has only adsorbed onto the surfaces of the C-S-H particles and is not chemically incorporated into the structure of C-S-H.

Particle size analysis (Fig. 3c) of the C-S-H–PCE nanocomposite via dynamic light scattering revealed a bimodal particle size distribution. According to this, the C-S-H–PCE precipitate contains

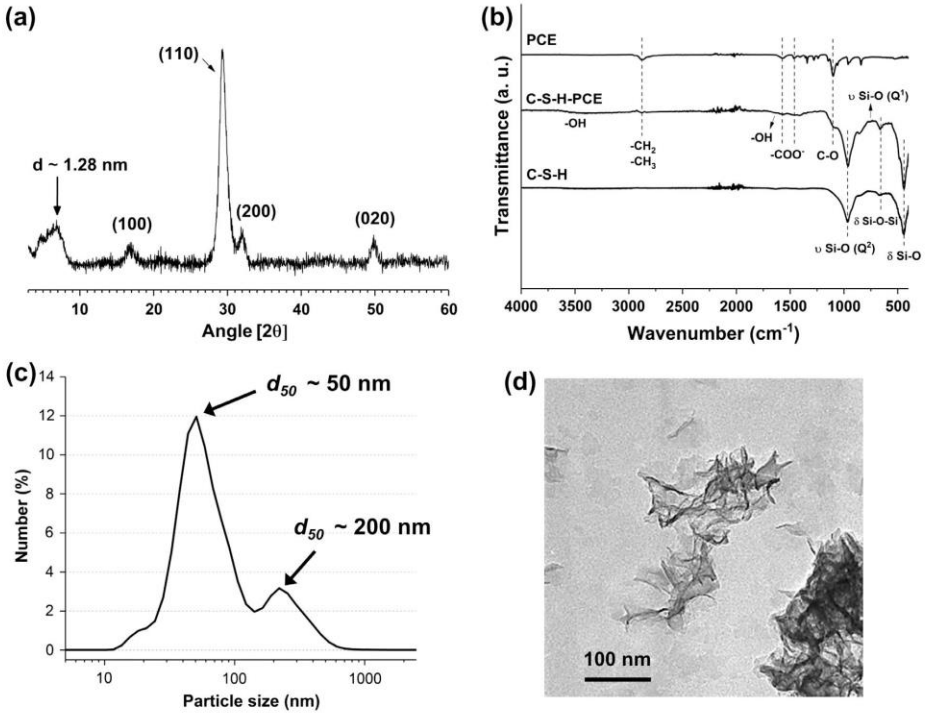

Fig. 3. (a) XRD pattern, (b) FT-IR spectra, (c) particle size distribution and (d) TEM image of the synthesized C-S-H–PCE nanocomposite.

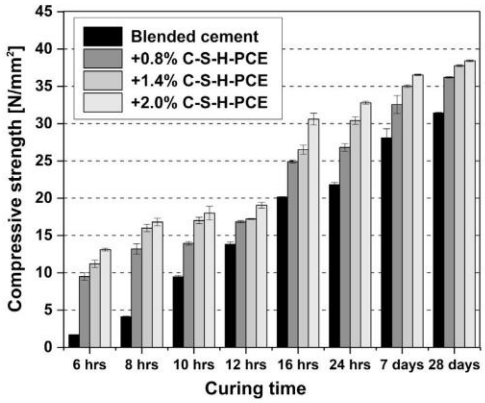

Fig. 4. Compressive strength of mortar samples after 6, 8, 10, 12, 16, 24 h, 7 and 28 days of curing at 23 °C and >95% relative humidity.

a larger fraction of small particles ($d_{50} \sim 50$ nm) and a minor fraction of particles with $d_{50} \sim 200$ nm. Presumably, the small particle fraction is responsible for the seeding (strength accelerating) effect in cement. Moreover, a TEM image (Fig. 3d) reveals a foil-like morphology for the synthesized C-S-H–PCE nanocomposite, with an average length of ~50 nm and a thickness of ~5 nm.

3.2. Early strength development of mortar

Mortars admixed with 0.8, 1.4 and 2.0 wt% of the C-S-H–PCE nanocomposite were prepared, and their compressive strengths were determined after 6, 8, 10, 12, 16, 24 h, 7 and 28 days of curing.

The results displayed in Fig. 4 and Table 5 demonstrate that addition of the C-S-H–PCE compound clearly promotes the strength development, in particular after 6–24 h of curing. Also, a higher dosage (2.0 wt%) of the accelerating admixture increased the compressive strength significantly. Most impressively, the 6 h compressive strength values of 9.5, 11.2 and 13.1 N/mm^2 obtained from 0.8, 1.4 and 2.0 wt% respectively of C-S-H–PCE were 470–690% over that of the control sample. Thereafter, the difference between the control sample and the admixed samples decreased. For example, at 8 h the increase in compressive strength of the mortar containing the nanocomposite had dropped to 220–300% over the control sample. Generally, higher C-S-H–PCE dosages resulted in higher strength values, albeit the increase was relatively minor, considering the extra cost involved. Interestingly, even after 28 days of curing the compressive strength of the mortar specimens containing the C-S-H–PCE accelerator still exhibited 15–22% higher strength than the control sample.

The results clearly demonstrate that even in highly blended (e.g. 35 wt% fly ash) cements the C-S-H–PCE nanocomposite can boost the early strength considerably, in spite of the low clinker factor of such cements. However, for such blended cements higher dosages (0.8–2.0 wt%) of the nanocomposite are required compared to pristine OPC where 0.3–0.6 wt% appear to be sufficient [19].

3.3. Effectiveness in concrete

3.3.1. Properties of fresh concrete

All concrete samples prepared were adjusted to a slump value of 16 ± 0.5 cm (Table 4). The slump of the control sample (no C-S-H–PCE nanocomposite present) was adjusted to 16 ± 0.5 cm by using the IPEG-PCE superplasticizer (SP). Addition of the C-S-H–PCE nanocomposite to the concrete always increased concrete fluidity (presumably because of free dissolved PCE polymer present in the nanocomposite) and allowed to decrease the dosage of the IPEG-PCE required to achieve the slump of ~16 cm. With increasing dosage of the nanocomposite the SP consumption decreased even further. For instance, in the concrete sample holding 2.0 wt % of the C-S-H–PCE compound, the required dosage of SP was only 0.08 wt% which presents a 62% decrease compared to the control sample without the C-S-H–PCE (Table 4). This result indicates that the C-S-H–PCE nanocomposite not only enhances the early strength of concrete (see section below), but also significantly improves its workability.

3.3.2. Early strength development

The results on the compressive strength development of the concrete samples with and without the C-S-H–PCE nanocomposite are displayed in Fig. 5 and Table 5.

At first, the effect of dosage of the C-S-H–PCE nanocomposite (0.8 wt% or 2.0 wt%) on the strength development of concrete after 6–12 h of curing was studied. Like in mortar, it was found that the concrete samples holding nanocomposite always produced considerably higher compressive strengths compared to the control sample. Furthermore, again only a slight improvement in compressive strength at higher dosages of the C-S-H–PCE nanocomposite was found. Thus, based on more favorable cost-effectiveness, all further tests were conducted using exclusively 0.8% bwoc of the nanocomposite.

Fig. 6 presents the compressive strength results for concretes containing 0.8% wt C-S-H–PCE nanocomposite cured over a time period from 6 h to 28 days. The results demonstrate that the nanocomposite provides its most pronounced effect in the first hours of cement hydration (especially at 6–12 h). For example, at 6 h the compressive strength of the concrete holding the nanocomposite was 600% higher than that of the control. Interestingly, and different to common salt-based accelerators such as e.g. $CaCl_2$, the 28 day compressive strength still was ~9% higher than that of the

Table 5
Compressive strength enhancement (%) of mortar and concrete samples at different curing times.

Sample	Compressive strength enhancement (%)[a] at							
	6 h	8 h	10 h	12 h	16 h	24 h	7 days	28 days
Mortar								
0.8% C-S-H–PCE	460	220	48	22	24	23	16	15
1.4% C-S-H–PCE	560	290	80	25	32	39	25	20
2.0% C-S-H–PCE	670	310	90	38	52	50	30	22
Concrete								
0.8% C-S-H–PCE	600	230	155	90	34	24	6	9

[a] Strength enhancement = $\frac{\text{Strength of sample} - \text{Strength of control cement}}{\text{Strength of control cement}} \times 100\%$

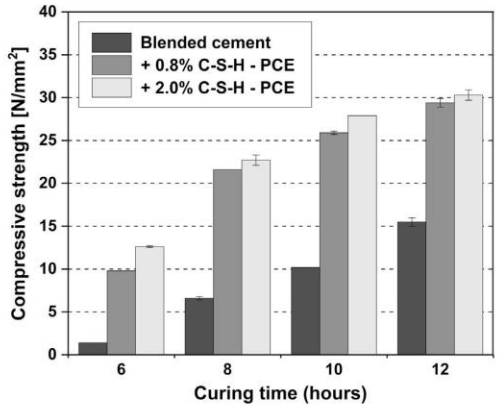

Fig. 5. Compressive strength of concrete specimens holding 0%; 0.8% or 2.0% bwoc of the C-S-H–PCE nanocomposite, measured after 6–12 h of curing at 23 °C, >95% relative humidity.

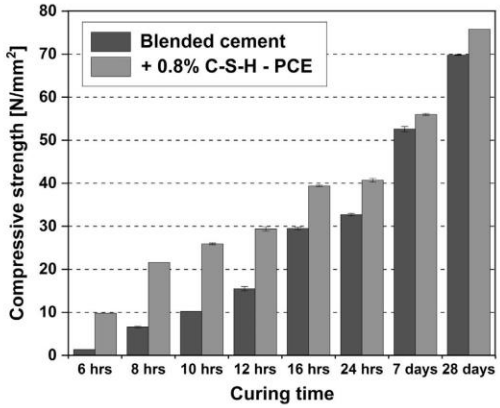

Fig. 6. Compressive strength of concrete specimens holding 0% or 0.8% bwoc of the C-S-H–PCE nanocomposite, cured from 6 h to 28 days.

control sample. Obviously, there is no penalty for the superior early strength gained by the C-S-H–PCE accelerating admixture.

These results imply that the C-S-H–PCE nanocomposite presents a superior seeding material which can drastically enhance the early strength of concrete based on a fly ash blended cement, especially during the first 12 h of hydration, without any negative effect on the final strength (28 days). This finding makes a more widespread use of such blended cements considerably more attractive and can help to reduce the negative environmental impact from cement production.

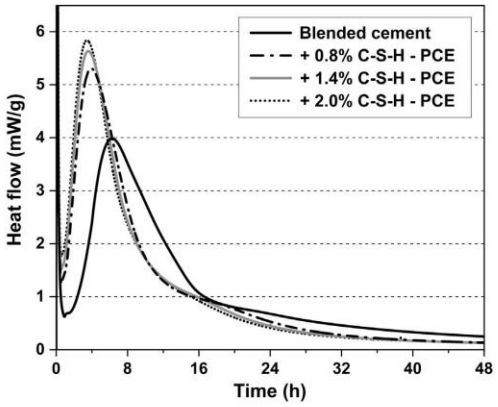

Fig. 7. Time – dependent heat evolution of the fly ash-blended cement admixed with 0.8, 1.4 and 2.0% bwoc of the C-S-H–PCE nanocomposite.

3.4. Mechanistic investigations

3.4.1. Calorimetry

The impact of the C-S-H–PCE nanocomposite on the hydration of the fly ash blended cement was observed via isothermal heat flow calorimetry (Fig. 7 and Table 6).

It was observed that addition of the C-S-H–PCE nanocomposite significantly accelerated cement hydration by shifting the peak assigned to the silicate hydration to earlier times. At the same time, the total heat released during the accelerating period increased. This main peak stems from the nucleation and growth of the C-S-H and Portlandite phases, indicating enhanced hydration of the silicate phases [30].

Like in the test on compressive strengths (Figs. 4-6), the accelerating effect was dependent on the dosage of the C-S-H–PCE compound. And, again similar to the strength tests, also here in the calorimetry higher dosages of the additive produced only a relatively minor improvement.

The cumulative heat flow of the cement pastes with and without C-S-H–PCE nanocomposite are illustrated in Table 6 and Fig. 8.

The results clearly show an increased heat flow for the blended cement admixed with the nanocomposite starting after ~1.5 h. A larger dosage of the additive achieved only a slightly higher total heat release. For example, the cumulative heat released during the first 6 h was 58.0 J/g for the reference cement, and 95.7, 103.5 and 108.7 J/g at 0.8, 1.4 and 2.0 wt% addition of C-S-H–PCE, respectively.

As can be seen, the C-S-H–PCE admixture acts as a seeding material and greatly reduces the activation energy barrier which needs to be overcome to initiate C-S-H nucleation [22,25]. This way, hydration of the silicate phases C_3S and C_2S commences much earlier. In view of the low clinker content of the cement used in the study here (only 65 wt%), the pronounced accelerating effect of the

Table 6
Maximum rate of heat flow and cumulative heat of the fly ash cement admixed with C-S-H–PCE nanocomposite.

Samples	Maximum rate of heat flow		Cumulative heat (J/g)			
	t_{max} (h)	q_{max} (mW/g)	6 h	10 h	12 h	24 h
Blended cement	6.2	4.0	58.0	108.2	125.6	171.2
+0.8% C-S-H–PCE	3.9	5.3	95.7	135.9	146.6	184.2
+1.4% C-S-H–PCE	3.6	5.6	103.5	140.4	151.3	187.5
+2.0% C-S-H–PCE	3.4	5.8	108.7	144.2	155.2	189.3

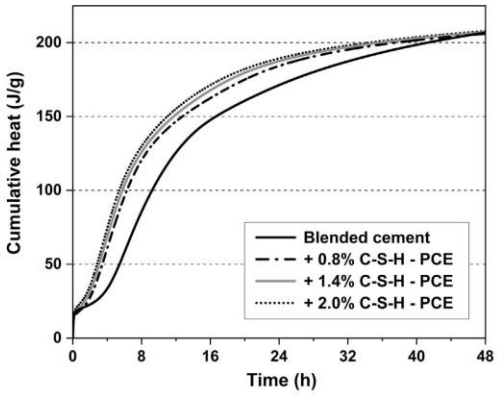

Fig. 8. Cumulative heat of hydration of the fly ash cement admixed with 0.8, 1.4 and 2.0% bwoc of the C-S-H–PCE nanocomposite.

nanocomposite is surprising. It gave rise to speculations as to whether the nanocomposite can even promote the pozzolanic reaction of fly ash. This was investigated in the following experiments.

3.4.2. Effect on pozzolanic reaction

In-situ XRD was carried out of the hydrating fly ash cement with and without C-S-H–PCE nanocomposite to track the silicate hydration via the amount of Portlandite produced during the first 48 h of hydration [31]. In our evaluation, the strong reflection signifying Portlandite at 18° 2θ (ICDD: 44-1481) was used [32] (Fig. 9).

It was found that when the cement was admixed with the nanocomposite, the reflection assigned to Portlandite was much more pronounced and appeared very early (after ~2 h). This indicates again that the C-S-H–PCE nanocomposite strongly promotes the silicate hydration.

Moreover, the relative intensities of the Portlandite reflections appearing at 18° 2θ were plotted over time (Fig. 10). For the neat cement, an increase in intensity was clearly observed during the

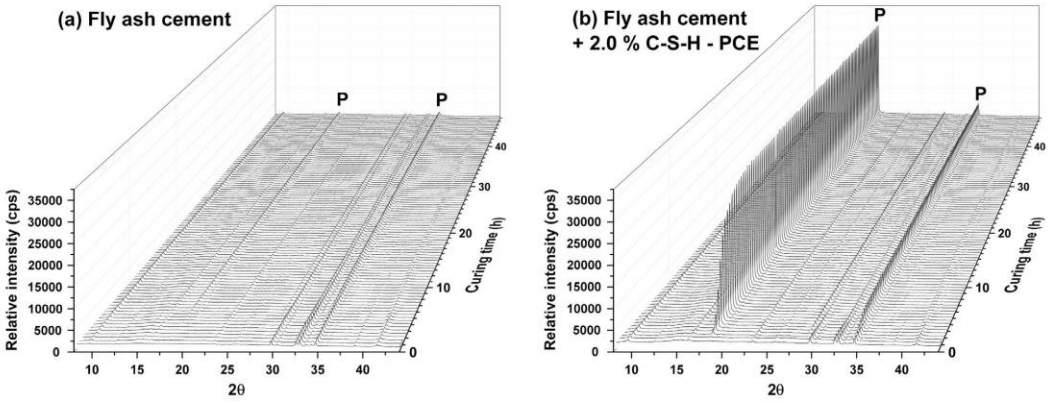

Fig. 9. In situ XRD patterns over 48 h of hydration of (a) fly ash cement paste and (b) this cement admixed with 2.0 wt% of C-S-H–PCE nanocomposite. P represents the reflections for Portlandite at 18° and 34.1° 2θ (ICDD: 44-1481), respectively.

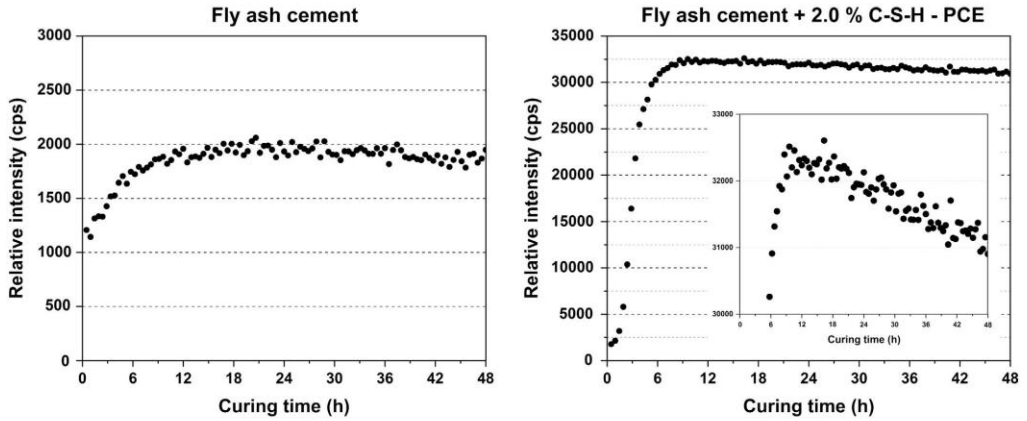

Fig. 10. Intensity of Portlandite reflections at 18° 2θ from in-situ XRD measurements of fly ash cement hydrated with and without C-S-H–PCE nanocomposite.

first 12 h until it leveled out to a constant value. However, when the seeding admixture was used, the increase occurred significantly earlier, was much more pronounced and already peaked at ~9 h of curing. Most remarkably, after that the amount of Portlandite decreased slightly, but steadily. This observation suggests that Portlandite is consumed over time through another reaction, presumably the pozzolanic reaction of fly ash which also produces C-S-H [32]. For fly ash cements, it is well established that the decrease in Portlandite resulting from the pozzolanic reaction typically commences only after 28 days of curing [33–35]. Whereas here, in this fly ash cement admixed with 2.0 wt% of C-S-H–PCE, this decrease already shows at about 15 h of hydration, and thus much earlier than in the non-seeded cement (see insert in Fig. 10).

These findings infer that the C-S-H–PCE nanocomposite accelerates both the hydration of the silicate phases present in the clinker, and – most interestingly – even the pozzolanic reaction of the fly ash.

4. Conclusions

A C-S-H–PCE nanocomposite was successfully synthesized via co-precipitation of aqueous Na_2SiO_3 and $Ca(NO_3)_2$ in an IPEG-PCE solution. The C-S-H–PCE nanocomposite promotes the early strength development of mortar or concrete prepared from a fly ash blended cement considerably, particularly in the first 12 h of hydration, without reducing final strength (28 days). Furthermore, the C-S-H–PCE accelerating admixture improves the workability of fresh mortar and concrete and allows to reduce the superplasticizer dosage required to achieve a certain spread flow or slump value.

Moreover, in situ XRD measurements revealed that the C-S-H–PCE nanocomposite not only accelerates the hydration of the silicate phases present in the clinker, but also promotes the pozzolanic reaction of the fly ash substantially, as was evidenced by a continuous consumption of Portlandite starting at ~9 h of curing. This effect distinguishes the C-S-H–PCE nanocomposite from all other salt-based accelerators such as calcium nitrate or formate which stimulate the silicate reaction, but have no impact at all on the pozzolanic reaction.

Acknowledgements

The authors would like to thank Ms. Benjaluk Na Lampang and Dr. Punnaman Norrarat (Siam Research and Innovation Company; SRI) for conducting the mortar and concrete tests. V.K. is most indebted to SCG Cement-Building Materials for financial support of her study.

References

[1] C.A. Hendriks, E. Worrell, D. de Jager, K. Blok, P. Riemer, Emission reduction of greenhouse gases from the cement industry, in: The proceeding of the greenhouse gas control technologies conference, 2004. http://www.wbcsdcement.org/pdf/tf1/prghgt42.pdf (accessed 23.08.04).
[2] World Business Council for Sustainable Development (WBCSD) and International Energy Agency (IEA), Cement technology roadmap 2009: carbon emissions reductions up to 2050, 2009, 1–36.
[3] P.C. Hewlett, Lea's chemistry of cement and concrete, fourth ed., Butterworth-Heinemann Publishing, Oxford, 2003.
[4] J. Qian, C. Shi, Z. Wang, Activation of blended cements containing fly ash, Cem. Concr. Res. 31 (2001) 1121–1127.
[5] C.Y. Lee, H.K. Lee, K.M. Lee, Strength and microstructural characteristics of chemically activated fly ash–cement systems, Cem. Concr. Res. 33 (2003) 425–431.
[6] K. Riding, D.A. Silva, K. Scrivener, Early age strength enhancement of blended cement systems by $CaCl_2$ and diethanol-isopropanolamine, Cem. Concr. Res. 40 (2010) 935–946.
[7] K. Hoang, H. Justnes, M. Geiker, Early age strength increase of fly ash blended cement by a ternary hardening accelerating admixture, Cem. Concr. Res. 81 (2016) 59–69.
[8] L. Zhao, X. Guo, C. Ge, Q. Li, L. Guo, X. Shu, J. Liu, Investigation of the effectiveness of PC@GO on the reinforcement for cement composites, Constr. Build. Mater. 113 (2016) 470–478.
[9] Y. Gu, Q. Ran, X. Shu, C. Yu, H. Chang, J. Liu, Synthesis of nanoSiO_2@PCE core-shell nanoparticles and its effect on cement hydration at early age, Constr. Build. Mater. 114 (2016) 673–680.
[10] B. Han, Z. Li, L. Zhang, S. Zeng, X. Yu, B. Han, J. Ou, Reactive powder concrete reinforced with nano SiO_2-coated TiO_2, Constr. Build. Mater. 148 (2017) 104–112.
[11] P. Sikora, K. Cendrowski, A. Markowska-Szczupak, E. Horszczaruk, E. Mijowska, The effects of silica/titania nanocomposite on the mechanical and bactericidal properties of cement mortars, Constr. Build. Mater. 150 (2017) 738–746.
[12] J.J. Thomas, H.M. Jennings, J.J. Chen, Influence of nucleation seeding on the hydration mechanisms of tricalcium silicate and cement, J. Phys. Chem. C 113 (2009) 4327–4334.
[13] R. Alizadeh, L. Raki, J.M. Makar, J.J. Beaudoin, I. Moudrakovski, Hydration of tricalcium silicate in the presence of synthetic calcium-silicate-hydrate, J. Mater. Chem. 19 (2009) 7937–7946.
[14] M.H. Hubler, J.J. Thomas, H.M. Jennings, Influence of nucleation seeding on the hydration kinetics and compressive strength of alkali activated slag paste, Cem. Concr. Res. 41 (2011) 842–846.
[15] K. Owens, M.I. Russell, G. Donnelly, A. Kirk, P.A.M. Basheer, Use of nanocrystal seeding chemical admixture in improving Portland cement strength development: application for precast concrete industry, Adv. Appl. Ceram. 113 (8) (2014) 478–484.
[16] G. Land, D. Stephan, Preparation and application of nanoscaled C-S-H as an accelerator for cement hydration, in: K. Sobolev, S.P. Shah (Eds.), Nanotechnology in Construction: Proceedings of NICOM5, Springer International Publishing, Cham, 2015, pp. 117–121.
[17] L. Nicoleau, T. Gädt, L. Chitu, G. Maier, O. Paris, Oriented aggregation of calcium silicate hydrate platelets by the use of comb-like copolymer, Soft Matter. 9 (2013) 4864–4874.
[18] J. Plank, E. Sakai, C.W. Miao, C. Yu, J.X. Hong, Chemical admixtures – chemistry, applications and their impact on concrete microstructure and durability, Cem. Concr. Res. 78 (2015) 81–99.
[19] J. Sun, H. Shi, B. Qian, Z. Xu, W. Li, X. Shen, Effects of synthetic C-S-H/PCE nanocomposites on early cement hydration, Constr. Build. Mater. 140 (2017) 282–292.
[20] L. Nicoleau, Accelerated growth of calcium silicate hydrates: experiments and simulations, Cem. Concr. Res. 41 (2011) 1339–1348.
[21] L. Nicoleau, The acceleration of cement hydration by seeding: influence of the cement mineralogy, ZKG Int. 1 (2013) 40–49.
[22] V. Kanchanason, J. Plank, C-S-H–PCE nanocomposites for enhancement of early strength of cement, 19th Ibausil, Bauhaus-Universität Weimar, Tagungsband 1, Weimar, Germany, 2015. pp. 759–766.
[23] V. Kanchanason, J. Plank, C-S-H–PCE nanocomposites for enhancement of early strength of Portland cement, in: C. Shi, Y. Yao (Eds.), 14th ICCC, Beijing, China (2015) Proceedings CD, Section 4: Admixtures.
[24] V. Kanchanason, J. Plank, Effectiveness of C-S-H–PCE nanocomposites possessing globular and foil-like morphology on early strength development of Portland cement, 2nd International Conference on the Chemistry of Construction Materials (ICCCM), Munich Germany, October 10 – 12, GDCh-Monographie 50, 2016, pp. 85–88.
[25] V. Kanchanason, J. Plank, Role of pH on the structure, composition and morphology of C-S-H–PCE nanocomposites and their effect on early strength development of Portland cement, Cem. Concr. Res. 102 (2017) 90–98..
[26] ASTM C595/C595M-17, Standard Specification for Blended Hydraulic Cements, ASTM International, West Conshohocken, PA, 2017.
[27] ASTM C33/C33M-16, Standard specification for concrete aggregates, ASTM International, West Conshohocken, PA, 2002.
[28] ASTM C109/C109M-08, Standard Test Method for Compressive Strength of Hydraulic Cement Mortars (Using 2-in. or [50-mm] Cube Specimens), ASTM International, West Conshohocken, PA, 2016.
[29] ASTM C192/C192M-16a, Standard Practice for Making and Curing Concrete Test Specimens in the Laboratory, ASTM International, West Conshohocken, PA, 2016.
[30] H.F.W. Taylor, Cement chemistry, second ed., Thomas Telford Publishing, London, 1997.
[31] S.T. Bergold, F. Goetz-Neunhoeffer, J. Neubauer, Quantitative analysis of C-S–H in hydrating alite pastes by in-situ XRD, Cem. Concr. Res. 53 (2013) 119–126.
[32] S. Dittrich, J. Neubauer, F. Goetz-Neunhoeffer, The influence of fly ash on the hydration of OPC within the first 44 h – a quantitative in situ XRD and heat flow calorimetry study, Cem. Concr. Res. 56 (2014) 129–138.
[33] E. Sakai, S. Miyahara, S. Ohsawa, Hydration of fly ash cement, Cem. Concr. Res. 35 (2005) 1135–1140.
[34] K. De Weerdt, M. Ben Haha, G. Le Saout, K.O. Kjellsen, H. Justnes, B. Lothenbach, Hydration mechanisms of ternary Portland cements containing limestone powder and fly ash, Cem. Concr. Res. 41 (2011) 279–291.
[35] E. Tkaczewska, Mechanical properties of cement mortar containing fine-grained fraction of fly ashes, Open J. Civil Eng. 3 (2013) 54–68.

5.3.2 Slag blended cement

In this part, the performance of a C-S-H – PCE nanocomposite on the strength development of mortar made from slag blended cement (35 wt. % slag) was studied. Moreover, the working mechanism of the C-S-H – PCE composite which nanocomposite was used in the slag blended cement was elucidated via in-situ XRD and calorimetric measurements.

It was found that the C-S-H – PCE nanocomposite considerably improved the strength development of mortar, particularly within the first 24 hours, without a decrease in the final strength at 28 days of hydration (**Figure 36**).

Interestingly, the nanocomposite also improved the strength development of the mortar during all stages of hydration (6 hrs - 28 days). While, the compressive strength of the mortar prepared from slag cement without nanocomposite showed lower strength values than the OPC.

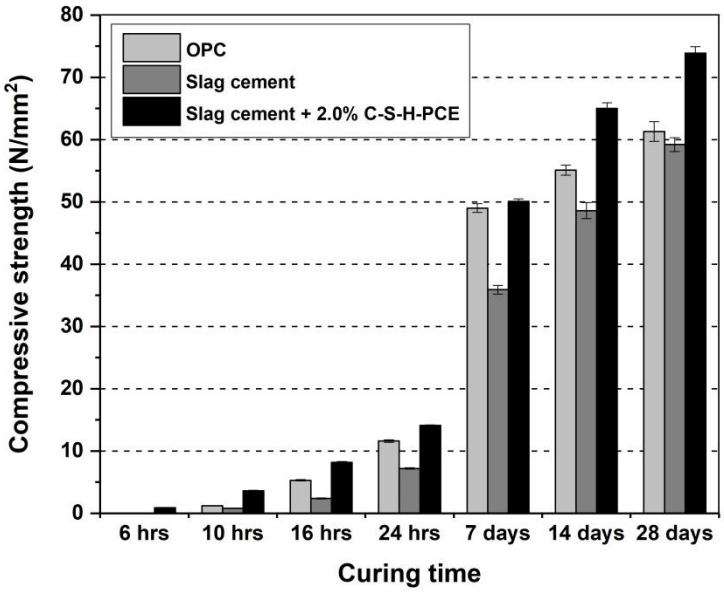

Figure 36: Compressive strength of mortar samples prepared from slag cement (w/b = 0.45) after 6, 10, 16, 24 hours, 7, 14 and 28 days of curing at 20 ° C and > 95 % relative humidity

Hydration of the slag blended cement was tracked by isothermal heat flow calorimetry (**Figure 37**). The results revealed that addition of the C-S-H – PCE nanocomposite to the slag cement significantly accelerated cement hydration and increased the total heat released during the accelerating period which can be assigned to the nucleation and growth of the C-S-H and Portlandite phases from the silicate phases (C_3S, C_2S) in cement.

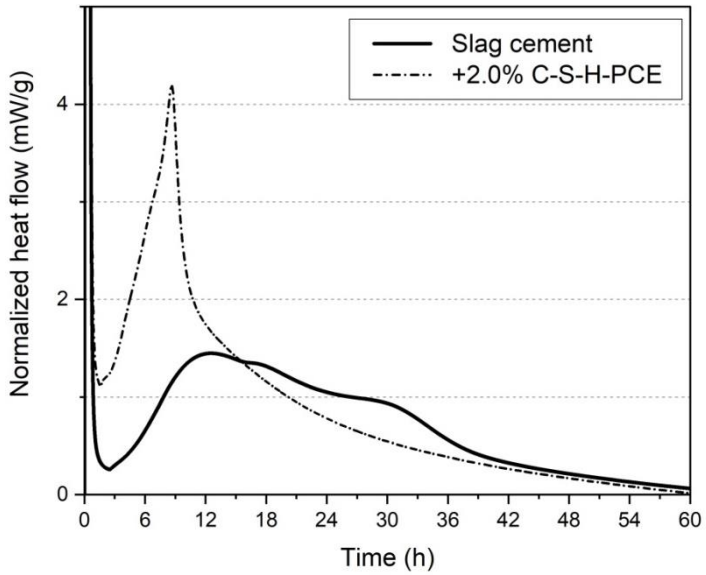

Figure 37: Heat evolution of the slag-blended cement (w/b = 0.45) admixed with 2.0 % bwoc of the C-S-H – PCE nanocomposite

The hydration products such as hemi carboaluminate (Hc) and Portlandite were monitored via in-situ XRD measurement. The relative intensities of the Hc and Portlandite reflections appearing at 10.8 and 18 ° 2θ were plotted over time (**Figure 38**). A continuous consumption of Portlandite starting at ~ 12 hours of curing was found. Additionally, an increase in the amount of Hc generated in the slag cement admixed with the C-S-H – PCE nanocomposite was observed after ~ 12 hours of curing, while the formation of Hc in the neat slag blended cement was detected only after 24 hours. These evidences suggest that Portlandite is

consumed over time through two reactions; presumably the pozzolanic reaction of slag which also produces C-S-H, and the formation of Hc.

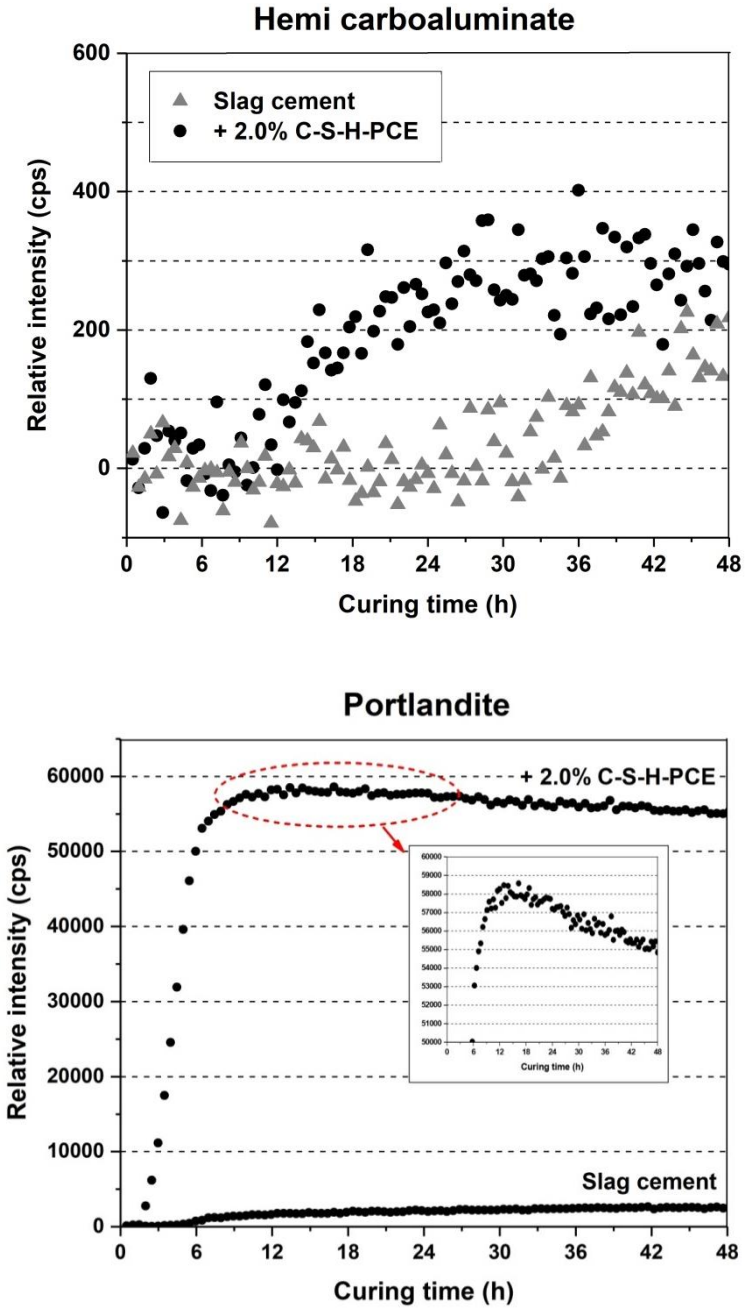

Figure 38: Intensity of hemi carboaluminate (top) and Portlandite (bottom) reflections at 10.8 and 18 ° 2θ respectively from in-situ XRD measurements of the slag cement, hydrated with and without C-S-H – PCE nanocomposite

5.3.3 Calcined clay blended cement

In this section, the effectiveness of a C-S-H – PCE nanocomposite on the strength development of mortar produced from a calcined clay-blended cement (35 wt. % calcined clay) is reported. Furthermore, the impact of the nanocomposite on the pozzolanic reaction in the blended cement was studied via in-situ XRD and calorimetric measurements. As C-S-H – PCE, the product described in paper #6 was selected (Ca/Si = 1.0, pH = 11.7 and 20 ° C).

It was observed that the C-S-H – PCE nanocomposite significantly improved the strength development of a mortar without a reduction in the final strength after 28 days of curing (**Figure 39**). Most impressively, after the first 24 hours the increase was ~ 100 % over that of the control sample. Thereafter, the difference between the control sample and the admixed samples decreased, but still were ~ 10 - 20 % higher than that of the control sample.

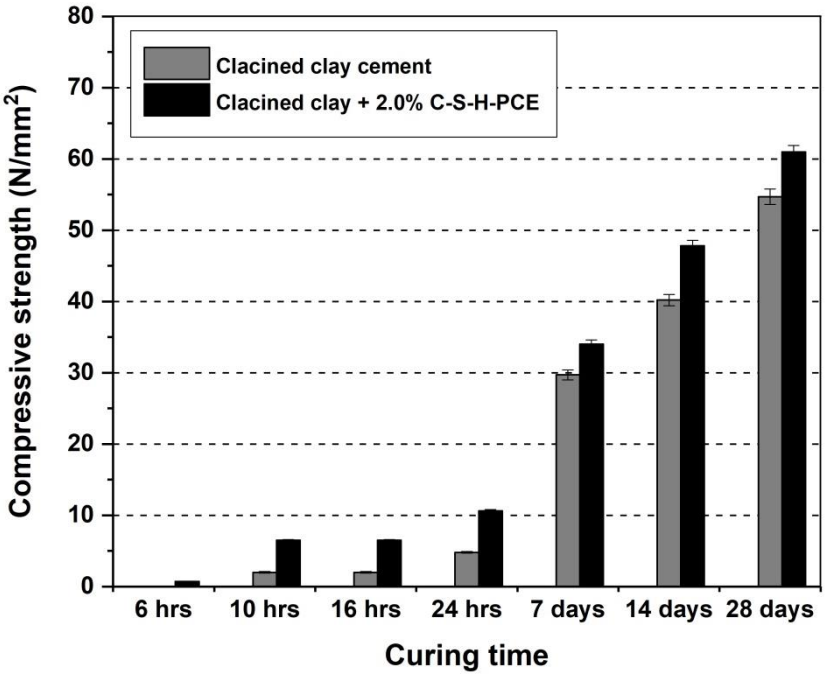

Figure 39: Compressive strength of mortar samples made from a calcined clay-blended cement (w/b = 0.5) after 6, 10, 16, 24 hours, 7, 14 and 28 days of curing at 20 ° C and > 95 % relative humidity

Hydration of the calcined clay blended cement was monitored by isothermal heat flow calorimetry (**Figure 40**). It was found that addition of the C-S-H – PCE nanocomposite to the clacined clay-blended cement considerably accelerated the hydration of the silicate phases present in the clinker and also increased the total heat released during the accelerating period. This behavior was nearly the same as observed in the hydration of the slag blended cement.

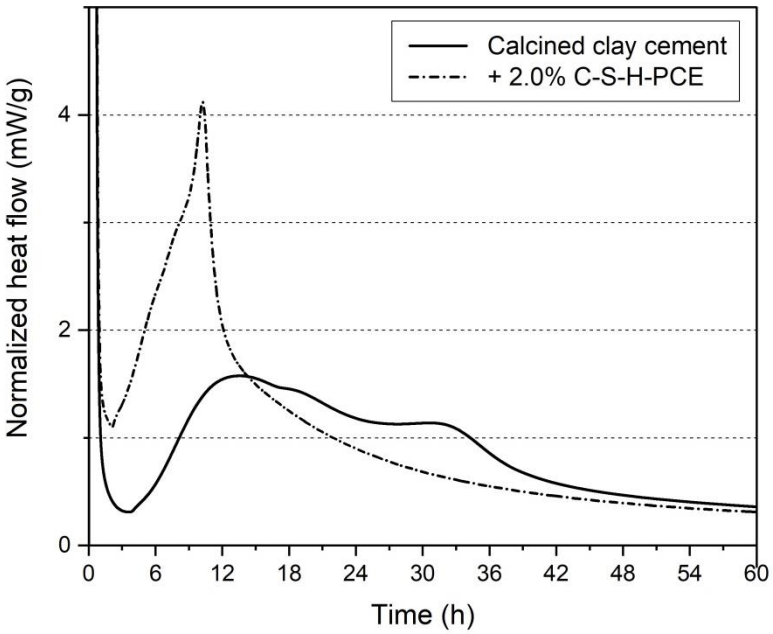

Figure 40: Heat evolution of the calcined clay-blended cement (w/b = 0.5) admixed with 2.0 % bwoc of the C-S-H – PCE nanocomposite

Furthermore, the impact of the nanocomposite on the pozzolanic reaction was studied via XRD measurements. These experiments were conducted to find an explanation for the superior early strength development observed for the calcined clay-blended cement as shown in **Figure 39**.

Figure 41 shows the XRD plot of the relative intensities of the hemi carboaluminate (Hc) and Portlandite reflections appearing at 10.8 and 18 ° 2θ over time, respectively, as monitored via in-situ XRD measurement. An extremely early and strong formation of Hc in

the clacined clay cement admixed with the C-S-H – PCE nanocomposite was observed after ~ 8 hours of curing, while the amount of Hc generated in the neat calcined clay cement increased only after ~ 24 hours. Moreover, a very early consumption of Portlandite starting at ~ 18 hours was detected in the calcined clay cement with the nanocomposite (**Figure 41**). This indicates that the C-S-H – PCE nanocomposite can also accelerate the pozzloanic reaction of calcined clay and stimulate the formation of Hc in the calcined clay cement.

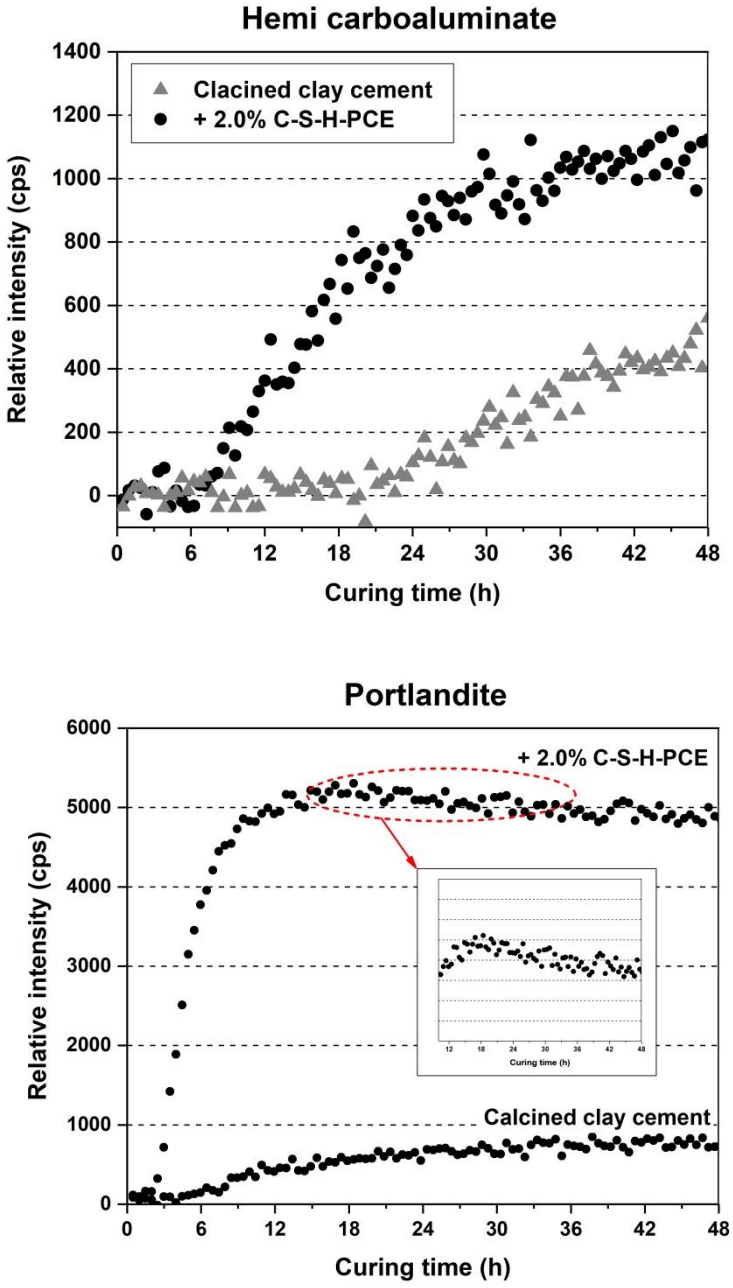

Figure 41: Intensity of hemi carboaluminate (top) and Portlandite (bottom) reflections at 10.8 and 18 ° 2θ respectively from in-situ XRD measurements of the calcined clay cement, hydrated with and without C-S-H – PCE nanocomposite

5.4 Nucleation and growth of the C-S-H – PCE nanocomposites

This part describes the effect of an isoprenyl oxy poly(ethylene glycol) (IPEG) based PCE on the nucleation and crystallization of C-S-H nanofoils.

First, the early nucleation and crystallization of C-S-H between 12 seconds and 24 hours precipitated from $Ca(NO_3)_2$ and Na_2SiO_3 solutions at a Ca/Si ratio of 1.0 in the presence of an IPEG-PCE superplasticizer was investigated by capturing the initial precursors of C-S-H via transmission electron microscopy (TEM). Moreover, the effectiveness of the C-S-H – PCE nanocomposites prepared at different ageing times on the early strength development of mortar was measured.

It was observed that in this precipitation reaction, at first a metastable precursor of C-S-H formed at the beginning exhibits a globular morphology and later converts to C-S-H nanofoils following a non-classical nucleation mechanism. The presence of the IPEG-PCE strongly delays the transformation from globular to nanofoil-like C-S-H for several hours because of a layer surrounding the globules. Because of this slow conversion, particularly small C-S-H nanofoils are produced with excellent seeding effect. Furthermore, the C-S-H nanofoils prepared after 24 hours of ageing exhibit a stronger seeding effect for the hydration and early strength development of cement than those taken from shorter ageing times.

Paper #7

Early nucleation and crystal growth of C-S-H – PCE nanocomposites used as strength enhancers in cement

V. Kanchanason, J. Plank

The 12th International Conference on Superplasticizers and Other Chemical Admixtures in Concrete, Beijing, China, October 28 - October 31, 2018.

(Submitted on 15th December 2017)

EARLY NUCLEATION AND CRYSTAL GROWTH OF C-S-H – PCE NANOCOMPOSITES USED AS STRENGTH ENHANCERS IN CEMENT

Vipasri Kanchanason and Johann Plank

Biography:

Vipasri Kanchanason is a Ph.D. student at the Chair for Construction Chemistry at Technische Universität München, Germany. Her research focuses on calcium silicate hydrate – polycarboxylate ether (C-S-H – PCE) nanocomposites for enhancement of early strength of cement.

Johann Plank is Full Professor at the Institute of Inorganic Chemistry of Technische Universität München, Germany. Since 2001, he holds the Chair for Construction Chemistry there. His research interests include cement chemistry, chemical admixtures, organic-inorganic nanocomposites, latex polymers, colloid chemistry, dry-mix mortars, concrete, oil well cementing and hydraulic fracturing.

ABSTRACT

The influence of an isoprenyl oxy poly(ethylene glycol) (IPEG) based PCE on the nucleation and crystallization of C-S-H precipitated from aqueous solutions of $Ca(NO_3)_2$ and Na_2SiO_3 was investigated. It was found that in the absence of IPEG-PCE, globular nanoparticles of C-S-H with a diameter of ~50 nm are formed. Subsequently, within an hour the globules convert to C-S-H nanofoils with ~150 nm length following a non-classical nucleation mechanism. In the presence of the PCE, the initial globules show a core-shell structure

whereby a layer; presumably PCE polymer, coats the C-S-H core. The shell around the C-S-H globules delays the conversion to the nanofoils for several hours and leads to significantly smaller foils and a superior seeding material in cement.

Keywords: calcium silicate hydrate; polycarboxylate; non-classical nucleation; globules; nanofoils; early strength

INTRODUCTION

The nucleation and crystallization of inorganic minerals is described by two theories. The first, classical nucleation theory is based on the formation and growth of nuclei [1]. The second, non-classical nucleation concept presents that the morphology of the precritical clusters can differ significantly from that of the final bulk crystal [2,3].

Calcium silicate hydrate (C-S-H) is well-known as the main hydration product of ordinary Portland cement. C-S-H presents ~ 60 % of hardened cement and results from the hydration of the tricalcium silicate (C_3S) and dicalcium silicate (C_2S) phases via dissolution-precipitation steps [4]. It presents the binding phase and is also responsible for the strength properties and durability of hardened cement. Generally, C-S-H exhibits low crystallinity and in concrete typically exhibits a Ca/Si molar ratio of ~ 1.6 [5]. The layered structure of C-S-H consists of linear silicate chains which are aligned in segments of “dreierketten” and share oxygen atoms with calcium ions in plane [6].

Polycarboxylate (PCE) superplasticizers are known high range water reducing admixtures for concrete. PCEs improve the rheology via an electrosteric dispersing effect [7]. The structure of anionic comb-like PCE copolymers consists of carboxylate anchor groups at the backbone which are a negatively charged and responsible for the adsorption onto the positively charged

surface sites of cement particles such as from hydration products like ettringite [8-12]. While the non-ionic side chains of PCEs are normally made of polyethylene glycol (PEG) which is accountable for the steric effect promoting dispersing ability [8]. It has been found that specific PCE polymers can exert a noticeable retarding effect on the hydration of the calcium silicates, C_3S and C_2S. Some studies even suggest that these admixtures can induce changes to the nanostructure of C-S-H which can negatively impact the mechanical properties of concrete [13].

Generally, the external surfaces of C-S-H contain silanol groups which are ionized in high alkaline condition and are able to complex with dissolved calcium ions [14]. Consequently, the surfaces of C-S-H exhibit a slightly positive charge which can facilitate the adsorption of anionic comb-like copolymers such as PCE superplasticizers [15].

Synthetic C-S-H – PCE nanocomposites are well-known seeding materials to enhance the early strength of Portland cement and blended cements [15]. They are composed of C-S-H nanofoils which are dispersed via PCE polymers adsorbed onto their positively charged surfaces [16]. A particularly small size of the C-S-H seeds is required to achieve such superior seeding efficiency and consequently, a much enhanced early strength development of concrete [17,18]. In previous works, we have investigated the effect of pH on the structure, composition and morphology of the nanocomposites [17]. However, the effect of reaction and ageing time on the composition and performance of these nanocomposites has not yet been disclosed.

Thus, in this study the very early nucleation and subsequent crystallization of C-S-H (12 seconds - 24 hours) precipitated from $Ca(NO_3)_2$ and Na_2SiO_3 solutions at a Ca/Si ratio of 1.0 in the presence of an IPEG-PCE superplasticizer was investigated by capturing the initial precursors of C-S-H via transmission electron microscopy (TEM). Moreover, the

effectiveness of the C-S-H – PCE nanocomposites prepared at different ageing times on the early strength development of mortar was determined.

RESEARCH SIGNIFICANCE

C-S-H – PCE nanocomposites are being used for early strength enhancement of concrete. However, the formation of these nanocomposites is not yet completely understood and the time-dependence of their effectiveness has not been revealed so far. The ultimate purpose of our study was to explain why the C-S-H – PCE nanocomposites is so much superior over conventional C-S-H nanofoils prepared according to exactly the same method.

EXPERIMENTAL PROCEDURE

Materials

The starting materials used in the synthesis of C-S-H were $Ca(NO_3)_2{\cdot}4H_2O$ (PanReac AppliChem, Germany), $Na_2SiO_3{\cdot}5H_2O$ (VWR Prolabo BDH Chemicals, Germany) and HNO_3 (65 wt. %; VWR Prolabo BDH Chemicals, Germany). As PCE superplasticizer, a commercial IPEG-PCE (Sunrise Co., Ltd., Shanghai, China) was used and the pH value of the PCE solution was adjusted by using NaOH (Merck KGaA, Germany). The chemical structure of the IPEG-PCE is presented in **Fig. 1** and its properties are listed in **Table 1**.

Furthermore, a slowly hydrating Ordinary Portland Cement (OPC) sample (API Class G oil well cement, corresponding to a CEM I 32.5R) obtained from Dyckerhoff GmbH (Germany) was used for testing the early strength development of mortars. Its phase composition was determined by quantitative XRD including *Rietveld* refinement and thermogravimetric analysis. The results are listed in **Table 2**. Its specific surface area (*Blaine*) and mean particle

size (*d50* value) were found at 3,000 cm^2/g and 11 μm, respectively.

Preparation of C-S-H and C-S-H – PCE

The C-S-H and C-S-H – PCE nanocomposite were prepared by the co-precipitation method. Aqueous $Ca(NO_3)_2$ and Na_2SiO_3 solutions were combined in water or the IPEG-PCE solution to obtain either pure C-S-H or the C-S-H – PCE nanocomposite. The initial molar ratio of CaO/SiO_2 based on the starting materials was 1.0. First, 4.2 g of the IPEG-PCE solution (concentration 40 wt. %) were diluted with 20.8 mL of water resulting in a 6.7 wt. % PCE solution which was adjusted to pH = 8.5 ± 0.1 by using aqueous 30 wt. % NaOH. Next, solutions of 4.2 g (18 mmol) of $Ca(NO_3)_2 \cdot 4H_2O$ dissolved in 2.7 mL of water and 3.8 g (18 mmol) of $Na_2SiO_3 \cdot 5H_2O$ in 7.2 mL of water were prepared in a water bath at 75 ° C. After that, both solutions were added continuously and at a constant dosing rate to water or the PCE solution within 8 minutes while stirring at 20 ° C. Morphologies of the resulting C-S-H and C-S-H – PCE respectively were monitored over time via TEM microscopy, first during addition of the $Ca(NO_3)_2/Na_2SiO_3$ solutions (at 12 sec and 2 min), and then 0 h, 3 h, 6 h and 24 h after completion of the addition of the $Ca(NO_3)_2/Na_2SiO_3$ solutions.

Characterization techniques

Micrographs of the C-S-H and C-S-H – PCE samples were collected by transmission electron microscopy (TEM) performed on a JEOL JEM 2011 instrument (JEOL, Japan) equipped with a LaB_6 cathode. Suspensions of pure C-S-H and the C-S-H – PCE nanocomposite respectively were diluted with isopropanol and dispersed in an ultrasonic bath for 2 minutes. After that, 4 μL of the dispersed samples were dropped on a 300 mesh Cu grid with carbon support films (Quantifoil Micro Tools GmbH, Germany) with a plasma-treated surface. The size of the C-S-H and C-S-H – PCE nanofoils and the thickness of the PCE layer on the C-S-H particles were assessed by using ImageJ software.

Mortar testing

The C-S-H – PCE precipitates were tested for their effectiveness as strength enhancing admixture in a standard mortar prepared according to DIN EN 196-1. The dosage of the C-S-H – PCE nanocomposite was 0.35 % (as solid) by weight of cement (bwoc). The water-to-cement (w/c) ratio of the mortar was 0.44. The mortar was cast into 40 x 40 x 160 mm steel prism molds and cured at 20 ± 1 ° C and 90 % relative humidity for 16 hours. After curing, the compressive strengths were measured on a test apparatus provided by Toni Technik (Berlin, Germany).

EXPERIMENTAL RESULTS AND DISCUSSION

Nucleation and crystallization of C-S-H

The early nucleation and crystallization of C-S-H synthesized from Na_2SiO_3 and $Ca(NO_3)_2$ in the absence and presence of an IPEG-PCE copolymer were observed via TEM imaging. Samples taken during the synthesis at 12 seconds and 2 minutes from the beginning of the combination of $Ca(NO_3)_2$/Na_2SiO_3 reveal polydisperse C-S-H and C-S-H – PCE particles exhibiting globular morphology with diameters in the range of ~ 30 – 60 nm (**Fig. 2**). Most interestingly, a thin layer (thickness ~ 5 – 7 nm) surrounding the C-S-H globules was observed on the C-S-H – PCE precipitates, resulting in a core-shell structure. When addition of the raw materials was finished (0 hour of ageing), the C-S-H formed in water only (no PCE present) exhibits a mixture of globules and nanofoils while the C-S-H precipitated in the presence of the IPEG-PCE consists of globules only (**Fig. 3**).

Furthermore, the appearance of the globular C-S-H and C-S-H – PCE precursors was monitored over time via TEM imaging (**Fig. 3**). For the pure C-S-H, the transformation from

globular to foil-like morphology had immediately started after the combination of the $Ca(NO_3)_2/Na_2SiO_3$ solutions was completed. At 3 hours, the initial C-S-H globules had entirely disappeared while a network of C-S-H nanofoils with lengths of > 150 nm was observed. However, TEM imaging of the C-S-H – PCE precipitates revealed a delayed transformation from the initial globules to the nanofoils. At 3 hours of ageing, still a mixture of globules and foils was present while after 6 hours of ageing, the C-S-H globules had completely transformed to foils with lengths of ~ 30 – 50 nm (and thus much smaller than for C-S-H).

The results suggest that following a non-classical nucleation mechanism, early on C-S-H is formed as a metastable droplet which then transforms to the thermodynamically more stable, foil-like morphology. Apparently, the IPEG-PCE delays the conversion of the globules to the nanofoils significantly.

Effectiveness of C-S-H – PCE as strength enhancer

The 16 hour compressive strengths of mortars admixed with 0.35 wt. % of the C-S-H – PCE particles obtained at various ageing times are shown in **Fig. 4**. It was found that the C-S-H – PCE nanocomposites generally increased the early strength of mortar. Moreover, the compressive strength values were significantly higher for mortars seeded with foil-like C-S-H – PCE prepared after 3 hours of ageing than with globular C-S-H – PCE particles obtained at 0 hour. The C-S-H – PCE nanofoils precipitated after 24 hours of ageing showed the best strength development and achieved ~ 10 N/mm^2, representing an 84 % increase over the neat cement. Whereas, the globule-like C-S-H – PCE nanocomposites (prepared at 0 hour of ageing) containing numerous agglomerated droplets were less effective as seeding material and increased the compressive strength only by ~ 25 %. Thus, the enhancement in early strength of mortar depends on the morphology of the synthesized C-S-H – PCE

nanocomposites which is controlled by the ageing period following the combination of the $Ca(NO_3)_2$/Na_2SiO_3 solutions.

CONCLUSIONS

The early nucleation and crystallization of C-S-H prepared by co-precipitation from $Ca(NO_3)_2$ and Na_2SiO_3 in the absence and presence of an IPEG-PCE superplasticizer was studied. It was found that the initially formed, metastable precursor of C-S-H exhibits a globular morphology and later converts to C-S-H nanofoils following a non-classical nucleation mechanism. The presence of the IPEG-PCE strongly delays the conversion from globular to nanofoil-like C-S-H for several hours because of a layer surrounding the globules. The foil-like particles prepared after 24 hours of ageing exhibit the strongest seeding effect for the hydration and early strength development of cement.

ACKNOWLEDGMENTS

The authors would like to thank Prof. S. Weinkauf and her team from the center of Electron Microscopy at TUM's Chemistry department for capturing the TEM images. V. Kanchanason wishes to thank SCG Cement-Building Materials for financial support of her study at TU München.

REFERENCES

1. Gibbs, J., "Equilibrium of Heterogeneous Substances," *Transactions of the Connecticut Academy of Arts and Sciences*, V. 3, 1876, pp. 108-248.
2. De Yoreo, J.J., Gilbert, P.U.P.A., Sommerdijk, N.A.J.M., Penn, R.L., Whitelam, S., Joester, D., Zhang, H., Rimer, J.D., Navrotsky, A., Banfield, J.F., Wallace, A.F., Michel, F.M., Meldrum, F.C., Cölfen, H., Dove, P.M., "Crystallization by Particle Attachment in Synthetic, Biogenic, and Geologic Environments," *Science*, 2015, V. 349, pp. 6247-6256.
3. Rieger, J., Frechen, T., Cox, G., Heckmann, W., Schmidt, C., Thieme, J., "Precursor Structures in the Crystallization/Precipitation Processes of $CaCO_3$ and Control of Particle Formation by Polyelectrolytes." *Faraday Discuss*, V. 136, 2007, pp. 265-277.
4. Bullard, J.W., Jennings, H.M, Livingston, R.A., Nonat, A., Scherer, G.W., Schweitzer, J.S., Scrivener, K.L., Thomas, J.J., "Mechanisms of Cement Hydration," *Cement and Concrete Research*, V. 41, 2011, pp. 1208-1223
5. Richardson, I.G., "The Nature of C-S-H in Hardened Cements," *Cement and Concrete Research*, V. 29, 1999, pp. 1131-1147.
6. Taylor, H.F.W., "Cement Chemistry," 2nd Edition, Thomas Telford Publishing, London, 1997, 142 pp.
7. Uchikawa, H., Hanchara, S., Sawaki, D., "The Role of Steric Repulsion Force in the Dispersion of Cement Particles in Fresh Paste Prepared with Organic Admixture," *Cement and Concrete Research*, V. 27, No. 1, 1997, pp. 37-50.
8. Yoshioka, K., Sakai, E., Daimon, M., Kitahara, A., "Role of Steric Hindrance in the Performance of Superplasticizers for Concrete," *Journal of the American Ceramic Society*, V. 80, No. 10, 1997, pp. 2667-2671.
9. Plank J., Hirsch C., "Superplasticizer Adsorption on Synthetic Ettringite," *Seventh*

CANMET/ACI Conference on Superplasticizers in Concrete (Editor V. M. Malhotra), SP-217-19, ACI, Berlin, 2003, pp. 283-298.

10. Plank J., Sachsenhauser B., "Impact of Molecular Structure on Zeta Potential and Adsorbed Conformation of α-allyl-ω-methoxypolyethylene Glycol – Maleic Anhydride Superplasticizers," *Journal of Advanced Concrete Technology*, V. 4 (2), 2006, pp. 233-239.
11. Plank J., Hirsch C., "Impact of Zeta Potential of Early Cement Hydration Phases on Superplasticizer Adsorption," *Cement and Concrete Research*, V. 37, 2007, pp. 537-542.
12. Zingg, A., Winnefeld, F., Holzer, L., Pakusch, J., Becker, S., Gauckler, L., "Adsorption of Polyelectrolytes and its Influence on the Rheology, Zeta Potential, and Microstructure of Various Cement and Hydrate Phases," *Journal of Colloid and Interface Science*, V. 323, 2008, pp. 301-312.
13. Winnefeld, F., Becker, S., Pakusch, J., Götz, T., "Effects of the Molecular Architecture of Comb-shaped Superplasticizers on their Performance in Cementitious Systems," *Cement and Concrete Composites*, V. 29, 2007, pp. 251-262.
14. Viallis-Terrisse, H., Nonat, A., Petit, J.C., "Zeta-Potential Study of Calcium Silicate Hydrates Interacting with Alkaline Cations," *Journal of Colloid and Interface Science*, V. 253, 2001, pp. 140-149.
15. Kanchanason K., Plank J., "C-S-H – PCE Nanocomposites for Enhancement of Early Strength of Portland Cement," *in: C. Shi, Y. Yao (Eds.) 14th ICCC*, Beijing, China, 2015, Proceedings CD, Section 4: Admixtures.
16. Nicoleau L., Gädt T., Chitu L., Maier G., Paris O., "Oriented Aggregation of Calcium Silicate Hydrate Platelets by the Use of Comb-like Copolymer," *Soft Matter*, V. 9, 2013, pp. 4864-4874.

17. Kanchanason K., Plank J., “Role of pH on the Structure, Composition and Morphology of C-S-H–PCE Nanocomposites and their Effect on Early Strength Development of Portland Cement,” *Cement and Concrete Research,* V. 102, 2017, pp. 90-98.
18. Kanchanason K., Plank J., “Effectiveness of a Calcium Silicate Hydrate – Polycarboxylate Ether (C-S-H–PCE) Nanocomposite on Early Strength Development of Fly Ash Cement,” *Construction and Building Materials*, 2017, submitted.

TABLES AND FIGURES

List of Tables:

List of Figures:

Table 1 – Molecular properties and specific anionic charge density of the IPEG-PCE sample

Molar masses (g/mol)		Polydispersity index	Specific anionic charge density in NaOH at pH = 11.7
M_w	M_n	(*PDI*)	(µeq/g)
35,100	15,700	2.2	2,750

Table 2 – Phase composition of the OPC sample as determined by quantitative XRD using *Rietveld* refinement

Content (wt.-%)									
C_3S, m	C_2S, m	C_3A, c	C_4AF	Lime	Arcanite	Hemihydrate[a]	Gypsum[a]	Anhydrite	Total
59.3	19.5	1.7	14.1	<0.3	<0.1	0.2	4.6	<0.1	99.7

[a] Determined by thermogravimetry

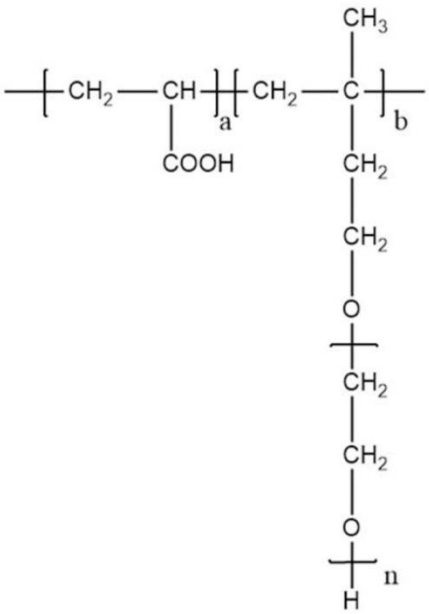

Fig. 1 – Chemical structure of the IPEG PCE sample used in the study.

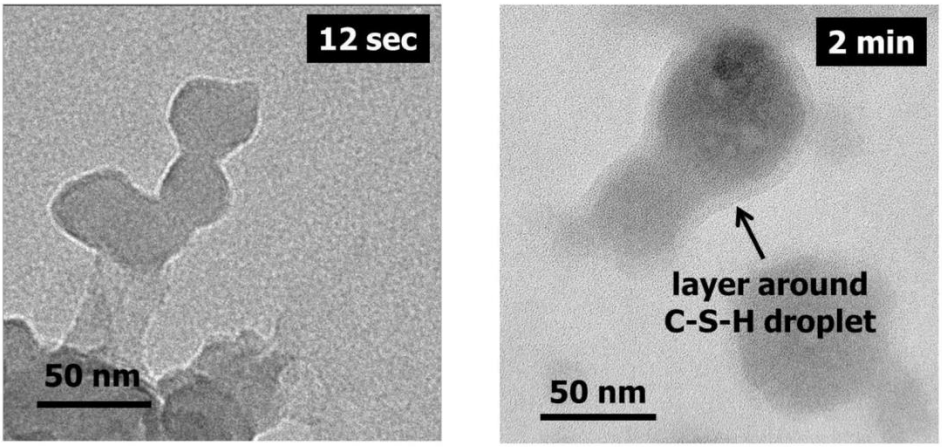

Fig. 2 – TEM images of C-S-H particles formed in the absence (left) and presence (right) of an IPEG-PCE polymer; images taken from samples acquired after addition of the $Ca(NO_3)_2/Na_2SiO_3$ solutions over 12 seconds and 2 minutes, respectively.

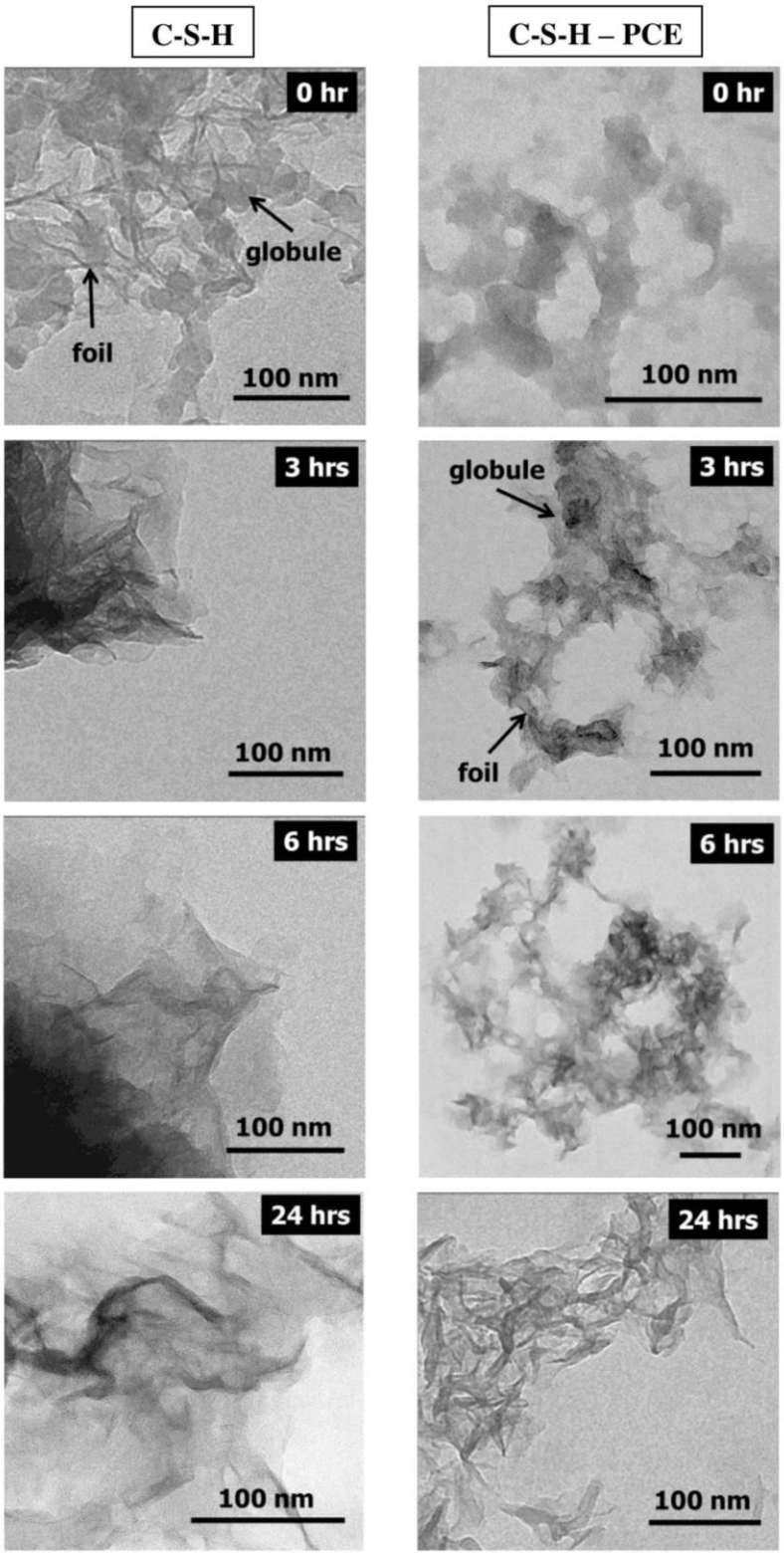

Fig. 3 – TEM images of C-S-H and C-S-H – PCE precipitates after 0, 3, 6 and 24 hours of ageing, respectively.

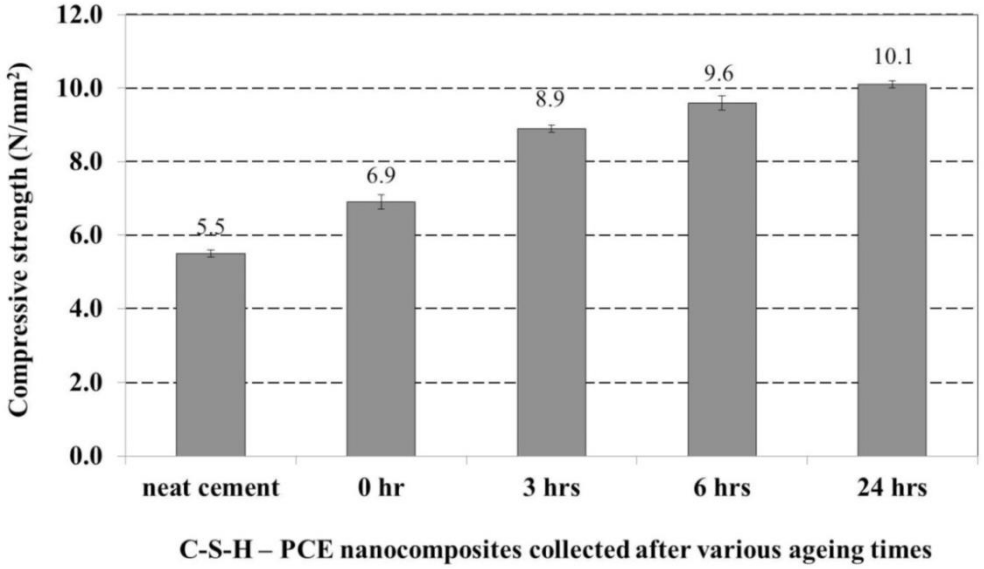

Fig. 4 – Compressive strengths of mortars cured for 16 hours and admixed with 0.35 % bwoc of the C-S-H – PCE nanocomposites collected after different ageing times.

16

6 Summary and outlook

This thesis focused on the synthesis of C-S-H – PCE nanocomposites that are used as seeding materials to accelerate the hydration of cement, resulting in enhanced early strength of Portland cement and blended cements. The mode of action of these nanocomposites in cement was also highlighted.

C-S-H – PCE nanocomposites were successfully synthesized by the co-precipitation method from Na_2SiO_3 and $Ca(NO_3)_2$ solutions in the presence of PCE copolymers. It was observed that the particle size and the characteristics of the synthetic C-S-H – PCE compounds are the key to obtain a strong seeding effect in cement.

In the first part of this thesis, the size of C-S-H particles was controlled using PCE copolymers of specific molecular structure. A PCE polymer possessing very long pendant groups (114 EO units) and low grafting density (molar ratio of MAA : MPEG-MA = 6 : 1) can produce the smallest particle sizes for the C-S-H – PCE composite, which exhibit the strongest seeding effect for the hydration of cement. Consequently, this nanocomposite achieves the largest gain in the early strength of mortar.

In the second part of this thesis, among the various conditions used for the synthesis of C-S-H – PCE nanocomposites, the pH value was found to play the most important role in obtaining a superior seeding material. The reason is that the pH value strongly affects the nanostructure, composition and morphology of the C-S-H – PCE products, and also impacts the PCE adsorption on C-S-H which generally controls the particle size of the C-S-H – PCE product. Furthermore, the structure of C-S-H – PCE nanocomposite precipitated at the optimal pH value (of 11.7) is semi-crystalline and consists of shorter, non-branched silicate chains. Moreover, this nanocomposite contains the highest amount of ultra-small nanofoils,

which shows an optimal seeding effect in cement and the highest early strength development of mortar.

In the third part of this thesis, effectiveness of the C-S-H – PCE admixture on early strength development of fly ash and slag blended cements was investigated. It was found that addition of the C-S-H – PCE nanocomposite drastically increases the early strength development of mortar and concrete, particularly during the first 24 hours of hydration, without a decrease in final strength (28 days). A mechanistic study revealed that the C-S-H – PCE nanocomposite greatly accelerates the reaction of the silicate phases present in the clinker. Moreover, it can also stimulate the pozzolanic reaction of fly ash, slag and calcined clay, consequently leading to higher early strength values there as well.

In the last part of this thesis, the effect of an IPEG PCE on the time-dependent nucleation and crystallization of C-S-H was studied via TEM. The results reveal that the initial precipitation product consists of a metastable C-S-H precursor which exhibits a globular morphology and then converts to C-S-H nanofoils, following a non-classical nucleation mechanism. In the presence of the IPEG-PCE, the conversion from C-S-H globules to the nanofoils is delayed for several hours because a layer, presumably of PCE polymer, coats the globules. Moreover, it was found that the C-S-H – PCE nanofoils aged for 24 hours show the strongest seeding effect for the hydration and early strength development of cement.

The work documented in this thesis includes a study on the effect of various parameters during synthesis of C-S-H – PCE nanocomposites and their effectiveness in cements. Further studies are suggested to improve the performance of this nanocomposite and to investigate other beneficial points, as follow:

- Use of other PCEs (e.g. amphoteric PCEs, star-shaped PCE) to stabilize the C-S-H particles

- Study of the interaction of C-S-H with polymers other than PCEs such as phosphated comb polymers, polyethylene imines, polyamidoamines, polyvinylalcohol, etc.
- Further control of the size of the C-S-H particles by adjusting process parameters such as the droplet size of the raw material solutions, by using a high speed mixer (e.g. homogenizer) or micro reactor.
- Application of the C-S-H – PCE nanocomposites in other blended cements such as limestone blended cements, etc.
- Clarification of the composition of the layer surrounding the metastable C-S-H globules found at very early nucleation when PCE is present.
- Study of the very early nucleation and crystallization of C-S-H in actual cement: does it also involve an amorphous, metastable, globular precursor?

7 Zusammenfassung und Ausblick

Der Fokus dieser Arbeit liegt in der Synthese von C-S-H – PCE Nanokomposit-Materialen, die Kristallisationskeime bilden und somit eine beschleunigende Wirkung auf die Zementhydratation haben, wodurch die Frühfestigkeit von Portland- und Kompositzementen deutlich erhöht werden kann. Darüber hinaus war ein weiteres Ziel dieser Dissertation, den Wirkmechanismus dieser Nanokomposite im Zement näher zu untersuchen.

Die Synthese der C-S-H – PCE Nanokomposite erfolgte mittels Co-Präzipitation aus Na_2SiO_3- und $Ca(NO_3)_2$ - Lösungen in Anwesenheit von PCE-Fließmitteln. Hierbei wurde beobachtet, dass die Kristallkeimbildung im Zement von der Partikelgröße und den Materialeigenschaften der synthetisierten C-S-H – PCE-Verbindungen abhängt.

Im ersten Teil der Arbeit wurde die Größe der C-S-H Partikel durch die molekularen Eigenschaften der PCEs gesteuert. Ein PCE-Polymer mit einer sehr langen Seitenkette (114 EO-Einheiten) und einer niedrigen Seitenkettendichte (molares Verhältnis MAA : MPEG-MA = 6:1) ergab die geringste Partikelgröße für die C-S-H – PCE-Nanokomposite. Sie waren am besten als Kristallisationskeime für die Hydratation der Silikatphasen (C_3S und C_2S) geeignet. Folglich ergaben diese Nanokomposite die höchste Zunahme an Frühfestigkeit bei den Mörtelproben.

Im zweiten Teil der Arbeit stellte sich von allen getesteten Reaktionsbedingungen der pH-Wert als entscheidendes Kriterium heraus, um möglichst wirkungsvolle Kristallisationskeime zu erhalten. Die Gründe hierfür sind, dass der pH Wert stark die Nanostruktur, die Zusammensetzung und die Morphologie der C-S-H – PCE-Nanokomposite beeinflusst und auch die PCE-Adsorption beeinflusst, wodurch prinzipiell die Partikelgröße der C-S-H Produkte reguliert wird. Die Nanokomposite, die bei einem pH-Wert von 11.7 hergestellt werden, sind semi-kristallin und bestehen aus kürzeren, unverzweigten Silikatketten.

Außerdem enthält dieses Nanokomposit die höchste Menge an ultra-kleinen Nanofolien, welche optimale Keimbildner im Zement sind und somit die beste Frühfestigkeitsentwicklung ergeben.

Im dritten Teil der Arbeit wurde die Effektivität der C-S-H – PCE-Nanokomposite auf die Frühfestigkeitsentwicklung von Zementen mit Flugasche und Schlacke untersucht. Es stellte sich heraus, dass die Zugabe von C-S-H – PCE-Nanokomposit die Frühfestigkeit von Mörtel und Betonproben – insbesondere in den ersten 24 Stunden der Zementhydratation – sehr stark erhöht, ohne jedoch die Endfestigkeit nachteilig zu beeinflussen (28 Tage). Eine mechanistische Studie ergab, dass die C-S-H – PCE-Nanokomposite die Hydratation der silikatischen Phasen, die im Klinker erhalten sind, stark beschleunigen. Außerdem kann es die puzzolanische Reaktion von Flugasche, Schlacke anregen und calcinierten Tonen, womit die sehr hohen Frühfestigkeitswerte dieser Zemente erklärt werden können.

Im letzten Teil der Arbeit wurde der Effekt eines IPEG-PCE auf die Keimbildung und Kristallisation von C-S-H mittels TEM untersucht. Die Ergebnisse Zeigten, dass zuerst metastabile C-S-H-Vorstufen, die eine tröpfchenförmige Morphologie aufweisen, gebildet werden und sich nach einem nicht-klassischen Nukleationsmechanismus in C-S-H-Nanofolien umwandeln. In Gegenwart des IPEG-PCEs findet die Transformation der C-S-H-Tröpfchen zu Nanofolien einige Stunden später statt, da eine Schicht, die vermutlich aus PCE besteht, die Tröpfchen umhüllt. Außerdem zeigte sich, dass C-S-H-Nanofolien, die 24 Stunden gealtert wurden, die besten Kristallisationskeime für die Hydratation und die Frühfestigkeitsentwicklung von Zement darstellen.

Die Dissertation beschäftigte sich außerdem mit dem Einfluss verschiedener Reaktionsparamater auf die Eigenschaften von C-S-H – PCE-Nanokomposite und deren Effektivität in Zement. Weitere Studien sollten sich mit der Verbesserung der Wirksamkeit

dieser Nanokomposite beschäftigen. Dazu sollten folgende Punkte eingehend untersucht werden:

- Einsatz anderer PCEs zur Stabilisierung der C-S-H Partikel, wie z.B. von amphoteren PCEs, sternförmigen PCEs, etc.
- Untersuchung der Wechselwirkung von C-S-H mit andern Polymeren wie z.B. Phosphat-Polymeren, Polyethyleniminen, Polyamidoamine, Polyvinylalkoholen, etc.
- Kontrolle der C-S-H Partikelgröße durch Anpassen der Prozessparamater wie z.B. der Tröpfchengröße bei der Zugabe der Ausgangslösugen ($Ca(NO_3)_2$, Na_2SiO_3) durch Einsatz eines Hochgeschwindigkeitsmixers oder eines Mikroreaktors
- Einsatz von C-S-H – PCE-Nanokompositen in anderen Kompositzementen.
- Chemische Identifizierung der Schicht um die metastabilen C-S-H-Tröpfchen Kügelchen, die zu Beginn der C-S-H-Bildung gefunden wurde
- Untersuchungen zur frühen Nukleation und Kristallisation von C-S-H im eigentlichen Zement: verläuft die Nukleation von C-S-H dort ebenfalls über eine amorphe, metastabile, tröpfchenförmige Vorstufe wie bei der hier angewandten Copräzipitationsmethode?

References

[1] C.A. Hendriks, E. Worrell, D. de Jager, K. Blok, P. Riemer, *Emission reduction of greenhouse gases from the cement industry*, In: The proceeding of the greenhouse gas control technologies conference. http://www.wbcsdcement.org/pdf/tf1/prghgt42.pdf, **2004** (accessed 23.08.04).

[2] World Business Council for Sustainable Development (WBCSD) and International Energy Agency (IEA), *Cement technology roadmap 2009: carbon emissions reductions up to 2050*, **2009**, 1-36.

[3] W. Shen, L. Cao, Q. Li, W. Zhang, G. Wang, C. Li, *Quantifying CO_2 emissions from China's cement industry*, Renewable and Sustainable Energy Reviews, 50, **2015**, 1004-1012.

[4] R. M. Edmeades, P.C. Hewlett, *Cement admixtures*, In: P.C. Hewlett Lea's chemistry of cement and concrete, fourth ed., Butterworth-Heinemann Publishing, Oxford, **2003**, 841-905.

[5] J. Qian, C. Shi, Z. Wang, *Activation of blended cements containing fly ash*, Cement and Concrete Research, 31, **2001**, 1121-1127.

[6] C.Y. Lee, H.K. Lee, K.M. Lee, *Strength and microstructural characteristics of chemically activated fly ash–cement systems*, Cement and Concrete Research, 33, **2003**, 425-431.

[7] K. Riding, D.A. Silva, K. Scrivener, *Early age strength enhancement of blended cement systems by $CaCl_2$ and diethanol-isopropanolamine*, Cement and Concrete Research, 40, **2010**, 935-946.

[8] K. Hoang, H. Justnes, M. Geiker, *Early age strength increase of fly ash blended cement by a ternary hardening accelerating admixture*, Cement and Concrete Research, 81, **2016**, 59-69.

[9] H.F.W. Taylor, *Hydration of the calcium silicate phases*, In: Cement Chemistry, 2nd Edition, Thomas Telford Publishing, London, **1997**, 123-166.

[10] J.J. Thomas, H.M. Jennings, J.J. Chen, *Influence of nucleation seeding on the hydration mechanisms of tricalcium silicate and cement*, Journal of Physical Chemistry C, 113, **2009**, 4327-4334.

[11] R. Alizadeh, L. Raki, J.M. Makar, J.J. Beaudoin, I. Moudrakovski, Hydration of tricalcium silicate in the presence of synthetic calcium-silicate-hydrate, Journal of Materials Chemistry, 19, **2009**, 7937-7946.

[12] M.H. Hubler, J.J. Thomas, H.M. Jennings, *Influence of nucleation seeding on the hydration kinetics and compressive strength of alkali activated slag paste*, Cement and Concrete Research, 41, **2011**, 842-846.

[13] L. Nicoleau, T. Gädt, L. Chitu, G. Maier, O. Paris, *Oriented aggregation of calcium silicate hydrate platelets by the use of comb-like copolymer*, Soft Matter, 9, **2013**, 4864-4874.

[14] V. Kanchanason, J. Plank, *C-S-H – PCE nanocomposites for enhancement of early strength of Portland cement*, In: C. Shi, Y. Yao (Eds.) 14th ICCC, Beijing, China, **2015**, Proceedings CD, Section 4: Admixtures.

[15] J. Sun, H. Shi, B. Qian, Z. Xu, W. Li, X. Shen, *Effects of synthetic C-S-H/PCE nanocomposites on early cement hydration*, Construction and Building Materials, 140 **2017**, 282-292.

[16] V. Kanchanason, J. Plank, *C-S-H – PCE nanocomposites for enhancement of early strength of cement*, 19. ibausil, Bauhaus-Universität Weimar, Tagungsband 1, Weimar, Germany, **2015**, 759-766.

[17] L. Nicoleau, *Accelerated growth of calcium silicate hydrates: experiments and simulations*, Cement and Concrete Research, 41, **2011**, 1339-1348.

[18] L. Nicoleau, *The acceleration of cement hydration by seeding: influence of the cement mineralogy*, ZKG Int 1, **2013**, 40-49.

[19] I.G. Richardson, *The calcium silicate hydrates*, Cement and Concrete Research, 38 **2008**, 137-158.

[20] E. Kaldis. *Principles of the vapour growth of single crystals*. In: C. H. L. Goodman, editor, Crystal Growth: Theory and Techniques Vol.1, Plenum, London, **1974**, 49-191.

[21] P. Cubillas, M. Anderson. *Synthesis mechanism: crystal growth and nucleation*. In: J. Čejka, A. Corma, S. Zones, editors, Zeolites and Catalysis: Synthesis, Reactions and Applications, Wiley-VCH Verlag GmbH & Co. KGaA, Weinheim, Germany, **2010**, 1-55.

[22] H. Cölfen, M. Antonietti, *Physico-chemical principles of crystallization*, Mesocrystals and Nonclassical Crystallization, John Wiley & Sons, Ltd., **2008**, 7-50.

[23] H. Cölfen, M. Antonietti, *Nonclassical crystallization*, Mesocrystals and Nonclassical Crystallization, John Wiley & Sons, Ltd., **2008**, 73-101.

[24] J.J. De Yoreo, P.U.P.A. Gilbert, N.A.J.M. Sommerdijk, R.L. Penn, S. Whitelam, D. Joester, H. Zhang, J.D. Rimer, A. Navrotsky, J.F. Banfield, A.F. Wallace, F.M. Michel, F.C. Meldrum, H. Cölfen, P.M. Dove, *Crystallization by particle attachment in synthetic, biogenic, and geologic environments*, Science, 349, **2015**, 6247-6256.

[25] J. Rieger, T. Frechen, G. Cox, W. Heckmann, C. Schmidt, J. Thieme, *Precursor structures in the crystallization/precipitation processes of $CaCO_3$ and control of particle formation by polyelectrolytes*. Faraday Discuss, 136, **2007**, 265-277.

[26] L.B. Gower, D.J. Odom, *Deposition of calcium carbonate films by a polymer-induced liquid-precursor (PILP) process*, Journal of Crystal Growth, 210, **2000**, 719-734.

[27] L.B. Gower, *Biomimetic model systems for investigating the amorphous precursor pathway and its role in biomineralization*, Chemical Reviews, 108, **2008**, 4551-4627.

[28] D. Gebauer, A. Völkel, H. Cölfen, *Stable prenucleation clusters*, Science, 322, **2008**, 1819-1822.

[29] D. Gebauer, H. Cölfen, *Prenucleation clusters and non-classical nucleation*, Nano Today, 6, **2011**, 564-584.

[30] L. Châtelier, *Recherches expérimentales sur la constitution des mortiers hydrauliques*, Dunod, **1904**.

[31] K. Scrivener, A. Nonat, *Hydration of cementitious materials, present and future*, Cement and Concrete Research, 41, **2011**, 651-665.

[32] J.W. Bullard, H.M. Jennings, R.A. Livingston, A. Nonat, G.W. Scherer, J.S.

Schweitzer, K.L. Scrivener, J.J. Thomas, *Mechanisms of cement hydration*, Cement and Concrete Research, 41, **2011**, 1208-1223.

[33] L. Nicoleau, A. Nonat, *A new view on the kinetics of tricalcium silicate hydration*, Cement and Concrete Research, 86, **2016**, 1-11.

[34] S. Garrault-Gauffinet, A. Nonat, *Experimental investigation of calcium silicate hydrate (C-S-H) nucleation*, Journal of Crystal Growth, 200, **1999**, 565-574.

[35] L. Nicoleau, A. Nonat, D. Perrey, *The di- and tricalcium silicate dissolutions*, Cement and Concrete Research, 47 (5), **2013**, 14-30.

[36] J. Bisschop, A. Kurlov, *A flow-through method for measuring the dissolution rate of alite and Portland cement clinker*, Cement and Concrete Research, 51, **2013**, 47-56.

[37] F. Bellmann, T. Sowoidnich, B. Möser, *Formation of an intermediate phase and influence of crystallographic defects on dissolution of C_3S*, In: Á. Palomo, A. Zaragoza, J.C. López Agüí (Eds.), Proceedings of the XIII. International Congress on the Chemistry of Cement, Madrid (Spain), **2011**, p. 320.

[38] F. Bellmann, T. Sowoidnich, H.M. Ludwig, D. Damidot, *Dissolution rates during the early hydration of tricalcium silicate*, Cement and Concrete Research, 72, **2015**, 108-116.

[39] A.C. Lasaga, *Kinetic theory in the earth sciences*, Princeton University Press, Princeton (New Jersey, USA), **1998**.

[40] P. Fierens, J.P. Verhaegen, *Hydration of tricalcium silicate in paste - kinetics of calcium ions dissolution in the aqueous phase*, Cement and Concrete Research 6, **1976**, 337-342.

[41] P. Juilland, E. Gallucci, R.J. Flatt, K. Scrivener, *Dissolution theory applied to the induction period in alite hydration*, Cement and Concrete Research, 40, **2010**, 831-844.

[42] P. Suraneni, R.J. Flatt, *Use of micro-reactors to obtain new insights into the factors influencing tricalcium silicate dissolution*, Cement and Concrete Research, 78, **2015**, 208-215.

[43] D.L. Kantro, S. Brunauer, C.H. Weise, *Development of surface in the hydration of calcium silicates. II. Extention of investigations to earlier and later stages of hydration*, Journal of Physical Chemistry, 66 (10), **1962**, 1804-1809.

[44] H.N. Stein, J.M. Stevels, *Influence of silica on the hydration of $3CaO{\cdot}SiO_2$*, Journal of Applied Chemistry, 14 (8), **1964**, 338-346.

[45] S. Garrault, A. Nonat, *Hydrated layer formation on tricalcium and dicalcium silicate surfaces: Experimental study and numerical simulations*, Langmuir, 17, **2001**, 8131-8138.

[46] S. Garrault, T. Behr, A. Nonat, *Formation of the C-S-H layer during early hydration of tricalcium silicate grains with different sizes*, Journal of Physical Chemistry B, 110 **2006**, 270-275.

[47] S. Garrault, E. Finot, E. Lesniewska, A. Nonat, *Study of C-S-H growth on C_3S surface during its early hydration*, Materials and Structures, 38, **2005**, 435-442.

[48] E.M. Gartner, *A proposed mechanism for the growth of C-S-H during the hydration of tricalcium silicate*, Cement and Concrete Research, 5, **1997**, 665-672.

[49] E.M. Gartner, K.E. Kurtis, P.J.M. Monteiro, *Proposed mechanism of C-S-H growth tested by soft X-ray microscopy*, Cement and Concrete Research, 30, **2000**, 817-822.

[50] A.J. Allen, R.C. Oberthur, D. Pearson, P. Schofield, C.R. Wilding, *Development of the fine porosity and gel structure of hydrating cement systems*, Philosophical Magazine Part B, 56, **1987**, 263-268.

[51] H.M. Jennings, *A model for the microstructure of calcium silicate hydrate in cement paste*, Cement and Concrete Research, 30, **2000**, 101-116.

[52] A.J. Allen, J.J. Thomas, H.M. Jennings, *Composition and density of nanoscale calcium–silicate–hydrate in cement*, Nature Materials, 6, **2007**, 311-316.

[53] H.M. Jennings, J.J. Thomas, J.S. Gevrenov, G. Constantinides, F.-J. Ulm, *A multitechnique investigation of the nanoporosity of cement paste*, Cement and Concrete Research, 37, **2007**, 329-336.

[54] H.M. Jennings, J.W. Bullard, J.J. Thomas, J.E. Andrade, J.J. Chen, G.W. Scherer, *Characterization and modeling of pores and surfaces in cement paste: correlations to processing and properties*, Journal of Advanced Concrete Technology, 6 (1), **2008**, 1-25.

[55] E. Ntafalias, P.G. Koutsoukos, *Spontaneous precipitation of calcium silicate hydrate in aqueous solutions*, Crystal Research and Technology, 45 (1), **2010**, 39-47.

[56] T. Maeshima, H. Noma, M. Sakiyama, T. Mitsuda, *Natural 1.1 and 1.4 nm tobermorites from Fuka, Okayama, Japan: Chemical analysis, cell dimensions, ^{29}Si NMR and thermal behavior*, Cement and Concrete Research, 33, **2003**, 1515-1523.

[57] E. Bonaccorsi, S.S. Merlino, A.R. Kampf, *The crystal structure of tobermorite 14 Å (plombierite), a C-S-H phase*, Journal of the American Ceramic Society, 88, **2005**, 505-512.

[58] E. Bonaccorsi, S. Merlino, H.F.W. Taylor, *The crystal structure of jennite, $Ca_9Si_6O_{18}(OH)_6 \cdot 8H_2O$*, Cement and Concrete Research, 34, **2004**, 1481-1488.

[59] S. Grangeon, F. Claret, Y. Linard, C. Chiaberge, *X-ray diffraction: a powerful tool to probe and understand the structure of nanocrystalline calcium silicate hydrates, Acta Crystallogr*, Section B: Structural Science, Crystal Engineering and Materials, 69, **2013**, 465-473.

[60] I.G. Richardson, *Model structures for C-(A)-S-H (I)*, Acta Crystallographica Section B, 70, **2014**, 903-23.

[61] H.F.W. Taylor, *Proposed structure for calcium silicate hydrate gel*, Journal of the American Ceramic Society, 69 (6), **1986**, 464-467.

[62] I.G. Richardson, G.W. Groves, *Models for the composition and structure of calcium silicate hydrate (C-S-H) gel in hardened tricalcium silicate pastes*, Cement and Concrete Research, **1992**, 1001-1010.

[63] I.G. Richardson, G.W. Groves, *The incorporation of minor and trace elements into calcium silicate hydrate (C-S-H) gel in hardened cement pastes*, Cement and Concrete Research, 23, **1993**, 131-138.

[64] I. G. Richardson and G. W. Groves, *Microstructure and microanalysis of hardened ordinary Portland cement pastes*, Journal of Materials Science, 28, **1993**, 265-77.

[65] I.G. Richardson, *The nature of hydration products in hardened cement pastes*, Cement and Concrete Composites, 22, **2000**, 97-113.

[66] R. Taylor, I.G. Richardson, R.M.D. Brydson, *Nature of C-S-H in 20 year old neat ordinary Portland cement and 10% Portland cement – 90% ground granulated blast furnace slag pastes*, Advances in Applied Ceramics, 106, **2007**, 294-301.

[67] E. Gallucci, X. Zhang, K. Scrivener, *Effect of temperature on the microstructure of calcium silicate hydrate (C–S–H)*, Cement and Concrete Research, 53, **2013**, 185-195.

[68] F. Deschner, F. Winnefeld, B. Lothenbach, S. Seufert, P. Schwesig, S. Dittrich, F. Goetz-Neunhoeffer, J. Neubauer, *Hydration of a Portland cement with high replacement by siliceous fly ash*, Cement and Concrete Research, 42, **2012**, 1389-1400.

[69] J.J. Thomas, H.M. Jennings, A.J. Allen, *Relationships between composition and density of tobermorite, jennite, and nanoscale $CaO–SiO_2–H_2O$*, Journal of Physical Chemistry C, 114, **2010**, 7594-7601.

[70] I.G. Richardson, *The nature of C-S-H in hardened cements*, Cement and Concrete Research, 29, **1999**, 1131-1147.

[71] I.G. Richardson, *Tobermorite/jennite- and tobermorite/calcium hydroxide-based models for the structure of C-S-H: Applicability to hardened pastes of tricalcium silicate, β-dicalcium silicate, Portland cement, and blends of Portland cement with blast-furnace slag, metakaolin, or silica fume*, Cement and Concrete Research, 34, **2004**, 1733-1377.

[72] H.F.W. Taylor, *Hydrated calcium silicates: part I. Compound formation at ordinary temperatures*, Journal of the Chemical Society, 3, **1950**, 3682-3690.

[73] J.A. Gard, H.F.W. Taylor, *Calcium Silicate Hydrate (II)*, Cement and Concrete Research, 6, **1976**, 667-678.

[74] A. Nonat, *Interactions between chemical evolution (hydration) and physical evolution (setting) in the case of tricalcium silicate*, Materials and Structures, 27 (4), **1994**, 187-195.

[75] A. Nonat. X. Lecoq, *The structure, stoichiometry and properties of C-S-H prepared by C_3S hydration under controlled condition*, In: P. Colombet et al. (Eds.), NMR Spectroscopy of Cement Based Materials, Springer-Verlag Berlin Heidelberg, **1998**, 197-207.

[76] B. Lothenbach, A. Nonat, *Calcium silicate hydrates: Solid and liquid phase composition*, Cement and Concrete Research, 78, **2015**, 57-70.

[77] A. Kumar, B.J. Walder, A.K. Mohamed, A. Hofstetter, B. Srinivasan, A.J. Rossini, K. Scrivener, L. Emsley, P. Bowen, *The atomic-level structure of cementitious calcium silicate hydrate*, Journal of Physical Chemistry C, 121 (32), **2017**, 17188-17196.

[78] H. Matsuyama, J.F. Young, *Effects of pH on precipitation of quasi-crystalline calcium silicate hydrate in aqueous solution*, Advances in Cement Research, 12 (1), **2000**, 29-33.

[79] A.W. Harris, M.C. Manning, W.M. Tearle, C.J. Tweed, *Testing of models of the dissolution of cements – leaching of synthetic CSH gels*, Cement and Concrete Research, 32, **2002**, 731-746.

[80] J.J. Chen, J.J. Thomas, H.F.W. Taylor, H.M. Jennings, *Solubility and structure of calcium silicate hydrate*, Cement and Concrete Research, 34, **2004**, 1499-1519.

[81] V. Kanchanason, J. Plank, *Role of pH on the structure, composition and morphology of C-S-H–PCE nanocomposites and their effect on early strength development of Portland cement*, Cement and Concrete Research, 102, **2017**, 90-98.

[82] M. Grutzeck, A. Benesi, B. Fanning, *Silicon-29 magic angle spinning nuclear magnetic resonance study of calcium silicate hydrates*, Journal of the American Ceramic Society, 72, **1989**, 665-668.

[83] G.M.M Bell, J. Bensted, F.P. Glasser, *Study of calcium silicate hydrates by solid-state high-resolution ^{29}Si nuclear magnetic resonance*. Advances in Cement Research, 3(2), **1990**, 23-37.

[84] X. Cong, R.J. Kirkpatrick, *^{29}Si MAS NMR study of the structure of calcium silicate hydrate*, Advanced Cement Based Materials, 3, **1996**, 144-156.

[85] I. G. Richardson, J. Skibsted, L. Black, R. J. Kirkpatrick, *Characterization of cement hydrate phases by TEM, NMR and Raman spectroscopy*, Advances in Cement Research, 22 (4), **2010**, 233-248.

[86] I. García-Lodeiro, A. Fernández-Jiménez, I. Sobrados, J. Sanz, A. Palomo, *C-S-H gels: interpretation of ^{29}Si MAS-NMR spectra*, Journal of the American Ceramic Society, 95 (4), **2012**, 1440-1446.

[87] E. Pustovgar, R.P. Sangodkar, A.S. Andreev, M. Palacios, B.F. Chmelka, R.J. Flatt, J.B. d'Espinose de Lacaillerie, *Understanding silicate hydration from quantitative analyses of hydrating tricalcium silicates*, Nature Communications, **2016**, 1-9.

[88] H. Viallis, P. Faucon, J.-C. Petit, A. Nonat, *Interaction between salts (NaCl, CsCl) and calcium silicate hydrates (C-S-H)*, Journal of Physical Chemistry B, 103, **1999**, 5212-5219.

[89] E.T. Rodriguez, I.G. Richardson, L. Black, E. Boehm-Courjault, A. Nonat, J. Skibsted, *Composition, silicate anion structure and morphology of calcium silicate hydrates (C-S-H) synthesized by silica-lime reaction and by controlled hydration of tricalcium silicate*, Advances in Applied Ceramics, 114, **2015**, 362-371.

[90] D.E. Macphee, E.E. Lachowski, F.P. Glasser, *Polymerization effects in C-S-H: implications for portland cement hydration*, Advances in Cement Research, 1, **1988**, 131-137.

[91] Y. Okada, H. Ishida, T. Mitsuda, *29Si NMR spectroscopy of silicate anions in hydrothermally formed C-S-H*, Journal of the American Ceramic Society, 77, **1994**, 765-768.

[92] I. Kiur, B. Pollet, J. Virlet, A. Nonat, *C-S-H structure evolution with calcium content by multinuclear NMR*, In: P. Colombet et al. (Eds.), Nuclear Magnetic Resonance Spectroscopy of Cement-Based Materials, Springer-Verlag Berlin Heidelberg, **1998**, 119-141.

[93] P. Yu, R.J. Kirkpatrick, B. Poe, P.F. McMillan, X. Cong, *Structure of calcium silicate*

hydrate (C-S-H): near-, mid-, and far-infrared spectroscopy, Journal of the American Ceramic Society, 82 (3), **1999**, 742-748.

[94] N. Lequex, A. Morau, S. Philippot, P. Boch, *Extended X-ray absorption fine structure investigation of calcium silicate hydrates*, Journal of the American Ceramic Society 82, **1999**, 1299-1306.

[95] E. L'Hôpital, B. Lothenbach, G. Le Saout, D. Kulik, K. Scrivener, *Incorporation of aluminium in calcium-silicate-hydrates*, Cement and Concrete Research, 75, **2015**, 91-103.

[96] G. Zhu, H. Li, X. Wang, S. Li, X. Hou, W. Wu, Q. Tang, *Synthesis of calcium silicate hydrate in highly alkaline system*, Journal of the American Ceramic Society, 99 (8), **2016**, 2778-2785.

[97] S. Komarneni, R. Roy, D.M. Roy, C.A. Fyfe, G.J. Kennedy, A.A. Bothnerby, J. Dadok, A.S. Chesnick, *Al-27 and Si-29 magic angle spinning nuclear magnetic-resonance spectroscopy of Al-substituted tobermorites*, Journal of Materials Science, 20, **1985**, 4209-4214.

[98] I.G. Richardson, A.R. Brough, R. Brydson, G.W. Groves, C.M. Dobson, *Location of aluminum in substituted calcium silicate hydrate (C-S-H) gels as determined by 29Si and 27Al NMR and EELS*, Journal of the American Ceramic Society, 76, **1993**, 2285-2288.

[99] I. Lognot, I. Klur, A. Nonat, *NMR and infrared spectroscopies of C-S-H and AI-substituted C-S-H synthesised in alkaline solutions*, In: P. Colombet et al. (Eds.), Nuclear Magnetic Resonance Spectroscopy of Cement-Based Materials, Springer-Verlag Berlin Heidelberg, **1998**, 189-196.

[100] G.K. Sun, J.F. Young, R.J. Kirkpatrick, *The role of Al in C-S-H: NMR, XRD, and compositional results for precipitated samples*, Cement and Concrete Research, 36, **2006**, 18-29.

[101] X. Pardal, F. Brunet, T. Charpentier, I. Pochard, A. Nonat, *Al-27 and Si-29 solid-state NMR characterization of calcium-aluminosilicate-hydrate*, Inorganic Chemistry, 51, **2012**, 1827-1836.

[102] J. Haas, A. Nonat, *From C-S-H to C-A-S-H: experimental study and thermodynamic modelling*, Cement and Concrete Research, 68, **2015**, 124-138.

[103] E. L'Hopital, B. Lothenbach, D. Kulik, K. Scrivener, *Influence of calcium to silica ratio on aluminium uptake in calcium silicate hydrate*, Cement and Concrete Research, 85, **2016**, 111-121.

[104] L. Nachbaur, P.C. Nkinamubanzi, A. Nonat, J.C. Mutin, *Electrokinetic properties which control the coagulation of silicate cement suspensions during early age hydration*, Journal of Colloid and Interface Science, 202, **1998**, 261-268.

[105] H. Viallis-Terrisse, A. Nonat, J.C. Petit, *Zeta-potential study of calcium silicate hydrates interacting with alkaline cations*, Journal of Colloid and Interface Science, 253, **2001**, 140-149.

[106] A. Nonat, *The structure and stoichiometry of C-S-H*, Cement and Concrete Research, 34, **2004**, 1521-1528.

[107] C. Labbez, I. Pochard, B. Jönsson, A. Nonat, *CSH/solution interface: Experimental and Monte Carlo studies*, Cement and Concrete Research, 41, **2011**, 161-168.

[108] C. Labbez, A. Nonat, I. Pochard, B. Jönsson, *Experimental and theoretical evidence of overcharging of calcium silicate hydrate*, Journal of Colloid and Interface Science, 309, **2007**, 303-307.

[109] C. Labbez, B. Jönsson, I. Pochard, A. Nonat, B. Cabane, *Surface charge density and electrokinetic potential of highly charged minerals: experiments and Monte Carlo simulations on calcium silicate hydrate*, Journal of Physical Chemistry B, 110, **2006**, 9219-9230.

[110] T.T.H. Bach, E. Chabas, I. Pochard, C. Cau Dit Coumes, J. Haas, F. Frizon, A. Nonat, *Retention of alkali ions by hydrated low-pH cements: mechanism and Na^+/K^+ selectivity*, Cement and Concrete Research, 51, **2013**, 14-21.

[111] A. Grudemo, *Discussion following the paper by J.D. Bernal on "The structure of cement hydration compounds*", Proceedings of the 3rd International Symposium on the Chemistry of Cement, **1954**, 247-253.

[112] G. L. Kalousek, A. F. Prebus, *Crystal chemistry of hydrous calcium silicates: III,*

Morphology and other properties of tobermorite and related phases, Journal of the American Ceramic Society, 41 (4), **1958**, 124-132.

[113] A. Kumar, P. Bowen, K. Scrivener, *Synthetic calcium silicate hydrate with high calcium to silicon ratio*, In: C. Shi, Y. Yao (Eds.) 14th ICCC, Beijing, China, **2015**, Proceedings CD, Section 2: Hydration of Portland cement.

[114] Y. He, X. Zhao, L. Lu, L. Struble, S. Hu, *Effect of C/S ratio on morphology and structure of hydrothermally synthesized calcium silicate hydrate*, Journal of Wuhan University of Technology - Mater. Sci. Ed., 26 (4), **2011**, 770-773.

[115] A. Hartmann, D. Schulenberg, J.C. Buhl, *Synthesis and structural characterization of CSH-phases in the range of C/S = 0.41 - 1.66 at temperatures of the tobermorite xonotlite crossover*, Journal of Materials Science and Chemical Engineering, 3, **2015**, 39-55.

[116] T.C. Powers, *Structure and physical properties of hardened Portland cement paste.* Journal of the American Ceramic Society, 41 (1), **1958**, 1-6.

[117] R.F. Feldman, P. Serada, *A new model for hydrated Portland cement and its practical implications*, Engineering Journal Cananda, 53 (8-9), **1970**, 53-59.

[118] S. Papatzani, K. Paine, J. Calabria-Holley, *A comprehensive review of the models on the nanostructure of calcium silicate hydrates*, Construction and Building Materials, 74, **2015**, 219-234.

[119] H.M. Jennings, *A model for the microstructure of calcium silicate hydrate in cement paste*, Cement and Concrete Research, 30, **2000**, 101-116.

[120] H.M. Jennings, *Refinements to colloid model of C-S-H in cement: CM-II*, Cement and Concrete Research, 38, **2008**, 275-289.

[121] J.D. Bernal, J.W. Jeffery, H.F.W. Taylor, *Crystallographic research on the hydration of Portland cement*, A first report on investigations in progress, Magazine of Concrete Research, 4 (11), **1952**, 49-54.

[122] H. Stade, D. Müller, *On the coordination of Al in ill-crystallized C-S-H phases formed by hydration of tricalcium silicate and by precipitation reactions at ambient temperature*, Cement and Concrete Research, 17, **1987**, 553-561.

[123] I.G. Richardson, G.W. Groves, *Models for the composition and structure of calcium silicate hydrate (C-S-H) gel in hardened tricalcium silicate pastes*, Cement and Concrete Research, 22, **1992**, 1001-1010.

[124] I.G. Richardson, G.W. Groves, *The incorporation of minor and trace elements into calcium silicate hydrate (C-S-H) gel in hardened cement pastes*, Cement and Concrete Research, 23, **1993**, 131-138.

[125] T. Hirata, Japanese Patent JP 84 (**1981**) 2022 (S59-018338).

[126] K. Mitsui, T. Yonezawa, M. Kinoshita, T. Shimono, *Application of a new superplasticizer for ultra-high strength concrete*. In: 4th CANMET/ACI International Conference on Superplasticizers and Other Chemical Admixtures in Concrete, 148, **1994**, 27-46.

[127] H. Okamura, M. Ouchi, *Self-compacting concrete - Development, present and future*. In: First International RILEM Symposium on Self-Compacting Concrete, 7, **1999**, 3-14.

[128] J. Plank, C. Schröfl, M. Gruber, *Use of a supplemental agent to improve flowability of ultra-high performance concrete*, Proceedings of Ninth ACI international Conference, Superplasticizers and Other Chemical Admixtures in Concrete SP-262, **2009**, 1-16.

[129] V. S. Ramachandran, V. M. Malholta, *Superplasticizers*, In: V. S. Ramachandran (Ed), Concrete Admixture Handbook 2nd edition, Noyes Publications, Park Ridge, NJ, **1996**, 410-517.

[130] H. Uchikawa, S. Hanchara, D. Sawaki, *The role of steric repulsion force in the dispersion of cement particles in fresh paste prepared with organic admixture*, Cement and Concrete Research, 27 (1), **1997**, 37-50.

[131] E. Sakai, A. Ishida, A. Otha, *New trends in the development of chemical admixtures in Japan*, Journal of Advanced Concrete Technology, 4 (2), **2006**, 211-223.

[132] J. Plank, *PCE superplasticizers – chemistry, applications, and perspectives*, ZKG International 67, Drymix Special, 1, **2014**, 48-59.

[133] K. Yoshioka, E. Tazawa, K. Kawai, T. Enohata, *Adsorption characteristics of superplasticizers on cement component minerals*, Cement and Concrete Research, 32 (10), **2002**, 1507-1513.

[134] J. Plank and C. Hirsch, *Superplasticizer adsorption on synthetic ettringite*, In: V. M. Malhotra (Ed), Seventh CANMET/ACI Conference on Superplasticizers in Concrete (Editor), ACI, Berlin, SP-217-19, **2003**, 283-298.

[135] J. Plank, C. Hirsch, *Impact of zeta potential of early cement hydration phases on superplasticizer adsorption*, Cement and Concrete Research, 37, **2007**, 537-542.

[136] A. Zingg, F. Winnefeld, L. Holzer, J. Pakusch, S. Becker, L. Gauckler, *Adsorption of polyelectrolytes and its influence on the rheology, zeta potential, and microstructure of various cement and hydrate phases*, Journal of Colloid and Interface Science, 323, **2008**, 301-312.

[137] K. Yoshioka, E. Sakai, M. Daimon, A. Kitahara, *Role of steric hindrance in the performance of superplasticizers for concrete*, Journal of the American Ceramic Society, 80 (10), **1997**, 2667-2671.

[138] A. Ohta, T. Sugiyama, Y. Tanaka, *Fluidizing mechanism and application of polycarboxylate-based superplasticizers*, In: V. M. Malhotra (Ed), Fifth CANMET/ACI Conference on Superplasticizers in Concrete, ACI, Rome, SP-173, **1997**, 359 – 378.

[139] J. Plank, E. Sakai, C.W. Miao, C. Yu, J.X. Hong, *Chemical admixtures – Chemistry, applications and their impact on concrete microstructure and durability*, Cement and Concrete Research, 78, **2015**, 81-99.

[140] G. Gelardi, S. Mantellato, D. Marchon, M. Palacios, *Chemistry of chemical admixtures*, In: P.-C. Aïtcin, R.J. Flatt (Eds.), Science and Technology of Concrete Admixtures, Elsevier (Chapter 9), **2016**, 149-218.

[141] D. Rinaldi, T. Hamaide, C. Graillat, F. D'Agosto, R. Spitz, S. Georges, M. Mosquet, P. Maitrasse, *RAFT copolymerization of methacrylic acid and poly(ethylene glycol) methyl ether methacrylate in the presence of a hydrophobic chain transfer agent in organic solution and in water*, Journal of Polymer Science Part A: Polymer Chemistry, 47 (12), **2009**, 3045-3055.

[142] S. Pourchet, S. Liautaud, D. Rinaldi, I. Pochard, *Effect of the repartition of the PEG side chains on the adsorption and dispersion behaviors of PCP in presence of sulfate*, Cement and Concrete Research, 42, **2012**, 431-439.

[143] J. Plank, K. Pöllmann, N. Zouaoui, P.R. Andres, C. Schaefer, *Synthesis and performance of methacrylic ester based polycarboxylate superplasticizers possessing hydroxyl terminated poly(ethylene glycol) side chains*, Cement and Concrete Research, 38, **2008**, 1210-1216.

[144] S. Akimoto, S. Honda, T. Yasukohchi, *Additives for cement*, EP 0,291,073, **1992**.

[145] G. Albrecht, J. Weichmann, J. Penkner, A. Kern, *Copolymers based on oxyalkylene glycol alkenyl ethers and derivatives of unsaturated dicarboxylic acids*, EP 0,736,553, **1996**.

[146] D. Hamada, F. Yamato, T. Mizunuma, H. Ichikawa, *Additive mixture for cement-based concrete or mortar contains a copolymer of polyalkoxylated unsaturated acid and a mixture of alkoxylated carboxylic acid with a corresponding ester and/or an alkoxylated alcohol*, DE 10,048,139 A1, **2001**.

[147] M. Yamamoto, T. Uno, Y. Onda, H. Tanaka, A. Yamashita, T. Hirata, N. Hirano, *Copolymer for cement admixtures and its production process and use*, US 6,727,315, **2004**.

[148] L. Ferrari, J. Kaufmann, F. Winnefeld, J. Plank, *Interaction of cement model systems with superplasticizers investigated by atomic force microscopy, zeta potential, and adsorption measurements*, Journal of Colloid and Interface Science, 347, **2010**, 15-24.

[149] K. Yamada, T. Takahashi, S. Hanehara, M. Matsuhisa, *Effects of the chemical structure on the properties of polycarboxylate-type superplasticizer*, Cement and Concrete Research, 30, **2000**, 197-207.

[150] E. Sakai, K. Yamada, A. Ohta, *Molecular structure and dispersion-adsorption mechanisms of comb-type superplasticizers used in Japan*, Journal of Advanced Concrete Technology, 1 (1), **2003**, 16-25.

[151] C.Z. Li, N.Q. Feng, Y.D. Li, R.J. Chen, *Effects of polyethylene oxide chains on the performance of polycarboxylate-type water-reducers*, Cement and Concrete Research, 35, **2005**, 867-873.

[152] J. Plank, B. Sachsenhauser, *Impact of molecular structure on zeta potential and adsorbed conformation of A-allyl-ω-methoxypolyethylene glycol – maleic anhydride superplasticizers*, Journal of Advanced Concrete Technology, 4 (2), **2006**, 233-239.

[153] J. Plank, C. Schroefl, M. Gruber, M. Lesti, R. Sieber, *Effectiveness of polycarboxylate superplasticizers in ultra-high strength concrete: The importance of PCE compatibility with silica fume*, Journal of Advanced Concrete Technology, 7 (1), **2009**, 5-12.

[154] F. Winnefeld, S. Becker, J. Pakusch, T. Götz, *Effects of the molecular architecture of comb-shaped superplasticizers on their performance in cementitious systems*, Cement and Concrete Composites, 29 (4), **2007**, 251-262.

[155] G.H. Kirby, J.A. Lewis, *Comb Polymer Architecture Effects on the Rheological Property Evolution of Concentrated Cement Suspensions*, Journal of the American Ceramic Society, 87 (9), **2004**, 1643-1652.

[156] J. Plank, B. Sachsenhauser, *Experimental determination of the effective anionic charge density of polycarboxylate superplasticizers in cement pore solution*, Cement and Concrete Research, 39, **2009**. 1-5.

[157] C. Gay, E. Raphäel, *Comb-like polymers inside nanoscale pores*, Advances in Colloid and Interface Science, 94, **2001**, 229-236.

[158] T. Nawa, *Effect of chemical structure on steric stabilization of polycarboxylate-based superplasticizer*, Journal of Advanced Concrete Technology, 44, **2006**, 225-232.

[159] R.J. Flatt, I. Schober, E. Raphael, C. Plassard, E. Lesniewska, *Conformation of adsorbed comb copolymer dispersants*, Langmuir, 25, **2009**, 845-855.

[160] G. Gelardi, R.J. Flatt, *Working mechanism of water reducers and superplasticizers*, In: P.-C. Aïtcin, R.J. Flatt (Eds.), Science and Technology of Concrete Admixtures, Elsevier (Chapter 11), **2016**, 257-278.

[161] H. Hommer, *Interaction of polycarboxylate ether with silica fume*, Journal of the European Ceramic Society, 29, **2009**, 1847-1853.

[162] A. Habbaba, J. Plank, *Interaction between polycarboxylate superplasticizers and amorphous ground granulated blast furnace slag*, Journal of the American Ceramic Society, 93, **2010**, 2857-2863.

[163] M. Lesti, S. Ng, J. Plank, *Ca^{2+}-mediated interaction between microsilica and polycarboxylate comb polymers in a model cement pore solution*, Journal of the American Ceramic Society, 93 (10), **2010**, 3493-3498.

[164] A. Habbaba, J. Plank, *Surface chemistry of ground granulated blast furnace slag in cement pore solution and its impact on the effectiveness of polycarboxylate superplasticizers*, Journal of the American Ceramic Society, 95, **2012**, 768-775.

[165] S. Ng, J. Plank, *Study on the interaction of Na-montmorillonite clays with polycarboxylate based superplasticizers*, In: V.M. Malhotra (Ed.), 10th CANMET/ACI Conference on Superplasticizers and Other Chemical Admixtures in Concrete (Proceeding Papers), ACI, Prague, **2012**, 407-421.

[166] S. Ng, J. Plank, *Interaction mechanisms between Na montmorillonite clay and MPEG-based polycarboxylate superplasticizers*, Cement and Concrete Research, 42, **2012**, 847-854.

[167] L. Lei, J. Plank, *A study on the impact of different clay minerals on the dispersing force of conventional and modified vinyl ether based polycarboxylate superplasticizers*, Cement and Concrete Research, 60, **2014**, 1-10.

[168] L. Nicoleau, G. Albrecht, K. Lorenz, E. Jetzlsperger, D. Fridrich, T. Wohlhaupter, R. Dorfner, H. Leitner, M. Vierle, D. Schmitt, M. Bräu, C. Hesse, S. Montero Pancera, S. Zuern, M. Kutschera, *Plasticizer-containing hardening accelerator composition*, US 2011,0269,875 A1, **2011**.

[169] L. Nachbaur, P.C. Nkinamubanzi, A. Nonat, J.C. Mutin, *Electrokinetic properties which control the coagulation of silicate cement suspensions during early age hydration*, Journal of Colloid and Interface Science, 202, **1998**, 261-268.

[170] A. Popova, G. Geoffroy, M.F. Renou-Gonnord, P. Faucon, E. Gartner, *Interactions between polymeric dispersants and calcium silicate hydrates*, Journal of the American Ceramic Society, 83 (10), **2000**, 2556-2560.

[171] A. Picker, L. Nicoleau, A. Nonat, C. Labbez, H. Cölfen, *Identification of binding peptides on calcium silicate hydrate: A novel view on cement additives*, Advanced Materials, 26, **2014**, 1135-1140.

[172] T. Sowoidnich, T. Rachowski, C. Rößler, A. Völkel, H.M. Ludwig, *Calcium complexation and cluster formation as principal modes of action of polymers used as superplasticizer in cement systems*, Cement and Concrete Research, 73, **2015**, 42-50.

[173] C.A. Orozco, B.W. Chun, G. Geng, A.H. Emwas, P.J.M. Monteiro, *Characterization of the bonds developed between calcium silicate hydrate and polycarboxylate-based superplasticizers with silyl functionalities*, Langmuir, 33, **2017**, 3404-3412.

[174] A. Picker, L. Nicoleau, Z. Burghard, J. Bill, I. Zlotnikov, C. Labbez, A. Nonat, H. Cölfen, *Mesocrystalline calcium silicate hydrate: A bioinspired route toward elastic concrete materials*, Science Advances, 3, **2017**, 1-6.

[175] V. Kanchanason, J. Plank, *Effectiveness of C-S-H – PCE nanocomposites possessing globular and foil-like morphology on early strength development of Portland cement*, Proceeding of 2nd ICCCM International Conference on the Chemistry of Construction Materials, Technische Universität München, Munich, Germany, GDCh-Monograph, 50, **2016**, 85-88.

[176] E. Cappelletto, S. Borsacchi, M. Geppi, F. Ridi, E. Fratini, P. Baglioni, *Comb-shaped polymers as nanostructure modifiers of calcium silicate hydrate: A 29Si solid-state NMR investigation*, Journal of Physical Chemistry C, 117, **2013**, 22947-22953.

[177] J.J. Beaudoin, H. Dramé, L. Raki, R. Alizadeh, *Formation and properties of C-S-H–PEG nano-structures*, Materials and Structures, 42 (7), **2009**, 1003-1014.

[178] J.J. Beaudoin, H. Dramé, L. Raki, R. Alizadeh, *Formation and characterization of calcium silicate hydrate-hexadecyltrimethylamonium nanostructures*, Journal of Materials Research, 23, **2008**, 2804-2815.

[179] J.J. Beaudoin, B. Patarachao, B., L. Raki, R. Alizadeh, *The interaction of methylene blue dye with calcium-silicate-hydrate*, Journal of the American Ceramic Society, 92, **2009**, 204-208.

[180] J.J. Beaudoin, L. Raki, R. Alizadeh, *A 29Si MAS NMR study of the modified C-S-H nanostructures.* Cement and Concrete Composites, 31, **2009**, 585-590.

[181] H. Matsuyama, J.F. Young, *Synthesis of calcium silicate hydrate/polymer complexes: part I. anionic and nonionic polymers*, Journal of Materials Research, 14 (8), **1999**, 3379-3387.

[182] H. Matsuyama, J.F. Young, *Synthesis of calcium silicate hydrate/polymer complexes: part II. Cationic polymers and complex formation with different polymers*, Journal of Materials Research, 14 (8), **1999**, 3389-3396.

[183] H. Matsuyama, J.F. Young, *Intercalation of polymers in calcium silicate hydrate: A new synthetic approach to biocomposites?*, Chemistry of Materials, 11, **1999**, 16-19.

[184] S.C. Mojumdar, L. Raki, *Preparation and properties of calcium silicate hydrate-poly (vinyl alcohol) nanocomposite materials*, Journal of Thermal Analysis and Calorimetry, 82, **2005**, 89-95.

[185] S.C. Mojumdar, L. Raki, *Preparation, thermal, spectral and microscopic studies of calcium silicate hydrate-poly(acrylic acid) nanocomposite materials*, Journal of Thermal Analysis and Calorimetry, 85, **2006**, 99-105.

[186] J. Minet, S. Abramson, B. Bresson, C. Sanchez, V. Montouillout, N. Lequeux, *New layered calcium organosilicate hybrids with covalently linked organic functionalities*, Chemistry of Materials, 16, **2004**, 3955-3962.

[187] J. Minet, S. Abramson, B. Bresson, A. Franceschini, H.V. Damme, N. Lequeux, *Organic calcium silicate hydrate hybrids: a new approach to cement based nanocomposites*, Journal of Materials Chemistry, 16, **2006**, 1379-1383.

[188] J. Plank, F. Yang, O. Storcheva, *Study of the interaction between cement phases and polycarboxylate superplasticizers possessing silyl functionalities*, Journal of Sustainable Cement-Based Materials, 3 (2), **2014**, 77-87.

[189] I. Odler, *Hydration, setting and hardening of Portland cement*, In: P.C. Hewlett (Ed), Lea's chemistry of cement and concrete, fourth ed., Butterworth-Heinemann Publishing, Oxford, **2003**, 241-297.

[190] K.L. Scrivener, P. Juilland, P.J.M. Monteiro, *Advances in understanding hydration of Portland cement*, Cement and Concrete Research, 78, **2015**, 38-56.

[191] D. Marchon, R.J. Flatt, *Mechanisms of cement hydration*, In: P.-C. Aïtcin, R.J. Flatt (Eds.), Science and Technology of Concrete Admixtures, Elsevier (Chapter 8), **2016**, 129-145.

[192] H. Minard, S. Garrault, L. Regnaud, A. Nonat, *Mechanisms and parameters controlling the tricalcium aluminate reactivity in the presence of gypsum*, Cement and Concrete Research, 37 (10), **2007**, 1418-1426.

[193] E. Gallucci, M. Mathur, K. Scrivener, *Microstructural development of early age hydration shells around cement grains*, Cement and Concrete Research, 40, **2010**, 4-13.

[194] J. Stark, B. Möser, F. Bellmann, *Nucleation and growth of C-S-H phases on mineral admixtures*, Advances in Construction Materials, **2007**, 531-538.

[195] V. S. Ramachandran, *Accelerators*, In: V. S. Ramachandran (Ed.), Concrete Admixture Handbook 2nd edition, Noyes Publications, Park Ridge, NJ, **1996**, 185-285.

[196] S. Baueregger, L. Lei, M. Perello, J. Plank, *Use of a nano clay for early strength enhancement of Portland cement*, In: K. Sobolev, S. P. Shah (Eds.), Nanotechnology in Construction – Proceedings of NICOM5, Chicago (USA), May 24-26, **2015**, 199-206.

[197] ACI Committee 212, *Chemical admixtures for concrete*, ACI Manual of Concrete Practice, **1995**, pp. 212.3R-10.

[198] A.M. Rosenberg, *Study of the mechanism through which calcium chloride accelerates the set of Portland cement*, In Proceedings of the Journal of the American Concrete Institute, **1964**, 1261-1268.

[199] V.H. Dodson, E. Farkas, A.M. Rosenberg, *Non-corrosive accelerator for setting of cements*, US Patent No. 3,210,207, **1965**.

[200] R.L. Angtadt, F.R. Hurley. *Accelerator for Portland cement,* US Patent No. 3,427,175, **1969**.

[201] V.S. Ramachandran, *Action of triethanolamine of the hydration of tricalcium aluminate,* Cement and Concrete Research, 3 (1), **1973**, 41-54.

[202] J. Neubauer, F. Goetz-Neunhoeffer, U. Holland, D. Schmitt, *Crystal chemistry and microstructure of hydrated phases occurring during early OPC hydration*, Proceedings of the 12th International Congress on the Chemistry of Cement, Montreal, Canada, **2007**.

[203] S. Aggoun, M. Cheikh-Zouaoui, N. Chikh, R. Duval, *Effect of some admixtures on the setting time and strength evolution of cement pastes at early ages*, Construction and Building Materials, 22 (2), **2008**, 106-110.

[204] K. Riding, D.A. Silva, K. Scrivener, *Early age strength enhancement of blended cement systems by $CaCl_2$ and diethanol-isopropanolamine*, Cement and Concrete Research, 40, **2010**, 935-946.

[205] K. Hoang, H. Justnes, M. Geiker, *Early age strength increase of fly ash blended cement by a ternary hardening accelerating admixture*, Cement and Concrete Research, 81, **2016**, 59-69.

[206] G. Land, D. Stephan, *Preparation and application of nanoscaled C-S-H as an accelerator for cement hydration*, In: K. Sobolev, S.P. Shah (Eds.), Nanotechnology in Construction: Proceedings of NICOM5, Springer International Publishing, Cham. **2015**, 117-121.

[207] V. Kanchanason, J. Plank, *Relationship between the structure and morphology of C-S-H – PCE nanocomposites and their accelerating effect in cement*, Tagung Bauchemie, Bauhaus-Universität Weimar, Tagungsband 1, Weimar, Germany, GDCh-Monograph, 52, **2017**, 36-40.

[208] L. Nicoleau, G. Albrecht, K. Lorenz, E. Jetzlsperger, D. Fridrich, T. Wohlhaupter, R. Dorfner, H. Leitner, M. Vierle, D. Schmitt, M. Bräu, C. Hesse, S. Montero Pancera, S.

Zuern, M. Kutschera, *Plasticizer-containing hardening accelerator composition*, US 8,653,186 B2, **2014**.

[209] L. Nicoleau, T. Gaedt, H. Grassl, *Hardening accelerator composition*, WO 2014/026938 A1, **2014**.

[210] L. Nicoleau, H. Leitner, *Hardening accelerator composition for cementitious compositions*, WO 2014/026940 A1, **2014**.

[211] C. Hesse, L. Nicoleau, *Hardening accelerator composition*, WO 2014/114782 A1, **2014**.

[212] K. Owens, M. I. Russell, G. Donnelly, A. Kirk, P.A.M. Basheer, *Use of nanocrystal seeding chemical admixture in improving Portland cement strength development: application for precast concrete industry*, Advances in Applied Ceramics, 113 (8), **2014**, 478-484.

[213] J. Pizoń, P. Miera, B.Ł. Piekarczyk, *Influence of hardening accelerating admixtures on properties of cement with ground granulated blast furnace slag*, Procedia Engineering, 161, **2016**, 1070-1075.

[214] J. Pizoń, *Long-term compressive strength of mortars modified with hardening accelerating admixtures*, Procedia Engineering, 195, **2017**, 205-211.